Determination and Characterization of 20th Century Global Sea Level Rise

by

Chung-Yen Kuo

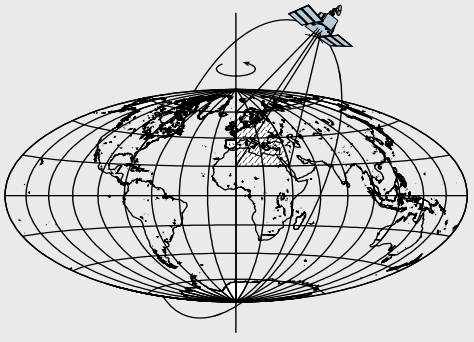

Report No. 478

Geodetic Science and Surveying
Department of Geological Sciences
The Ohio State University
Columbus, Ohio 43210

April 2006

DETERMINATION AND CHARACTERIZATION OF 20th CENTURY GLOBAL SEA LEVEL RISE

BY

CHUNG-YEN KUO

Report No. 478

Geodetic Science and Surveying

Department of Geological Sciences

The Ohio State University

Columbus, Ohio 43210, USA

April 2006

ABSTRACT

Sea level rise has been widely recognized as a measurable signal and as one of the consequences of a possible anthropogenic (human-induced) effect on global climate change. The small rate of sea level rise, 1–2 mm/yr during the last century [Church et al., 2001, *Chapter 11, Changes in Sea Level, in the Third Assessment Report (TAR) of the Intergovernmental Panel for Climate Change (IPCC), Working Group I,* Houghton et al., 2001], could only be partially explained by a number of competing geophysical processes, each of which is a complex process within the Earth-atmosphere-ocean-cryosphere-hydrosphere system. In particular, the observed 20th Century sea level rise rate of 1.84±0.35 mm/yr [Douglas, 2001; Peltier, 2001] could not explain up to one half of the predicted 20th Century global sea level rise based on the IPCC TAR estimate of 1.1 mm/yr (0.6 mm/yr of melted water from ice sheets and glaciers, and 0.5 mm/yr from the steric effect in the ocean) [Church et al., 2001] and remains an enigma [Munk, 2002]. The quest to resolve the controversy [Meier and Wahr, 2002] and to further understand sea level change [Chao et al., 2002] is well underway including efforts being conducted during the current IPCC Fourth Assessment Report (FAR), 2003–2007.

In this study, we provide a determination of the 20th Century (1900–2002) global sea level rise, the associated error budgets, and the quantifications or characterization of various geophysical sources of the observed sea level rise, using data and geophysical models. We analyzed significant geographical variations of global sea level change including those caused by the steric component (heat and salinity) in the ocean, and sea level redistribution resulting from ice sheets and glacier melting in consequence of self gravitation, and the effects of glacial isostatic adjustment (GIA) since the Pleistocene affecting sea level signals in the observations. In particular, relative sea level data from up to 651 global long-term (longest record is 150 years) tide gauges from Permanent Service for Mean Sea Level (PSMSL) and other sources, and geocentric sea level data from multiple satellite radar altimetry (1985–2005) have been used to determine and characterize the 20th Century global sea level rise. Altimeter and selected tide gauge data have been used for sea level determination, accounting for relative biases between different altimeters and offsets between the tide gauges, effects of thermosteric sea level variations, vertical motions affecting tide gauge sea level measurements, sea level redistribution due to ice melt resulting from self gravitation, and barotropic ocean response due to atmospheric forcing. This study is also characterized by the role of the polar ocean in the global sea level study and addressing the question whether there is a detectable acceleration of sea level rise during the last decade. Vertical motions have been estimated by combining geocentric sea level measurements from satellite altimetry (TOPEX/POSEIDON, T/P) and long-term relative (crust-fixed) sea level records from global tide gauges using the Gauss-Markov model with stochastic constraints. The study provided a demonstration of improved vertical motion solutions in semi-enclosed seas and lakes, including Fennoscandia and the Great Lakes region, showing excellent agreement with independent GPS observed radial velocities, or with predictions from GIA models. In general, the estimated uncertainty of the observed vertical motion is <0.5 mm/yr, significantly better than other studies. Finally, improved algorithms to account for nonlinear vertical motions caused by other geodynamic processes than GIA including post-seismic deformations, have been developed and applied to tectonically active regions such as Alaska and

compared well with GPS velocities and other studies. This novel technique could potentially provide improved vertical motion globally where long-term tide gauge records exist.

The thermosteric sea level trend of the upper (0–500 m) layers of the ocean accounts for about 70% of the variations when deeper ocean (0–3000 m) is considered using the World Ocean Altas 2001 (WOA01). The estimated global thermosteric sea level trend of 0.33 mm/yr (0–500 m) and 0.43 mm/yr (0–3000 m) agrees well with other studies [Levitus et al., 2005; Ishii et al., 2005]. A detailed analysis using *in situ* temperature and salinity data from the Ocean Station Data (OSD), in the Eastern Pacific (where the *in situ* data are more abundant) is conducted to assess the contributions of respective roles of thermal and salinity effects on sea level changes. The analysis indicates that the estimated thermosteric sea level trends integrated from 0–500 m and from 0–1000 m depths using OSD are almost identical at ~0.64 mm/yr in the Eastern Pacific ocean. In this region, the halosteric (salinity) sea level trend is small, at the 0.04 mm/yr level for both the 0–500 m and 0–1000 m cases. The result is consistent with Miller and Douglas [2004], which analyzed data from selected oceanic regions including the Eastern Pacific, Eastern Atlantic, and Caribbean. In general, observed sea level (from tide gauges or altimetry) and thermosteric sea level are highly correlated except in regions of high mesoscale variability. A detailed comparison of the estimated thermosteric sea level trends with the observed sea level trend near proximities of global tide gauges (~50 years, 1950–2004, up to 597 sites) indicates that the thermosteric sea level trends account for 36% and 68% of the observed global sea level trend, for the 0–500 m and 0–3000 m cases, respectively, indicating the importance of deeper ocean thermal effects. Comparison of global thermosteric sea level trend with altimetry observed sea level trends indicates that the results are dependant on data spans used: thermosteric sea level trend (0–500 m) accounts for over 81% of total observed sea level using T/P altimetry during 1993–2003, while accounts for only 26% when data span extends to 1985–2005 using multiple altimetry. The primary reason is the presence of long-period oceanic variability (interannual, decadal or longer) in trend estimates causing inconsistent conclusions. Comparison of thermosteric sea level trend with sea level observed by selected tide gauges reaches different conclusions depending on the choice and number of tide gauges (1955–1996) used: thermosteric sea level trend (0–3000 m) accounts for over 88% of the observed sea level from 27 tide gauges, while it accounts for only 38% if 515 tide gauges are used.

A study using temporal gravity field measurements observed by the Gravity Recovery and Climate Experiment (GRACE) in terms of oceanic mass variations at long-wavelength (>800 km) and monthly sampling demonstrates its potential use, when combined with satellite altimetry, to improve steric sea level trend estimates over the Southern Ocean, where the OSD is extremely sparse or non-existent.

The global (covering within $\pm 81^0.5$ latitude) sea level trend (corrected for IB) observed by multiple satellite altimetry (GEOSAT, ERS-1, T/P, ERS-2, GFO, JASON and ENVISAT, data covering 1985–2002 except for 1988–1991), and by ~530 tide gauges are 2.8±0.5 mm/yr (corrected for GIA geoid effect) and 2.7±0.4 mm/yr, respectively, indicating excellent agreement. The observed sea level trend using multiple satellite altimeters covering 1985–2004 is 2.9±0.5 mm/yr, although the data span is still too short to yield reliable trend estimates. The multiple altimeter data sets allow coverage in the polar oceans, as opposed to only using data from T/P (coverage within $\pm 66^0$), and have a longer data span (~19 years versus 10 year for T/P). The data

have been calibrated against each other and with tide gauge data for robust determination of their relative biases with respect to T/P. The 20th Century (1900–2002) global sea level trend determined from 651 tide gauge stations is 1.6±0.4 mm/yr, while the trend estimate for the last 50 years (1948–2002) is similar, but used 620 tide gauges. The atmospheric effect via the barotropic IB correction (globally averaged at ~0.11 mm/yr and over 50 years at global tide gauge locations) to sea level (tide gauges or altimetry) observations is warranted as it reduces variances of the data and causes improved agreements between altimetry and tide gauge sea level data. The multiple altimeter data allows sea level studies in the Arctic and Sub-Arctic Oceans, which have been less studied. The sea level trend in the Sub-Arctic Ocean, bounded by latitude 55°N–82°N and longitude 315°E–60°E, is estimated at 1.8 mm/yr using primarily ERS-1 and ERS-2 altimetry, which have been calibrated by TOPEX/POSEIDON in the lower latitude (±66^0 latitude) oceans and remove constant offsets and a latitude-dependent bias. The sea level trend can mostly be explained by atmospheric forcing and thermosteric effects. In the Arctic Ocean, sea level trend during 1948–2002 is estimated at 1.9–2.0 mm/yr using tide gauges after correction of land motion using different GIA models. After applying the inverted barometric (IB) correction, the sea level rate reduces to 1.5–1.6 mm/yr, indicating that the barotropic response of the ocean contributes significantly more to the sea level trend in the Arctic Ocean than for the global ocean.

In an attempt to estimate the global sea level trend and to quantify some of the known contributions in the 20th Century using data from sparsely distributed long-term tide gauges and ~20 years of satellite altimetry, we assume that the *spatial patterns* of sea level trends from melt water sources (Antarctica, Greenland and mountain glaciers), the thermosteric effects, and geoid change and land uplift due to GIA are known, while their *magnitudes* are unknown. We ignored contributions from fresh water imbalances due to continental hydrological processes [Milly et al., 2003; Ngo-Duc et al., 2005], human-impoundment of water in reservoirs or lakes [Chao et al., 1994; Sahagian et al., 1994] and other effects, including permafrost melt [Zhang et al., 2005]. Using two different estimators, the Weighted Least Squares (WLS) and the Elementwise-Weighted Total Least Squares (EW-TLS), and using long-term tide gauges and satellite altimetry, we estimate the respective contributions of each of the sources to the global sea level rise. The EW-TLS technique is found to be more stable while the WLS technique produces solutions with larger error of ~0.3 mm/yr in a simulated study. The EW-TLS solution yields the estimated 20th Century (1900–2002) sea level trend contributions by melt water from the Antarctic and Greenland ice sheets and mountain glaciers to be 0.80±0.14 mm/yr, 0.56±0.12 mm/yr and 0.31±0.08 mm/yr, respectively; the estimated contribution from the thermosteric effect is 0.06±0.04 mm/yr, and the estimated scale of the GIA (ICE-4G) model to correct tide gauge sea level data is 1.27±0.08, indicating that the correction should be higher by 27%. The resulting 20th Century (1900–2002) globally averaged sea level trend is estimated to be 1.73±0.42 mm/yr (95% confidence or 2σ) after summing the above forcing factors. The estimate of the resulting last 50 year (1948–2002) global sea level trend is 1.74±0.48 mm/yr (95% confidence or 2σ).

Finally, we address the issue of whether the sea level trend acceleration is detectable. An analysis indicates that the minimum data span to obtain a stable rate of sea level trend from 27 selected tide gauges [Douglas, 2001] is 20 years or more, while one should use a 30-year or longer data span to derive a stable thermosteric sea level trend from WOA01. It is concluded

that, with 95% confidence, there is no statistically significant evidence of sea level acceleration during 1900–2000 from tide gauge data, and during 1950-2000 from thermosteric data.

The estimated 20th Century global sea level rise is compared with the more recently estimated total geophysical effects contributing to global sea level rise of 1.41–1.53 mm/yr, which include the sum of the steric effect (~0.4 mm/yr) [e.g., Levitus et al., 2005; Antonov et al., 2005], mountain glacier melting (~0.51 mm/yr) [e.g., Arendt et al., 2002; Dyurgerov and Meier, 2005; Raper and Braithwaite, 2005; and others], ice sheet mass imbalance (~0.45 mm/yr) [e.g., Krabill et al., 2004, Rignot et al., 2005, Thomas et al., 2005], hydrological imbalance (~0.0–0.12 mm/yr) [Milly et al., 2003, Ngo-Duc et al., 2005], and anthropogenic effect (~0.05 mm/yr) [Dork Sahagian, pers. comm.]. This study (1.74±0.48 mm/yr) reduces the existing discrepancy [Chruch et al., 2001] to 0.21–0.33 mm/yr between the total observed and predicted contributions to 20th Century global sea level rise. However, the estimated individual contributions of the ice sheet imbalance and the oceanic steric effect remain significantly different from the current results from observations, and not much progress has been made since the last IPCC study on the effect of hydrologic imbalance and anthropogenic causes. Much future work remains to improve our understanding of the complex processes governing global sea level changes.

ACKNOWLEDGMENT

The Report describes the PhD dissertation research completed by Chung-Yen Kuo on November, 2005, supervised by C.K. Shum and other PhD Committee Members including Douglas Alsdorf, Michael Bevis, Laury Miller, and Yuchan Yi. Tide gauge records provided by PSMSL, University of Hawaii sea level center, Geographical Survey Institute, Japan, LEGOS/ROSAME, France, and numerous other collaborators. Water level gauge data in the Great Lakes are provided by NOAA CO-OPS and MEDS in Canada. The ICE4G/VM2 PGR model is provided by Richard Peltier and BIFROST PGR model is provided by Jerry Mitrovica and Glenn Milne. Global ocean circulation model outputs are provided by Ichiro Fukumori and Tony Song. Various ocean model outputs in the Arctic and Sub-Arctic Oceans are provided by Andrey Proshutinsky. Global ocean temperature and salinity data are provided by Sydney Levitus, Masayoshi Ishii and Josh Willis. GEOSAT and GFO satellite altimetry data are provided by US Navy via NOAA's Laboratory for Satellite Altimetry. ERS-1/-2 and ENVISAT data are provided by ESA/ESRIN via IFREMER. TOPEX/POSEIDON and JASON-1 data are provided by NASA/JPL PODAAC and CNES AVISO. Altimeter data with repeated orbits are stored in form of the Ohio State University stackfile maintained by Yuchan Yi. GRACE data products are provided by University of Texas Center for Space Research via JPL/PODAAC. Modeled geographical patterns of sea level changes due to continuing ice mass variations are provided by Jerry Mitrovica and Mark Tamisiea. Finally, we acknowledge many fruitful discussions and inspiring advice on the research from the incomplete list of colleagues mentioned above, as well as from Geoff Blewitt, Anny Cazenave, Bruce Douglas, Masayoshi Ishii, Laury Miller, Hans-Peter Plag, Josh Willis, Philip Woodworth and many others. This research is supported by grants from NOAA under NA16RG2252, NA86RG0053 (R/CE-5) and NA030AR4170060 (R/CE-8), and NASA's Ocean and Ice, Cryosphere, Physical Oceanography and Interdisciplinary Science Programs (NNG04GA53G, NAG5-9335, NAG5-12585, JPL-1265252).

.

TABLE OF CONTENTS

CHAPTER 1

INTRODUCTION

1.1 Global Sea Level Rise

Global sea level rise has a substantial impact on the economic and human societal well being. The impacts of sea level rise are summarized by Nicholls and Leatherman [1994] which include inundation of low-lying areas, erosion of beaches and bluffs, salt intrusion into aquifers and surface waters, higher water tables, and increased flooding and storm surge damage. These effects have a significant impact on the economic and human societal well being in the coastal regions because sea level rise causes land loss near the coasts, which are the most populated regions of the world. United States Census Bureau figures [Culliton et al., 1990] show that nearly 50 percent of the residents of the country reside in coastal counties. Stewards of the world's wetland, one of our most sensitive environmental zones, are concerned that a rapid change in the sea level might dramatically reduce the size of arable wetlands.

The Earth's Quaternary climate has been characterized on the Milankovitch time scales of 100,000 years by interlinked changes in temperature, greenhouse gases dominated by CO_2, cryosphere, and sea level. Sea level rise has been widely recognized as a measurable signal and as one of the consequences of a possible anthropogenic (human-induced) effect on global climate change. The small rate of sea level rise signal, 1–2 mm/yr during the last century [Church et al., 2001, *Chapter 11, Changes in Sea Level, in the Third Assessment Report (TAR) of the Intergovernmental Panel for Climate Change (IPCC), Working Group I*, Houghton et al., 2001], could only be partially explained by a number of competing geophysical processes, each of which is a complex process within the Earth-atmosphere-ocean-cryosphere-hydrosphere system. They include geological changes of the ocean basin, redistribution of atmosphere masses and water from ice sheet and glacier melting, visco-isostatic rebound of the lithosphere and mantle from Pleistocene deglaciation, resulting gravity changes, thermosteric and halosteric sea level variations of the oceans, the extraction of ground water and storage of water in man-made reservoirs, astronomical and atmospheric tides, and changes in coastal sedimentation and erosion. Among these processes, the dominant effects include the melting of continental ice sheets and mountain glaciers, and the steric (thermosteric and halosteric) effects of the ocean [Pattulo et al., 1955], especially if the warming trend continues.

A contemporary definition of sea level changes refers to a height change with respect to the origin of the current realization of the International Terrestrial Reference System (ITRF) [IERS, D. McCarthy (Ed.), 1996]. This "geocentric" measurement is independent of the crust and the solid Earth motions. The more commonly recognized term "relative sea level change" is the measurement with respect to a reference datum located on the crust of the solid Earth (i.e., from tide gauge stations). The signal of global sea level rise desirable to be quantified includes those due to mass redistribution (from ice melting) and due to volume (due to thermal expansion and salinity contraction) changes in the global ocean. In this study, the classical term "eustatic sea level", which is defined as "the change of global sea level brought about by an alteration to

the volume of the world ocean," is not used. In discussions of changes on geological time-scales, eustatic sea level also includes changes in average sea level caused by a change of the shape of the ocean basin. The use of this term in some presently published literatures is inconsistent with its original definition, i.e., it has been used to denote the mass change of sea level. As a result, also adopted by the IPCC glossary, this term is not used to avoid further confusion.

1.2 Determination of Global Sea Level Rise Using Altimetry and Tide Gauges

Global sea level rise that is desirable to be quantified is caused by mass and volume changes of the ocean, which will have a direct impact on human-societal well-beings on time scales of decades and centuries. However, to accurately determine the sea level changes and the rate of sea level changes is a complex problem. Recently the most common instruments used to determine global sea level changes are tide gauges and satellite altimetry.

Satellite altimetry is a developed technology in oceanography to synoptically map the surfaces of the global ocean. It is able to observe global oceanic topography and its changes with unprecedented accuracy (several cm Root Mean Square (RMS) in sea surface heights) and resolutions (up to 50 km spatial scale and weekly temporal sampling). The basic concept of satellite altimetry is relatively straightforward. The observational principle is to measure a range R from a satellite to a ocean surface. The radar altimeter transmits an electromagnetic radar pulse with known power and radar frequency to the sea surface and measures its round-trip travel time (t) when the radar pulse is partially reflected back to the receiving antenna onboard the satellite from the instantaneous sea surface. As a result, the observed measurement in satellite radar altimetry is actually a time series of the received power distributions of the reflected pulses, which is often referred to as the altimeter waveforms. The range R from the satellite to the sea surface can be expressed as:

$$R = ct/2 \tag{1.1}$$

where c is the speed of light in vacuum.

However, several corrections must be applied to the observed altimeter heights before they can be used in oceanographic and other applications. The altimeter measurement models can be summarized as follows [Gumma, 1997]:

$$h_{alt} = R + h_a + h_i + h_e + h_s + \varepsilon \tag{1.2}$$

where h_a are the atmospheric refraction corrections, including atmosphere delays from the ionosphere, wet and dry troposphere. h_i is the instrument correction. h_e are the geophysical corrections including ocean tides, solid Earth tides, pole tides, relativistic light-time, and atmospheric pressure loading. h_s is the sea state bias correction, including electromagnetic (EM) and skewness biases. ε are other random and systematic errors in the altimeter measurements.

To be useful for oceanography, the position and velocity of the satellite or the orbit of the satellite must be known. Or, after computing a precise orbit, the orbital height (H) from the satellite to a specified reference ellipsoid, is known. Sea surface heights (ssh) relative to a specified reference ellipsoid are written as follows:

$$h_{ssh} = H - h_{alt} \tag{1.3}$$

Since the launch of GEOS-3, a satellite carrying a radar altimeter in 1975, there have been a number of historic and current operating altimeter missions flown, and numerous scientific results of these missions have been published. Table 1.1 presents a list of the past, current and future altimeter missions and their orbital parameters [Cheng, 2001; Urban, 2000; Guman, 1997].

Satellite radar altimetry has a potential to definitively measure the long-term (decades) global sea level changes with a spatial scale of 50 km or longer and a temporal sampling of days, and with an accuracy approaching 1 mm/yr [e.g., Nerem and Mitchum, 2001; Shum et al., 2000, 2001a, 2001b; Urban et al., 1999, 2001b]. One of the first plans for using satellites to observe global sea surface heights was formulated at the 1969 NASA's Williamstown Conference of Solid Earth and Ocean Physics [Kaula, 1969]. Altimeter derived sea level trends using TOPEX/POSEIDON (T/P) data covering global ocean from $66°N$ to $66°S$ have been extensively been published [e.g., Nerem and Mitchum, 2001; Cabanes et al., 2001b; Cazenave and Nerem, 2004]. Other high-latitude observing altimetry missions in addition to T/P have also been used to determine sea level changes [e.g., Guman, 1997]. Stringent technical details are needed to exploit the use of multiple radar altimeters for the measurements of the global sea level. For instance, relative biases between different altimeter systems with different accuracies depending on geographical locations or even time could be a significant limitation. The US/WOCE (operated by University of Hawaii) and the Great Lakes tide gauges have been used to "link" or determine the relative instrument biases between different altimeter systems [Guman, 1997; Urban et al., 1999, 2001b; Shum et al., 2000]. However, because of the potential problems including degrading of instruments and instrument biases dependent on satellite orientation and thus on geographical locations, necessitates multiple absolute calibration sites, preferably globally distributed for the continuous monitoring of each of the altimetry systems. The ~20 years altimetry measurements from multiple missions (Table 1.1), including GEOSAT GM/ERM, ERS-1/-2, GFO, ENVISAT, TOPEX/POSEIDON and JASON-1, may still be limited to resolve a robust sea level trend estimates primarily because of the low frequency (interannual, decadal or longer) signals in the ocean which are either as long as or longer than the data span (see Chapter 7).

The stringent observational requirements necessitate the knowledge of the altimeter instrument bias, its drift, and its link with current and historic altimetric systems. Absolute radar altimeter calibration and its monitoring are critical and a number of dedicated calibration sites have been established. Since 1992, operational calibration sites for T/P include the Harvest Platform, California [Christensen et al., 1994; Haines et al., 2003], Bass Strait, Tasmania [White et al., 1994, Watson et al., 2003], and the British Channel [Murphy et al., 1996]. Since then, other dedicated altimeter absolute calibration sites for multiple altimeters have been established or planned, including the North Sea [Schöne et al., 2002], Corsica Island [Bonnefond et al.,

2003], Vanuatu, South West Pacific [Calmant et al., 2001], Baltic Sea [Liebsch et al., 2002], Catalunya, Spain (M. Rocca, personal communication), Mediterranean Sea [Schüler et al., 2003], and Lake Erie [Cheng et al., 2002; Shum et al., 2003a]. Among the absolute altimeter calibration sites, the Arguello Inc. Harvest Oil Platform [Christensen et al., 1994], located 10 km offshore of central California has the longest altimeter absolute calibration data records [Haines et al., 2003] and has demonstrated the ability to estimate altimeter bias and drifts due to the instruments as well as geophysical algorithm errors for the reduction of the altimeter measurements to geocentric sea surface height measurements. The evaluation of altimeter systems over large lakes has a number of advantages including minimal tides and a smaller dynamic variability compared to the ocean. Moreover, long-term water level or tide gauge records usually exist in lakes and Morris and Gill [1994] have conducted absolute calibration of the TOPEX/POSEIDON altimeter over the Great Lakes. Shum et al. [2004] reported more recent absolute calibration results for both TOPEX/POSEIDON and JASON-1 altimeters over Lake Erie and the rest of the Great Lakes. This study used knowledge from existing absolute radar altimeter calibration results and developed a method to cross-calibrate different altimeters as well as compare with tide gauges, to generate a consistent, long-term (~20 year) lake level data set spanning from 1984–2005, with data gaps from 1988–1991.

In contrast to the short-term altimetry data, tide gauges provide longer than 50 years of data records with the longest record reaches 150 years. However, there are some important factors that affect the determination of sea level changes. First, tide gauges are monitoring heights of sea surfaces relative to a fixed point on the adjacent land. Hence vertical crustal motions due to local subsidence, tectonic uplift, and primarily the Glacial Isostatic Adjustment (GIA) or Post-Glacial Rebound (PGR), which is the physical phenomenon of the visco-elastic response of the solid Earth (mostly mantle) due to the ice accumulation and melting during the cycles of glaciation and deglaciation, resulting in crust-fixed tide gauge (relative) sea level measurements not representing the true sea level signals. As an example, the rate of the sea level changes at Churchill Falls in Hudson Bay, Canada, derived from long-term tide gauge data is about –9 to –10 mm/yr [Tushingham, 1992; Shum et al., 2002], with most of the observed sea level rate signal due to vertical land motion (crustal uplift and geoid change). Assuming that the mean sea level rise is 1.8 mm/yr [Douglas, 2001] and the observed geoid deformation (from absolute gravimeter measurement) is 0.9 mm/yr [Lambert et al., 1998], the vertical motion with respect to the center mass of the Earth is about 11.7–12.7 mm/yr, which agrees with the solutions of GPS and absolute gravity [Larson and Dam, 2000]. It is obvious GIA must be taken into account when determining the global sea level trend using tide gauges. The second problem is the incompleteness of tide gauge records, such as large data gaps, the length of records, and jumps of tide gauge benchmarks due to human (surveying) errors or land motions such as earthquakes. A large data gap could severely embroil the accuracy of the estimated sea level trend, so a robust algorithm to determine the rate of a time series is required. Douglas [1997, 2001] mentioned that they do not use short tide gauge records because of the low frequency fluctuations of sea level which influence the determination of the sea level trend. However, Cabanes et al. [2001b], Mitrovica et al. [2001], and Munk [2002] are among recent studies which suggested that the current estimation of sea level using selected long-term (>50 years) tide gauges (e.g., up to 27 gauges are chosen by Douglas [1997, 2001]) may be under-sampling the sea level signal. The fundamental problem is that the tide gauge stations are not globally distributed. For example, there are almost no tide gauge sites with long-term records in the

Southern Ocean, including Antarctica, while the sea level change signals have significant geographical variations. Most of the available tide gauges are located in the northern hemisphere. Nevertheless, Douglas [1992, 1997, 2001] and Woodworth [1990] are among the studies indicating that very long (>70 years) tide gauge records do not require global coverage and widely located tide gauge stations show a very consistent sea level trend and there is also a lack of evidence of acceleration in the observed sea level trend. However, significant spatial variations of sea level signals have been shown by studies including Levitus et al. [2000] on the oceanic variations due to thermal expansion during the past 5 decades, and by Conrad and Hager [1997] and Mitrovica et al. [2001] on the sea level redistribution due to ice mass variations resulting from self gravitation in the surface load. Shum et al. [2001a] and this study advocate the use of as many geographically located tide gauge data records as possible, even those with shorter records than 50 years, to mitigate the problem to observe or model sea level trends with known, significant spatial or geographical variations.

The contemporary estimate of the 20th century sea level rise is determined primarily using data from coastal and island tide gauges after correcting for the GIA effect. The estimated sea level rise ranges from 1.5 to 2.4 mm/yr [Gornitz, 1982, 1995; Barnett, 1990; Peltier, 1988, 2001; Trupin and Wahr, 1990; Shennan and Woodworth, 1992; Douglas, 1991, 1992, 1997; Mitrovica and Davis, 1995; Ekman, 1988, 2000; Woodworth et al., 1999; Douglas et al., 2001; Mitrovica et al., 2001; Miller and Douglas, 2005]. There is a prediction that the 21st century sea level will be 13–94 cm higher than today, with one of the possible causes being the human-induced or anthropogenic greenhouse effects [Warrick et al., 1996]. One of the more recent determinations of the 20th Century sea level rise using tide gauges [Douglas et al., 2001; Peltier, 2001], 1.84±0.35 mm/yr, is slightly higher than the central value of the last IPCC study [Church et al., 2001] of 1.5 mm/yr, but within their estimated range of 1.0 to 2.0 mm/yr. The significance is that the currently observed 20th Century sea level rise at 1.8 mm/yr (without evidence of apparent acceleration) is much higher than the recent IPCC estimate [Church et al., 2001] of 0.6 mm/yr. In order for the "residual" 1.2 mm/yr to be accounted for during the 20th Century, if entirely from melted water, it would require 40,000 gigatons of fresh water; or if entirely thermal expansion, it requires ~10×10^{23} J of excess heat storage in the ocean. Either scenario is extremely unlikely to have happened. This controversy has caused the so-called "20th Century sea level: an enigma" [Munk, 2002] debate and prompted publishing of other studies, [e.g., Meier and Wahr, 2002].

In order to diminish the effects of vertical motions, Miller and Douglas [2005] demonstrated a morphological approach, based on the trends of relative sea level rise as a function of distance from the centers of the ice loads at last glacial maximum, to obtain the trend of sea level rise of about 2 mm/yr.

Presently researchers are trying to study sea level using the combined data of tide gauges and altimeters [Chambers et al., 2002; Church et al., 2004; Shum et al., 2002; Kuo et al., 2005]. Chambers et al. [2002] analyzed the low frequency signals of global mean sea level during the 1950–2000 period of time by interpolating sparse tide gauge data to a global grid using empirical orthogonal functions (EOFs) of sea level variability determined from TOPEX/POSEIDON altimeter data. Similarly, Church et al. [2004] reconstructed the grids of global mean sea level combining TOPEX/POSEIDON data and historical tide gauge data by using an improved EOF

approach and the estimated global sea level trend is 1.8±0.3 mm/yr for the time period 1950–2000. Nevertheless, Jakub et al. [2004] reported that the 50-year sea level reconstruction is moderately sensitive to the variations in the analysis variables, such as tide gauge selection criteria and the number of EOFs used. The greatest sensitivity is in the early years of the reconstruction when the least number of tide gauges are available. In addition, the geographical sea level trends from the reconstructed sea level fields using tide gauge data [Church et al., 2004] are highly correlated geographically with the standard deviations of the TOPEX/POSEIDON observed sea surface height anomalies after removal of the annual and semiannual signals, and a linear trend in the globally averaged sea level. There is no explanation for this phenomenon and it seems that the resulting 51-year sea level trend estimate reported by Church et al. [2004] could be the variations of TOPEX/POSEIDON sea level data. The errors of reconstructed sea level trends may be caused by the short-term altimeter data since the time-varying biases (e.g., trends) in the observations cannot be determined exactly and might be projected onto the leading EOFs. In addition, because the EOFs used as basis functions are computed over relatively short time spans of the altimeter data, true spatial patterns of global sea level change are not distinct in any of EOF mode [Hendricks et al., 1996]. Therefore trends in the tide gauge observations would likely be projected incorrectly into the TOPEX/POSEIDON EOFs which might lead to possible errors. As a result, any recovered sea level trends from the reconstruction could be in suspect [Chambers et al., 2002]. However, more study is needed to further examine the validity of this method.

Mission	Active Date (month/year)	Altitude (km)	Inclination (degree)	Repeated Period (Sidereal days)	Agency
GEOS-3	4/75–12/78	840	115	N/A	NASA
SEASAT	7/78–9/78	790	108	17	NASA
SEASAT	9/78–10/78			3	
GEOSAT GM	3/85–11/86	780	108	N/A	US Navy
GEOSAT ERM	11/86–12/89			17	
ERS-1 A	7/91–11/91	785	98.5	3	ESA
ERS-1 B	11/91–3/92			3	
ERS-1 C	4/92–12/93			35	
ERS-1 D	12/93–4/94			3	
ERS-1 E	4/94–9/94			168	
ERS-1 F	9/94–3/95			168	
ERS-1 G	4/95–6/95			35	
TOPEX/POSEIDON	8/92–12/05	1354	66	10	NASA & CNES
ERS-2	4/95–6/03	785	98.5	35	ESA
GFO	5/98–present	800	108	17	US Navy
ENVISAT	3/02–present	785	98.5	35	ESA
JASON-1	11/01–present	1354	66	10	CNES & NASA
Cryosat*	2005	720	92	369 30 sub-cycle	ESA
JASON-2	2008	1354	66	10	NOAA, NASA/ & CNES

Table 1.1: Altimeter missions. *CryoSat failed due to a launch failure on October 2005.

1.3 Acceleration of Sea Level Rise in the 1990s

Most studies show that the global sea level is rising (e.g., Douglas [2001]), so the current populated areas for humans are continuing to diminish. The other notable open question is whether global sea level rise is accelerating in the 1990s, which could make land areas disappear more quickly. Gregory et al. [2001] and Church et al. [2001] indicate an acceleration of sea-level rise during the 20th century and beyond in response to increasing concentrations of greenhouse gases through climate model projections. However, Douglas [1992] and Woodworth [1990] consider sea level records containing a considerable amount of interannual and decadal variability, and indicated no definite long-term acceleration of sea level has been identified using the 20th Century data alone. However, the other possible reason for not detecting sea level acceleration may be the sparseness of the tide-gauge network [Gregory et al., 2001].

The global sea level rise estimate in the 20th century has been reported at 1.8 mm/yr [Church et al., 2004; Douglas, 2001], which is consistent with the IPCC TAR estimate of 1.5±0.5 mm/yr for the 20th Century [Church et al., 2001]. In contrast to the 1.8 mm/yr sea level rise estimate derived from tide gauges, sea level trend estimate from satellite altimetry since 1993 has increased to 3.1±0.4 mm/yr [Cazenave and Nerem, 2004]. Although the sea level rise during the TOPEX/POSEIDON period or the last decade is observed to rise almost 50% faster than the average rate over the last Century, visual inspection and fitting a quadratic to the time series confirms there is no significant increase in the rate [Church et al., 2004].

Likewise, some researchers tried to examine if sea level is accelerating in the 1990s in terms of thermosteric sea level derived using *in situ* temperature data or ocean modeling [Willis et al., 2004; Carton et al., 2005]. Willis et al. [2004], Antonov et al. [2005] and Ishii et al. [2005] estimated the trends of thermosteric sea level during 1993–2003 using *in situ* temperature data. For example, Willis et al. [2004] combined temperature data with TOPEX/POSEIDON data and estimate the thermosteric sea level trends to be 1.6±0.3 mm/yr (integrating from 0–750 m depth), 1.23±0.2 mm/yr (0–700 m), and 1.8±0.2 mm/yr (0–500 m), respectively. For the time span of the past 5 decades (1955–2003), the estimated thermosteric sea level trend is ~0.4 mm/yr [Antonov et al., 2005], which is significantly (more than 4 times) lower than the 1993–2003 trend. The acceleration of sea level (thermosteric and total sea level) is being concluded [Carton et al., 2005; Hansen et al., 2005]. However, Willis et al. [2004] reported it is not possible to identify whether the recent increase in ocean warming is caused by an acceleration of heat uptake by the ocean or it is simply the decadal variability with the present time series since the warming rate in the early 1970s is comparable to the present rate.

In summary, recent studies reported similar (1.6–1.8 mm/yr) 20th century sea level rise [Shum et al. 2002b; Church et al. 2004; Kuo et al. 2005] as Douglas [2001], significantly different and controversial contributions of thermal expansion to the global sea level budget [Cabanes et al., 2001a; Miller and Douglas, 2004], and indicated that the global sea level observed by TOPEX/POSEIDON (T/P) altimetry [Cazenave and Nerem, 2004] and the thermal expansion [Willis et al., 2004] during the last decade are rising almost 50% faster than during the last century. In addition to the possibility that sea level rise (and thermal expansion) are accelerating during the last decade as implied by [Hansen et al., 2005] and a result of recent evidence on the Earth's energy imbalance (0.85±0.15 W/m^2 more absorption than emission of the Sun's energy), other potential causes of the discrepancy include (1) the mis-modeling of

longer term (>interannual) oceanic variability, (2) errors associated with the two primary instruments determining sea level (tide gauges and satellite altimetry), or all of the above. The tide gauge instrument errors are associated with inadequate knowledge to predict vertical motions due to glacial isostatic adjustment [Peltier, 2002] and tectonic motions at the global tide gauge sites, which directly affect sea level determination. This study attempts to address some of these problems.

1.4 Characterizations of Global Sea Level Rise

Global sea level rise can only be partially explained by a number of competing geophysical processes, each of which is a complex process within the Earth-atmosphere-ocean-cryosphere-hydrosphere system. The sea level variations measured by tide gauge data are results of a number of forcing factors, which include but are not limited to steric sea level, mass variations of ice sheets and mountain glaciers, ocean currents, atmospheric circulation, crustal vertical motions, and land water. Milly et al. [2003] showed that only 0.12 mm/yr equivalent mean sea level could be attributed to the land water contribution during 1981–1998 using dynamics (LaD) land surface model (LSM). Ngo-Duc et al. [2005] report a study using the ORCHIDEE model which estimates a small positive sea level trend of 0.08 mm/yr. Both models (Figure 1.1) display the similar interannual/decadal variability and a significant interannual signal except for 1993 when ORCHIDEE displays a downward trend not seen in the LaD simulation. During the period of 1975–1993, the ORCHIDEE simulation shows an increase of 0.32 mm/yr for the total land water contribution. This strong increase appears to reflect natural long-term (20–25 yr periodicities) variability rather than systematic changes in hydrological condition. For 50 years, the contribution of land water to sea level is close to 0 mm/yr. Additionally, the contribution of land water variations is a local phenomenon as compared with the effects of ice sheet melting like the Antarctic ice sheet mass balance. So far sea level studies have not include land water contributions to characterize global sea level [Plag and Jüttner, 2001; Plag, 2005]. There is also a potentially significant anthropogenic effect of human-impundment of water in reservoirs contributing to sea level rise or fall [Chao et al., 1994; Sahagian et al., 1994]. Additionally, other effects including permafrost melting [Zhang et al., 2005] could potentially contribute to global sea level rise.

Among the forcing mechanisms of sea level variations, the dominant effects are the melting of the continental ice sheets and mountain glaciers, and the steric (thermosteric and halosteric) effects of the ocean [Pattulo et al., 1955]. In addition, when tide gauge records are used to determine sea level, the knowledge of crustal vertical motions at the tide gauge benchmarks must be known or modeled. These effects, the vertical motion, steric sea level, and ice melting are discussed as follows.

I. Vertical Motion

Current observations used for environmental monitoring and coastal forecasting systems are primarily from tide gauges, which are measurements of the sea surface heights relative to a fixed point on the adjacent land. For that reason, the vertical crustal motions due to local subsidence, tectonic uplift, and primarily PGR, which is the physical phenomenon due to the cycles of glaciation and deglaciation since the last Ice Age, could contaminate the sea level

measurements from tide gauge stations. Currently, no global model or observations due to tectonic motions are available while co-seismic motions (instantaneous offsets due to earthquakes) are supposedly removed from the gauge records. Therefore, at present, the best one could do is to assume that vertical motion is caused only by GIA and adopt a GIA model for vertical motion corrections to determine sea level trends using global tide gauge data.

For the past 900,000 years, physical process due to the cycle of glaciation and deglaciation has a characteristic duration of about 100,000 years, the Milankovitch Cycles. During the cycle of the glaciation phase, ice sheets covered some regions of the northern hemisphere (Canada and Northwestern Europe) up to approximately 4 km thickness. Beginning at the Last Glacial Maximum (LGM) about 21,000 years ago, the ice sheets began to melt. Since the mass of ice sheets is reduced, the crust is uplifting in the ancient ice covered regions while crust is sinking in the other regions not covered by ice sheets, due primarily to the viscous relaxation of the mantle. Since the cycle of the deglaciation phase about 6,000 years ago, the crustal motion persists, which may surpass 1 cm per year (in the southeast Hudson Bay region of Canada) [Peltier, 1998]. This phenomenon is called GIA or PGR. The signal is significant for estimating global sea level rise and is non-negligible. Global GIA models have been developed including the ICE-3G [Tushingham and Peltier, 1991], ICE-4G (VM2) [Peltier, 1998], and the BIFROST model based on constraints from GPS estimates of crustal motions [Milne et al., 2001] with 12 sets of the Earth parameters, lithospheric thickness (LT), upper mantle viscosity (UMV), and lower mantle viscosity (LMV) (hereafter the BIFROST model). The BIFROST model adopted in this study (courtesy, J. Mitrovica and G. Milne) used the following parameters. LT is 70 or 120 km. UMV is 0.5×10^{21} Pas or 1×10^{21} Pas. LMV is 1×10^{21} Pas, 3×10^{21} Pas or 10×10^{21} Pas. Figure 1.2 shows two GIA models used in this study and their differences. The upper panel of Figure 1.2 is ICE4G (VM2), hereafter the ICE4G model, and the middle panel is the BIFROST model with the Earth parameters, LT=120km, LMV=1×10^{21} Pas, and UMV=3×10^{21} Pas. It should be noted that the negative values in this plot indicate crustal uplift. The relatively large uplift appears in the North America, Fennoscandia, and Antarctica in both models, which were covered by large ice sheets during the cycle of the glaciation phase. The significant difference between both models exists due presumably to different data processing, ice loading history, Earth parameters, and sea level modeling theory. Lower panel of Figure 1.2 shows the differences of the two models, the mean of which is equal to 0.13 mm/yr with a standard deviation of 0.63 mm/yr.

In addition to the use of GIA models, other studies attempt to determine vertical motions using geodetic measurements. The absolute vertical motion, which is relative to the center of the Earth, can be determined by means of absolute gravimeters [Pagiatakis et al., 2003], GPS [Johansson et al., 2002; Caccamise et al, 2005], satellite laser ranging, DORIS radiometric tracking system, and combining tide gauge and altimetry data [Cazenave et al., 1999; Lin, 2000]. Attempts to determine absolute crustal vertical motions by combining altimeter measured absolute sea level changes and tide gauge records of relative sea level changes indicated the uncertainties in excess of 2 mm/yr [Cazenave et al., 1999; Lin, 2000]. A more recent comprehensive study using the differences between 114 tide gauge rates and TOPEX/POSEIDON altimetry estimated rates with accuracies of 1-2 mm/yr for absolute

crustal vertical rates at about half of the tide gauge sites [Nerem and Mitchum, 2002]. Kuo et al. [2004b] and Shum at al. [2002] developed a technique, which uses historic tide gauge records (>50 years) and T/P altimeter data (10 years) by the stochastic adjustment within a semi-enclosed sea to improve the vertical motion estimates.

However, GIA models or estimated secular trends of vertical motions coming from phenomena such as tectonic uplift could not explain fully vertical motions. Vertical motions may contain a non-linear trend due to a postseismic deformation [Larsen et al., 2003] such as in Alaska. Larsen et al. [2003] reported analyzing various types of deformations which cause vertical motion is necessary to improve the accuracy of the estimates.

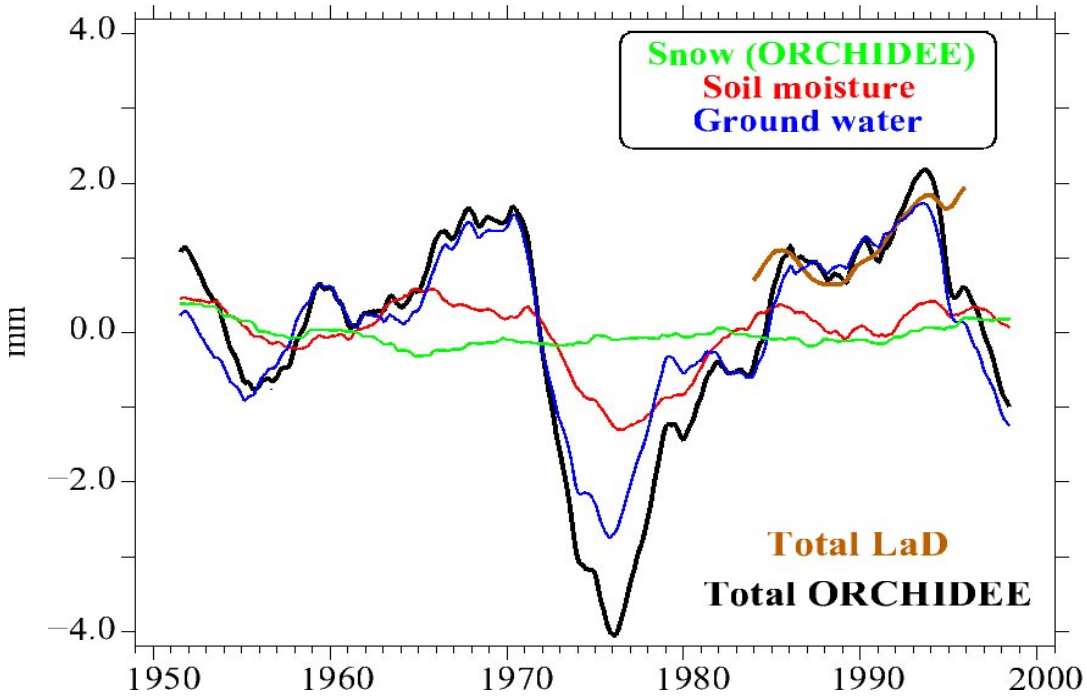

Figure 1.1: Five year moving average time series of water reservoirs changes expressed as equivalent global sea level anomalies for the past 50 years. Red curve: soil moisture; green curve: snow pack; blue curve: groundwater; black curve: sum of the above components, which represents the land water storage variations simulated by the ORCHIDEE model. Brown curve: land water storage variations simulated by the LaD model. Figure courtesy of Ngo-Duc et al. [2005].

II. Steric (Thermosteric and Halosteric) Sea Level

Steric sea level changes (thermosteric and halosteric) result from the density variations of sea water, which are induced by temperature and salinity variations [Pattullo et al., 1955]. The dominant effect is the thermosteric anomalies, which are about 10 times greater than halosteric anomalies. For global averages, the rate of halosteric sea level changes is an order of magnitude smaller than the thermosteric component but with the same sign, 0.05 mm/yr [Antonov et al., 2002]. Since there is no reliable salinity data in the worldwide ocean, halosteric sea level anomaly is not easy to be separated from thermosteric or mass variations.

Additionally, it is relatively small, so most studies ignore the halosteric sea level anomaly [Cabanes et al., 2001a; Chen et al., 2000].

Chen at al., [2000] indicated that the thermosteric effect accounts for much of the observed seasonal variability of sea level change, especially when averaging over zonal regions using combination of WOA94 [Levitus and Boyer, 1994] and Optimum Interpolation Sea Surface Temperature (OISST) data [Reynolds and Smith, 1994]. Cabanes et al. [2001a] shows the thermosteric sea level variation integrated from 0 to 500 m has been determined at 3.1±0.4 mm/yr (1992–1998), agreeing with the sea level rise (3.2±0.2 mm/yr) derived from TOPEX only (1992–1998) and concluded that thermosteric sea level of the upper ocean (0–500 m) predominately accounted for TOPEX/POSEIDON observed sea level rise. However, Shum et al. [2001a] show a comparison between the sea level trend from 16-year altimetry data and 0–3000 m thermosteric trend and indicate that the thermosteric trend is only about 30% of the observed sea level trend from 16-year altimetry. Miller and Douglas [2004 and 2005] also reported a disagreement of the conclusions reported by Cabanes et al. [2001a]. They present an analysis of tide gauge records and hydrographic (*in situ* temperature and salinity) observations in the Pacific and Atlantic Oceans showing that gauge-measured sea level rates, which reflect both mass and volume changes, are 2–3 times higher than hydrographic based rates, which only reflect volume changes. In addition, Willis et al. [2004], Antonov et al. [2005], and Ishii et al. [2005] reported that the rapid thermosteric sea level trends range from 1.2 to 1.8 mm/yr in the 1990s, which is not large enough to cover the sea level rise signal observed by TOPEX/POSEIDON.

As it is known that grid temperature data are organized from *in situ* temperature profiles that lack in the southern hemisphere, so the grid temperature data have relatively larger errors in this region [Lombard et al., 2005; Miller et al., 2004]. Recently, NASA/DLR's Gravity Recovery and Climate Experiment (GRACE) mission, utilizing a new technique, has been successfully providing monthly observations of the Earth's gravity field since the satellites were launched in 2002 [Tapley et al., 2004a]. These observations are represented in spherical harmonic coefficients complete to degree 120 (~167 km wavelength) and spherical harmonic coefficients are going to provide us the results on land water storage [Wahr et al., 2004] and ocean mass variations [Chambers et al., 2004]. Chambers et al. [2004] and Kuo et al. [2004a] indicated global ocean mass variations derived by spherical harmonic coefficients from GRACE agree well with the steric-corrected sea level from TOPEX/POSEIDON data. However, Kuo et al. [2004a] pointed out steric-corrected sea level from altimeter data is not consistent with mass variations from the GRACE solution in the southern ocean. Nevertheless, combination of altimetry and GRACE data has the potential to provide a new approach to improve the steric sea level variations in the southern hemisphere while altimeter data measure sea level changes and GRACE provides ocean mass variations.

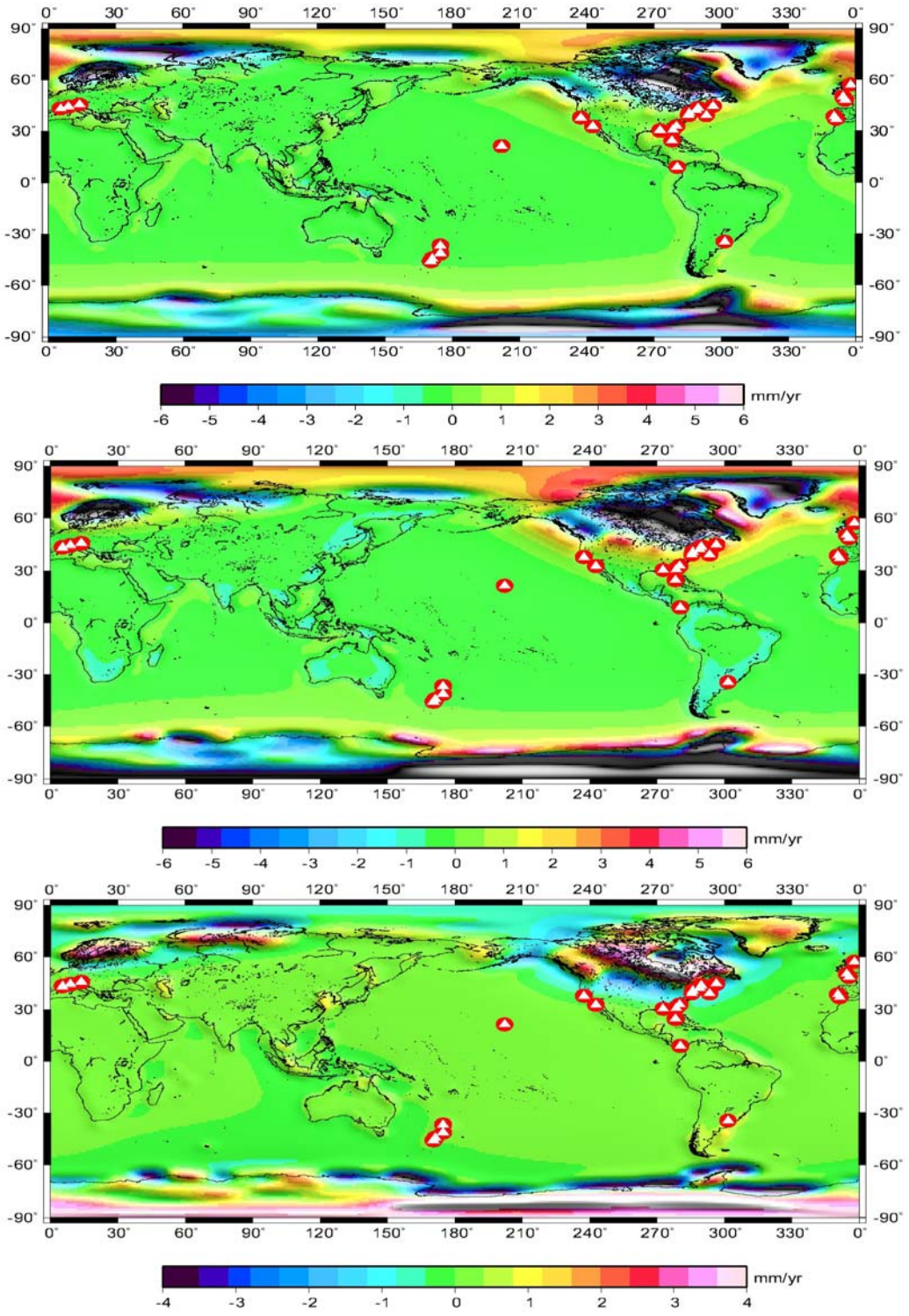

Figure 1.2: GIA models. Top: ICE4G (VM2). Middle: BIFROST. Bottom: Difference between ICE4G and BIFROSAT models. Red circles with white triangles are the locations of 27 long-term (>70 years) tide gauges [Douglas, 2001]

III. Sea Level Changes from Ice Sheet and Glacier Melting

On geological time scales (100,000 years), fluctuation of ice sheets in the northern and southern hemispheres has dominant variations in the global sea level. Beginning from the last Ice Age 21,000 years ago, global sea level has risen about 125 m as a result of the retreat of the great glacial ice sheets. This rise in sea level is presumably initiated by the shrinking of the marine Antarctic ice sheet, adding perhaps another 30 m to the global sea level [Nakada and Lambeck, 1988]. The ice sheet retreat appears to have been completed 6000 years ago. Since then, sea level appears to have been stable, rising by about 10 cm until the last Century [Varekamp et al., 1992]. The rate of the sea level rise appears to have accelerated, with a rise of approximately 15 cm over the past 100 years since the industrial revolution [Gornitz et al., 1982]. It is speculated that this rise of sea level and apparent acceleration is attributable to human activities, which resulted in a greenhouse effect, causing global climate change [e.g., Warrick et al., 1996; Church et al., 2001]. Recently, a number of studies have addressed global climate change and recent warming of the ocean [Levitus et al., 2000, 2001, 2005; Barnett et al., 2001].

The last IPCC study [Church et al., 2001] attributed the estimated contributions of continental ice sheet and glacier melts (Antarctica, Greenland, and mountain glaciers) to sea level during the 20^{th} Century at 0.0–0.4 mm/yr, which is in good agreement with geophysical constrain studies using observed gravity changes, i.e., secular variations of zonal harmonics up to degree 8 (Greenland's contribution is estimated at 0.5±0.5 mm/yr and Antarctica's contribution is at 0.12±0.10 mm/yr, with a total contribution of 0.6±0.5 mm/yr) [Trupin and Shum, 2001b]. Altimeter measurements of ice sheet elevation changes in Antarctica and Greenland provide a modern measurement in time series from 1991 and are to be continued when ICESAT, the laser altimeter mission, started its operation in 2002.

The current ice loading history largely assumes uniform spatial melting of ice sheets. The modern observations of ice sheet thickness changes (approximate from ice elevation changes) are using radar altimeters [e.g., Zwally et al., 1989; Wingham et al., 1998], airborne laser altimetry [Krabill et al., 2000], and the NASA ICESAT laser altimeter mission. These could provide a data source of non-uniform melting of ice sheets [Trupin and Shum, 2001b] and could potentially benefit the GIA modeling and thus the contribution of ice mass balance to sea level. The ice elevation data will be used as elevation change data and also as a data source for present-day ice loading history for Antarctica and Greenland. The approach [Trupin and Shum, 2001b] then could be used to accept data sources of non-uniform spatial melting of ice sheets to study the mass balance constrain to sea level (mass variations).

Any redistribution of surface mass, such as ice sheets, mountain glaciers, ocean mass, and hydrology, could deform the solid Earth and change the Earth's gravity fields, which can bring about the redistribution of oceanic mass and affect local sea level changes. Woodward [1888] demonstrated that the melting of an ice mass on a rigid Earth would lead to a highly non-uniform redistribution of sea level as a consequence of self gravitation in the surface load. Conrad and Hager [1997] are the first to extensively describe the geophysical basis of the phenomena. Plag and Jüttner [2001] and Plag [2005] determined the patterns of sea-level redistributions associated with present-day mass variations in the Antarctic and Greenland ice

complexes for a constant unit trend over the complete area of the ice sheet by solving the static sea level equation [Farrell and Clark, 1976]. Mitrovica et al. [2001] and Tamisiea et al. [2001] calculated the geographical patterns of sea level redistributions associated with present-day mass variations in the Antarctic and Greenland ice sheets as well as melting from a suite of smaller land-based ice sheets and glaciers tabulated by Meier [1984] based on an improved sea level theory [Milne et al., 1999] that extends previous work [Farrell and Clark, 1976] to include a varying geometry of shoreline and the influence of load-induced perturbations in the Earth's rotation vector. Figure 1.3 illustrates the predicted geometries of sea level changes due to continuing ice mass variations [Mitrovica et al., 2001] in the Antarctica and Greenland ice sheets, and of the mounting glaciers tabulated by Meier [1984]. For the sake of the convenience of the later discussion, the geographical patterns of sea level variations are normalized, which is to assume that a melting event in the ice source contributes 1 mm/yr of the global sea level rise corresponding to mass changes. Figure 1.3 shows that the effect of the Antarctic ice sheet melting generates a distinct zonal component of the geoid change, while the geometry due to ice sheet melting in Greenland illustrates more variations along the longitude in the northern hemisphere.

A flaw in determining global sea level variations using tide gauge data can be that the gauge stations are far from being adequately or evenly distributed. In order to mitigate this problem which is first pointed out by studies including Conrad and Hager [1997], Plag and Jüttner [2001], Mitrovica et al. [2001], Tamisiea et al. [2001], Blewitt et al. [2005], and Plag [2005], tide gauge data as observations can be used to estimated the amplitudes of the various forcing sources assuming that the geometries of sea level trend are known. The approach successfully estimated the amplitude of geometries due to forcing factors and interpolated sea level trends between gauges. Global sea level trend is estimated by Mitrovica et al. [2001] and Tamisiea et al. [2001] at 1.6–2.0 mm/yr, while the estimates by Blewitt et al. [2005] and Plag [2005] ranges from 0.70 to 0.95 mm/yr.

1.5 Summary

The dissertation will focus on the determination and the characterizations of global sea level rise using altimeter data, tide gauge records, and the assumed known geometries of sea level trends due to melting of three ice sources (Antarctica, Greenland, and mountain glaciers), GIA deformation patterns, and steric sea level data. Furthermore, vertical motions and steric sea level variations are analyzed in detail.

Chapter 2 focuses on the computation of vertical motions around tide gauge by combining satellite altimeter data and tide gauge records. The adjustment approach is introduced to compute absolute vertical motions by taking advantage of historical tide gauge records and accurate altimeter data, applicable to semi-enclosed ocean basins as well as open ocean where long-term tide gauges exist. Algorithm to account for nonlinear vertical motion due to co-seismic or itner-seismic deformation is presented and applied to regions near Alaska.

Chapter 3 describes the estimates of the steric (thermostric and halosteric) sea level trend using *in situ* temperature and salinity data or grid temperature data in the form of time series.

The steric (or thermosteric) sea level trend and sea level trend derived from altimetry and tide gauges are analyzed.

Chapter 4 describes the use of the GRACE gravity mission data, which measure oceanic mass variations. An analysis of mass variations derived from GRACE and steric-corrected altimeter data is conducted to investigate whether GRACE can be used to improve the steric sea level trend estimate in the Southern Ocean.

Chapter 5 describes to the methodologies for the determination of global sea level rise using multiple altimetry data (GEOSAT, ERS-1, ERS-2, TOPEX/POSEIDON, GFO, JASON-1, and ENIVSAT) and long-term tide gauge records. Sea level trends derived from altimeter and tide gauges are analyzed.

Chapter 6 describes the calibration of high-latitude observing ERS-1 and ERS-2 altimetry using TOPEX/POSEIDON for Arctic and Sub-Arctic sea level trend determination. Long-term sea level trend estimates using tide gauges are discussed.

The primary focus of Chapter 7 is to address the question on whether sea level trends derived from the 20th Century tide gauge data and thermosteric sea level are accelerating using statistical analysis including hypothesis testing. An analysis of the minimum data span required to obtain a stable sea level trend is conducted using tide gauges and thermosteric sea level data.

Chapter 8 provides an error budget to quantify the 20th Century sea level rise by an adjustment approach using altimeter and tide gauge data assuming the geographical patterns of sea level trend resulting from three ice sheet sources, thermosteric sea level, and GIA deformation are known. The characterization will provide a quantification of signals associated with specific geophysical processes to enhance the ability for prediction of sea level rise in the 21st century.

Chapter 9 presents the conclusions and future work.

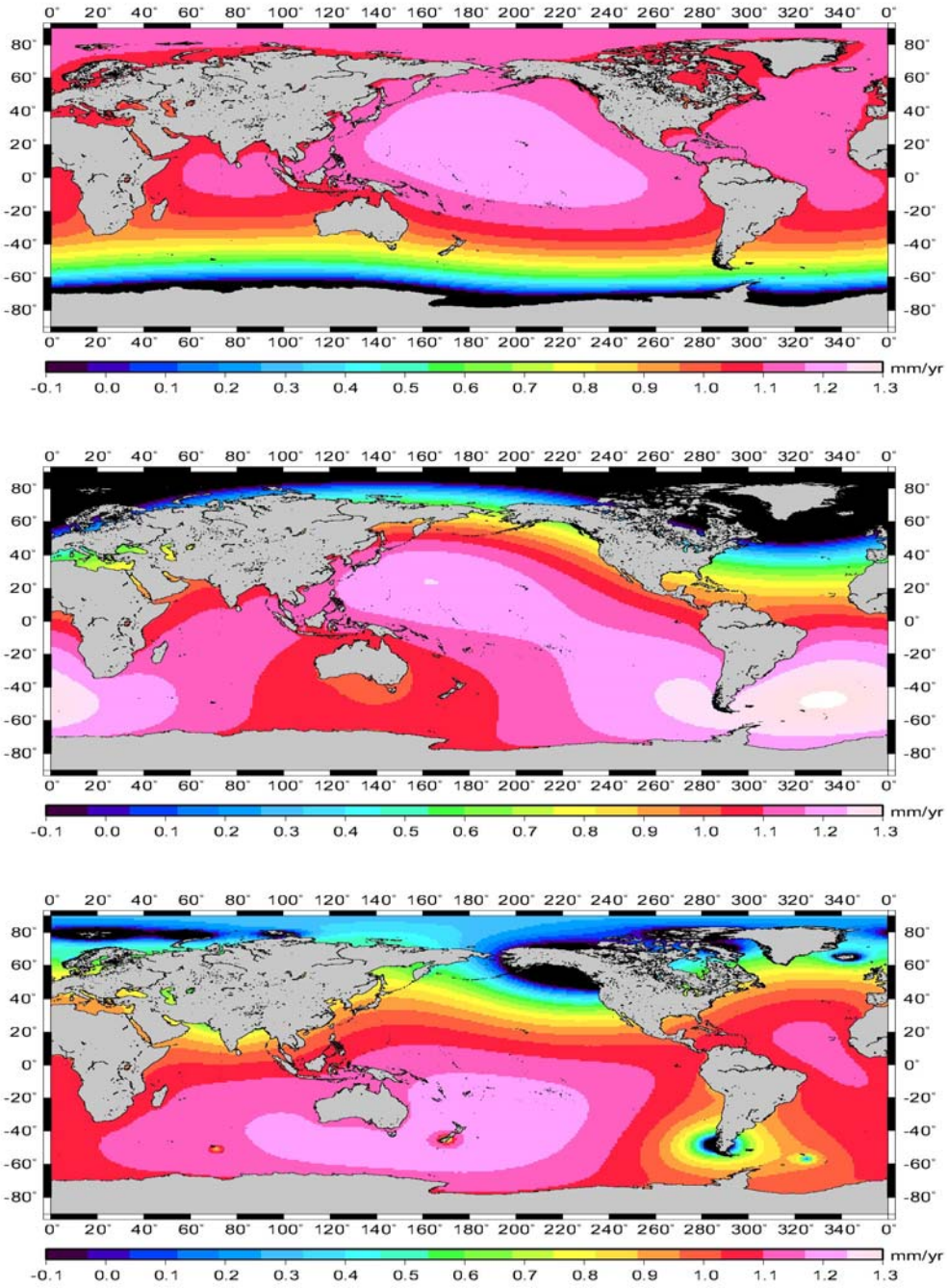

Figure 1.3: Predicted geometries of sea level trends due to continuing ice mass variations. Normalized global sea level variations computed for the case of ice melt from Antarctica (Top), Greenland (Middle) and the melting of the mountain glaciers tabulated by Meier [1984] (Bottom).

CHAPTER 2

VERTICAL MOTIONS DETERMINED BY COMBINING SATELLITE ALTIMETRY AND TIDE GAUGES

Tide gauges are mostly located along the coasts or near islands, and the records have been used to derive relative sea level change. Relative sea level change is the variation in the position of the mean sea surface relative to the solid Earth, or a benchmark on the crust of the solid Earth referencing to the tide gauge instrument. In most parts of the world, the benchmark locations to which the tide gauges are referenced are subject to Earth deformation processes such as earthquakes and their deformation cycles, plate tectonics, basin evolution, Glacial Isostatic Adjustment (GIA) or postglacial rebound (PGR), and anthropogenic effects such as local subsidence due to water usage, mining, oil, or natural gas drilling. Therefore, the signals of tide gauge records could contain both sea level changes and vertical motions.

Deformation processes have different spatial-temporal scales and thus affect the observations of sea level using tide gauges. Deformation processes can be episodic or continuous. For example, the interseismic deformation before an earthquake depends on the tectonic setting and can have both elastic and viscous components. The coseismic offset of an earthquake is almost completely elastic and the deformation reaches equilibrium after a few weeks. The postseismic deformation is viscous relaxation. Viscoelastic processes like GIA persist for several thousand years or longer and contribute to continuous rather than episodic deformations. Plate tectonics, e.g., subduction of lithospheric plates, add another component to solid Earth deformation affecting tide gauge sea level measurements. Hence the different temporal scales require a thorough analysis of the impact of deformations (here, especially the vertical component) on the sea level measurements by tide gauge records. The relative vertical motion of the solid Earth's surface, which is relative to a chosen benchmark, can be determined by means of strandlines, historic sea level data [Larsen et al., 2003; Mäkinen and Saaranen, 1998], and precise leveling [Mäkinen and Saaranen, 1998]. On the other hand, the absolute vertical motion, which is relative to the center of Earth, can be determined by means of absolute gravimeters [Pagiatakis et al., 2003], GPS [Johansson et al., 2002; Caccamise et al, 2005], satellite laser ranging, DORIS Doppler tracking system, and the combination of tide gauge and altimetry data [Cazenave et al., 1999; Lin, 2000]. Except for the method of combining altimeter and tide gauge data, the disadvantage of all other techniques is that they are time consuming, expensive, and labor intensive.

Attempts to determine absolute vertical crustal motions by combining altimeter measured absolute sea level changes and tide gauge records of relative sea level changes indicated uncertainties in excess of 2 mm/yr [Cazenave et al., 1999; Lin, 2000]. A more recent comprehensive study using the differences between 114 tide gauge and TOPEX/POSEIDON altimetry observed sea level over almost 1 decade to estimate absolute vertical crustal rates with accuracies of 1–2 mm/yr for about half of the tide gauge sites [Nerem and Mitchum, 2002]. Kuo et al. [2004b] and Shum et al. [2002a] developed a technique, which uses historic tide gauge records (>50 years) and one decade of T/P altimeter data in a stochastic adjustment withiin a

semi-enclosed sea to improve the vertical motion estimates. In this chapter, we describe in detail the vertical motion adjustment algorithms, including an extension of the algorithm to apply to open ocean regions such as Alaska. Vertical motion solutions are conducted and analyzed in the Great Lakes and near Alaska. The ability to improve vertical motion near the vicinity of long term tide gauges will improve the accuracy of relative sea level trend estimates.

2.1 Data Analysis

In this study, TOPEX/POSEIDON (T/P) data, available from the NASA/JPL Physical Oceanography Distributed Active Archive Center (PO.DAAC) in the Generation B Merged TOPEX/POSEIDON Geophysical Data Record (MGDR-B) format, are processed for the efficient access of global sea level data, into the so-called Ohio State University (OSU) stackfiles [Yi, 2000]. The instrument correction, media correction (unsmoothed dual-frequency ionosphere, TOPEX/POSEIDON Microwave Radiometer or TMR wet troposphere correction, and dry troposphere correction), geophysical corrections (solid Earth and ocean tide, pole tide, the BM4 sea state bias or SSB model augmented by a SSB correction model [Chambers et al., 2003]), Wallops drift correction for the TOPEX range, and correction for TMR drift [V. Zlotnicki, personal communication] are applied. Inverted barometer corrections are not applied to either the TOPEX/POSEIDON data or tide gauges. The ocean tide corrections are not applied to the TOPEX/POSEIDON data in the Great Lakes analysis because tide in Great Lakes is unknown and relatively small. In this study, 1-Hz TOPEX Side A (TSA) and TSB data of the TOPEX/POSEIDON mission from cycle 4 to cycle 365 are used before the TOPEX/POSEIDON orbit was changed to the interleave orbit.

In the Baltic Sea region, monthly averaged Revised Local Reference (RLR) tide gauge data for 25 stations around the Baltic Sea (Figure 2.1) from Proudman Oceanographic Laboratory's (POL's) Permanent Service for Mean Sea Level (PSMSL) are used in the study. This analysis used data records which ended in 2001. The record with the longest time span is from 1811 to 1999. All records used exceed 40 years. The RLR is defined to be approximately 7000 mm below mean sea level at each station.

For the Great Lakes region, daily water level gauge data of 29 stations in the USA published by the Center for Operational Oceanographic Products and Services (CO-OPS) and 22 stations in Canada from the Marine Environmental Data Service (MEDS) are used. These data are dynamic heights with respect to the International Great Lakes Datum 85 (IGLD 85) (Figure 2.2, circles denote water level gauge locations). In order to compare with TOPEX/POSEIDON data, dynamic heights are converted to Helmert orthometric heights [Heiskanen and Moritz, 1987]. Nevertheless, the difference between the dynamic heights and the orthometric heights is approximately a bias [Cheng, 2001]. For instance, the trend of the difference is smaller than 0.05 mm/yr at Holland West water level gauge in Lake Michigan and does not affect the determination of absolute vertical motions. Therefore, a datum transformation is not applied.

For the Alaska region, monthly averaged RLR tide gauge data of 15 stations around South Alaska from PSMSL are used in the study (denoted by circles and triangles in Figure 2.5 for their locations). The latest record in this analysis ended in 2002. The record with the longest

time span is from 1909 to 2002. All records used exceed 30 years except for SAND POINT and KODIAK.

2.2 Vertical Motion Adjustment: Algorithms and Results

2.2.1 Algorithm for Semi-enclosed Basins

The relationship between the rates of relative sea level change and absolute (or geocentric) vertical motion is straightforward. If we denote the former by $\dot{S}(\lambda,\varphi)$, and the latter by $\dot{u}(\lambda,\varphi)$, where φ is the co-latitude and λ is the longitude, we can simply write:

$$\dot{S}(\lambda,\varphi) = \dot{g}(\lambda,\varphi) - \dot{u}(\lambda,\varphi), \tag{2.1}$$

where $\dot{g}(\lambda,\varphi)$ is the rate of absolute sea level change, and the superscript $\bullet$ denotes time differentiation. We emphasize that the quantities $\dot{u}(\lambda,\varphi)$ and $\dot{g}(\lambda,\varphi)$ are measured relative to the Earth's center of mass. Altimetry data provide the rates of absolute sea level changes, while tide gauge records yield estimates of relative sea level changes. It should be noted that there is an inherent assumption that the drifts associated with both instruments (tide gauge and altimeter), which are inseparable from the signal, $\dot{u}(\lambda,\varphi)$, are small and negligible. Hence, for simplicity, an error term corresponding to combined drifts of both instruments is ignored. Accordingly, an estimated rate of vertical motion follows through the simple rearrangement of (1):

$$\dot{u}(\lambda,\varphi) = \dot{g}(\lambda,\varphi) - \dot{S}(\lambda,\varphi). \tag{2.2}$$

Because of the discrepancies of the spatial (only a few ground tracks close to the tide gauge station, e.g., within a 3° spatial averaging region) and temporal sampling, (monthly tide gauge data versus 9.99 day repeat track patterns for TOPEX/POSEIDON) and in order to reduce random noise in the data, the geocentric sea level change is determined by spatial (over the Baltic Sea) and temporal (monthly) averaging of TOPEX/POSEIDON data. This yields an averaged absolute or geocentric sea level trend in the Baltic Sea. Using Equation (2.2) and a least squares procedure, the averaged absolute vertical motion is determined by fitting the difference of both time series. In practice, residual seasonal and selected tidal periodicities as well as possible data gaps in tide gauge records are removed or accommodated by estimating appropriate parameters in a least squares adjustment computation. So far, this approach is similar to other contemporary studies [Lin, 2000; Nerem and Mitchum, 2002], and it is noted that only tide gauge data during the altimetry time span can be used, whereas historic data from tide gauges, even if available, cannot be considered in the present form of the algorithm.

To improve the algorithm, we introduce the following equation to compute relative vertical motion between two adjacent tide gauges using Equation (2.2):

$$\begin{aligned} r\dot{u}_{ij} &= \dot{u}_i(\lambda_i,\varphi_i) - \dot{u}_j(\lambda_j,\varphi_j) \\ &= \dot{g}_i(\lambda_i,\varphi_i) - \dot{S}_i(\lambda_i,\varphi_i) - \dot{g}_j(\lambda_j,\varphi_j) + \dot{S}_j(\lambda_j,\varphi_j) \end{aligned}, \tag{2.3}$$

where i and j are indices of tide gauge stations. In this study, we assume that $\dot{g}_i(\lambda_i, \varphi_i)$ and $\dot{g}_j(\lambda_j, \varphi_j)$ are identical, i.e., the absolute or geocentric sea level variations at both tide gauges are the same and thus can be eliminated in Equation (2.3). In this study, the two tide gauges which are used to compute the relative vertical motion (Equation 2.3) are subject to the criterion that the correlation coefficient between both relative sea level measurements should be > 0.6. In practice, we find that all 25 tide gauges in the Baltic Sea region fulfill the above criterion and that 85% have correlation coefficients >0.8.

The adjustment algorithm to obtain the best estimate of absolute vertical motion of the tide gauges in the network can be considered as a straightforward extension of the Gauss-Markov (GM) model with stochastic constraints written in a partitioned form [e.g., Koch, 1999]:

$$\begin{bmatrix} y_1 \\ z_0 \end{bmatrix}_{(n+l)\times 1} = \begin{bmatrix} A_1 \\ K \end{bmatrix}_{(n+l)\times m} \xi \; + \; \begin{bmatrix} e_1 \\ e_0 \end{bmatrix},$$
$$with \quad \begin{bmatrix} e_1 \\ e_0 \end{bmatrix} \sim \left(\begin{bmatrix} 0 \\ 0 \end{bmatrix}, \sigma_0^2 P^{-1} = \Sigma \right) \quad and \quad rank \begin{bmatrix} A_1 \\ K \end{bmatrix} = m, \tag{2.4}$$

where m is the size of the state vector, ξ; l is the number of constraint equations or the so-called pseudo-observations, z_0; n is the dimension of observation vector, y_1; A_1 is the observation-state relationship or the design matrix; e_1 and e_0 are random error vectors; K is the design matrix for the constraint equation; σ_0^2 is the unknown a priori variance associated with a weight matrix, P, and Σ is a variance-covariance matrix. Equation (2.4) can be written as:

$$y = A\xi + e \quad with \quad e \sim (0, \sigma_0^2 P^{-1} = \Sigma). \tag{2.5}$$

The solution of Equation (2.5) using the Best Linear Unbiased Estimation has the following form:

$$\hat{\xi} = (A^T PA)^{-1}(A^T Py), \tag{2.6}$$

$$\hat{D}\{\hat{\xi}\} = \hat{\sigma}_0^2 (A^T PA)^{-1},$$
$$with \quad \hat{\sigma}_0^2 = (y^T Py - A^T Py\hat{\xi}) / (n - m + l), \tag{2.7}$$

where $D\{\hat{\xi}\}$ is the dispersion matrix of the estimate, $\hat{\xi}$. The rates of the absolute vertical motions at 25 tide gauges around the Baltic Sea can then be estimated using tide gauge data (>40 years) as relative vertical motion observations between each pair of gauges (Equation 2.3) and using averaged TOPEX/POSEIDON altimeter and tide gauge data (1992–2001) over the entire Baltic Sea as the geocentric vertical motion constraint (Equation 2.2).

2.2.2 Vertical Motions in Fennoscandia

Absolute or geocentric vertical motion for each of the 25 Baltic Sea tide gauges are first estimated using Equation (2.2), or the technique similar to the one used by Nerem and Mitchum [2002]. The differences of the time series between each tide gauge record and averaged TOPEX/POSEIDON data (1992–2001) within 3° of the gauge locations are fitted in a least squares procedure solving for the vertical motion and parameters associated with annual and semi-annual periodicities. Table 2.1 shows the vertical motion solutions of the 25 tide gauges (Column 5), with the associated formal uncertainties and the correlation coefficients between the individual tide gauge and altimeter observed sea level. The correlation coefficients are between 0.87 and 0.98, indicating excellent agreement in observed relative sea level change by both instruments. The uncertainties are 1.5–8.3 mm/yr, with an average of 4.6 mm/yr, consistent with the results obtained by Nerem and Mitchum [2002]. It should be noted that the uncertainty increases when the correlation coefficient decreases. The averaged absolute vertical motion observation computed over the Baltic Sea region using TOPEX/POSEIDON and tide gauge data (1992–2001) is 6.7 ± 1.4 mm/yr, which will then be used as the constraint (z_0 in Equation 2.4) in the improved algorithm.

We next use the GM model with stochastic constraints (Equation 2.5) to solve for the absolute vertical motions at the Baltic Sea tide gauge locations. Let $\Sigma = \begin{bmatrix} \Sigma_0 & \Sigma_2 \\ \Sigma_2 & \Sigma_1 \end{bmatrix}$, a priori variance-covariance matrix Σ_1 is set equal to σ_{v1}^2, where σ_{v1} is the standard deviation of the averaged absolute vertical motion, which equals 1.4 mm/yr, and z_0 = 6.7 mm/yr. The diagonal elements of the Σ_0 matrix is set equal to $\sigma_{v2}^2 + \sigma_{v3}^2$, where σ_{v2} is the standard deviation of the computed relative vertical motion between each pair of the 25 tide gauges (Equation 2.3) and σ_{v3} is the assume priori error in the computed relative vertical motion and is set equal to 0.5 mm/yr. The choice of σ_{v3} is directly related to the uncertainty of sea level determination using tide gauges, e.g., Douglas [2001] reported global sea rising at 1.8 mm/yr with an uncertainty of 0.4 mm/yr. Here, we adopt σ_{v3} = 0.5 mm/yr. It is noted that any choice of σ_{v3} from 0.3–0.6 mm/yr produces negligible change in the vertical motion solutions. The off-diagonal elements of the Σ_0 matrix is set equal to $\sqrt{(\sigma_{v2,ij}^2 + \sigma_{v3}^2)(\sigma_{v2,jk}^2 + \sigma_{v3}^2)} \times 0.3$, which means the correlation coefficient of the computed relative vertical motions is 0.3 when two relative vertical motions are computed using the same tide gauge stations. Σ_2 matrix is set equal to $\sqrt{\sigma_{v1,i}^2 (\sigma_{v2,ij}^2 + \sigma_{v3}^2)} \times 0.1$, indicating that the correlation coefficient of the computed relative and absolute vertical motions is 0.1 when the relative and absolute vertical motions are computed using the same tide gauge station.

We first apply the adjustment algorithm using data (altimetry and tide gauges) only during 1992–2001. The vertical motion solutions and the associated uncertainties (Equation 2.6 and 2.7) are shown in Table 2.1 (Column 6). The uncertainty of the solutions as a result of the adjustment has been reduced significantly from an average error of 4.6 mm/yr to 1.1 mm/yr,

compared with the results (Column 5, Table 2.1) of the earlier approach [e.g., Lin, 2000; Nerem and Mitchum, 2002]. The vertical motion solutions also changed drastically, up to 10 mm/yr.

Finally, we applied the new method using tide gauge (monthly sampled sea level) data over 40 years (~1950–2001) and TOPEX/POSEIDON geocentric sea level data (1992–2001) to solve for the absolute vertical motions. The final vertical motion solution has a range of 1–12 mm/yr, with an average uncertainty estimated at 0.5 mm/yr (1σ, Column 7, Table 2.1).

Figure 2.1 shows the estimated vertical motion rates (circles) at the 25 tide gauge stations around the Baltic Sea and a comparison with the GPS observed rates (triangles) from 10 collocated sites of the BIFROST project [Johansson et al., 2002]. Nominal TOPEX/POSEIDON ground tracks are shown on the background of altimeter averaged sea level trend (mm/yr, 1992–2001) in the Baltic and adjacent seas. Our estimates of vertical motions, when compared with 10 independently determined GPS rates, have a difference of 0.2 ± 0.9 mm/yr, indicating excellent agreement (Fig. 2.2). The differences are probably caused by instrument errors (tide gauge, altimetry, and GPS), and because the tide gauges and BIFROST GPS stations are not necessarily collocated. The small mean differences provide a validation of both techniques (GPS and this study) and places bounds on the instrument stability.

Vertical crustal motion in Fennoscandia is dominated by GIA [Milne et al., 2001]. It is known that the deglaciation of the Fennoscandian ice sheet from the last glacial maximum (LGM, about 21 kyrs BP) to about 9 kyrs BP, and the ocean load associated with the global deglaciation phase, are reflected in ongoing vertical motion which peaks at ~11 mm/yr in the Gulf of Bothnia and trends toward zero at the periphery of the former ice sheet. This pattern is clearly reflected in the geographic variations of the estimated vertical motions and evident in Figure 2.1.

The dominance of GIA in the region has made it possible to constrain models of the GIA process through comparison of observations with forward predictions. As an example, Milne et al. [2001] have derived bounds on various Earth model parameters on the basis of a comparison of numerical predictions of GIA with BIFROST GPS estimates of 3-D crustal motions. One model which fits within these constraints is characterized by a lithospheric thickness of 120 km, an upper mantle viscosity of 5×10^{20} Pa s, and a lower mantle viscosity of 5×10^{21} Pa s, where the boundary between the latter two regions is at 670 km in depth. We have computed vertical motions using this Earth model, together with the ice history adopted by Milne et al. [2001] and compared these predictions with the 25 estimates of vertical motion obtained in this study (Table 2.2). The mean of difference is 1.4 mm/yr. In contrast, the mean of difference comparing the ICE4G combination of ice history and Earth model [Peltier, 2002] and the vertical motion solutions is 3.4 mm/yr. These values indicate that the residual between model predictions and our estimates of vertical motion are larger than the differences between the two sets of observations (this study and GPS rates, Figure 2.1). Further, the sensitivity of the difference to changes in the numerical model of GIA suggests that the technique described herein has the potential to contribute constraints on such models (whether in Fennoscandia or elsewhere).

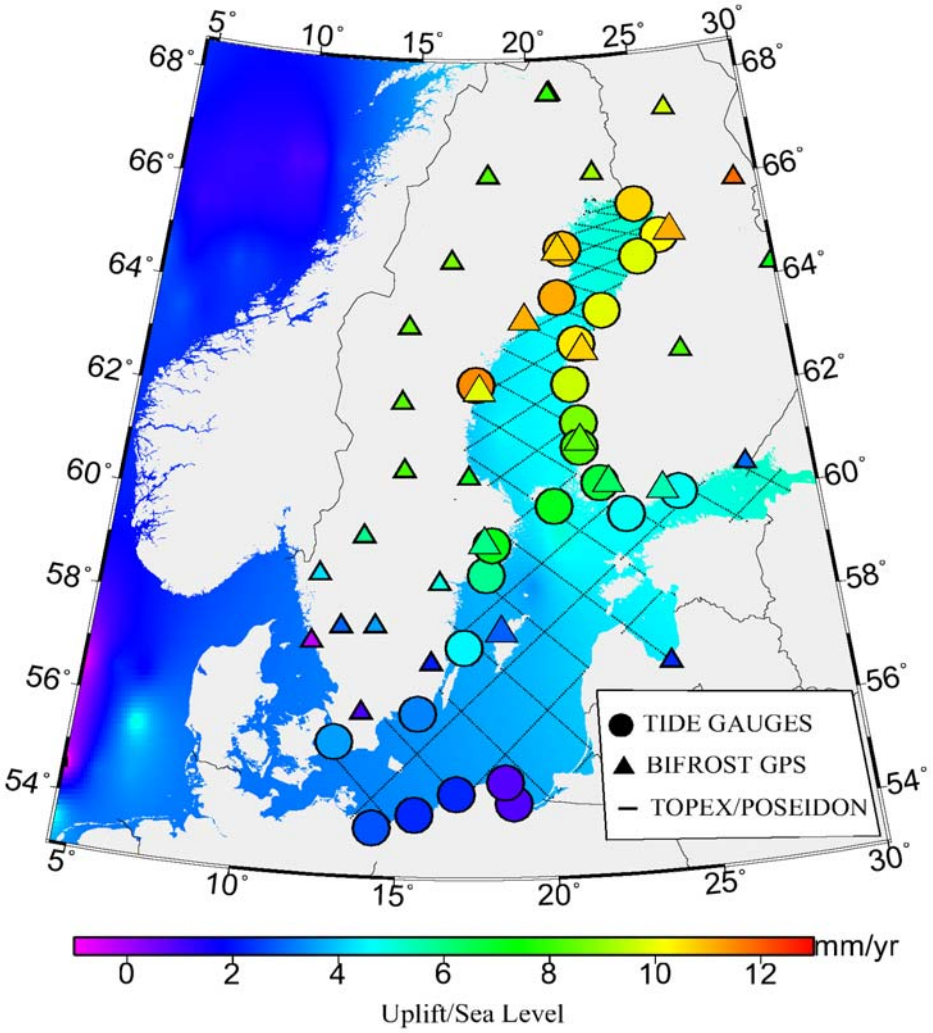

Figure 2.1: Estimates of absolute or geocentric vertical motions (circles) at 25 tide gauge sites in the Baltic Sea by combining TOPEX/POSEIDON decadal altimeter data and long-term (>40 years) tide gauge records. These estimates are compared with 10 collocated BIFROST GPS vertical rates (triangles) [Johansson et al., 2002]. TOPEX/POSEIDON ground tracks are shown on the background of altimeter averaged sea level trend (mm/yr, 1992–2002) in the Baltic and adjacent seas. Other inland BIFROST GPS vertical rates (triangles) are also shown.

Tide gauge	Data Span	Latitude (Degree)	Longitude (Degree)	Altimeter Minus Tide gauge Solution[1] (mm/yr) 1992–2001	Adjustment[2] (mm/yr) 1992-2001	Adjustment[3] (mm/yr) All Data
50051	1930-2001	55.52	12.90	3.6 ± 3.0 (0.90)	-0.7 ± 1.1	3.3 ± 0.5
50081	1887-2001	56.10	15.58	6.3 ± 2.2 (0.94)	2.6 ± 1.1	2.9 ± 0.5
50091	1887-2001	57.37	17.10	4.5 ± 2.6 (0.92)	2.7 ± 1.1	4.6 ± 0.5
50121	1887-2001	58.75	17.87	4.0 ± 1.5 (0.98)	4.9 ± 1.1	5.9 ± 0.5
50141	1889-2001	59.32	18.08	2.0 ± 1.6 (0.98)	5.4 ± 1.1	7.2 ± 0.5
50183	1968-2001	62.37	17.53	3.2 ± 2.8 (0.93)	12.6 ± 1.1	11.3 ± 0.5
50191	1892-2001	64.00	20.92	6.0 ± 3.2 (0.92)	20.6 ± 1.1	11.0 ± 0.5
50201	1916-2001	64.92	21.23	13.4 ± 3.4 (0.93)	15.9 ± 1.2	11.1 ± 0.5
60001	1920-1997	65.67	24.52	10.5 ± 8.3 (0.92)	16.1 ± 1.1	10.4 ± 0.5
60011	1889-1997	65.03	25.42	10.8 ± 8.2 (0.92)	16.5 ± 1.2	10.0 ± 0.5
60021	1922-1997	64.67	24.42	12.0 ± 7.9 (0.92)	18.8 ± 1.2	9.8 ± 0.5
60041	1914-1997	63.70	22.70	5.8 ± 8.2 (0.89)	13.8 ± 1.2	10.2 ± 0.5
60051	1883-1997	63.10	21.57	4.4 ± 7.7 (0.89)	12.0 ± 1.2	10.3 ± 0.5
60071	1926-1997	62.33	21.22	4.5 ± 6.2 (0.93)	10.9 ± 1.2	9.8 ± 0.5
60101	1910-1997	61.60	21.47	8.6 ± 4.2 (0.97)	8.8 ± 1.1	8.9 ± 0.5
60121	1933-1997	61.13	21.43	7.0 ± 4.2 (0.97)	7.5 ± 1.1	8.2 ± 0.5
60241	1922-1997	60.43	22.10	4.0 ± 4.1 (0.97)	3.8 ± 1.1	6.8 ± 0.5
60281	1924-1997	60.03	20.38	5.0 ± 3.5 (0.97)	4.6 ± 1.1	7.1 ± 0.5
60331	1887-1997	59.82	22.98	7.6 ± 4.6 (0.96)	4.9 ± 1.1	4.9 ± 0.5
60351	1879-1997	60.15	24.97	6.0 ± 4.3 (0.97)	4.1 ± 1.1	4.7 ± 0.5
110022	1951-1999	54.40	18.68	1.3 ± 3.7 (0.96)	-1.7 ± 1.2	0.8 ± 0.5
110047	1951-1999	54.80	18.42	-2.1 ± 3.8 (0.96)	-5.1 ± 1.1	1.3 ± 0.5
110057	1951-1999	54.58	16.87	1.4 ± 4.3 (0.95)	-1.7 ± 1.1	2.0 ± 0.5
110072	1951-1999	54.18	15.55	-4.8 ± 5.4 (0.90)	-4.9 ± 1.1	2.5 ± 0.5
110092	1811-1999	53.92	14.23	-7.5 ± 6.1 (0.87)	-5.1 ± 1.1	2.3 ± 0.5

Table 2.1: Vertical crustal motion solutions determined using decadal TOPEX/POSEIDON altimetry and long-term (>40 years) tide gauge data in the Baltic Sea.

[1]Altimeter Minus Tide gauge Solution, 1992–2001: Vertical motion solutions and the corresponding formal uncertainty are obtained differencing tide gauge and TOPEX/POSEIDON (TOPEX/POSEIDON) altimeter data within 3° of tide gauges using same data spans (1992–2001). Correlation Coefficients between altimeter and tide gauge sea level in parenthesis, indicating excellent agreements. The method used and resulting solution uncertainties are similar to Nerem and Mitchum [2002].

[2]Adjustment Solution, 1992–2001: Vertical motion solutions and uncertainties obtained using the Gauss-Markov adjustment method with employed data (altimetry and tide gauges) spanning only 1992–2001. Solution uncertainties are significantly reduced as compared to the above case.

[3]Adjustment Solution, All Data: Vertical motion solutions and uncertainties obtained using the Gauss-Markov adjustment method and using decadal (1992–2001) TOPEX/POSEIDON altimetry and long-term (>40 years, ~1950–2001) tide gauge data. Solution uncertainties are further reduced to 0.5 mm/yr (1σ) .

ICE4G	BIFROST Model LT=120 km UMV=$1x10^{21}$Pas LMV=$10x10^{21}$Pas	BIFROST Model LT=120 km UMV=$1x10^{21}$Pas LMV=$3x10^{21}$Pas
3.4±1.5	1.4±2.1	1.6±1.8

Table 2.2: Comparison of altimeter-tide gauge determined vertical motion with GIA models (ICE4G and BIFROST models). The comparison with the BIFROST models has less mean differences than with the ICE4G model.

2.2.3 Vertical Motions in the Great Lakes

The computation in the Great Lakes follows the procedure in the Baltic Sea region described above except for computing of absolute vertical motions using altimeter and water level gauge data. In contrast to the averaged absolute vertical motion observation computed over the Baltic Sea region using TOPEX/POSEIDON and tide gauge data, the absolute vertical motion at each water level gauge station is determined by averaging TOPEX/POSEIDON data through spatial area (constant radius) and time (monthly) in the Great Lakes area. A constant radius is chosen based on the correlation coefficients between the absolute sea level changes and relative sea level changes of water level gauge records, and on the data points of altimeters within the constant radius. In this study, TOPEX/POSEIDON measurements are mostly located at the center of the lakes, so TOPEX/POSEIDON data are averaged over each of the entire lake. For the Great Lakes region, TOPEX/POSEIDON and water level gauge records are highly correlated. The correlation coefficients between TOPEX/POSEIDON and water level gauge are larger than 0.95 while the correlation coefficients between water level gauges are larger than 0.9 except in Lake Erie (>0.8). Following the procedure outlined above for solving absolute vertical motions, we assumed the vertical motions fit a linear model.

The uncertainties are 0.6–1.6 mm/yr obtained by the traditional method [Nerem and Mitchum, 2002]. After adjustment, the uncertainties drop dramatically to <0.5 mm/yr (Table 2.3). Figure 2.3 illustrates the estimates of absolute vertical motions averaged in each lake compared with ICE4G model, BIFROST GIA model, and water level gauge analysis [Mainville and Craymer, 2003]. Our estimates represent similar results with the others except ICE4G has a smaller amplitude. Figure 2.4 shows the estimates of absolute vertical motions at gauge stations compared with ICE4G [Peltier, 2002], GPS velocity [M. Cline and R. Snay, National Geodetic Survey solution, personal communications, 2004], and water level gauge analysis [Mainville and Craymer, 2003]. Lake Superior, Lake Huron and Lake Ontario present uplift rates. Absolute vertical motions in Lake Erie are close to zero. The upper part of Lake Michigan is rising while the lower part is sinking. Absolute vertical motions are attributed to postglacial rebound because the crust is seeking equilibrium after the removal of a large ice sheet since the Last Ice Age in this region. Table 2.4 shows the statistics of the comparison between estimates and different PGR models. Models that account for the geoid effect match better with estimates of absolute vertical motions. Two better fitting GIA models are ICE3G and BIFROST with specific Earth parameters (M6 in Table 2.4). Means of difference of ICE3G and M6 with our estimates are –0.2±0.6 mm/yr and 0.0±0.6 mm/yr, respectively. In addition, vertical motions derived by water level gauge analysis [Mainville and Craymer, 2003] are consistent with our estimates as mean of difference is –0.1 mm/yr with a standard deviation of 0.5 mm/yr. The relative big difference

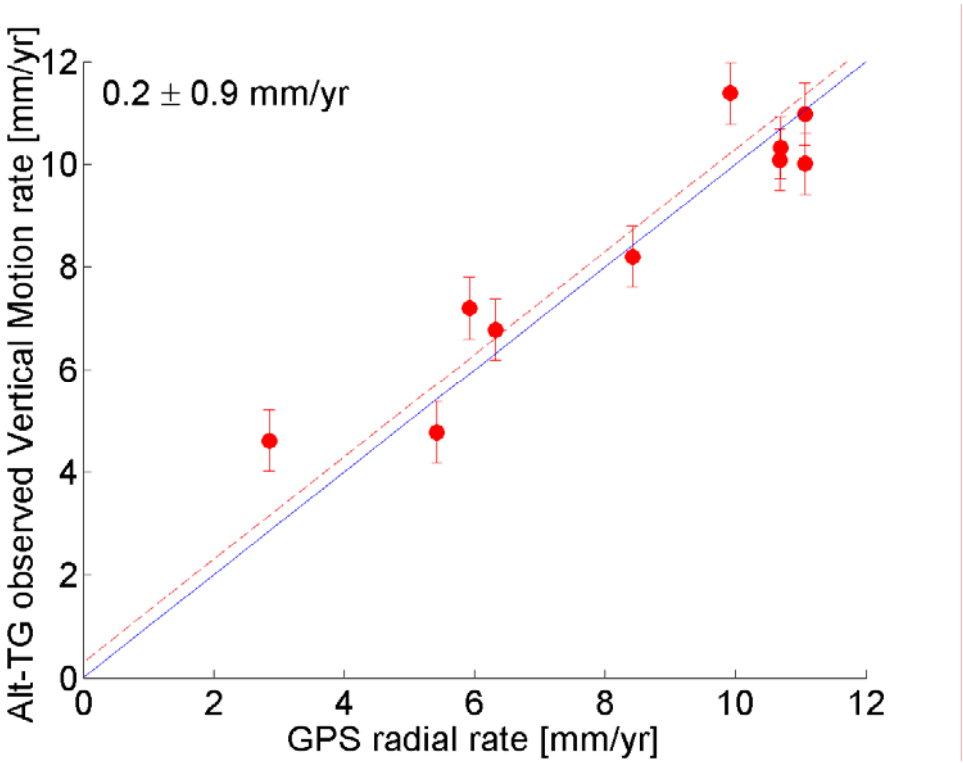

Figure 2.2: Comparison of 10 vertical motions (shown with uncertainties) derived from the combination of altimetry and tide gauge records with collocated BIFROST GPS vertical rates [Johansson et al., 2002].

Latitude (Degree)	Longitude (Degree)	Altimeter minus TG solution[1] (mm/yr)	Adjustment solution[2] (mm/yr)
Lake Erie			
281.11	42.88	2.0 ± 1.6	0.4 ± 0.4
279.93	42.15	2.7 ± 1.2	-0.5 ± 0.4
278.72	41.75	-1.8 ± 0.8	-1.5 ± 0.4
278.37	41.54	-1.0 ± 0.8	0.1 ± 0.4
277.27	41.55	0.0 ± 1.4	0.1 ± 0.4
276.53	41.69	-2.9 ± 1.6	-0.3 ± 0.4
276.74	41.96	-1.5 ± 1.3	-0.1 ± 0.4
276.88	42.15	-0.9 ± 1.3	0.2 ± 0.4
276.88	42.05	-2.1 ± 1.1	-1.0 ± 0.4
277.27	42.03	-0.6 ± 1.0	-0.3 ± 0.4
278.08	42.27	0.9 ± 0.8	-0.1 ± 0.4
278.78	42.67	-0.1 ± 0.8	-0.3 ± 0.4
279.80	42.78	1.0 ± 1.1	0.3 ± 0.4
280.75	42.87	1.5 ± 1.4	0.2 ± 0.4
Lake Huron			
277.36	43.85	1.5 ± 0.7	1.2 ± 0.3
276.15	43.64	-1.2 ± 1.1	0.6 ± 0.3
275.28	45.78	2.6 ± 0.7	2.1 ± 0.3
276.10	45.99	2.5 ± 0.7	2.7 ± 0.3

276.45	46.25	3.7 ± 0.7	3.3 ± 0.3
278.07	45.98	3.2 ± 0.7	3.1 ± 0.3
279.97	45.33	3.1 ± 0.7	3.1 ± 0.3
279.74	44.50	2.1 ± 0.7	2.0 ± 0.3
278.33	45.27	1.9 ± 0.6	2.8 ± 0.3
278.27	43.75	1.3 ± 0.7	0.4 ± 0.3
277.51	43.14	0.9 ± 0.9	0.8 ± 0.3
276.71	44.66	1.3 ± 0.8	1.7 ± 0.3
Lake Michigan			
273.56	43.95	0.6 ± 0.9	-1.2 ± 0.5
272.46	41.73	-0.7 ± 1.0	-0.6 ± 0.5
272.11	43.00	-0.8 ± 0.9	-1.3 ± 0.5
272.69	44.80	-1.5 ± 0.9	-0.2 ± 0.5
271.99	44.54	-2.3 ± 1.0	-1.0 ± 0.5
274.13	45.97	1.0 ± 0.9	1.0 ± 0.5
273.80	42.77	-0.2 ± 1.3	-0.7 ± 0.5
272.50	44.46	-0.6 ± 1.2	-0.4 ± 0.5
Lake Ontario			
283.66	44.13	1.3 ± 0.7	1.5 ± 0.3
283.49	43.46	1.1 ± 0.7	1.3 ± 0.3
282.37	43.27	1.1 ± 0.7	1.2 ± 0.3
280.78	43.23	0.8 ± 0.7	0.4 ± 0.3
280.23	43.33	0.5 ± 0.8	-0.1 ± 0.3
280.62	43.63	-0.1 ± 0.7	1.0 ± 0.3
281.83	43.95	2.0 ± 0.7	1.3 ± 0.3
283.48	44.22	1.6 ± 0.8	1.7 ± 0.3
Lake Superior			
275.37	46.49	3.4 ± 0.6	2.5 ± 0.4
272.62	46.55	0.7 ± 0.5	1.3 ± 0.4
270.68	46.88	0.7 ± 0.5	0.1 ± 0.4
267.91	46.78	-1.7 ± 0.7	-0.7 ± 0.4
269.66	47.75	1.3 ± 0.5	1.3 ± 0.4
270.78	48.42	0.8 ± 0.5	2.1 ± 0.4
272.48	48.83	4.7 ± 0.5	4.2 ± 0.4
275.10	47.97	4.2 ± 0.6	4.3 ± 0.4
275.42	46.53	3.8 ± 0.6	2.2 ± 0.4

Table 2.3: Vertical crustal motion solutions determined using decadal TOPEX/POSEIDON altimetry and long-term water level gauge data in the Great Lakes.

[1]Altimeter Minus Water Level Gauge Solution, 1992–2002: Vertical motion solutions and the corresponding formal uncertainty are obtained differencing water level gauge and TOPEX/POSEIDON (T/P) altimeter data within 3° of water level gauges using same data spans (1992–2002). The method used and resulting solution uncertainties are similar to Nerem and Mitchum [2002].

[2]Adjustment Solution, All Data: Vertical motion solutions and uncertainties obtained using the Gauss-Markov adjustment method with stochastic constraints and using decadal (1992–2002) TOPEX/POSEIDON altimetry and long-term water level gauge data.

#	Observation/Model	Mean of difference (mm/yr)	STD. (mm/yr)
M1	BIFROST LT=120 UMV=1 LMV=10	1.4	1.2
M2	BIFROST LT=120 UMV=1 LMV=10	1.3	1.0
M3	BIFROST LT=120 UMV=1 LMV=3	-0.1	0.9
M4	BIFROST LT=120 UMV=1 LMV=3	0.1	0.8
M5	BIFROST LT=120 UMV=.5 LMV=3	-0.2	0.7
M6	BIFROST LT=120 UMV=.5 LMV=3	0.0	0.6
M7	ICE4G LT=120 UMV=.5 LMV=3	0.1	0.9
M8	ICE4G LT=120 UMV=.5 LMV=3	-0.1	0.9
M9	ICE3G LT=120 UMV=1 LMV=2	-0.2	0.6
M10	Mainville and Craymer [2003] analysis	-0.1	0.5

Table 2.4: Mean of difference between PGR models and TG/Alt Observations. UMV/LMV in 10^{21} Pas, LT in km. M2, M4, M6, and M8 account for the geoid effect. LT=Lithospheric thickness; UMV=Upper mantle viscosity; LMV=Lower mantle viscosity. Mainville and Craymer [2003] analyzed only water level gauge data for relative vertical motion with respect to one gauge.

appears in the northern Lake Huron. However, our estimates show a large inconsistency with the GPS solutions. The large discrepancy may be caused by different solution methodologies, processing philosophy, using different reference frames or fixing different stations. At present, various GPS vertical solutions are largely inconsistent with each other even though different analysis centers or researchers primarily used similar data sets [Snay et al., 2002].

2.2.4 Vertical Motions in Alaska Region

In certain regions, absolute vertical motions could include a linear term and a nonlinear term. The quadratic deformation, which is a nonlinear term, is caused by the postseismic deformation [Larsen et al., 2003], like in Alaska. Analyzing various types of deformation causing vertical motions is necessary for improving the accuracy of the estimates. In particular, a separation of secular, periodic, instantaneous, and non-linear motions would be needed. In order to consider vertical motions using a quadratic model, both the absolute sea level change of altimeter data within a constant radius at the tide gauge station, i, and relative sea level change from tide gauge station, i, are computed in a time series (monthly). The difference between the relative and absolute sea level change at each epoch can be written according to Equation (2.1) as:

$$\begin{aligned} u_{i,t}(\lambda_i,\varphi_i) &= g_{i,t}(\lambda_i,\varphi_i) - S_{i,t}(\lambda_i,\varphi_i) \\ &= a_i + b_i(t-t_0) + c_i(t-t_0)^2 \end{aligned}, \qquad (2.8)$$

Where t is the time index (interval is monthly), t_0 is the reference time set as 1990 in this study; a is the bias, b is the coefficient of the linear term, and c is the coefficient of the quadratic term. The criterion for selecting a tide gauge station stands on the correlation coefficient between TOPEX/POSEIDON data and tide gauge records that should be larger than 0.8.

The difference of the records between two tide gauge stations (difference of two relative sea level changes), i and j, is written in light of Equation (2.4) as:

$$\begin{aligned} ru_{ij,t} &= -S_{i,t}(\lambda_i,\varphi_i) + S_{j,t}(\lambda_j,\varphi_j) = u_{i,t} - u_{j,t} \\ &= a_i + b_i(t-t_0) + c_i(t-t_0)^2 \\ &\quad - a_j - b_j(t-t_0) - c_j(t-t_0)^2 \end{aligned} \quad . \qquad (2.9)$$

Similarly, the correlation coefficient of two tide gauge records used to compute Equation (2.9) should also be larger than 0.8. Next, $g_{i,t}(\lambda_i,\varphi_i) - S_{i,t}(\lambda_i,\varphi_i)$ and $-S_{i,t}(\lambda_i,\varphi_i) + S_{j,t}(\lambda_j,\varphi_j)$ in Equation (2.8) and (2.9), respectively, are substituted into Equation (2.4) as observations so that unknown parameters, a, b, and c could be solved by Equation (2.6) and (2.7). We next use the GM model with stochastic constraints (Equation 2.5) to solve for the absolute vertical motions at all tide gauge locations. By fitting the same time span data of the absolute and relative vertical motions in Equation (2.8) and (2.9), the formal errors of trends are 1.5–2.5 mm/yr. This means the data in Equation (2.8) and (2.9) have equivalent accuracy even though they consist of different types of data (TOPEX/POSEIDON with tide gauge data and tide gauge with tide gauge data, respectively). Therefore, the diagonal elements of Σ_0 and Σ_1 are set equal to σ_v^2, where σ_v is equal to 10 mm. The off-diagonal elements of Σ_0 matrix and Σ_2 matrix are set equal to $\sigma_v^2 \times 0.3$, which means the correlation coefficient of the computed absolute or relative vertical motions is 0.3 when the absolute or relative vertical motions are computed using the same tide gauge data.

Larsen et al. [2003] have done a comprehensive analysis of vertical motions in this region. The absolute vertical motions were calculated via the adjustment by adopting their result of describing types of vertical motions. All tide gauge stations are separated into two regions (see Figure 2.5). One region contains YAKUTAT, SITKA, SKAGWAY, JUNEAU, KETCHIKAN, PRINCE RUPERT, and QUEEN CHARLOTTE CITY (triangles in Figure 2.5). Absolute vertical motions in this region are presented by a linear model except station YAKUTAT. The other region includes SAND POINT, KODIAK, ANCHORAGE, NIKISKI, SELDOVIA, SEWARD, VALDEZ, and CORDOVA (circles in Figure 2.5). Absolute vertical motions of most stations in this region are presented by a quadratic model because of the earthquake in 1964.

Table 2.5 shows the estimated coefficients of absolute vertical motions. In region I, YAKUTAT, SITKA, SKAGWAY, and JUNEAU stations have extremely rapid uplift rates that may be caused by regional GIA or regional tectonic stress [Barnes, 1984]. The global GIA model ICE4G in region I is only presented the uplift rate <1 mm/yr, which is significantly smaller than the estimates. The underestimate of the PGR model in this region is due to the limited knowledge of the last glacial maximum ice history [e.g., Tushingham and Peltier, 1991]. In region II, the linear model has been tested as well and the F ratio of linear and quadratic models can be defined as [Zhao et al., 1995]:

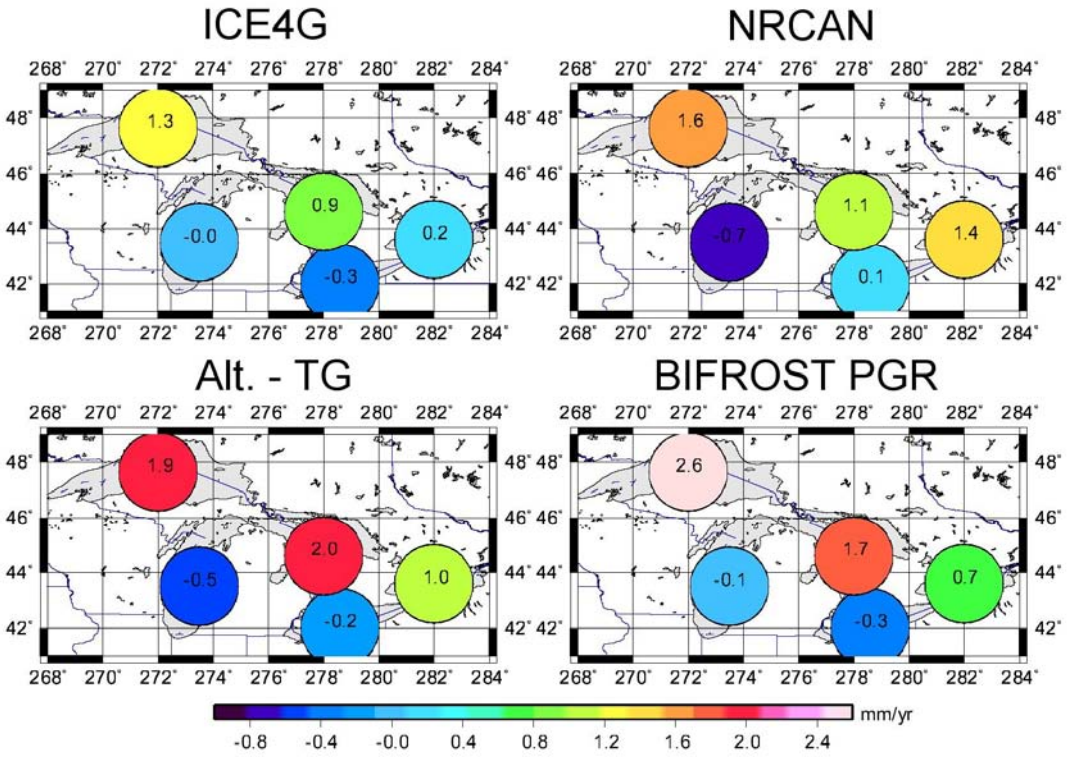

Figure 2.3: Estimates of absolute vertical motions averaged in each lake compared with ICE4G, BIFROST PGR, and water level gauge analysis [Mainville and Craymer, 2003].

$$F = \frac{(SSR_1 - SSR_2)/(DF_1 - DF_2)}{SSR_2 / DF_2}, \qquad (2.10)$$

where *SSR* is the sum of the squared residuals and *DF* is the number of degrees of freedom (number of data points minus number of unknown parameters). The subscripts 1 and 2 refer to models without and with the extra parameters, respectively. According to Equation (2.10), F is equal to 20.5, so the quadratic model passes the F test at the 0.1% level (F ratio >10.8) [Beyer, 1991]. ANCHORAGE, SEWARD, VALDEZ, and CORDOVA stations show the similar quadratic form in uplift rates. KODIAK and NIKISKI show subsidence of a quadratic term but there is a big data gap in the records of NIKISKI. This makes the estimates of NIKISKI less reliable. Table 2.6 shows the comparison of the absolute vertical motions derived by altimeter–tide gauges, tide gauges only [Larsen et al., 2003], and GPS vertical velocity solutions at four tide gauge stations which are provided by http://www.giseis.alaska.edu/Input/chris/gpsuplift.pdf. Figure 2.6 shows the comparison of the absolute vertical motions derived by altimeter-tide gauges (this study) and relative vertical motion only using tide gauges at 15 Alaskan sites [Larsen et al., 2003]. The rates of the estimates from this study and Larsen et al. [2003] shown in Table 2.6 are calculated in year 2000. The rate of absolute vertical motion at YAKUTAT observed by altimeter and tide gauges in 2000 is 10.5 mm/yr from the estimation of the quadratic model; however, there is an unknown shift of tide gauge data in January 1992 [Larsen et al., 2003]. If this shift is removed, the vertical motion rate increases ~3 mm/yr and equals 13.5

mm/yr. The mean of solution differences between Larsen et al. [2003] and this study in region I and region II are -1.0±0.7 mm/yr and -2.7±4.2 mm/yr, respectively. The results are consistent in region I within the uncertainty. In region II, significant discrepancy exists. By eliminating two stations, NIKISKI and KODIAK, the mean of difference is -4.8±1.2 mm/yr. The standard deviation decreases dramatically, however, it drastically increases the magnitude of the bias estimate. This bias may be caused by introducing different absolute sea level variations. Altimetric sea level trends are employed by this study while Larsen et al. [2003] used almost an equal rate of sea level trends. Figure 2.7 shows the comparison of the estimates and GPS solutions geographically. The comparison illustrates an extremely good agreement. Therefore, an approach we developed recently can be adopted in the open-ocean if the absolute sea level variations at different gauge stations could be assumed to be known or be modeled with sufficient accuracy.

Tide gauge	Linear	Quadratic
Region I (1950-2002)	(mm/yr)	(mm/yr) (mm/yr^2)
YAKUTAT	–	8.6 ± 1.2 0.09 ± 0.01
SITKA	1.4 ± 1.3	–
SKAGWAY	15.8 ± 1.3	–
JUNEAU	11.9 ± 1.2	–
KETCHIKAN	-0.3 ± 1.3	–
PRINCE RUPERT	-1.1 ± 1.3	–
QUEEN CHARLOTTE CITY	-0.5 ± 1.3	–
Region II (1973-2002)	(mm/yr)	(mm/yr) (mm/yr^2)
SAND POINT	-4.5 ± 1.5	–
KODIAK	–	7.7 ± 1.7 $-0.07 \pm .072$
ANCHORAGE	–	-3.0 ± 1.6 $0.35 \pm .060$
NIKISKI	–	7.5 ± 1.6 $-0.04 \pm .081$
SELDOVIA	6.8 ± 1.6	–
SEWARD	–	-1.0 ± 1.5 $0.28 \pm .041$
VALDEZ	–	-1.2 ± 1.5 $0.50 \pm .052$
CORDOVA	–	-7.5 ± 1.5 $0.27 \pm .044$

Table 2.5: Estimated coefficients of the absolute vertical motions.

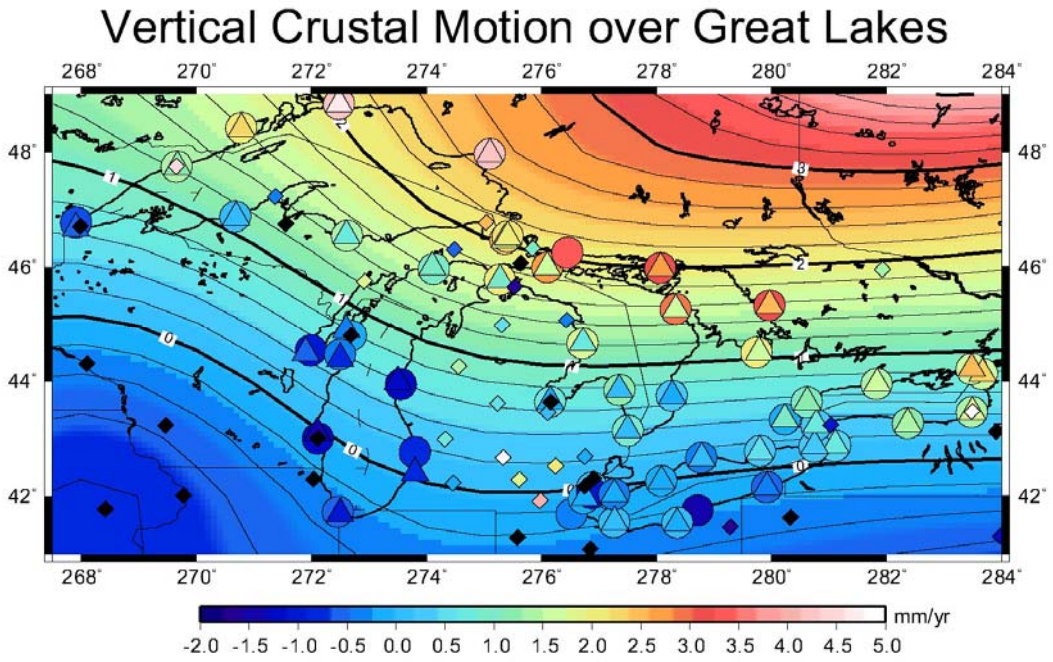

Figure 2.4: Estimates of absolute or geocentric vertical motions (circles) at 50 water level gauge sites in the Great Lakes by combining TOPEX/POSEIDON decadal altimeter data and long-term water level gauge records. The background is ICE4G [Peltier, 2002]. The diamonds are GPS velocities [NGS solution, M. Cline and R. Snay, personal communications, 2004]. The triangles present the vertical motions from water level gauges analysis [Mainville and Craymer, 2003].

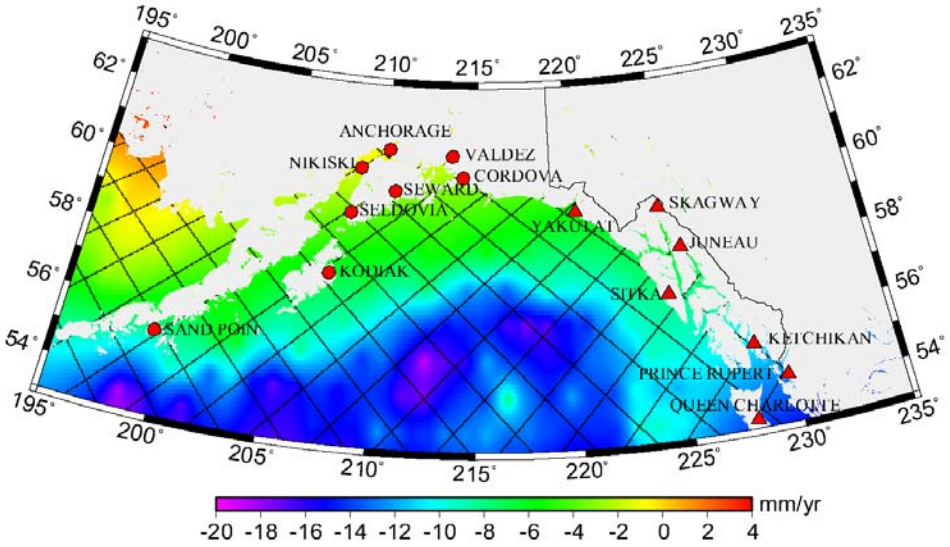

Figure 2.5: Tide gauge stations. All tide gauges are separated into two regions, triangles and circles. The background is altimetric sea level changes derived from Geosat, ERS-1, ERS-2 and TOPEX/POSEIDON.

Tide gauge	Alt. & Gauge (mm/yr)	GPS (mm/yr)	Gauge (mm/yr) Larsen et al. [2003]
YAKUTAT	13.5	13-14	13.7
SITKA	1.4	0 ~ -1	3.0
SKAGWAY	15.8	15 ~ 16	17.1
JUNEAU	11.9	11 ~ 12	13.6
KETCHIKAN	-0.3		0.0
PRINCE RUPERT	-1.1		-0.7
QUEEN CHARLOTTE CITY	-0.5		1.0
SAND POINT	-4.5		0.1
KODIAK	6.2		5.4
ANCHORAGE	4.4		10.4
NIKISKI	6.7		0.5
SELDOVIA	6.8		9.6
SEWARD	4.9		10.4
VALDEZ	8.8		12.9
CORDOVA	-1.8		3.8

Table 2.6: Comparison of the absolute vertical motions derived from altimeter–tide gauges, GPS vertical velocities, and tide gauges only [Larsen et al., 2003]. Uplift rates in year 2000.

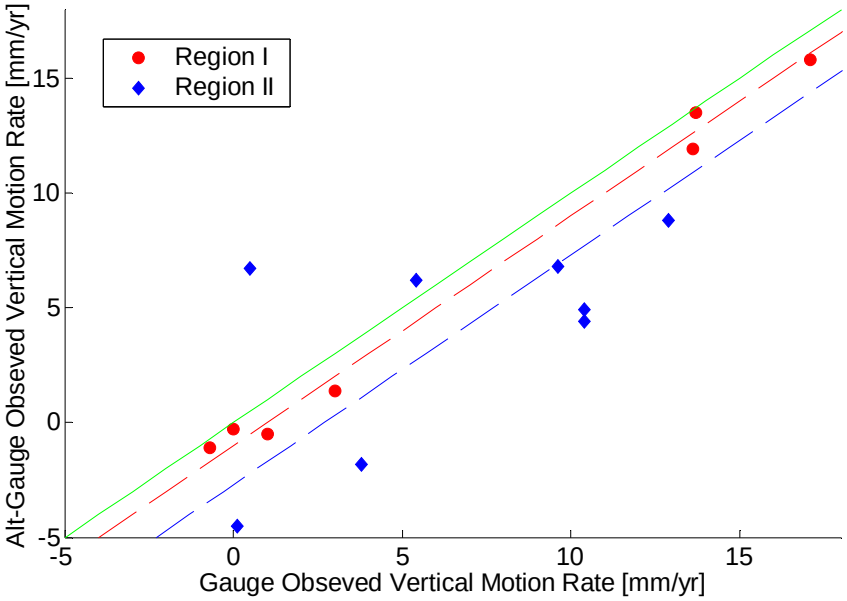

Figure 2.6: Comparison of the absolute vertical motions derived from altimeter-tide gauges using only 15 tide gauges [Larsen et al., 2003]. Red circles indicate tide gauge stations in region I and blue diamonds indicate tide gauges in region II. The green line indicates per agreement between the two independent solutions. The red dash line represents the mean of solution differences in region I and the blue dash line represents the mean of solution differences in region II.

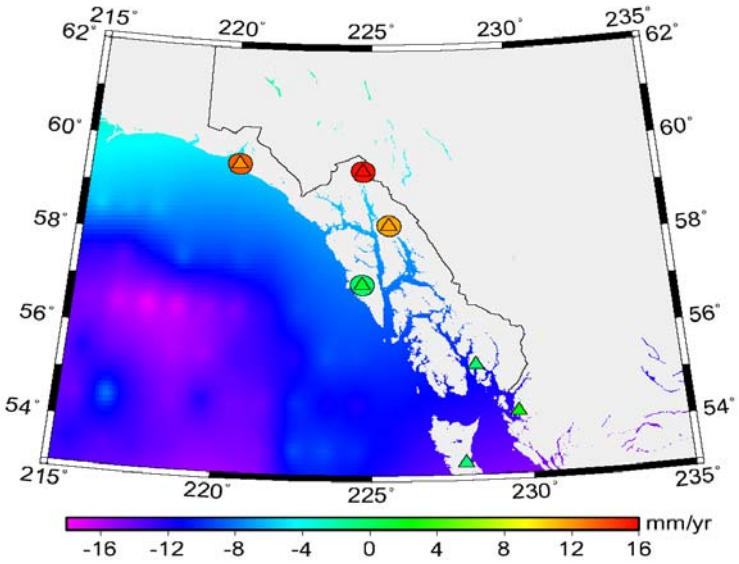

Figure 2.7: Geographical comparison of altimeter-tide gauge derived absolute vertical motions (triangles) and GPS solutions (circles).

2.3 Conclusion

A new method of estimating absolute vertical motions using both satellite altimetry and tide gauge data in Fennoscandia, Alaska, and the Great Lakes is presented. The technique is applied to Fennoscandia using 25 tide gauges and TOPEX/POSEIDON altimetry over the Baltic Sea. The estimated absolute vertical motions have an uncertainty of 0.5 mm/yr (1σ), which is significantly smaller than the traditional approach at 1–2 mm/yr [e.g., Nerem and Mitchum, 2002]. The improved accuracy is primarily due to an innovative adjustment technique, which optimally combines short-term altimetry (10 years) and long-term (>40 years) tide gauge records in a network adjustment. Comparison of the estimates with constraints provided by 10 collocated BIFROST GPS sites yields a difference of 0.2±0.9 mm/yr. The excellent agreement between the two independent solutions verifies the accuracy and robustness of our (and the GPS) technique. Comparisons of 25 estimates with predictions generated from numerical models of the GIA process yield larger discrepancies.

In the Great Lakes, the uncertainties are 0.6–1.6 mm/yr obtained by the traditional method [Nerem and Mitchum, 2002]. After adjustment, the uncertainties decrease dramatically to <0.5 mm/yr. In Lake Michigan and Erie, the lands are sinking, while the lands are uplifting in Lake Ontario, Superior, and Huron. By comparing the PGR models with the estimates, ICE3G and M6, as shown in Table 2.4, have better agreements with our estimates. In addition, vertical motions derived by tide gauge analysis [Mainville and Craymer, 2003] are consistent with our estimates as the mean of difference is –0.1 mm/yr with a standard deviation of 0.5 mm/yr. However, at present the estimates have a large discrepancy with GPS vertical solutions. The disagreement may be caused by unstable GPS solutions, which used different reference frames and the solutions used are based on absolute vertical solutions [e.g., Snay et al., 2002]. In

comparison, the BIFORST GPS vertical solution used a primarily kinematic solution approach [Johansson et al., 2002].

In Alaska, the uncertainties of estimates are larger than 1 mm/yr because the study region is not in a semi-enclosed or enclosed sea. In the open ocean, the assumption that the absolute sea level variations are equal at nearby gauges, is not exactly correct. However, our estimates agree well with the GPS solution and the solutions of Larsen et al. [2003] but is not consistent with the GIA model because of the limited knowledge of the last glacial maximum ice history. Therefore, this approach has potential to apply in the open ocean and deals with non-linear vertical motions.

The next step to improve the vertical motion determination is to lengthen the time span of altimeter data, which would produce a commensurate improvement in accuracy for the absolute vertical motion estimates. Extension of the TOPEX/POSEIDON data span using JASON and linking with GEOSAT (1984–1990), and using other altimetry data (e.g., GFO, ENVISAT, ERS-1/-2, JASON) could provide an avenue for this improvement. In the adjustment, the adjacent tide gauge stations are assumed to measure the identical sea level variations; however, this assumption could be wrong when the local phenomenon dominates the sea level like currents. Hence the assumption can be improved by introducing sea level trends from ocean general circulation models, such as the ECCO model [Fukumori et al., 1999]. In addition, detailed analysis of the correlations between the tide gauge data and altimeter data to formulate a more accurate error model could potentially improve the algorithm and the resulting vertical motion solutions. In summary, the developed technique potentially enables accurate vertical motion estimates where long-term tide gauge data records exist. The improvement of vertical motion at world tide gauge sites which are caused by GIA and other phenomena, will improve the determination of global sea level trend.

CHAPTER 3

STERIC SEA LEVEL

Steric sea level (thermosteric and halosteric) variations [Pattullo et al., 1955] represent the component of the sea level changes due to density variations, the thermosteric component due to changes in temperature, and the halosteric component caused by changes in salinity. Sea level will rise if the ocean warms or decreases in salinity and drops if it cools or increases in salinity, since the density of the water column changes. The dominating effect is thermosteric sea level, which is about 10 times greater than halosteric sea level. Since there is no reliable salinity data over an extended time period (last several decades) for the worldwide ocean, a halosteric anomaly is not easy to distinguish from mass or thermal variations, and it is relatively small. Recent studies often ignore the halosteric anomaly [e.g., Cabanes et al., 2001a].

The amount of steric sea level change depends not only on the temperature or salinity variation, but also on the depth over which the temperature of salinity changes, the average temperature and salinity of the water column, the water pressure, the process of mixing including nonlinear effects [Gille, 2004], and different diffusivities associated with bottom topography. For example, warm water expands more than cold water given the same input of heat. A small temperature change over 1000 meters of water causes a much larger steric sea level increase than a comparable temperature increase in the near-surface layers. Vertical mixing of salts and heat and tides is found to be by no means uniform, and it is one of the principal mechanisms including Earth rotation, winds, stable stratification, mesocale eddies, and upholding the meridional overturning circulation [e.g., Wunsch and Ferrari, 2004], which largely governs climate change [e.g, McPhaden and Zhang, 2002]. The importance of the contribution of thermal expansion to global sea level rise was speculated to be the missing link (for up to ~1 mm/yr) during the 1996 United Nation's Intergovernmental Panel for Climate Change (IPCC) sea level assessment study in an attempt to explain the large discrepancy between the observed and the geophysical predictions. The thermosteric sea level trend calculated based on the Levitus et al. [2000] study reveals that its contribution is only on the order of 0.5 mm/yr, however, the ocean is observed to be warming significantly during the last five decades. Recently, the salinity contribution to sea level rise [Antonov et al., 2002] is speculated to be important, and studies including Munk [2002], Wadhams and Munk [2004] attempted to explain the current discrepancy of observed and predicted sea level rise during the 20th Century [Church et al., 2001] by possibly missing accounting of fresh water masses contributed to the ocean. In particular, due to the recent (past decade) accelerated melting of sea ice in the Arctic region [e.g., Dyurgerov and Carter, 2004]. However, the conjecture requires accurate estimate of the halosteric sea level trend [Antonov et al., 2002], which still has a large uncertainty.

In situ temperature and salinity data have been collected by buoys, commercial ships and oceanographic cruises over the last few decades, which are distributed unevenly. Recently, Levitus et al. [2005] and Ishii et al. [2005] provided global grid temperature data sets based on objective analysis methods applied to the raw data for 1955–2003 and 1945-2003 respectively. By analyzing temperature profiles over the last half-century, it can be concluded that the ocean in

all basins are warmed. The rate of averaged thermosteric sea-level rise caused by ocean heating is estimated to be 0.40 mm/yr over 1955–1995 [Antonov et al., 2005], based on pentadal temperature data down to 3000 m. For the 0–700 m layers, the averaged thermosteric trends are 0.34 mm yr^{-1} and 1.23 mm yr^{-1} for the 1955–2003 and 1993–2003 periods, respectively [Antonov et al., 2005]. For the same two periods and same depth range (0–700 m), the trend of thermosteric sea level based on monthly ocean temperature data from Ishii et al. [2005] are 0.38±0.04 mm yr^{-1} and 1.8±0.2 mm/yr respectively. Cabanes et al. [2001a] indicate the rapid rise of thermosteric sea level is large enough to explain the entire sea level rise signal also observed by TOPEX/POSEIDON (T/P) altimeter during 1993-1998. However, Miller and Douglas [2004, 2005] conducted an analysis with results conflicting with the conclusions by Cabanes et al. [2001a]. Miller and Douglas [2004, 2005] indicates that the trend of mass variations is 2–3 times larger than the steric sea level trend, based on analysis using the *in situ* Ocean Surface Data (OSD) instead of using objectively analyzed data which perhaps have produced an unrealistically large sea level trend due to over smoothing. Recent studies including Willis et al. [2004], Antonov et al. [2005], and Ishii et al. [2005] reported that the rapid thermosteric sea level trends range from 1.2 to 1.8 mm/yr in the 1990s. These results agree with the conclusion of Miller and Douglas [2004, 2005].

In this chapter, determinations of the thermosteric sea level using grid temperature data from objective analysis, and the steric sea level, i.e., the effect of both the thermosteric and haleosteric sea level using the equation of the state to account for nonlinearity [Miller and Douglas, 2004; Gille, 2004] and using *in situ* temperature and salinity data (the so-called Ocean Station Data (OSD)) from NOAA's World Ocean Database 2001 (WOD01) compiled by S. Levitus et al., covering the time period from the last five decades, 1948–2000. We will also address the issue whether salinity change in the ocean would significantly change the global sea level trend estimate. The determined steric and thermosteric sea level trends are used to compare with global sea level observed by altimeters (last two decades) and tide gauges (last five decades) to provide a quantification of their respective contributions to global sea level change during the last 50 years.

3.1 Algorithm to Compute Steric Sea Level

The algorithm of computing steric sea level is extensively described in textbooks [e.g., Gill, 1982; Pond et al., 1983] and the concept is summarized concisely as follows. First of all, the definition of geopotential in oceanography is introduced. The quantity $dw = Mgdz$ is the amount of work done (which equals potential energy gained) in raising a mass M through a vertical distance dz against the force of gravity (ignoring friction), where g is the acceleration due to gravity. A quantity is called geopotential (Φ) such that the change of geopotential $d\Phi$ over the vertical distance dz is given by

$$d\Phi = gdz . \qquad (3.1)$$

The hydrostatic (pressure) equation in differential form can be expressed as

$dp = -\rho g dz$, so

$$d\Phi = -\rho^{-1} dp = -\alpha dp\,, \tag{3.2}$$

where ρ is the density of water, α is the specific volume, and p is the sea pressure.

There are standard algorithms to compute the values of the density and of dynamic heights. The density is calculated in terms of the specific volume anomaly δ, defined as the specific volume $\alpha = \rho^{-1}$ (unit is $m^3 kg^{-1}$) related to the value at the same pressure for a temperature of 0° C and a practical salinity of 35, i.e., Gill [1982],

$$\delta(S,T,p) = \alpha(S,T,p) - \alpha(35,0,p)\,, \tag{3.3}$$

where S is the salinity of sea water, T is the temperature of sea water, and p is the pressure at the corresponding depth of the ocean. $\alpha_{S,T,p}$, $\alpha_{35,0,p}$, and δ are derived from the density of sea water, ρ, which can be easily computed from the equation of state (Appendix A). The equation of state defined by the Joint Panel on Oceanographic Tables and Standards [UNESCO, 1981] fits available measurements with a standard error of 3.5 ppm for pressure up to 1000 bars, for temperatures between freezing and C, and for salinities between 0 and 42 [Millero and Poisson, 1981].

Integrating equation (3.2) from z_1 to z_2, the equation is expressed as

$$\int_1^2 d\Phi = \int_1^2 g dz = -\int_1^2 \alpha dp\,. \tag{3.4}$$

Now rewriting $\alpha(S,T,p) = \alpha(35,0,p) + \delta(S,T,p)$, we get

$$\Phi_2 - \Phi_1 = g(z_2 - z_1) = -\int_1^2 \alpha(35,0,p)dp - \int_1^2 \delta dp = -\Delta\Phi_{std} - \Delta\Phi\,. \tag{3.5}$$

The quantity $\Phi_2 - \Phi_1$ is called the geopotential distance between the levels z_1 and z_2 where pressures will be p_1 and p_2. The quantity $\Delta\Phi_{std}$ is called the "standard geopotential distance" while the second quantity $\Delta\Phi$ is called either "geopotential anomaly" or "dynamic height." Geopotential Anomaly (Dynamic height) can be derived by:

$$D(p_1,p_2) = \int_{p_1}^{p_2} \delta(S,T,p)dp = \int_{p_1}^{p_2} \alpha(S,T,p)dp - \int_{p_1}^{p_2} \alpha(35,0,p)dp\,. \tag{3.6}$$

The use of dynamic heights is preferred over the use of geometric heights in oceanography and meteorology because energy is generally lost or gained when a parcel of fluid moves along a surface of equal geometric height but not when it moves along a surface of equal dynamic height. This is similar to the situation in the land where we like to use height or elevation of fluid (e.g., hydrology) referenced to dynamic or orthometric heights (or equipotential surface) other than to ellipsoidal height. Even though $D(p_1, p_2)$ is called dynamic

heights, its unit is energy, m^2/s^2. For numerical convenience, oceanographers in the past have used a unit called dynamic meter so that 1 dynamic meter = $10\,m^2/s^2$. Therefore, $D(p_1, p_2)$ in dynamic meters is almost numerically equivalent to the geometric meter ($z_2 - z_1$). For example, if:

$$D(p_1, p_2) = 980\,m^2/s^2 = 98 \quad dynamic \quad meter = 100 meter (if \quad g = 9.8\,m/s^2) \approx 98 meter$$

The relationship is given here because sometimes raw data of dynamic heights is given in the form of dynamic meters instead of meters.

After choosing a long-time-averaged temperature, pressure, and salinity as reference datum, the steric sea level can be expressed as:

$$h_{steric} = \int_{p_1}^{p_2} \alpha(S,T,p)dp - \int_{p_1}^{p_2} \alpha(S_0,T_0,p_0)dp_0 = \int_{z_1}^{z_2} \left(\frac{1}{\rho(S,T,p)} - \frac{1}{\rho_0(S_0,T_0,p_0)}\right)dz \tag{3.7}$$

where $S_0, T_0,$ and p_0 are the mean salinity, temperature, and pressure, respectively.

3.2 Data Analysis

3.2.1 Ocean Station Data (OSD) from World Ocean Database 2001 (WOD01)

WOD01, containing observed and standard level profile and plankton and surface data, represent an update of the World Ocean Database products first released as World Ocean Atlas 1994 (WOA94) [Levitus, et al., 1994], followed by World Ocean Database 1998 (WOD98) [Boyer, et al., 1998], and World Ocean Database 2001 [Conkright et al., 2002]. WOD01 expands on WOD98 by including new variables, data sets, and data types. The Ocean Station Data (OSD) or the *in situ* data in WOD01 include all bottle data, Salinity/Temperature with Depth (STD), low resolution Conductivity-Temperature-Depth (CTD) data, some surface only data, and plankton taxonomic and biomass measurements. The amount of data in the northern hemisphere is much more abundant than that in the southern hemisphere (Figure 3.1).

3.2.2 World Ocean Atlas 2001 (WOA01)

The data set of 1°×1° grid temperature anomalies [Stephens et al., 2002] are provided as yearly means (averages) for the upper 700 m from 1955 to 2003 and five-year (pendatal) means down to 3000 m from 1955 to 1998 by Levitus et al. [2005], updating the earlier work [Levitus et al., 2000]. They computed gridded time series at non-uniformly spaced depth levels using the raw temperature profiles, based on an objective analysis scheme. By analyzing the data set, Levitus et al. [2005] reported that globally-averaged ocean heat content (0–300 m) increased by 14.5×10^{22} joules between 1955 and 1998, corresponding to a net ocean mean temperature warming of 0.037°C during the past 50 years at a rate of 0.20 Wm^{-2} (per unit area of Earth's total

surface area). For the world ocean the linear trend of heat content (0–3000 m layer for 1955–1998) is 0.33×10^{22} J/year.

In addition, annual temperature and salinity data from WOA01 are in the format of one-degree objectively analyzed mean [Stephens et al., 2002]. Maximum depth for annual objective analyses reaches 5500 m (33 layers).

3.2.3 Analysis Using Alternate Ocean Subsurface Temperature Data

The Ishii et al. [2005] data set consists of 1°×1° grid temperature fields given as monthly means covering the topmost layer to 700 m from 1945 to 2003. The analysis and quality control schemes are mostly the same as Ishii et al. [2003]. The analysis domain is the same as Ishii et al. [2003] except for including the Black Sea and adding two layers, 600 m and 700 m depths, to the previous 14 layers from 0 m to 500 m depths. The apparent sea level decrease rate in 1991, which is caused by changing the observational data from the World Ocean Database 1994 (WOD94) to the operational database of the global telecommunication system and Japanese domestic communication lines, has been corrected to the expendable bathythermograph (XBT) data. This new analysis data agrees well with Levitus et al. [2005]. According to the objective analysis data, Ishii et al. [2005] reported the linear trend of steric sea level is 0.38±0.04 mm/yr between the period of 1945-2003 with the corresponding heat content change of $0.23 \pm 0.03 \times 10^{22}$ J/yr. Hereafter, the term "Ishii05" refers to the data set generated by Ishii et al. [2005].

3.3 Thermosteric Sea Level

In this Section, the comparison of thermosteric sea level variations using WOA01 and Ishii05 will be analyzed. In Equation (3.7), pressure data are needed but they are not available in data set; however, they can be computed simply from the depth data. In addition, annual temperature and salinity data are used as reference values. Thermosteric sea level variations are determined using yearly temperature data of WOA01, averaged yearly data of Ishii05, and pendatal (five-year average) data of WOA01 using Equation (3.7). Figure 3.2 shows the time series of thermosteric sea level variations (mm), which are averaged globally and weighted by areas for 1945–2003, 1955–2003, and 1947–1996, respectively. In the top panel of Figure 3.2, the red and blue curves represent the thermosteric sea level variations integrated from 0 to 500 m using Ishii05 ("I500" hereafter) and using WOA01 ("L500" hereafter), respectively. The estimated sea level trends of I500 are 0.30±0.05 mm/yr during 1955–2003, and 0.20±0.04 mm/yr during 1945–2003, respectively. The estimated sea level trend of L500 is 0.28±0.04 mm/yr during 1955–2003. In the bottom panel of Figure 3.2, the red and blue curves represent the thermosteric sea level changes integrated from 0 to 700 m using Ishii05 ("I700" hereafter) and using WOA01 ("L700" hereafter), respectively. The estimated sea level trends of I700 are 0.36±0.06 mm/yr during 1955–2003 and 0.23±0.04 mm/yr during 1945–2003, respectively. The estimated sea level trend of L700 is 0.33±0.04 mm/yr during 1955–2003. The difference of estimated sea level trend from I500 and I700, for both 1945-2003 and 1955–2003, is 0.1–0.13 mm/yr, which is twice the estimated (formal) uncertainty. This discrepancy is presumably due to interdecadal or longer variability in the ocean. The green curve represents the thermosteric sea level trend integrated from 0 to 3000 m using temperature data from WOA01 ("L3000"

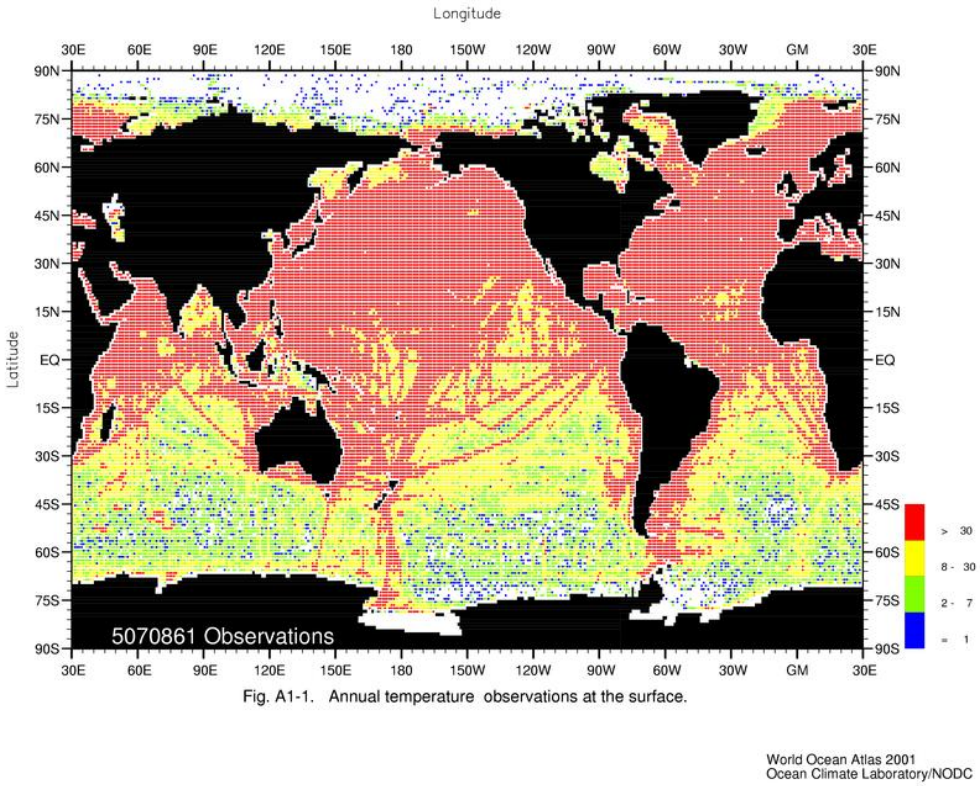

Figure 3.1: Number of annual temperature observations at the surface (WOA01 data). Figure courtesy Stephens et al. [2002].

hereafter). The sea level trend of L3000 is 0.44±0.05 mm/yr during 1957–1998. In terms of sea level trends, the thermosteric sea level trend from Ishii05 is slightly larger than the trend estimated from WOA01; however, the discrepancy is smaller than the formal error of the estimated trends, and is thus statistically insignificant. As a result, the trends of thermosteric sea level from both data sources agree reasonably well.

In all curves, the thermosteric sea level shows large decadal/interdecadal or longer fluctuations. In particular, a long period of significant rise from the end of the 1960s to the early of the 1980s followed by a rapid decrease during the 1980s and then an increase at the end of the 1980s. Compare I500 with L500 or I700 with L700, there is a 5 mm difference in amplitude in the 1980s.

In both time series of I500 and I700, there is a jump from 1995 to 1996 individually. The amplitudes of the jumps are 7.2 mm in I500 and 8.5 mm in I700, which are relatively larger than sea level changes in any other time span. In an attempt to shed some light on the cause of the jump, L500 is used to compute the geographical differences between 1994 and 1995, between 1995 and 1996, between 1996 and 1997, and between 1997 and 1998 individually (Figure 3.3). All plots of geographical differences show heat balance except for the differences between 1995 and 1996. The geographic differences of 1996 and 1997 and of 1997 and 1998 show the relatively larger positive and negative thermosteric sea level anomalies in the Equatorial Pacific Ocean while the geographic difference of 1994 and 1995 presents smoother. The heat content increased in the West Pacific Ocean near Australia from 1995 to 1996 but there is no heat

content decreasing in other regions of the world. This situation causes a jump of thermosteric sea level from 1995 to 1996 but at present there is still no natural phenomenon to explain this observed jump in thermosteric sea level.

Figure 3.4 indicates the geographical trends of L500 (upper panel), I500 (middle panel), and the geographical discrepancy between L500 and I500 globally (bottom) during 1955–2003. The global averages of L500 and I500 computed using area weights are 0.28 mm/yr and 0.30 mm/yr, respectively. The mean of the differences of thermosteric sea level between L500 and I500 is 0.02 mm/yr with a standard deviation of 0.27 mm/yr. Figure 3.5 illustrates the same as Figure 3.4 except that it uses L700 and I700 data sets. The global averages of L700 and I700 computed using area weights are 0.33 mm/yr and 0.36 mm/yr, respectively. The mean of the differences of thermosteric sea level between L700 and I700 is 0.03 mm/yr with a standard deviation of 0.31 mm/yr. Figure 3.6 shows the geographical trends of L3000 during 1947–1996 with a global average by area weights of 0.43 mm/yr. The thermosteric sea level integrating from 0 m to a deeper depth shows a slightly larger trend; however, the discrepancy of trends is only twice of the formal error and only half of the standard deviation of differences between I500 and L500 (0.27 mm/yr) or I700 and L700 (0.31 mm/yr).

In addition to further examining the global average of thermosteric sea level trends, spatial correlation coefficients are also calculated to check local trends of different models and different integration depths. The correlation coefficients of I500 with L500, and I700 with L700 are 0.83 and 0.84, respectively. The high correlation indicates that even though the temperature data are from two models used slightly different data processing methods and data sets, the estimated thermosteric sea level trends show remarkable consistency. The correlation coefficients of L500 with L3000, L700 with L3000, and L500 with L700 are 0.75, 0.78 and 0.98, respectively. The computed correlation coefficients indicate that L500, L700 and L300 are highly correlated and the geographical distributions are significantly similar even for different thermosteric sea levels with integrations down to different depths. The difference only exists on the amplitude of trends. To check the results more carefully, it is noted that the largest thermosteric sea level trend appears in the Gulf Stream (Figures 3.4–3.6). The result shows the same phenomenon as Levitus et al. [2005], which states that the North Atlantic Ocean contributes most to the increase in heat content during the last 5 decades. However, the North Atlantic anomaly has also been previously reported by Miller and Douglas [2004], who also noted that while the raw (*in situ*) hydrographical data show a narrow (~100 km) band of high temperature confined to the Gulf Stream, the interpolated Levitus data set exhibits a much wider, unrealistic temperature anomaly. Miller and Douglas [2005] also indicated WOA98v2-derived dynamic heights in the slope water region show a dramatic rise but the surrounding observed values do not, and is thus likely an artifact of the large (444 to 888 km) variable radius of influence used in the WOA98v2 objective analysis. In addition, geographical trends of Ishii05 (I500 and I700) are smoother than WOA01 (L500 and L700). This is presumably caused by different numerical procedures for interpolating the *in situ* data.

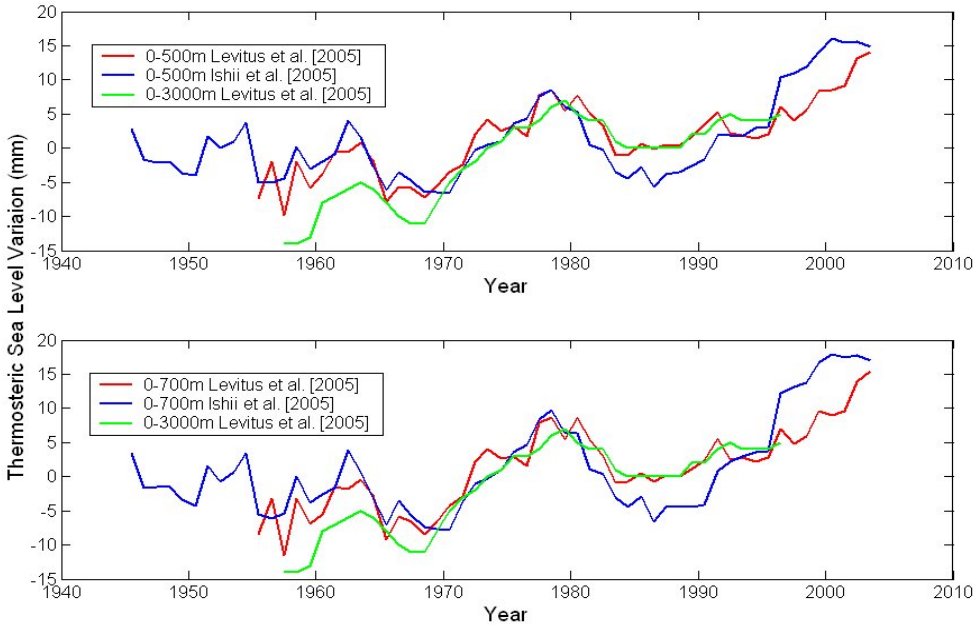

Figure 3.2: Global averaged, area-weighted thermosteric sea level variations during 1955–2003. The thermosteric sea level is calculated using Ishii05 and WOA01 and integrated from 0 –500 m, 0–700 m, and 0–3000m.

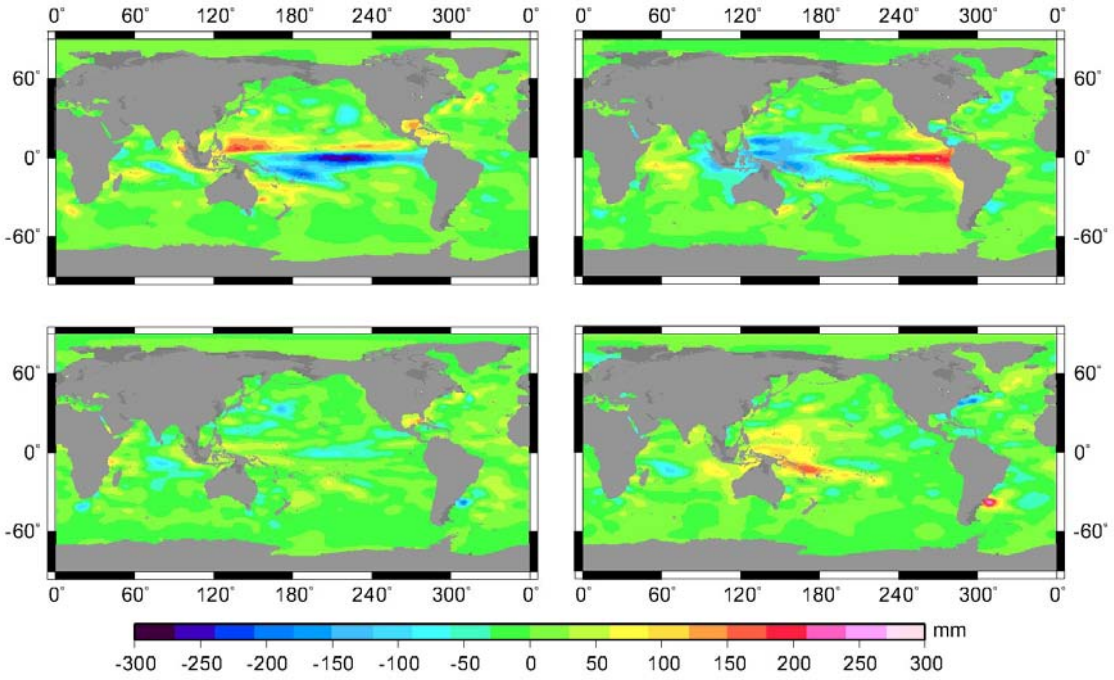

Figure 3.3: Difference of annual thermosteric sea level (mm), 0–500 m using Ishii05. Left-Top: Thermosteric sea level difference of 1997 and 1998. Right-Top: Thermosteric sea level difference of 1996 and 1997. Left-Bottom: Thermosteric sea level difference of 1994 and 1995. Right-Bottom: Thermosteric sea level difference of 1995 and 1996.

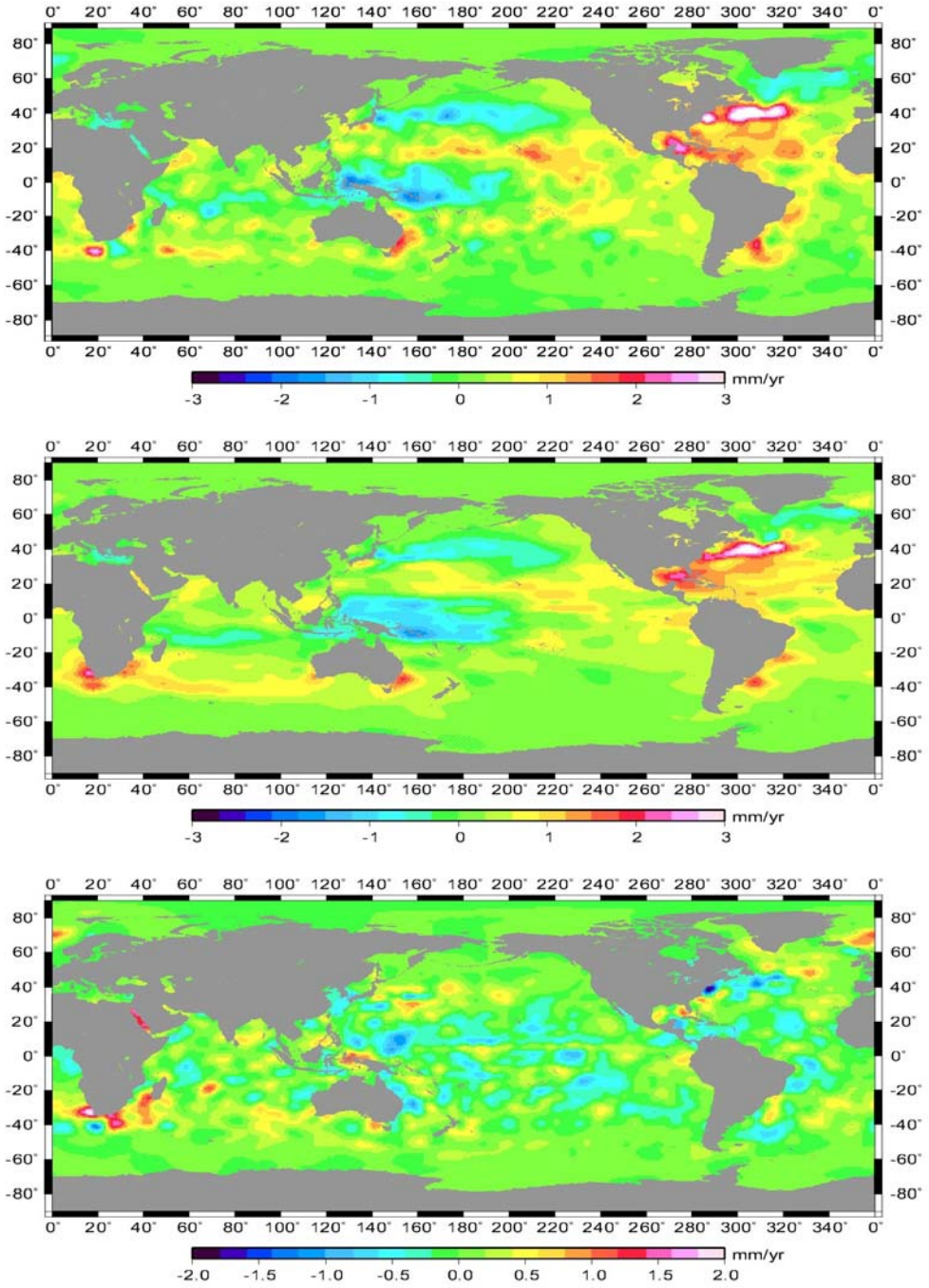

Figure 3.4: Geographical trends of thermosteric sea level, 0–500 m, during 1955–2003. Top: Yearly temperature data from WOA01 [Levitus et al., 2005]. Mean area-weighted trend is 0.28 mm/yr. Middle: Yearly temperature data from Ishii05 [Ishii et al., 2005]. Mean area-weighted trend is 0.30 mm/yr. Bottom: Geographical differences of trends between L500 and I500 . Mean of differences is 0.02±0.27 mm/yr.

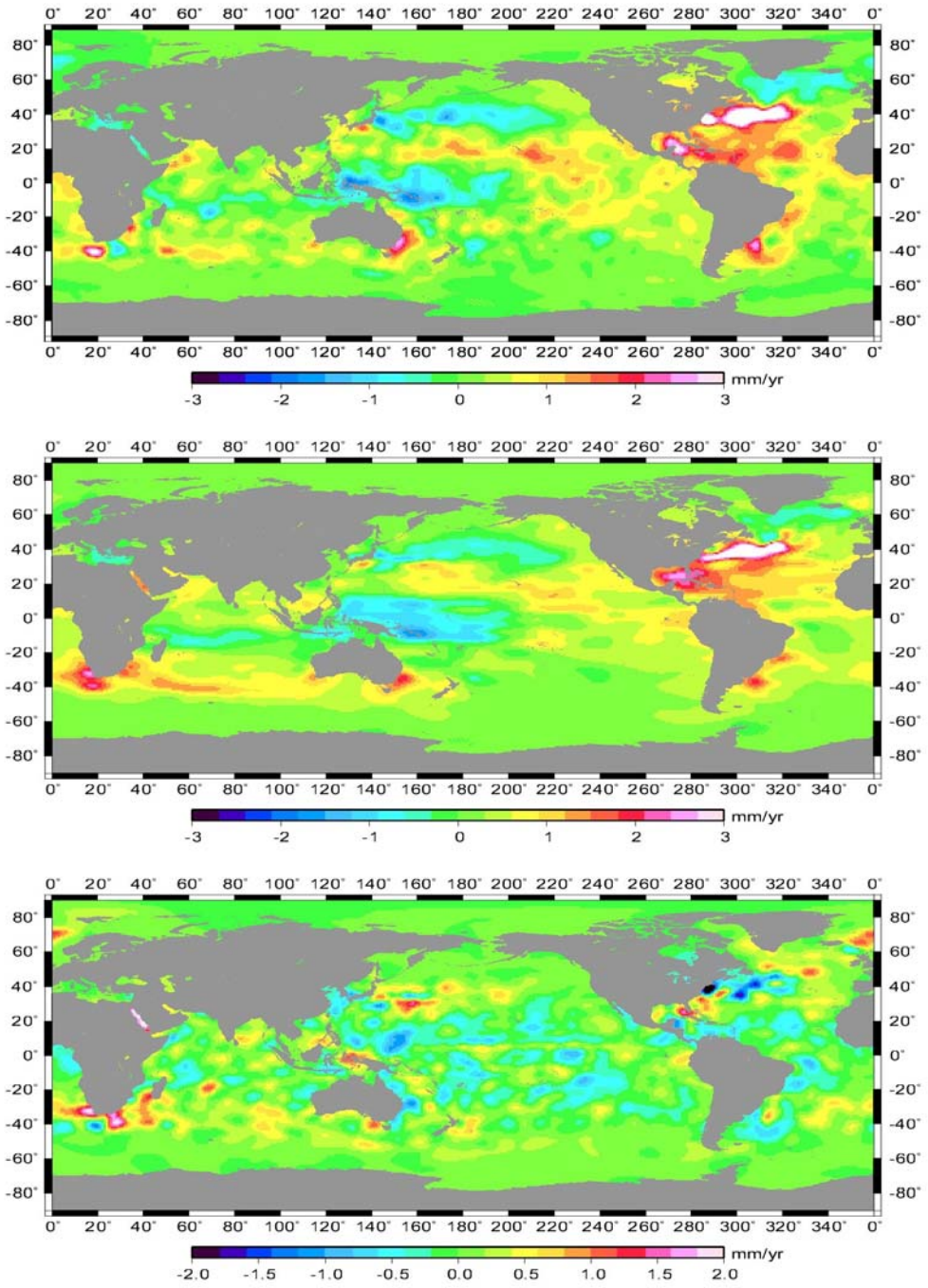

Figure 3.5: Geographical trends of thermosteric sea level, 0–700 m, 1955–2003. Top: Yearly temperature data from WOA01 [Levitus et al., 2005]. Mean area-weighted trend is 0.33 mm/yr. Middle: Yearly temperature data from Ishii05 [Ishii et al., 2005]. Mean area-weighted trend is 0.36 mm/yr. Bottom: Geographical differences of trends between L700 and I700. Mean of difference is 0.03±0.31 mm/yr.

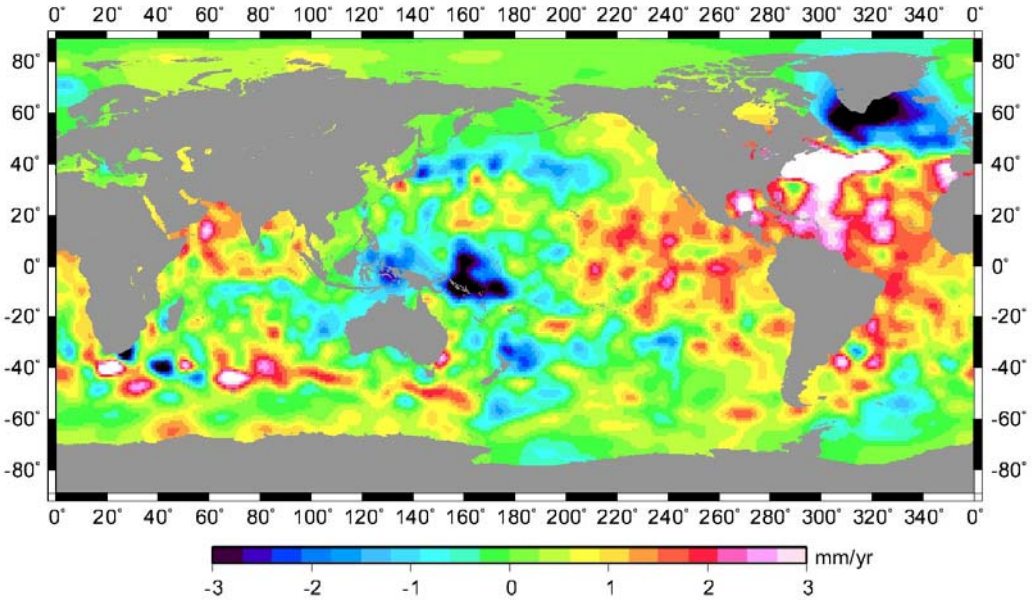

Figure 3.6: Geographical trends of thermosteric sea level variations, which are integrated from 0 to 3000 m, using pentadal temperature data of WOA01 [Levitus et al., 2005]. Mean area-weighted trend estimate is 0.43 mm/yr.

3.4 Haleosteric Sea Level and Thermosteric Sea Level

Steric sea level consists of thermosteric sea level and halosteric sea level. WOA01 and Ishii05 only contain temperature data, which can be used to calculate thermosteric sea level, so halosteric sea level is not considered in the analysis conducted in the above Sections. Antonov et al. [2002] reported the global rate of halosteric sea level change an order of magnitude smaller than the thermosteric sea level trend but with the same sign at 0.05 mm/yr. Assuming that the global salinity content remains constant, a simple thermodynamic analysis shows that there is no global distribution effect from halosteric expansion to affect sea level change [J. Willis, personal communications] and it is estimated that the halosteric effect amounts to only ~3% of the volume change in global sea level due to mass addition as a result of sea ice melting, causing decreased regional salinity. However, regional halosteric variations could potentially be larger.

In this Section, the effect of halosteric sea level in the (total) steric sea level variations is analyzed. The analysis is focused in the Eastern Pacific, a region bounded by tide gauge sites at Honolulu, San Francisco, San Diego, and Balboa, Panama [Miller and Douglas, 2004]. The region covers latitude 0^o to 40^o and longitude 200^o to 280^o. Selecting this region has several characteristics that make it ideal for this study: low mesoscale variability, narrow continental margins, and large numbers of hydrographic observations [Miller and Douglas, 2004].

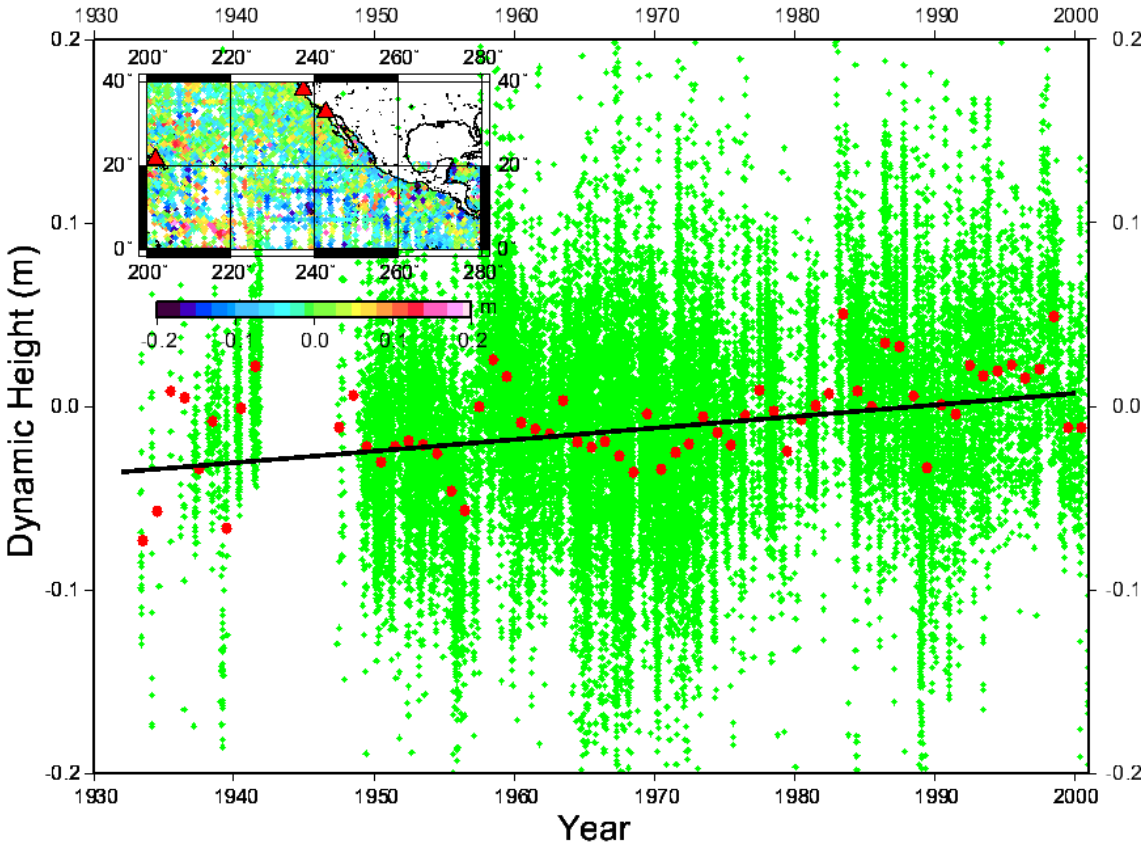

Figure 3.7: Geographical distribution and time series of steric sea level. Steric sea level is integrated from 0 to 500 m, 1930–2000. Red circles are yearly averages. Triangles represent three tide gauge stations as described in the text.

Steric sea level and thermosteric sea level (1933–2000) are calculated using OSD at each measurement locations, which are integrated from 0 down to 500 m and to 1000 m individually similar to the approach described by Miller and Douglas [2004]. Figure 3.7 shows the geographical distribution (color dots, figure inset) and time series (green dots) of steric sea level, which is integrated from 0 down to 500 m. The total number of measurements is 30,166. Red circles are yearly averages of individual data (green dots). After averaging individual data points to monthly steric sea level variations, the estimated secular trend is 0.69±0.09 mm/yr by simultaneously fitting bias, trend, semi-annual, and annual signals. Strong decadal/interdecadal signals exist. Figure 3.8 shows the geographical distribution (color dots) and time series (green dots) of steric sea level, which is integrated from 0 down to 1000 m. The number of measurements drops dramatically to 9,364 but the trend of monthly steric sea level remains consistent at 0.68±0.15 mm/yr, which is one third of the observed global sea level trend of 1.8 mm/yr [Douglas, 2001]. In this region, thermosteric sea level trend is also estimated. Table 3.1 shows the trends of steric and thermosteric sea level, which are integrated from 0–500 m and 0–1000 m (columns 1 to 4). Steric and thermosteric sea level have nearly the same trend, which means halosteric sea level contributes slightly to the steric sea level, about 0.01–0.04 mm/yr. The result has the same sign as the estimate reported by Antonov et al. [2002], 0.05 mm/yr. The rate of global halosteric sea level change is an order of magnitude smaller than the thermosteric

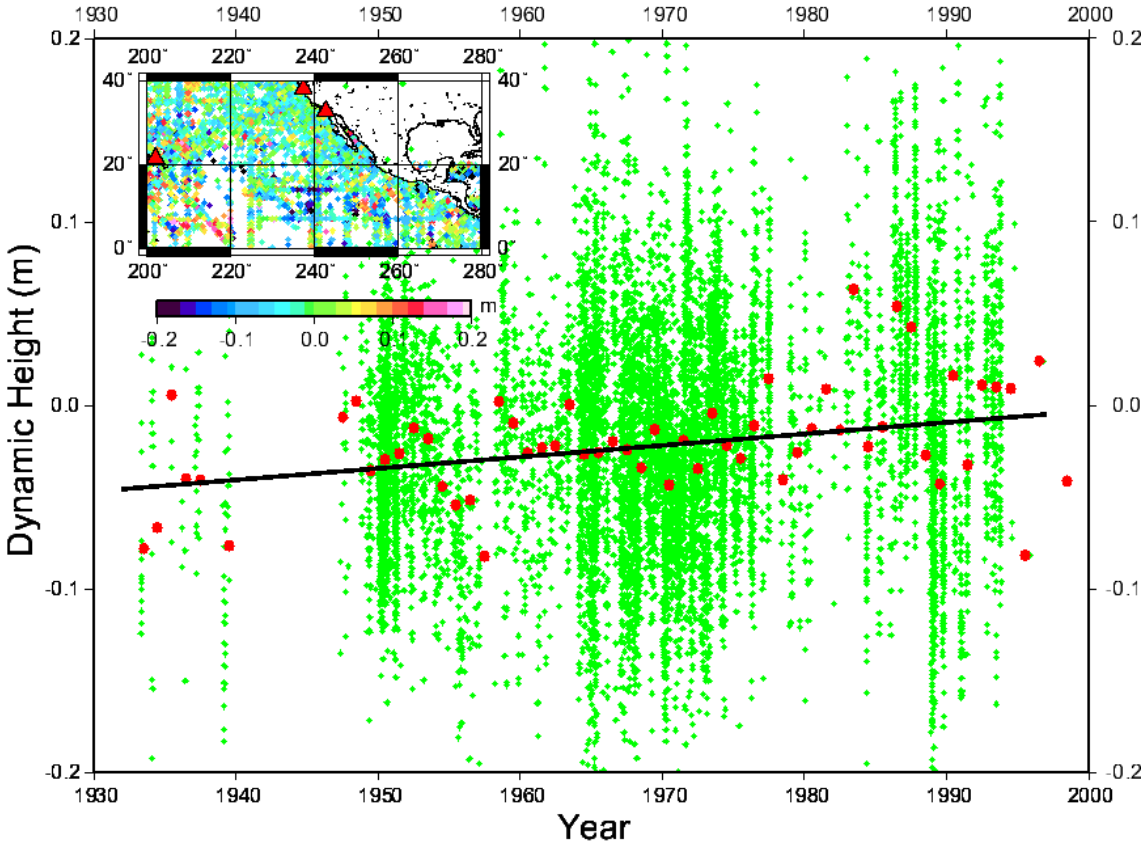

Figure 3.8: Geographical distribution and time series of steric sea level, 1933–1996. Steric sea level is integrated from 0 to 1000 m. Red circles are yearly averages. Triangles represent three tide gauge stations as described in the text.

sea level trend but both components are positive contributing to the rise of the global sea level. However, the magnitude of halosteric sea level is smaller than the (formal) uncertainty, indicating the trend estimate is unreliable. One more reason to consider only the thermosteric sea level is that salinity changes are not only caused by the change of the water volume but also by water mass, such as sea ice melting and terrestrial fresh water fluxes. Furthermore, we calculated the trend of 0–500 m thermosteric and steric sea level using only the same measurements used for the 0–1000 m case for more exact comparison (columns 5 and 6, 0.65±0.10 and 0.64±0.09 mm/yr, respectively). All cases show excellent agreement of the estimated trends, indicating that the (total) steric and thermosteric sea level trends have no significant difference in the studying area, or that the halosteric sea level trend is negligible.

The objective analysis data are also used to compute thermosteric sea level in order to compare with *in situ* data (OSD). The trend of L500 is 0.62±0.13 mm/yr in the region latitude 0^o to 40^o and longitude 200^o to 280^o and the trend of L1000 is 0.63±0.07 mm/yr. There is essentially no difference when using the objective analysis data (WOA01) or *in situ* data in this testing area. Accordingly, the objective analysis data and *in situ* data have the consistency of thermosteric sea level trends if the number of *in situ* measurements used to establish the objective analysis model is sufficiently large and perhaps the more important reason is that the

region does not have significant slope gradients of steric sea level manifested by strong mesoscale variabilities.

Steric sea level 0–1000 m	Thermosteric sea level 0–1000 m	Steric sea level 0–500 m	Thermosteric sea level 0–500 m	Steric sea level 0–500 m (I)	Thermosteric sea level 0–500 m (I)
0.68±0.15 mm/yr	0.64±0.14 mm/yr	0.69±0.09 mm/yr	0.66±0.08 mm/yr	0.65±0.10 mm/yr	0.64±0.09 mm/yr

Table 3.1: Trends of steric sea level and thermosteric sea level, which are integrated from 0 m to 1000 m and 500 m using OSD.

0–500 m (I): At the same measurement points as used in 0–1000 m

3.5 Comparison of Observed Sea Level with Thermosteric Sea Level

Cabanes et al. [2001a] show the 0–500 m thermosteric anomaly case is 3.1±0.4 mm/yr (1992-1998), agreeing with the sea level rise (3.2±0.2 mm/yr) from TOPEX-only (1992–1998) and concluded that "the upper (0-500 m) ocean thermal expansion predominately accounted for TOPEX observed sea level rise." In addition, the observed (25 tide gauges) sea level trend for 1955–96 is 1.6±0.15 mm/year, a value that agrees well with the global mean thermosteric sea level trend (0–3000 m), at 1.4±0.10 mm/year. Shum et al. [2001a] shows the comparison of the sea level changes determined from 16-year altimetry data with 0–3000 m and 0–500 m thermosteric sea level trend and indicates thermosteric sea level trend accounts for only ~30% of the observed sea level from multiple altimetry. In addition, the selection of more tide gauges (much more than the 25 gauges) would arrive at a similar conclusion during 1950–1998. Miller and Douglas [2004, 2005] also reported a disagreement with conclusions by Cabanes et al. [2001a]. They present an analysis of tide gauge and hydrographic (*in situ* temperature and salinity) observations in the Pacific and Atlantic Oceans showing that tide gauge observed sea level trend, which contains both mass and volume change, is 2–3 times higher than hydrographic data estimated trends, reflecting only volume change. Lombard et al. [2005] later present a reanalysis of the Cabanes et al. [2001a] study, with results primarily agreeing with the conclusions by Miller and Douglas [2004].

In this Section, efforts on comparing sea level variation using more tide gauge records and longer altimeter data with thermosteric sea level using WOA01 has been made. The computation of sea level changes using altimeters is described in detail in Chapter 5. The upper panel of Figure 3.9 shows thermosteric sea level (L500, L700, and L3000) and sea level variations derived by TOPEX/POSEIDON. The estimated sea level trend is relatively larger than the thermosteric sea level trend, which are 1.3 and 2.7 mm/yr during 1993–2003, respectively (column 1 in Table 3.2). The lower panel of Figure 3.9 shows the comparison of thermosteric sea level variations with the sea level variations observed by multiple satellite altimetry (GEOSAT/GM, GEOSAT/ERM, ERS-1, ERS-2, TOPEX/POSEIDON, T/P Interleave Mission, GFO, ENVISAT, and JASON-1). The comparison reaches the same result as the above

comparison. In addition, the trends of sea level and thermosteric sea level during different time spans are determined and shown in Table 3.2. During 1993–2003, the observed altimetry sea level trend is twice as much as thermosteric sea level. During 1993–1996, the difference between sea level trend and thermosteric sea level trend is only about 0.6 mm/yr except L3000. Nevertheless, the uncertainties of trends are 0.7–0.9 mm/yr. During 1985–2003 and 1985–1996, the observed sea level trends are 4–5 times higher than thermosteric sea level trends. Note that the use of longer data span (1985–2003 for multiple altimetry data span, as compared to 1993–2003 for the T/P only data span), the comparison with thermosteric sea level trend estimates for the same data span has an entirely different conclusion than when the shorter data span (T/P data span of 10 years) is used. The difference is due to the presences of decadal or longer signals making the trend estimate unreliable. Our result essentially further confirms that mass variations of sea level contribute more than water volume changes [Miller and Douglas, 2004; 2005].

Sea level variations can also be computed using tide gauges to compare with thermosteric sea level. First of all, we compared sea level variations derived from 27 tide gauge records [Douglas, 2001] with L500, L700, and L3000 (Figure 3.10). Sea level variations are determined by averaging 27 gauges at the same epoch and then averaging them to a yearly time series. Similarly, thermosteric sea level variations are determined by averaging data within 6 degrees of 27 gauge stations. Next, the sea level and thermosteric sea level trends are estimated using linear regression using only data when both measurements exist at the same epoch. The trends of L3000 and sea level derived from tide gauges are 1.82±0.14 mm/yr and 1.61±0.14 mm/yr, respectively. It agrees well with Cabanes et al. [2001a]. However, the trends of L500 and L700, at 1.38 mm/yr and 1.15 mm/yr respectively, are relatively lower than L3000. The correlation coefficients of tide gauge records and corresponding thermosteric sea level also indicate worse correlation at most of the stations which are located near the vicinity of the Gulf Stream (Tables 3.3, 3.4, and 3.5). Moreover, the ccorrelation coefficient of trends between thermosteric sea level and tide gauge sea level are 0.32, 0.55, and 0.57 for the cases L3000, L700, and L500 respectively. Trends of L500 have higher correlations with sea levels derived from 27 gauges since the trends of L500 agree well with tide gauge records in the Gulf Stream area.

Next, significantly more tide gauges (than 27) are used for the comparison. The criteria to select tide gauges are discussed in Chapter 5. There are 615 gauge stations selected for the analysis. Figure 3.11 shows the comparison of tide gauge sea level with thermosteric sea level. It should be noted that the number of gauges is not constant and not necessarily equal to 651 because there may not be thermosteric sea level data within 6 degrees of some stations which would cause the station to be edited in this study. The trends of thermosteric sea level in three cases (L500, L700 and L3000) are 0.68±0.10 mm/yr, 0.74±0.10 mm/yr, and 0.89±0.06 mm/yr, respectively. In contrast, the tide gauge sea level trends are 1.91±0.10 mm/yr, 1.97±0.10 mm/yr, and 1.32±0.11 mm/yr, respectively, and which are significantly higher than the thermosteric sea level trends. Despite the discrepancy between sea level trend and thermosteric sea level trend, both time series are highly correlated. Correlation coefficients of sea level with L500, L700, and L3000 are 0.80, 0.78, and 0.90 respectively. It should be noted that the sea level and the thermosteric sea level do not necessarily represent the real sea level and thermosteric sea level since substantial spatial averaging of measurements was done leading to this analysis, especially when substantial data gaps occur temporally and spatially. The results shows that the thermosteric sea level trend accounts for 36%, 38%, and 68%, respectively for the cases 0–500

m, 0–700 m, and 0–3000 m, of the observed tide gauge sea level trends, again confirming the conclusion of Miller and Douglas [2004], but with significantly more tide gauges.

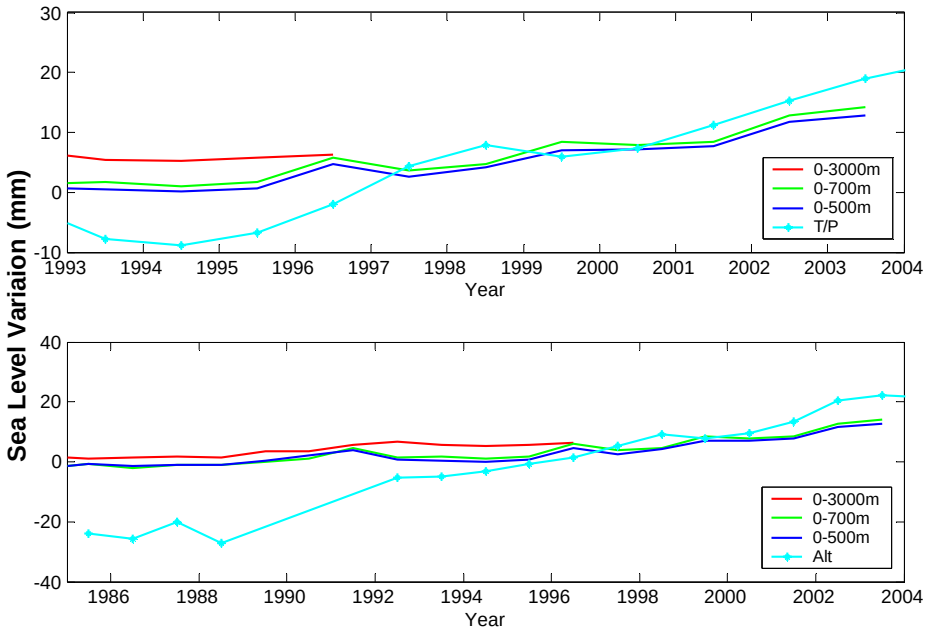

Figure 3.9: Comparison of altimetry (T/P, 1993–2003, and multiple altimetry, 1984–2003) observed sea level and thermosteric sea level from WOA01.

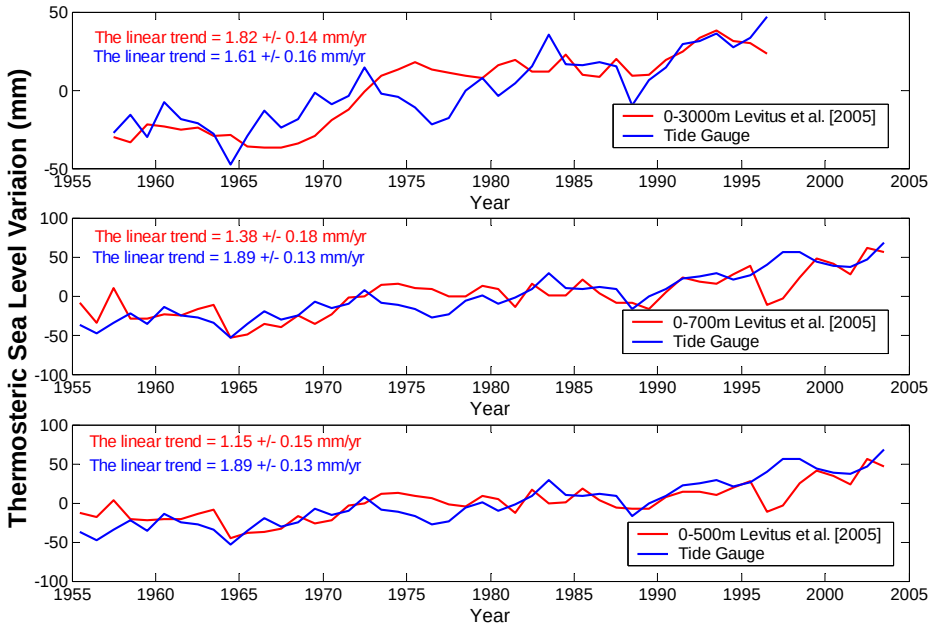

Figure 3.10: Comparison of thermosteric sea level within 6 degrees of 27 tide gauge stations and tide gauge observed sea level [Douglas, 2001].

Unit: mm/yr	1993-2003	1993-1996	1985-2003	1985-1996
T/P Only	2.76±0.21	1.93±0.93	N/A	N/A
Multiple Altimetry	N/A	N/A	2.60±0.13	2.54±0.27
0-500m	1.26±0.12	1.35±0.71	0.67±0.09	0.35±0.13
0-700m	1.26±0.15	1.29±0.78	0.76±0.08	0.49±0.13
0-3000m	N/A	0.28±0.12	N/A	0.53±0.08

Table 3.2: Comparison of estimated altimetry sea level and thermosteric sea level trends using WOA01 using different data spans.

3.6 Conclusions and Discussions

In this study, grid temperature data of WOA01 and Ishii05 have been used to compute the thermosteric sea level and its trend. The thermosteric sea level and the steric sea level and their trends are also determined using OSD (*in situ* data) in a selected area where data are more abundant. Sea level variations derived from tide gauge data and altimeters are compared with thermosteric sea level. In this analysis, global thermosteric sea level trend of upper (0–500 m) layers is about 70% of the deep ocean (0–3000m) when using the objective analysis data, whereas the thermosteric sea level trends integrated from 0–500 m and 0–1000 m have near identical trends in the Eastern Pacific whether they are determined using OSD (*in situ* data) or WOA01 (objectively analyzed grid data). The discrepancy in sea level between using OSD and WOA01 data in other regions, may be caused by inadequate sampling by *in situ* profiles, particularly in the Southern Hemisphere or Gulf Stream [Miller and Douglas, 2004]. Therefore, a more careful analysis on the deep ocean such as 500–3000 m or 500–5500 m is needed.

Halosteric sea level provides a relatively small contribution to steric sea level, which is verified using OSD and the sign is positive. The rise of halosteric sea level means the decrease of salinity, which may be interpreted in terms of both sea ice melting and fresh water added to the oceans. Melting of sea ice does not change sea level while fresh water flowing to the oceans from the continents does. Assuming reasonable bounds for the contribution of sea ice melting, Wadhams and Munk [2004] find a mass contribution to the ocean of 0.6 mm/year, a significantly large contribution to sea level and thus the result remains controversial. Presumably the error bar on this estimate is at least as large as the estimate itself, and that the computation relies on the accuracy of the Antonov et al. [2002] estimate of the halosteric sea level rise of 0.05 mm/yr during the last 5 decades.

Global thermosteric sea level contributes to the global sea level about 0.2–0.5 mm/yr with perhaps not well-determined uncertainty. It only accounts for 1/2 to 1/5 of global sea level; however, thermosteric sea level and sea level are highly correlated. Undoubtedly, steric sea level is a critical component of the global sea level signal, and warrants further study. On the other hand, if we can estimate mass variation or fresh water flowing into oceans more accurately over the past 50 years, it will provide a useful constraint on contributions of steric sea level. Recently measurements from spaceborn gravimetry by the NASA/DLR Gravity Recovery and Climate Experiment (GRACE) mission provide a new observation for land water storage [Wahr et al.,

2004] and ocean mass variations [Chambers et al., 2004]. This data set provides a new approach to study steric sea level and global sea level. In the next Chapter, we analyze ocean mass variation by comparing GRACE measurements with steric-corrected sea level derived by satellite altimetry to address the question whether GRACE can be used to constrain steric sea level in the Southern Ocean, which has the least abundance of *in situ* thermal and salinity data. Finally, the AGOS arrays are beginning to lengthen the spatial and temporal coverage of the steric measurements in the ocean, and combining with satellite altimetry and GRACE. It is expected that the quantification and understanding of steric sea level will improve in the decades to come.

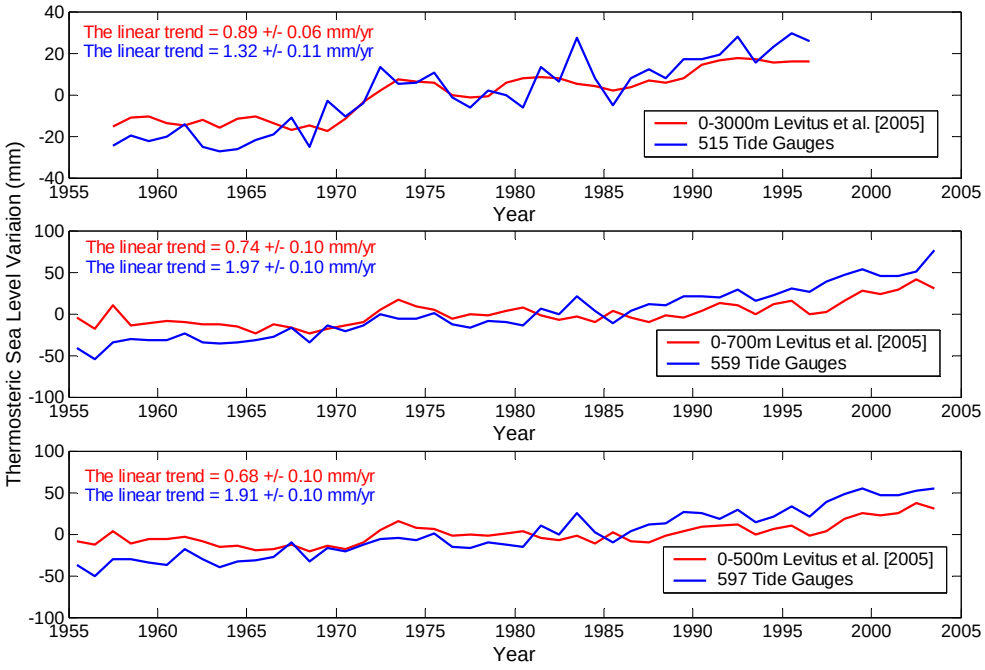

Figure 3.11: The comparison of thermosteric sea level within 6 degree of 515–597 tide gauges and tide gauge observed sea level changes.

Station ID	Trend of sea level corrected by ICE4G(mm/yr)	Trend of thermosteric sea level (mm/yr)	Correlation Coefficient
170011	0.81	-1.76	0.02
170161	0.73	-1.36	-0.38
190091	0.57	-1.06	-0.13
210021	0.53	2.36	0.05
210031	1.75	2.82	0.38
230051	-0.68	0.35	-0.31
250011	0.61	0.55	0.33
270061	0.24	0.50	0.15
690002	0.38	-1.89	0.02
690032	2.62	0.63	0.51
690022	2.18	-0.06	0.13
690012	2.21	-1.84	-0.06
760031	1.42	0.54	0.18
823031	1.86	0.47	0.39
823081	2.11	0.66	0.67
840011	0.64	1.26	0.08
860151	4.09	5.61	0.32
940041	1.40	2.28	0.55
940071	1.95	1.76	0.67
960021	2.36	1.56	0.35
960041	2.55	1.34	0.22
960081	1.22	5.77	0.71
960091	2.95	5.15	0.75
960121	1.46	6.34	0.61
960171	1.23	5.92	0.57
960181	1.23	5.08	0.48
970011	1.30	5.52	0.80

Table 3.3: Tide gauge sea level trends and thermosteric sea level trends (L3000). Correlation coefficients of tide gauge sea level with the corresponding thermosteric sea level.

Station ID	Trend of sea level corrected by ICE4G(mm/yr)	Trend of thermosteric sea level (mm/yr)	Correlation Coefficient
170011	1.35	-0.18	0.20
170161	1.19	0.34	0.43
190091	0.96	0.16	0.41
210021	0.55	-0.08	-0.14
210031	1.66	-0.32	-0.18
230051	-0.36	0.23	-0.02
250011	0.84	0.13	0.11
270061	0.72	-0.01	-0.03
690002	0.36	-0.15	0.53
690032	2.39	0.52	0.37
690022	1.93	0.14	0.39
690012	1.89	-0.31	0.37
760031	1.37	0.58	0.57
823031	1.86	0.37	0.68
823081	1.87	0.68	0.77
840011	0.73	1.13	0.29
860151	4.52	5.66	0.31
940041	1.61	1.34	0.34
940071	1.89	1.77	0.57
960021	2.41	1.17	0.37
960041	2.66	1.36	0.50.
960081	1.17	3.18	0.52
960091	3.13	2.87	0.43
960121	1.71	3.41	0.33
960171	1.41	2.75	0.39
960181	1.09	2.44	0.30
970011	1.35	3.18	0.59

Table 3.4: Tide gauge sea level trends and thermosteric sea level trends (L700). Correlation coefficients of tide gauge sea level with the corresponding thermosteric sea level.

Station ID	Trend of sea level corrected by ICE4G(mm/yr)	Trend of thermosteric sea level (mm/yr)	Correlation Coefficient
170011	1.35	-0.17	0.21
170161	1.19	0.42	0.53
190091	0.96	0.28	0.49
210021	0.55	-3.22	-0.08
210031	1.66	-0.29	-0.14
230051	-0.36	0.17	-0.01
250011	0.84	0.06	0.06
270061	0.72	-0.06	-0.04
690002	0.36	-0.10	0.59
690032	2.39	0.33	0.37
690022	1.93	0.06	0.37
690012	1.89	-0.30	0.39
760031	1.37	0.60	0.57
823031	1.86	0.37	0.68
823081	1.87	0.63	0.76
840011	0.73	1.02	0.29
860151	4.52	4.74	0.31
940041	1.61	1.17	0.34
940071	1.89	1.59	0.61
960021	2.41	1.15	0.51
960041	2.66	1.26	0.61
960081	1.17	2.30	0.51
960091	3.13	2.22	0.48
960121	1.71	2.64	0.34
960171	1.41	2.22	0.38
960181	1.09	2.07	0.26
970011	1.35	2.59	0.56

Table 3.5: Tide gauge sea level trends and thermosteric sea level trends (L500). Correlation coefficients of tide gauge sea level with the corresponding thermosteric sea level.

CHAPTER 4

SOUTHERN OCEAN MASS VARIATION STUDIES USING GRACE

The Southern Ocean provides a major link among the world oceans via complex processes associated with the melting and accumulation of the Antarctic ice sheet and the surrounding sea ice. Sea ice growth and melting affect Southern Ocean circulation and are regarded as an important forcing mechanism for the dense water formation that contributes to deep ocean circulation [Aoki, 2004]. The high-latitude ocean is strongly stratified by the warmth of its surface water [Sigman et al., 2004]. The circulation of the Southern Ocean is dominated by the zonal Antarctic Circumpolar Current (ACC), which isolates the Antarctic continent and maintains its low temperature. The ACC is primarily strongly wind-forced and is the only current that connects with other major current systems. Understanding the role of Southern Ocean circulation in climate change, its interactions with ice and atmosphere, and the potential quantification of natural and anthropogenic climate-forcing mechanisms require long-term observations and improvement in modeling. While the warming layers of subsurface of the Southern Ocean since 1950 [Gille, 2002; 2003] appears to be confirmed by satellite altimetry at least for the past decade [Cabanes et al., 2001b; Shum et al., 2003b], the forcing mechanisms responsible remain speculative. *In situ* data are extremely sparse and for example, accurate satellite altimetry like TOPEX/POSEIDON or JASON-1 is limited by their coverage and unable to observe the polar oceans beyond latitude $\pm 66^0$. However, current and future high-latitude observing satellite geodetic sensors exist, including satellite altimetry such as GFO, ERS-2, ENVISAT, ICESat (laser) and CryoSat; and spaceborne gravimetry. These sensors, with the exception of CryoSat which suffered a launch failure in October 2005, provide an opportunity to study the ocean dynamics of the seasonally or permanently sea ice covered Southern Ocean and its link to climate change.

Measuring and understanding the static and time-varying gravity field and its relationship to climate change phenomena are among the scientific objectives of the NASA/DLR Gravity Recovery And Climate Experiment (GRACE) satellite mission [Tapley et al., 2004a]. The two GRACE co-orbiting satellites are in a near-circular orbit with a mean altitude of 500 km and a mean inclination of 89^0, which enables near-polar coverage and also exhibits a ground track pattern oriented nearly along meridians on the surface of the Earth.

The GRACE mission has been successfully providing monthly observations of the Earth's gravity field since the satellites were launched in 2002 [Tapley et al., 2004a]. These observations are represented in spherical harmonic coefficients complete to degree 120 (~167 km wavelength), and have demonstrated to represent Earth's water mass redistribution at monthly temporal resolutions at a much longer spatial resolution [Tapley et al., 2004b]. Wahr et al. [2004] show that the current GRACE gravity field solutions can be used to recover monthly changes in water storage, both on land and in the ocean, to accuracies of 1.5 cm of thickness when smoothed over 1000 km spatial scale, and that the annual amplitude of large hydrological basins including the Amazon could be determined to accuracies of 1.0–1.5 cm. Chambers et al. [2004] show that the averaged GRACE ocean mass variation (within $\pm 66^0$ latitude) at annual

frequency (8.6±1.1 mm amplitude, $265^0 \pm 8^0$ phase) agrees well with the variations computed using 11 years of averaged TOPEX/POSEIDON altimetry observing sea level after correcting for steric (theromosteric and halosteric) components using analyzed monthly mean fields of WOA01. Song and Zlotnicki [2005] found good agreements between GRACE ocean mass variations and the non-Boussinesq ocean model for the annual component by subtracting the tropical Pacific Ocean bottom pressure signals from the sub-Arctic signals due to the 2002–2003 ENSO oscillation. Zlotnicki et al. [2005] compared GRACE ocean mass variations with two ocean circulation models near the polar oceans in the Pacific and concluded that the RMS are 24 mm (comparable to the signal) in the Arctic Ocean and 12 mm (much smaller than the signal) in the Southern Ocean, respectively. In part because of the GRACE near-polar orbital inclination geometry, the apparent trackiness in the North-South direction represents higher degree and order harmonic errors. In addition, the oceanic signal, while much smaller than the hydrological signal, is larger in the polar region than in the equatorial region. This aspect is also indicated by Andersen and Hinderer [2005], who estimated GRACE errors of 5 mm RMS near the poles to 13 mm around the equator.

In this Chapter, we compare the GRACE observed mass variations with the NASA/JPL Estimating the Circulation and Climate of the Ocean (ECCO) model [Fukumori et al., 1999] ocean bottom pressure, and with the steric-corrected high-latitude observing satellite altimetry (ENVISAT, $\pm 81.5^0$) ocean mass variations in the Southern Ocean to conduct a preliminary assessment of the first release of GRACE data. We will assess the potential of combining data from GRACE and high-latitude observing satellite altimetry in providing steric sea level measurements in the Southern Ocean where *in situ* ocean data are sparse or non-existent.

4.1 Data Processing

4.1.1 Ocean Mass Variations from Satellite Altimetry

Satellite altimeters such as TOPEX/POSEIDON and ENVISAT observe geocentric sea surface heights, while *in situ* hydrographic data such as the World Ocean Database 2001 (WOD01) or grid data from World Ocean Atlas 2001 (WOA01) [Stephens et al., 2002] provides steric sea level from temperature and salinity data. One method to infer observed ocean mass variations is to subtract the computed steric sea level from sea level derived from satellite altimetry [e.g., Chambers et al., 2004; Kuo et al., 2005]. Although WOA01 data covers global ocean (90^0N–70^0S) over the 50 year data span, the availability of data over the Southern Ocean is very sparse [Stephens et al., 2002]. In this study we make an approximation to use the WOA01 temperature and salinity data in the form of global objectively analyzed mean of 1^0 by 1^0 grids of 50-year averaged monthly and annual climatology to compute the steric sea level anomalies. The maximum depth for the annual analyzed mean maps reaches 5,500 m (33 layers) and for monthly mean maps, the maximum depth reaches 1,500 m (24 layers). The steric sea level anomalies are computed by integrating from 0 m depth down to 1000 m according to Equation (3.7) with annual analyzed mean fields as a reference. Steric sea level anomalies for 0–1500 m are also computed and there are no significant differences between the computed values. The 0–1000 m depth values are selected. The equation of the state (Appendix A) is used and nonlinear mixing effects of temperature and salinity data are taking into account for computing the monthly climatological steric sea level anomalies by removing the annual mean dynamic heights.

Figure 4.1 shows the geographical (upper panel) dynamic heights globally integrated from 0–1000 m and over the Southern Ocean (lower panel) using annual mean fields by Equation (3.5). In the upper panel, the density of sea-water in the equatorial ocean is relative smaller than in the higher latitude oceans. In the ocean near Antarctica or Arctic Ocean, the density of sea-water is larger, which means sea-water in these two regions is colder than the other area.

In this study, TOPEX/POSEIDON and ENVISAT radar altimeter data are used in the form of sea level anomalies with all standard and altimeter-specific instrument, atmosphere and geophysical corrections, along with associated improved corrections such as new sea state bias models, tide models, and radiometer correction, etc. Figure 4.2 (upper panel) shows the ocean mass variations observed by steric-corrected radar altimeter (TOPEX) between $\pm 66^0$ latitude bounds on February 2003 with respect to October 2003. The higher mass variations appear in the equatorial Pacific Ocean while the lower show in the western Pacific Ocean. Besides, ocean mass variations on February are generally higher than on October in southern ocean.

4.1.2 ECCO Ocean Model

Ocean models with adequate resolutions and sophisticated physical modeling are limited in the Southern Ocean primarily because of limited observations (e.g., TOPEX/POSEIDON altimeter covering only within $\pm 66^0$ latitude) and complicated dynamics due to the presence of sea ice and ice shelves. One of the promising models is the NASA/JPL's ECCO model [see Fukumori et al., 1999 for an early version of this model; see also http://www.ecco-group.org]. In this study the model run denoted kf049f, was run, which assimilated TOPEX/POSEIDON altimeter data and temperature profiles (WOCE hydrography, XBTs and profiling floats) and based on the Massachusetts Institute of Technology general circulation model (MITgcm) [Marshall et al., 1997]. The ECCO model is a nonlinear primitive equation model using the Boussinesq approximation with a vertical resolution of 46 layers from 5 m to 5,615 m, a spatial resolution of 1^0 and a near-global model domain from 72.5^0S to 72.5^0N latitude. See Lee and Fukumori [2003] for additional information about the model and its configuration. In order to overcome the vast computational requirements of the oceanic analyses, a partitioned Kalman filter and smoother [Fukumori, 2002] are employed to assimilate the observations. The model is volume conserving and does not conserve mass. Therefore, model sea level is adjusted by a time-varying, spatially uniform value assuming that total mass of the model ocean is time-invariant [Greatbatch, 1994]. The ocean model resolves spatial variability of mass, but does not simulate changes of the ocean's total mass content.

4.1.3 CPC (Climate Prediction Center) Monthly Water Storage Model

The Land Data Assimilation System (LDAS) is one of the land surface models developed at NOAA Climate Prediction Center (CPC) [Fan et al., 2003]. It is a 1x1 degree monthly grid data covering Jan. 1980 to Dec. 2004. LDAS is forced by observed precipitation, derived from CPC daily and hourly precipitation analyses, downward solar and long-wave radiation, surface pressure, humidity, 2-m temperature and horizontal wind speed from NCEP reanalysis. At the surface, it consists of all components affecting energy and water mass balance, including snow cover, depth, and albedo. However, the output only comprises soil temperature and soil moisture in four layers below the ground.

4.1.4 GRACE Ocean Mass Variations

In this study, 19 monthly gravity field solutions (April/May 2002–April 2004) from the initial release of GRACE science data products (the so-called Level 2 or L2 data products) are used [Tapley et al., 2004b]. Here the October 2003 gravity field is chosen as the reference field, which is subtracted from the other gravity fields to obtain 18 residual gravity field solutions. Most of the GRACE analysis so far have primarily used the isotropic or Gaussian filtering of a given radius which assumes that the signal-to-noise level decreases with increasing degree [Wahr et al., 2004; Chambers et al., 2004; Andersen and Hinderer, 2005; Tapley et al., 2004a; Zlotnicki et al., 2005; Song and Zlotnicki, 2005]. Davis et al. [2004] used the F-Test to select GRACE coefficients representing significant reduction of the annual signal variance in the data. First of all, the correlation of GRACE L2 was tried to be analyzed, with combination of ECCO and CPC. Spherical harmonic coefficients based on grid water mass redistribution data considering the Earth's elastic response to the load can be computed as follows [Wahr et. al., 1998]:

$$\begin{Bmatrix} \overline{C}_{nm}(t) \\ \overline{S}_{nm}(t) \end{Bmatrix} = \frac{3(1+k_n)\sigma_w}{4\pi R\sigma_E(2n+1)} \iint h(\theta,\lambda,t)\overline{P}_{nm}(\cos\theta) \begin{Bmatrix} \cos m\lambda \\ \sin m\lambda \end{Bmatrix} \sin\theta d\theta d\lambda , \qquad (4.1)$$

where $\overline{C}_{nm}$ and $\overline{S}_{nm}$ are the spherical harmonic coefficients; n is degree and m is order; θ is co-latitude and λ is longitude; h is water thickness. k_n is the load Love number of degree n that describes the Earth's elasticity; σ_w is the density of water (1000 kg m^{-3}). $\overline{P}_{nm}$ is the fully normalizing associated Legendre function; σ_E is the average density of the Earth (5517 kg m^{-3}).

CPC hydrology model and ECCO model only have data on land and in ocean respectively. Therefore, globally grid data can be accessed by combining CPC and ECCO models. After computing spherical harmonic coefficients of the combination of CPC and ECCO data according to Equation (4.1), the phase correlation coefficients are calculated using the spherical harmonic coefficients of 15-month GRACE L2 solutions and the combination of CPC and ECCO. Figure 4.3 indicates spatial correlation coefficients between the harmonic coefficients of GRACE L2 and the combined geophysical models. High correlations are found mostly at low degree and order (n and m < 15), but some of the higher degree (15 < n < 30) and lower order (m < 15) are also well correlated. It indicates the estimates of GRACE L2 are not only degree dependent but also order dependent. Therefore, in this study, a non-isotropic filtering of the GRACE L2 data products with a 500 km (latitude) by 1000 km (longitude) filter is performed [Shum et al., 2004; Han et al., 2005b], which is an extension of the filter based on selection of coefficients with high correlations with signals computed from geophysical (hydrological and ocean) models [Kuo et al., 2004a].

Water thickness variations can be derived by a formula [Wahr et. al., 1998] using spherical harmonic coefficients:

$$\Delta h(\theta,\lambda) = \frac{a\sigma_E}{3\sigma_w} \sum_{n=0}^{\infty} \sum_{m=0}^{n} \overline{P}_{nm}(\cos\theta) \frac{(2n+1)}{(k_n+1)} \times (C_{nm}\cos(m\lambda) + S_{nm}\sin(m\lambda)) . \qquad (4.2)$$

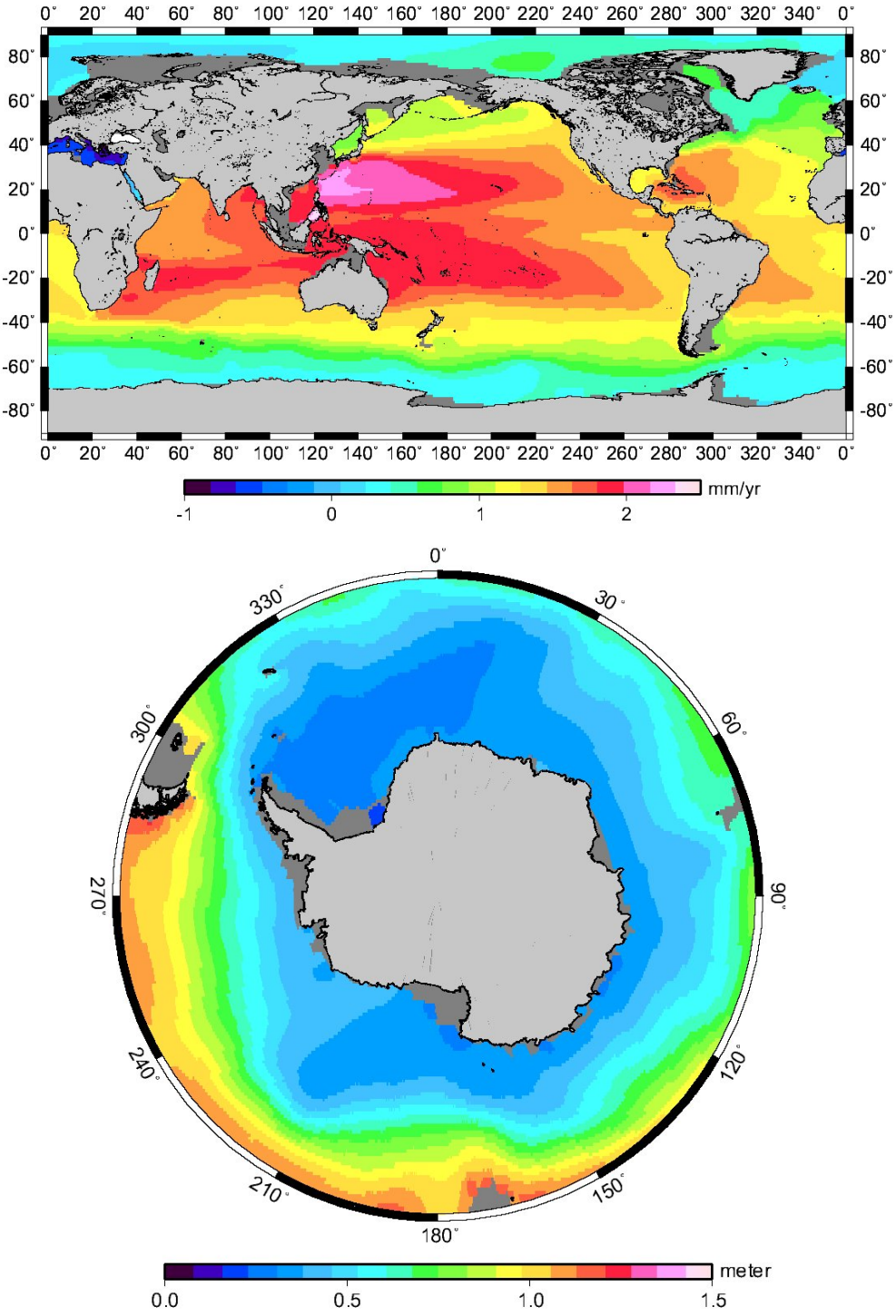

Figure 4.1: Dynamic heights computed for 0–1000 m using analyzed annual mean fields of WOA01 (Top). Southern Ocean projection is shown on lower panel.

To be noticed, when comparing ocean mass variations derived by GRACE and steric-corrected sea level derived from altimeters, $(1+k_n)$ should be eliminated since the loading effect is included in the measurements of altimeters yet. For the sake of reducing noise involved in coefficients, Non-isotropic filter could be applied to harmonic coefficients. Non-isotropic filter, $W(\theta,\lambda,\theta',\lambda')$, depends only on the angle γ between two points (θ,λ) and (θ',λ') [Swenson et. al., 2002].

$$W(\theta,\lambda,\theta',\lambda') = W(\gamma) = \frac{b}{2\pi}\frac{\exp[-b(1-\cos\gamma)]}{1-e^{-2b}},$$
$$b = \frac{\ln(2)}{(1-\cos(r_{1/2}(m)/a))}, \tag{4.3}$$

where $r_{1/2}(m)/a$ is the half width of the Non-isotropic smoothing function. a is the mean radius of the Earth. $r_{1/2}(m)$ should be written as:

$$r_{1/2}(m) = r_o - (r_o - r_1)\frac{m}{m_{\max}}, \tag{4.4}$$

where m is the order, m_{max} is the maximum order (usually the same value as the maximum degree), r_o is the smallest averaging radius, and r_1 is the largest averaging radius. The coefficients after smoothing are

$$\begin{bmatrix}\hat{C}_{nm}\\ \hat{S}_{nm}\end{bmatrix} = W_{nm}\begin{bmatrix}C_{nm}\\ S_{nm}\end{bmatrix}, \tag{4.5}$$

where

$$W_{nm} = \frac{2\pi}{\sqrt{2n+1}}\int_0^{\pi} W(\gamma)\overline{P}_{n0}(\cos\gamma)\sin\gamma d\gamma .$$

Here, W_{nm} could be computed recursively as following:

$$W_{0m} = 1,$$
$$W_{1m} = \frac{1+e^{-2b}}{1-e^{-2b}} - \frac{1}{b},$$
$$W_{n+1,m} = -\frac{2n+1}{b}W_{nm} + W_{n-1,m}. \tag{4.6}$$

There is an indication of large scatter of GRACE estimated J_2 coefficients as compared to satellite laser ranging (SLR) solutions [Ries, 2004] and instead of substituting the J_2 coefficients using the SLR solutions, they were chosen not to be included [Wahr et al., 2004]. Ries [2004] also indicates good agreement between GRACE and SLR solutions for C_{21}, S_{22}; however, worse

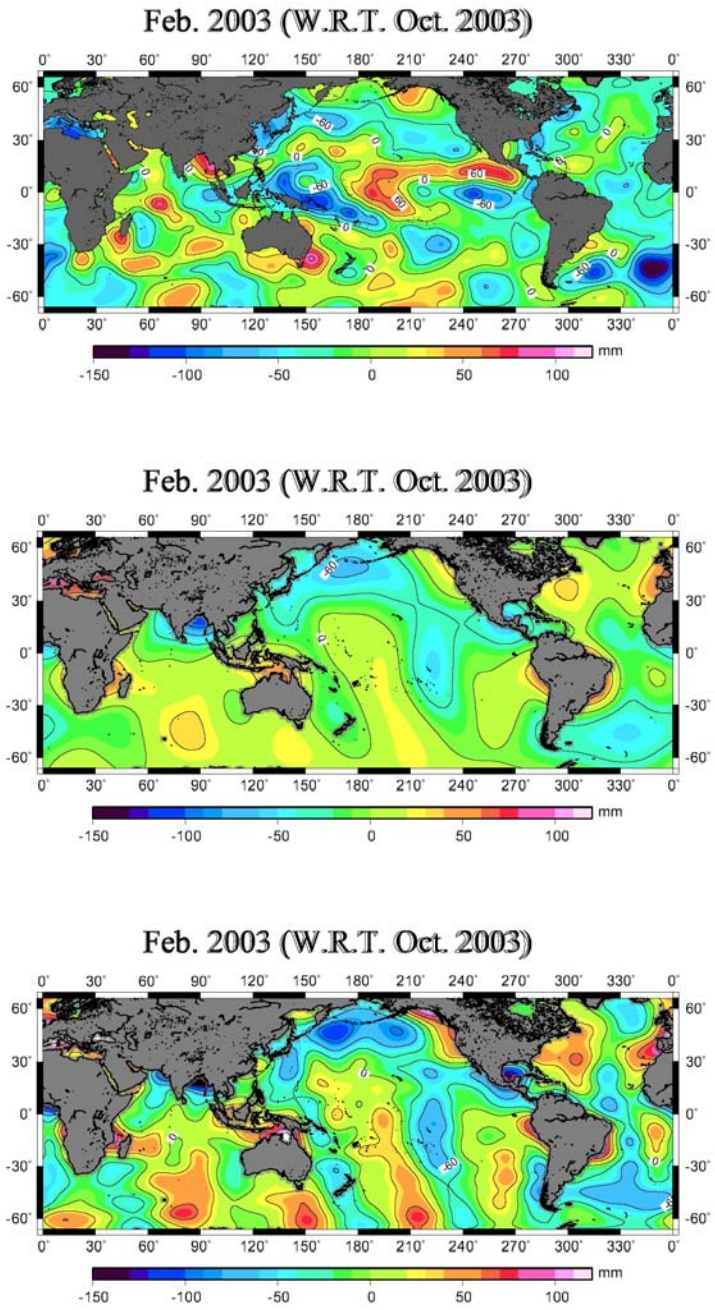

Figure 4.2: Ocean mass variations derived from steric-corrected TOPEX ($\pm 66^0$ latitude) (top), GRACE using isotropic filter(1000 km radius), and GRACE using non-isotropic filter (500 km by 1000 km) in February 2003 (with respect to October 2003).

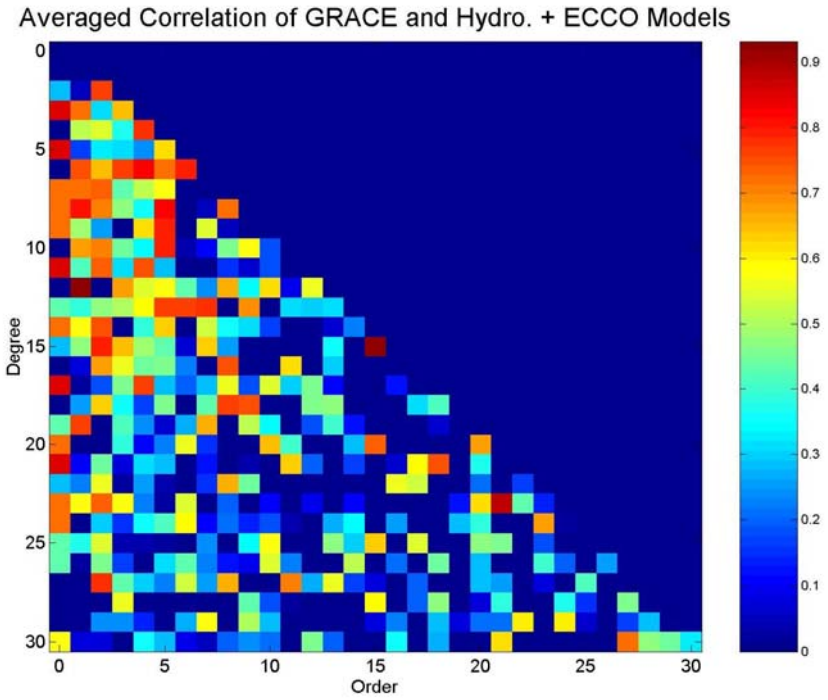

Figure 4.3: Correlation coefficients between GRACE L2 and geophysical models.

agreement for S_{21} and S_{22}. C_{20} or $-J_2$ is the only coefficient not used here. The secular rate of low degree zonals ($n = 2$ to 5) to GRACE is not removed, since only seasonal signals are assessed and the effects are relative small with the order of $<10^{-11}$ as well. In addition, pole tides [Walhr, 1985] and geocentric (degree one coefficients) corrections are applied to the GRACE data. The pole tides are easily computed as described in Wahr [1985]. Modeling the pole tide requires knowledge of proportionality constants, the so-called Love numbers, and a time series of perturbations to the Earth's rotation axis, a quantity that is now measured routinely with space techniques. Geocenter correction is derived using geocentric vector (X_{cm}, Y_{cn}, Z_{cm}) from Lageos-1 and Lageos-2 SLR [J. Ries, personal communications] in accordance with Chen at al. [1999]. Figure 4.4 shows the components X (top), Y (middle), Z (bottom) of observed geocenter solutions from Lageos-1 and Lageos-2 SLR and interpolated values at GRACE measured epoch charactered by circles. In terms of degree one fully normalized Stokes coefficients ($C_{1,1}, S_{1,1}, C_{1,0}$) can be expressed as:

$$C_{1,1} = X_{cm} / R / \sqrt{3},$$
$$S_{1,1} = Y_{cm} / R / \sqrt{3},$$
$$C_{1,0} = Z_{cm} / R / \sqrt{3}. \qquad (4.7)$$

Nerem et al. [2005] reported different geocenter models applied to correct harmonic coefficients derived by GRACE affect the estimates of annual amplitudes and phases of global ocean mass variations significantly.

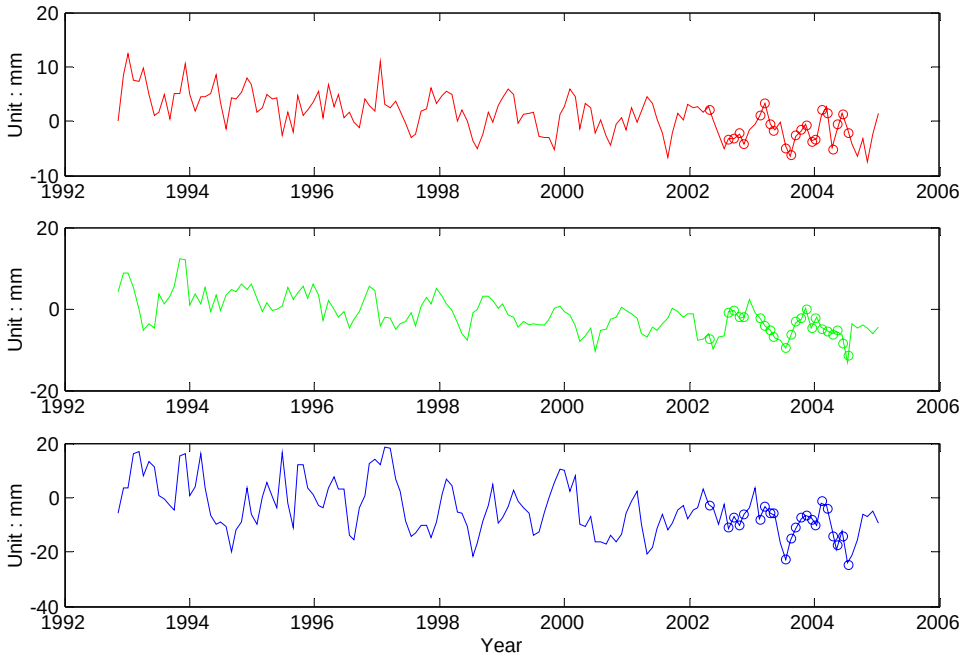

Figure 4.4: Components, X (top), Y (middle), and Z (bottom), of observed geocenter solutions from Lageos-1 and Lageos-2 SLR. The circles are the interpolations at GRACE time [J. Ries, personal communications].

Since GRACE observes ocean mass variation in the form of ocean bottom pressure, as a result of combined atmosphere and ocean forcing, atmospheric effect sensed by GRACE does not have to be removed to compare with steric-corrected satellite altimetry [e.g., Chambers et al., 2004]. Here, GRACE product was selected to be used, which has already been de-aliased by a barotropic ocean model and to compare with inverted barometer corrected altimetry ocean mass variations.

Figure 4.2 shows the ocean mass variations observed by GRACE using isotropic filter (1000 km radius) (middle) and the non-isotropic filter (500 km latitude and 1000 km longitude) [Han et al., 2005b] (bottom) in February 2003 relative to October 2003. The mass variations from GRACE by the isotropic filter show much less signals; however, the N-S trackiness or error pattern is more pronounced in the non-isotropic filtered GRACE observations.

In addition, an alternatively processed GRACE data product was employed as *in situ* (at altitude) potential differences using the GRACE inter-satellite ranging measurements (the so-called Level 1B, or L1B data) based on energy conservation principle [Han, 2004c; Han et al., 2004a]. The resulting *in situ* potential differences are used in a regional inversion [Han et al., 2004b] for GRACE observations with enhanced spatial and temporal scales [Han et al., 2005a] over the Southern Ocean (-60^0 south poleward).

	Amplitude (mm)	Phase (^{0}) (from Jan 1)
Steric-Corrected TOPEX	9.3 ± 0.6	270 ± 3.5
GRACE (this study, with J_2)	9.1 ± 0.6	238 ± 3.6
GRACE (no geocenter correction)	5.4 ± 0.4	272 ± 4.5
GRACE (this study)	7.3 ± 0.7	246 ± 5.3
GRACE, Chambers et al [2004]	8.6 ± 1.1	265 ± 8

Table 4.1: Comparison of estimated annual amplitudes and phases of global ocean mass variations from steric-corrected TOPEX, non-isotropic filtered GRACE, and other studies using GRACE [Chamber et al., 2004] and using hydrological models [Cazenave et al., 2000].

4.2 Results and Discussions

Table 4.1 shows the comparison of global annual signals (amplitudes and phases, phases are defined in degrees from January 1) estimated using 18-months of the ocean mass variations observed by GRACE, with steric-corrected TOPEX variations and other studies. It is shown that excluding of J_2 changes the amplitude by more than 1.8 mm. Chambers et al. [2004] study (isotropic filtered GRACE ocean mass variations) and this study have good agreement with 0.7 mm in amplitude and 19^o (~19 days) in phase differences. The agreement of (non-isotropic filtered) GRACE and steric-corrected altimeter ocean mass variations is within 2 mm of the amplitude and within 24^o of the phase. In addition, estimated annual amplitude increases obviously and phase drops around 20^0 after geocenter corrections are applied.

Fig. 4.5 shows the comparisons of the area-averaged ocean mass variations from GRACE, steric-corrected TOPEX altimetry, and ECCO (kf049f run) ocean bottom pressure for the time period 2002–2004. All three data types (in a global average) show good agreements, except that ECCO model ocean bottom pressure tends to become more negative after the end of 2003. Table 4.2 (left) shows that the RMS of the difference and the correlation coefficient between GRACE and steric-corrected TOPEX (global ocean) is 4.60 mm and 0.80, respectively, indicating good agreement; compared to 9.04 mm and 0.61 between GRACE and ECCO, indicating worse agreement.

Next, study region is focused on the Southern Ocean with the evidence that the ocean mass variations are much larger in the polar ocean than that of the variations near the equator or in the mid-latitude [Zlotnicki et al., 2005; Song and Zlotnicki, 2005]. Three different GRACE data products for 18 monthly solutions from April/May 2002 to April 2004 (referenced to October 2003) were used for the Southern Ocean study. They are (1) the GRACE L2 product using isotropic filter with 1000 km smoothing radius [e.g., Chambers et al., 2004], (2) the non-isotropic filtered L2 GRACE data product with 500 km (latitude) by 1000 km (longitude) smoothing [Shum et al., 2004, Han et al., 2005b], and (3) regionally inverted GRACE gravity field using *in situ* potential (denoted as L1C data product) [Han et al., 2005a]. Fig. 4.6 shows the comparison of the monthly averaged ocean mass variations geographically (February 2004 with respect to October 2003) in Southern Ocean derived by the steric-corrected ENVISAT (top left), and the three different GRACE data types, the non-isotropic filtered GRACE (top right), GRACE regional inversion or L1C (bottom left), and isotropic filtered GRACE (bottom right).

Fig. 4.7 shows the comparison of monthly ocean mass variations from GRACE (non-isotropic filtering), GRACE regional inversion (L1C), steric-corrected ENVISAT altimetry, and ECCO model ocean bottom pressure, from April 2002–April 2004. Table 4.2 (right) shows the RMS of differences and correlation coefficients between GRACE L1C and steric-corrected ENVISAT altimetry are 22.9 mm and 0.46, respectively, which are considerably better agreement than between GRACE (non-isotropic filtered data) and ENVISAT, at 41.8 mm and 0.39, respectively. It should be noted that the steric sea level anomaly is climatology and that the data are largely missing or very sparse in the Southern Ocean. GRACE observations with non-isotropic filter are considerably different from the preliminary regional inversion solution (Fig. 4.6 and 4.7) and Table 4.2 (middle column, RMS of difference is 28.3 mm and a correlation of only 0.15). At present, it is difficult to assess which GRACE observation types or steric-corrected ENVISAT altimetry is more correct.

Global ($\pm 66^0$) RMS (mm)/Correlations		Southern Ocean (-60^0 to -75^0) RMS (mm)/Correlations		
GRACE vs TOPEX	GRACE vs ECCO	GRACE vs ENVISAT	GRACE vs GRACE L1C	GRACE L1C vs ENVISAT
4.60/0.80	9.04/0.61	41.75/0.39	28.32/0.15	22.91/0.46

Table 4.2: Comparison of GRACE data products and steric-corrected altimetry (TOPEX and ENVISAT) in the global and southern ocean.

The vicinity (longitude: 15E to 65 E; Latitude: 50S to 75S) of the Japanese Antarctica station, Syowa station, is at the outset of the Shirase Glacier drainage basin and located in the Lutzow-Holm Bay, E. Antarctica. Fig. 4.8 shows the comparison of monthly ocean mass variations observed by steric-corrected ENVISAT altimeter, GRACE L2 with non-isotropic filter, and the ocean bottom pressure of ECCO model in the Lutzow-Holm Bay, E. Antarctica study area (latitude: 50S to 750S and longitude: 15E to 65E), from January 2002–June 2004 (except ENIVSAT, which spans from January 2003– June 2004). Red curve represents steric-corrected ENVISAT altimetry observed ocean mass variations. Steric sea level anomalies are integrated from 0–1000 m using WOA01 objective analyzed temperature and salinity data accounting for nonlinearity. Blue curve represents the monthly mass variations of GRACE L2 (without J2 coefficients) with non-isotropic smoothing (500 km by 1000 km) [Shum et al., 2004; Han et al., 2005a]. Cyan curve represents the monthly variations of ocean bottom pressure data from the ECCO model. The RMS of differences between GRACE and ENVISAT, GRACE and ECCO, ENVISAT and ECCO, are 33.0 mm, 21.2 mm, and 23.0 mm, respectively. Correlation coefficients are 0.15, 0.20 and 0.70. The steric-corrected ENVISAT altimeter shows high correlated with ECCO model. The relatively poor comparison is expected due to the poor coverage and accuracy of hydrographic (WOA01) data in the study region and the error due to potential inadequate sampling of ENVISAT data due to ice-covered ocean. Figure 4.9 shows the comparison of the two GRACE mass variation products: the non-isotropic filtered (L2) data [Han et al., 2005b] and the *in situ* processed GRACE data (so-called L1C data product) [Han et al., 2005a] in the Lutzow-Holm Bay, E. Antarctica study area, January 2002 – June 2004. It is noted that there are significant differences with RMS 15.4 mm between the two data products and correlation coefficient is 0.56. In particular, the first annual amplitude of the non isotropic

L2 data is smaller than that of the subsequent year, while the L1C data product has similar annual amplitudes.

4.3 Conclusions

We provide an assessment of the first release of the GRACE observations of the Southern Ocean mass variation (April/May 2002–April 2004) using ENVISAT radar altimetry corrected for steric sea level using NOAA's World Ocean Atlas 2001 climatology, and the ocean bottom pressure data of ECCO model. The annual signal of ocean mass variations in general agrees well between the GRACE and the steric-corrected TOPEX altimetry globally. Among the three GRACE data products used, the isotropic filtered GRACE observations using a 1000 km radius smoother, the non-isotropic filtered GRACE data using a 500 km (latitude) by a 1000 km (longitude) smoother, and a preliminary solution of regional inversion using GRACE *in situ* potential measurements, the last data product has the best agreement with RMS difference of 22.9 mm and a correlation of 0.46 with the ocean mass variations derived by the steric-corrected ENVISAT altimetry. In East Antarctica, RMS of difference between L1C and GRACE L2 is 15.4 mm and the correlation coefficient is 0.56. The causes of the discrepancy can be attributed to the error in the steric sea level due primarily to lack of data in the Southern Ocean, and possible ENVISAT data sampling problem due to sea ice. The chapter presents a study to assess the role of GRACE observed long-wavelength mass variations in potentially improving the estimates of the steric sea level over Southern Ocean.

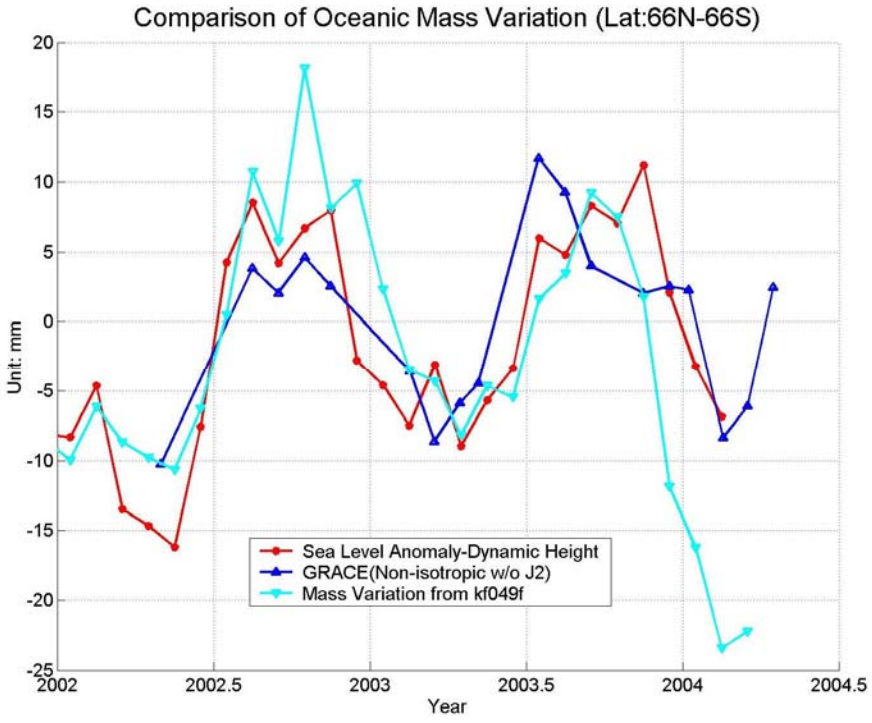

Figure 4.5: Comparisons of monthly area-averaged ($\pm 66^0$ latitude) ocean mass variations from GRACE, steric-corrected TOPEX altimetry, and ECCO ocean bottom pressure for the time period 2002–2004.

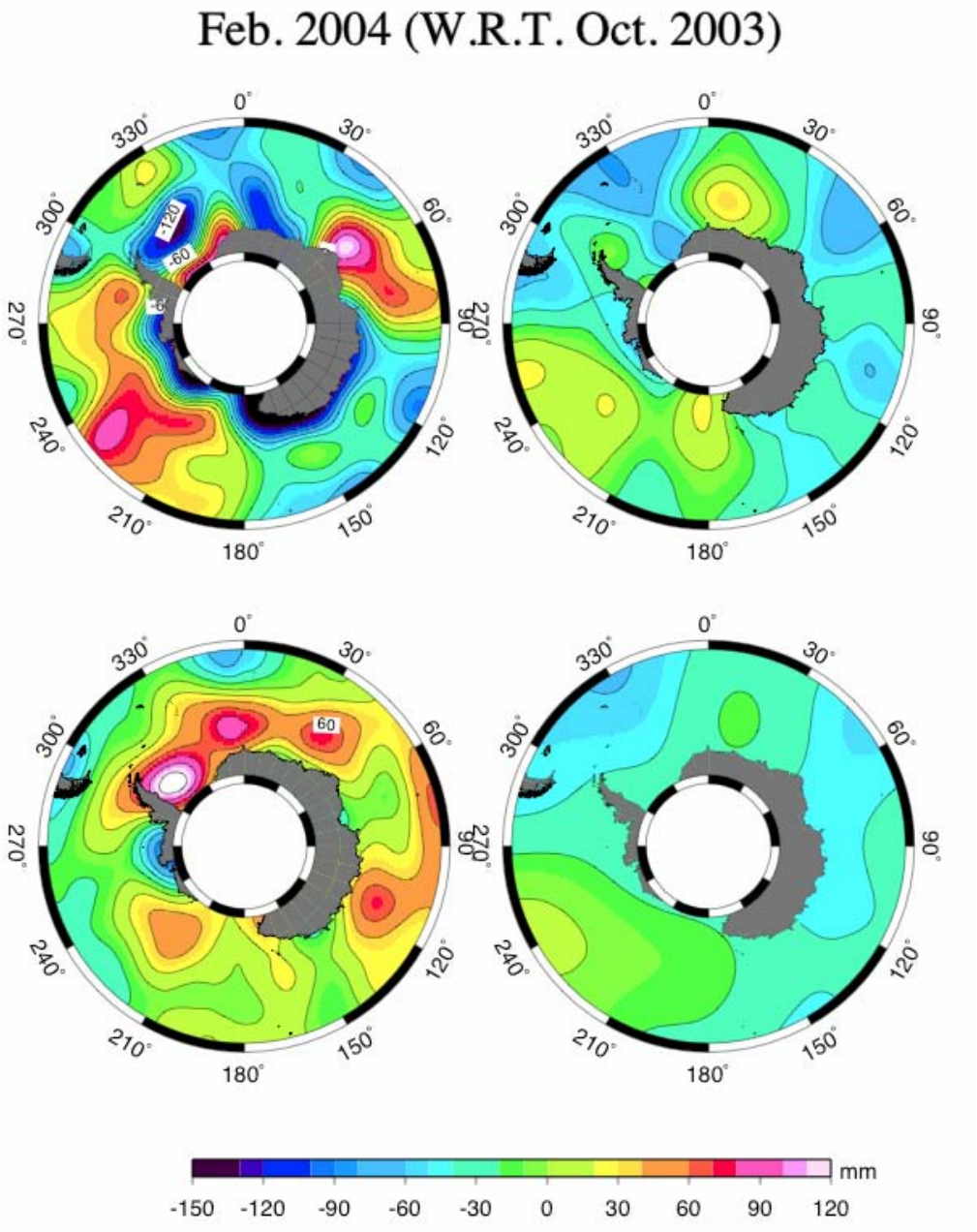

Figure 4.6: Comparison of monthly (February 2004 with respect to October 2003) ocean mass variations in Southern Ocean derived from steric-corrected ENVISAT (top left), non-isotropic filtered GRACE (top right), GRACE regional inversion or L1C (bottom left), and isotropic filtered GRACE (bottom right).

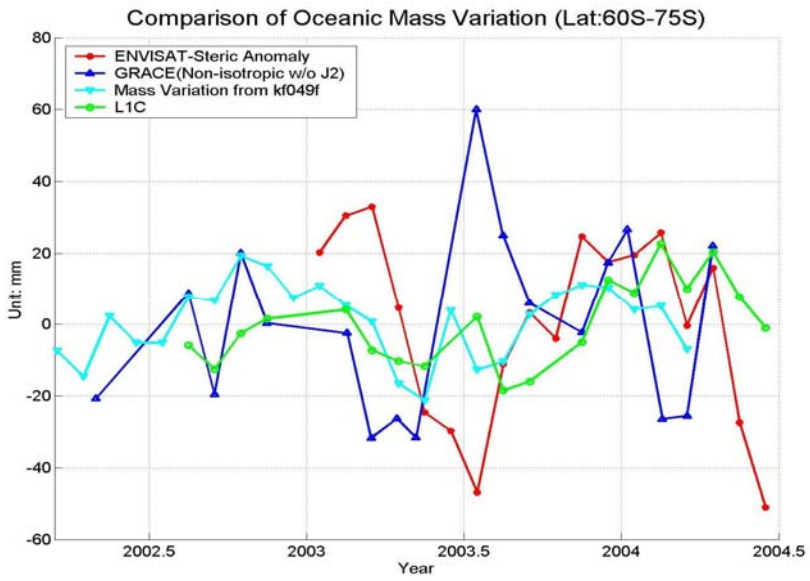

Figure 4.7: Comparison of monthly area-averaged ocean mass variation in Southern Ocean derived from GRACE (non-isotropic filtering), GRACE regional inversion (L1C), steric-corrected ENVISAT altimetry, and ECCO model ocean bottom pressure.

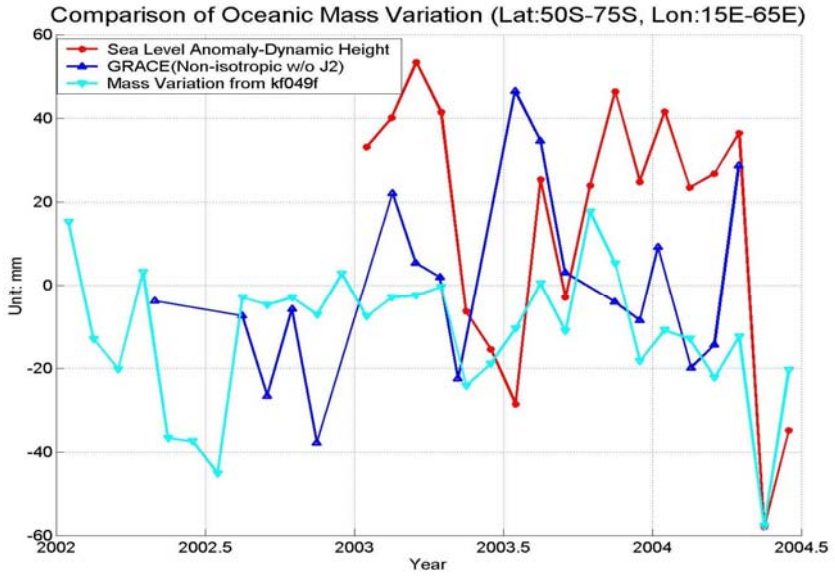

Figure 4.8: Comparison of monthly ocean mass variations derived from steric-corrected ENVISAT, non-isotropic filtered GRACE, and ECCO model in the Lutzow-Holm Bay, E. Antarctica study area, January 2002 – June 2004

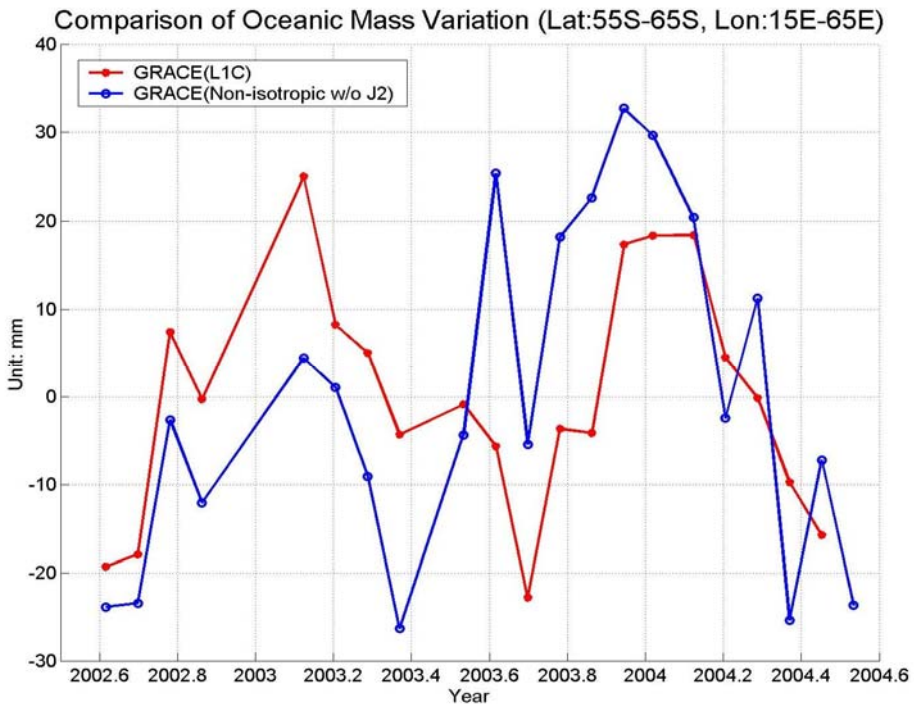

Figure 4.9: Comparison of the two GRACE mass variation products: the non-isotropic filtered data [Han et al., 2005b] and the *in situ* processed GRACE data (so-called L1C data product) [Han et al., 2005a] in the Lutzow-Holm Bay, E. Antarctica study area, January 2002 – June 2004.

CHAPTER 5

GLOBAL SEA LEVEL TREND OBSERVED BY SATELLITE ALTIMETRY AND TIDE GAUGE RECORDS

Global sea level variations have been determined using tide gauge records collected over the last century [Gornitz, 1982, 1995; Barnett, 1990; Peltier, 1988, 2001; Trupin and Wahr, 1990; Shennan and Woodworth, 1992; Douglas, 1991, 1995, 1997; Mitrovica and Davis, 1995; Ekman, 1998, 2000; Woodworth et al., 1999; Douglas et al., 2001; Mitrovica et al., 2001; Shum et al., 2002b; Church et al., 2004; Miller and Douglas, 2005], resulting in determinations of the rate of global mean sea level rise in the range of 1.5 to 2.4 mm/yr, with the suggestion of a possible acceleration since the middle of the last century [Barnett, 1984; Woodworth, 1990]. The advantage of tide gauge records is that long records up to 150 years are available. However, there are two major limitations using tide gauges for long-term sea level trend determination. First, the locations of tide gauge stations do not distribute evenly and globally. Most stations are situated along the continental coastlines in the northern hemisphere, especially in the western equatorial Pacific ocean, while others are located on islands or in the southern hemisphere coastlines, with almost no long-term gauges near Antarctica. As a result, the determination of sea level trends is not necessarily in agreement using different methods and weights. The second problem is crustal vertical motions at tide gauge benchmarks, resulting in the difficulty to separate vertical motions and absolute sea level variations. At present, the applicable solution is to apply PGR corrections using a specific model [Douglas, 2001; Peltier, 2001]. However, vertical motions still contain signals other than PGR, such as tectonic motions, local land subsidence, and post-seismic deformation due to earthquakes. Consequently the error caused by vertical motions in determination of global sea level trend still exits apparently. Miller and Douglas [2005] demonstrated a morphological approach, based on the trends of relative sea level rise as a function of distance from the centers of the ice loads at last glacial maximum. The resulting rate of sea level rise is close to 2 mm/yr, which is argued that they do not depend on PGR models.

The other emerging observational technique, satellite altimetry, can overcome the limitations of tide gauges when they are used for sea level trend determination. Altimeter measurements of sea surface topography are geocentric sea surface heights, which are relative to the center mass of the Earth using accurately determined satellite orbit defined in a well-maintained terrestrial reference frame. Therefore, vertical motions do not affect the sea level measurements from altimeters. In addition, altimeters can provide nearly global coverage of measurements and some of altimeters are designed as repeated orbits, which measure the almost same locations one cycle after the other, capable of averaging which further improve the accuracy of sea level measurements, for instance, TOPEX/POSEIDEN has a 9.9-day repeated orbit. However, the limitation of satellite altimetry is its much shorter time span (~10–20 years), whereas tide gauges have records longer than 150 years.

Satellite radar altimeters have a potential to definitively measure the long-term (decades) global sea level changes with a spatial scale of 50 km and with an accuracy approaching 1 mm/yr [e.g., Nerem and Mitchum, 2001; Shum et al., 2000, 2001a, 2001b, 2002b; Urban et al., 1999,

2001b]. Altimeter derived sea level using TOPEX data alone [e.g., Nerem and Mitchum, 2001; Cabanes et al., 2001b; Cazenave and Nerem, 2004] with less than 10 years of data is inhibited by interannual and decadal signals of the ocean and only covers $66°N$ to $66°S$ when large-scale interannual and longer period natural variations of the ocean are substantial [Sturges, 1990]. One possible way to deal with this shortcoming is to link two or more satellite altimetry missions occurring at different times in order to create a longer combined time series and extend the coverage to global area (up to latitude $\pm 81.5^0$). If the relative instrument biases between altimeter systems are well known via absolute calibrations [e.g., Haines et al., 2003] and cross-calibrations, the consequence would be a better observation of long-term global sea level rise. Stringent technical details are needed to exploit the use of multiple radar altimeters for measuring global sea level. WOCE (and Great Lakes) tide gauges have been used to "link" or determine the relative instrument biases between different altimeter systems [Guman et al., 1997; Urban et al., 1999, 2001; Shum et al., 2000]. However, the ~20-year (1984–2005, with data gaps in 1988–1992) altimetry data (GEOSAT, ERS-1/-2, GFO, TOPEX/POSEIDON, ENVISAT, and JASON-1) probably still could not resolve the true 20^{th} century sea level changes because of the presence of low frequency signals as long as or longer than the data span (see also Chapter 7).

Satellite altimeters have their own limitations. Errors in orbit determination, media and geophysical corrections, and the altimeter bias drift could significantly render altimetry useless for sea level determination. Nevertheless, improved instrument, media, and geophysical corrections have been periodically updated to constantly improve the accuracy of the resulting sea level data. In addition, routine operation of dedicated absolute calibration sites (e.g., Harvest for TOPEX/POSEIDON and JASON) has also enabled to monitor the altimeter instruments.

In this Chapter, the trends of global sea level variations are determined using tide gauge data and altimeter data individually. A comparison of sea level variations derived from altimeters and tide gauges at the same time span will be analyzed to understand the discrepancy of resulting estimated trends. Additionally, the estimated biases of altimeters relative to TOPEX/POSEIDON are described as well.

5.1 Global Sea Level Trends Observed by Satellite Altimetry

5.1.1 Satellite Altimeters

(1) TOPEX/POSEIDON:

The TOPEX/POSEIDON satellite was launched on August 10, 1992, by the cooperation of the United States National Aeronautics and Space Administration (NASA) and the French Centre d'Etudes Spatials (CNES). The satellite measures oceanographic signals, especially the ocean tides, in order to observe and to understand the ocean circulation. It equips two altimeters working alternatively because of sharing the same antenna. The U.S. TOPEX altimeter reaches a precision about 2 cm, and the French POSEIDON altimeter measures with a precision about 3 cm. TOPEX/POSEIDON makes measurements with a precision of 1.7 cm and overall accuracy of 4.7 cm. The high accuracy of TOPEX/POSEIDON attributes to the following improvements. The TOPEX Microwave Radiometer measures the water vapor path delay for correcting the altimeter range. The dual-frequency (Ku-band and C-band) altimeter measures the electron

content of the ionosphere allowing the correction of path delay for TOPEX. The correction for POSEIDON is derived from DORIS ionosphere maps. In addition, the orbit of TOPEX/POSEIDON is about 550 km higher than ERS-1 and GEOSAT, significantly reducing gravity and atmospheric drag effects on the satellite. The success of TOPEX/POSEIDON creates a good foundation for monitoring ocean from space and has ensured the place of satellite oceanography as both a prominent and bountiful area of scientific study [Urban, 2000].

The TOPEX altimeter has redundant A and B hardware. A low degradation of TOPEX Side-A (TSA) has been noticed from cycle 130. Therefore, after 6-year of exclusive Side-A operation, the TOPEX Science Working Team and the Jet Propulsion Laboratory engineers decided to evaluate the performance of Side B. Since 15:04 UTC on February 10, 1999, TOPEX Side-B (TSB) has been switched on for the future operation [TOPEX Team, 2000; Hayne and Hancock, 2000]. On September 15, 2002 TOPEX/POSEIDON was maneuvered off its initial orbit into an orbital position halfway between that of JASON tracks, which is flying along the former TOPEX/POSEIDON ground tracks. Since then, the two spacecraft have been operational, scanning the ocean surfaces to obtain a sampling grid twice as dense as before. This interleave mission demonstrates the scientific capabilities of a constellation of optimized altimetric satellites.

(2) GEOSAT

The U. S. Navy launched GEOSAT (GEOdetic SATellite) on March 12, 1985, and it began mapping the marine geoid. Data from initial 18 months of its Geodetic Mission (GM) were classified because of military value, but after 1996 the high spatial resolution data set became publicly available. Following the GM, GEOSAT started a 17-day Exact Repeat Mission (ERM) beginning November 8, 1986, which focused on the study of mesoscale oceanographic features. The quantity of GEOSAT ERM data decreased due to tape recorder failure in October of 1989. Because GEOSAT ERM follows the groundtrack of the first half of the SEASAT mission, the data from this phase therefore have been available to the public since 1986.

GEOSAT lacked a microwave radiometer to measure water vapor along the altimeter path and the satellite is equipped with only a single-frequency Ku-band (13.6 GHz) altimeter. The correction for the ionosphere path delay was calculated by models (e.g., the IRI model or the GPS Ionosphere Maps). GEOSAT provided valuable data for the study of global mean sea level variations, reaching an instrumental precision of 5 cm.

(3) ERS-1

The ERS-1 satellite was launched on July 17, 1991 by the European Space Agency (ESA). Generally the mission is to observe the Earth's atmosphere and ocean. Specifically, ERS-1 served wide objectives, which include understanding coastal zones and global ocean processes, improving global weather information, and applying remote sensing data to coastal, ocean and ice exploitation. The precision of the ERS-1 single-frequency Ku-band radar altimeter is reported as about 3 cm. The ERS-1 Microwave Radiometer (EMR1) detected water vapor in troposphere to correct path delay. Precise Range and Range-rate Equipment (PRARE) was the primary tracking system for ERS-1. After PRARE was damaged due to radiation, Satellite Laser Ranging

(SLR) tracking supplied adequate data for precise orbits to be computed to support the altimetry mission.

(4) ERS-2

ERS-2, the follow-on from ERS-1, was launched by ESA on April 21, 1995. ERS-2 is almost identical to ERS-1 including the radar altimeter and the microwave radiometer. For one year, ERS-1, ERS-2, and TOPEX/POSEIDON actively measured the oceans, and in the meantime ERS-2 followed ERS-1 by exactly one day in an identical orbit. The PRARE tracking system on ERS-2 is fully-working, thus the orbit accuracy, about 3.5 cm, is better than ERS-1 relying on SLR tracking only. ERS-1 was subsequently placed in stand-by mode in 1996 and retired in 2000.

(5) GFO-1

The GEOSAT Follow-On 1 (GFO-1) satellite was launched by the U.S. navy on February 10, 1998. The mission of GFO-1 is to measure ocean topography. The real-time data is available to scientific and commercial users through NOAA (National Oceanic and Atmospheric Administration). The satellite follows the 17-day repetitive orbit of GEOSAT ERM. GFO-1 is currently operational, with an accuracy of sea surface height measurements of about 5 cm rms.

(6) JASON-1

Following the success of the TOPEX/POSEIDON mission, JASON-1 was launched into a similar orbit to TOPEX/POSEIDON on December 7, 2001 by cooperation between NASA and CNES. The purpose of JASON-1 mission is to provide near-real-time data on sea surface height (SSH) in order to observe the oceans, and further to predict climate. Orbiting at an altitude (1,336 kilometers) higher than TOPEX/POSEIDON, JASON-1 gained precision through minimizing both atmosphere drag and the Earth's gravity. JASON-1 is the first of a series of altimeter satellites designed to be operational for decades. JASON-1 is scheduled to be taken over by its successor, JASON-2, in 2008.

(7) ENVISAT

The ENVISAT satellite (Environmental Satellite) was launched on March 1st, 2002 by ESA. It is the follow-on of the ERS missions. Its mission is to observe the Earth's ocean, land, ice, and atmosphere for the purpose of climatological and environmental research. ENVISAT carries ten optical and radar instruments among them with a radar altimeter. The altimeter is mainly for topography of the Earth's surfaces as well as correcting orbit along with three other complementary instruments on board. Its orbital period is 35 days same as ERS-2 and some of the ERS-1 phases. ENVISAT is expected to have at least five-year lifetime in its orbit offering near-real time data for scientific, operational, and commercial uses.

5.1.2 Determination of Sea Level Changes Using Altimeter Data

A number of issues should be noticed when global sea level variations are derived from multi-satellite altimeters. First of all, geophysical corrections should be identical, such as ocean tide corrections. Secondly, a reference surface that measurements of sea surface heights from altimeters are referred to should be selected when global sea level change is determined by the satellite altimetry method. Some examples of reference surfaces are geoid models, reference ellipsoids, and models combining the geoid and mean dynamic topography such as a mean stackfile surface and a high resolution mean sea surface model derived from altimeter data. The effect of using different reference surfaces in the determination of global sea level change is demonstrated by Guman [1997] and he reported that mean stackfile surface is a better surface and there is only slight difference of using a mean stackfile surface and using a high resolution mean sea surface model. In this study, a mean sea surface model, OSUMSS95 [Yi, 1995], is selected to be a reference surface in order to derive sea level anomalies utilizing multi-satellite altimetry missions. The reason to employ OSUMSS95, not a mean stackfile surface, is the mean stackfile surfaces determined by different altimetry missions have relative biases depending on locations, so the relative biases are difficult to be determined precisely. Besides, the mean stackfile of GEOSAT/GM altimeter is not available since it is not a repeated mission.

In addition to removing a reference surface from sea surface heights observed by altimeters, the relative biases and datum shifts should be considered carefully as well. All biases and datum shifts of altimeter data are derived with respect to TOPEX/POSEIDON altimeter (Table 5.1) provided by Yi [personal communication] except for JASON and GFO-1. TOPEX interleave mission is assumed to have no bias relative to TOPEX/POSEDON. The procedure to determine the biases of GFO-1 and JASON with respect to TOPEX/POSEIDON is described as follows. First of all, the “fast delivery” tide gauge records are provided by World Ocean Circulation Experiment (WOCE), with a latency of only 1–3 months and excellent for validation and comparison with altimeters. There are a total of 151 tide gauges available, which give monthly measurements referring to a reference. Secondly, altimeter measurements are averaged within 3 degree of every gauge station in form of a monthly time series. To avoid measuring different signals by altimeter and tide gauges, the correlation coefficients of tide gauge records with JASON, TOPEX interleave mission, GFO-1, and TOPEX/POSEDON are calculated. It is noted that no inverted barometer (IB) corrections are applied to both altimeter measurements and gauge records to make consistency, while PGR corrections are applied to gauge records. If the correlation coefficient is <0.8, the measurements at this gauge station are edited. In contrast, when the correlation coefficient is >0.8, the mean of difference between gauge records and altimeter data at a station is used for the comparison. The bias of an altimeter relative to TOPEX/POSEIDON is computed by averaging the differences of means at all stations, which are determined by subtracting the mean of difference between the altimeter and gauge data from the mean of difference between TOPEX and gauge data. The purpose of introducing tide gauge records is to link the measurements of two altimeters that do not have an overlap in time span. In this study, GFO and TOPEX/POSEDON have the overlap in time span, so do TOPEX interleave mission and JASON-1. For that reason, the biases are determined by simply averaging the means of differences between two altimeters at all stations. The procedure can avoid the errors contributed by tide gauge records and reduce the discrepancy caused by the case where the altimeter and the gauge do not measure at the exact same location. However, the limitation

exists when there is only short overlap of time span for both instruments. Figure 5.1(a) shows the biases between GFO and TOPEX/POSEIDON at tide gauge stations. The mean of the differences is 28 mm, which is consistent with 30.0 mm determined by Shum et al. [2001b]. Figure 5.1(b) shows the bias between JASON and TOPEX interleave mission at tide gauge stations. The mean of difference is 95.5 mm, which has also a good agreement with 98 mm derived by Shum et al. [2003a]. This approach only attains a value for the global bias. However, in this study, even if the global bias is not accurately determined, the residual geographical biases are further removed simultaneously with sea level trends and other parameters in a least squares adjustment.

For GEOSAT altimeter, not only the relative bias but also the datum shift with respect to TOPEX/POSEIDON is considered. Datum shift of GEOSAT is estimated using the formula:

$$dx\cos(\varphi)\cos(\lambda) + dy\cos(\varphi)\sin(\lambda) + dz\sin(\varphi), \qquad (5.1)$$

where φ and λ are latitude and longitude. Required parameters are shown in Table 5.1. Geographically dependent biases and datum (x-, y-, z-) shifts are due to geographically correlated gravity errors in the altimetric satellite orbits, reference frame errors, inherent weakness in tracking instrument to vertical component (z-axis) (e.g., Tranet Doppler tracking for GEOSAT, GPS tracking), and altimeter instrument problems. Here, all the biases and datum shifts are all relative to TOPEX/POSEIDON, the most accurate altimeter system before JASON and ENVISAT.

After removing the effects of the reference surface, the relative bias, and the datum shift from sea surface heights observed by an altimeter, the residuals are called sea level anomalies (SLA) or sea level variations in this study. Afterward, two kinds of approaches to determine sea level variations are proposed. The first method is to determine the rate of sea level variations using a time series, which is obtain by averaging sea level anomalies globally with area weights in a 9-day time interval. The other approach is to store sea level anomalies in $1^\circ \times 1^\circ$ grid and the rate of sea level variations are individually estimated in each grid. As a result, the geographic sea level trends can be determined. The formula to fit the rates of sea level variations can be expressed as:

$$SLA = a_i + bt + c\sin(2\pi t) + d\cos(2\pi t) + e\sin(4\pi t) + f\cos(4\pi t), \qquad (5.2)$$

where a_i is the residual bias. i is the index of altimeter missions (1-9). b is the secular rate of sea level. c and e are amplitude of the sine term, respectively. d and f are the amplitude of the cosine term. SLA is the measurement of sea level anomaly.

The unknown parameters a_i, b, c, d, e and f could be estimated using least squares algorithm that is to best fit the measurements of sea level variations in each grid or the time series. Furthermore, outliers are considered for 99% confidence of t-distribution.

5.1.3 Recovery of Residual Biases and Trends

Whether the residual biases and the trend of altimeter data can be exactly detected based on Equation (5.2) may not be clearly evident. Therefore, this Section intends to clearly demonstrate the recovery of residual biases and trend by a numerical simulation experiment when a known value of offset is added to the global time series of SLA, and then the offset is 'recovered' using our developed methodology. Figure 5.2 shows the time series with error bars of global ($\pm 81^0$ latitude) sea level variations from various altimeters with all known corrections applied including instrument drifts and IB corrections. Biases of altimeters relative to TOPEX/POSEIDON and datum shifts in Table 5.1 have been removed. Error bars shown in Figure 5.2 are 4.2 mm, 5.0 mm, 5.0 mm, 6.7 mm, 7.0 mm, 6.7 mm; 11 mm, 10 mm, and 10 mm for TOPEX/POSEIDON, TOPEX interleave mission, JASON-1, ERS-1, ERS-2, ENVISAT, GEOSAT/GM, GEOSAT/ERM, and GFO, respectively, which are given empirically. Obviously, there are still small biases relative to TOPEX/POSEIDON exist. Equation (5.2) is introduced here again to estimate the residual biases and global sea level trend by weighting altimeter data in accordance with error bars. Four cases are examined and the outcome of the residual biases relative to TOPEX/POSEIDON and the trend are addressed in Table 5.2. Case I shows the relative residual biases and the trend of 2.7 mm/yr using the original time series of Figure 5.2. The maximum relative residual bias equals -13.0 mm, GEOSAT/ERM altimeter. The relative residual bias of TOPEX interleave mission is equal to -0.7 mm, which confirms the assumption there is no bias between TOPEX/POSEIDON and TOPEX interleave mission. In Case II, the values present the result by using the same time series as Case I except for adding a known 20 mm offset to GEOSAT/GM and GEOSAT/ERM. Accordingly the biases and the trend are recovered perfectly. Similarly, a known 20 mm offset is added to ERS-1 and ERS-2 in case III and it is also added to GFO and ENVISAT in CASE IV to examine. The 20 mm offset could be recovered in all cases and estimated global sea level trend is identical at 2.7 mm/yr. The conclusion from the simulated study confirms the robustness of our methodology in the estimated trend of global sea level variations even if the relative biases in Table 5.1 may still have small and negligible errors.

	GEOSAT/GM	GEOSAT/ERM	ERS-1	ERS-2
Relative bias	-103 mm	-116 mm	Phase C : 394 mm Phase E : 400 mm Phase F : 400 mm Phase G : 434 mm	53 mm
Datum shift	dx = -44.6 mm dy = 15.2 mm dz = -138.2 mm	dx = -40.7 mm dy = -0.5 mm dz = -141.4 mm		
	ENVISAT	JASON-1	TOPEX interleave mission	GFO-1
Relative bias	481 mm	95.5 mm	0 mm	28 mm

Table 5.1: Relative Bias Estimates and Datum Shift between Altimeter Systems.

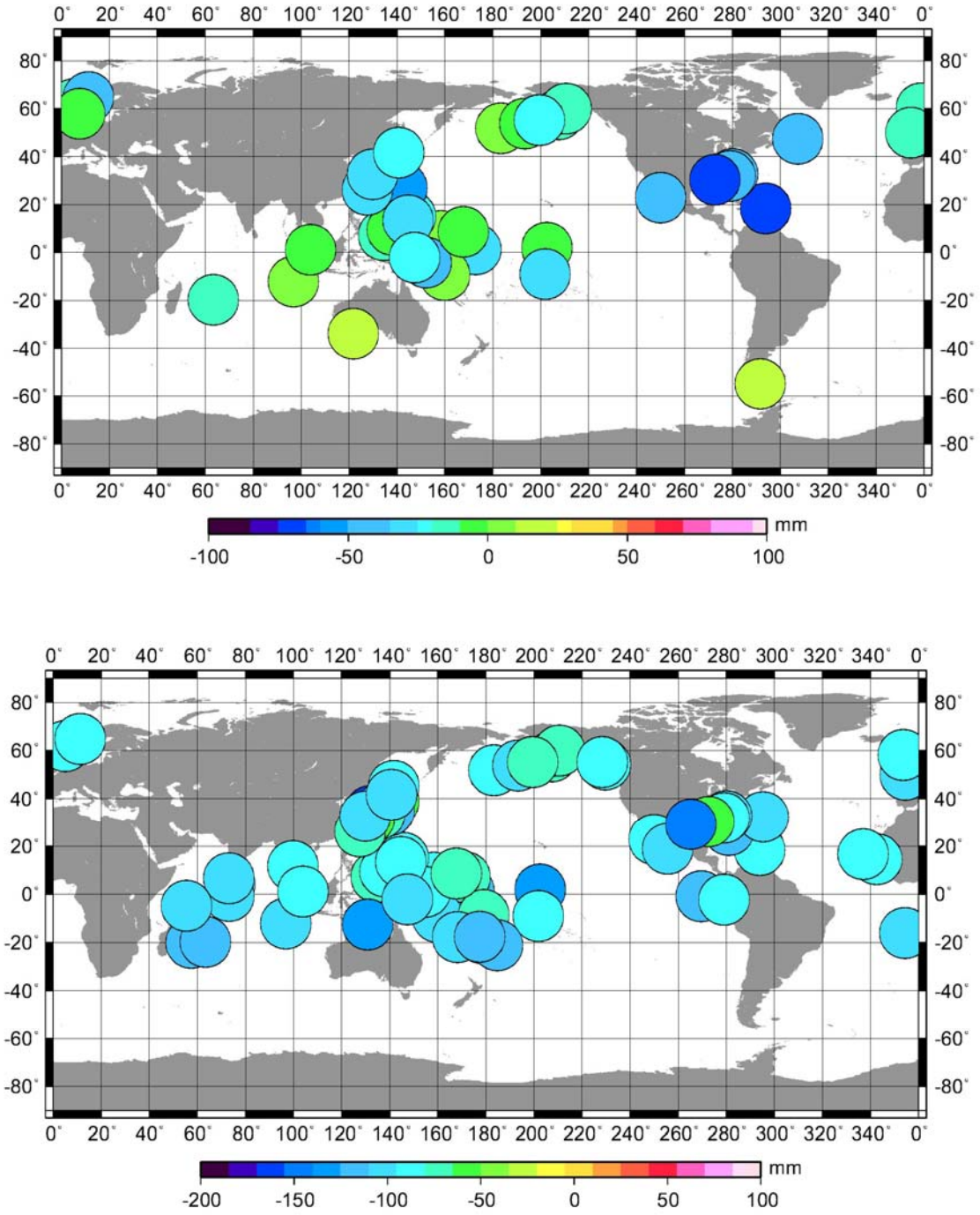

Figure 5.1: (a) Top: Bias between GFO-1 and TOPEX/POSEIDON at tide gauge stations. Mean of differences is 28 mm. (b) Bottom: Bias between JASON and TOPEX interleave mission at tide gauge stations. Mean of differences is 95.5 mm.

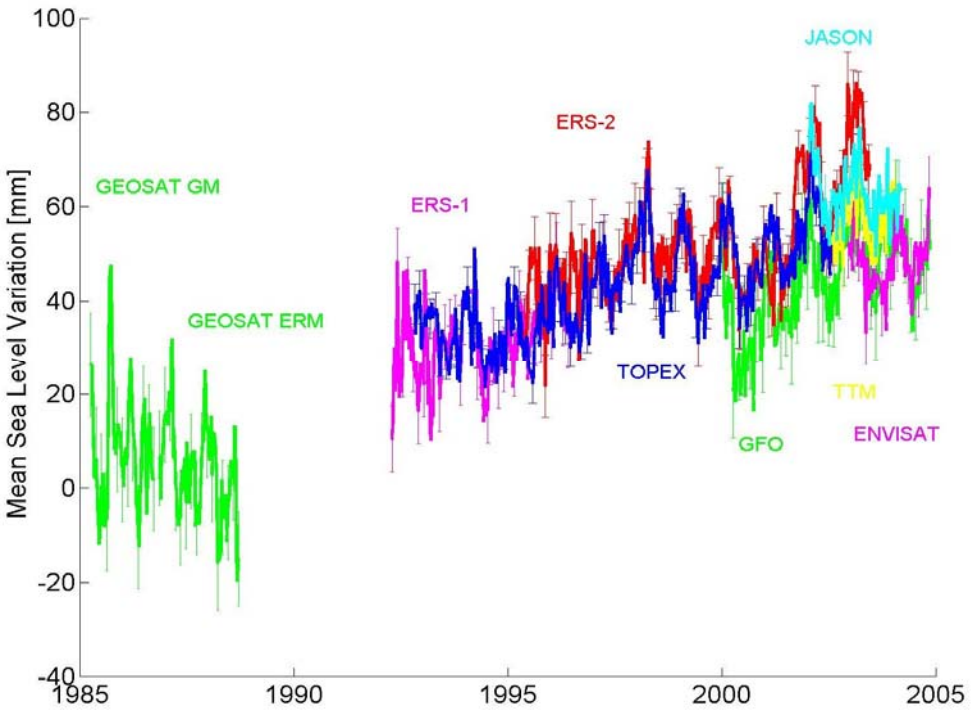

Figure 5.2 Global sea level variations (latitude $\pm 81^0.5$, with error bars) observed by altimeters (1985-2004) with all known corrections applied including instrument drifts and IB correction.

5.1.4 Results and Discussions

The geographical rates of sea level changes (latitude $\pm 81°$) with resolution $1° \times 1°$ grid are determined by Equation (5.2) using GEOSAT/ERM, GEOSAT/GM, GFO, ERS-1, ERS-2, ENVISAT, TOPEX/POSEIDON, TOPEX interleave mission, and JASON-1 ($i = 9$) altimeters without IB corrections (Figure 5.3). Global averaged trend with area weights within latitude $\pm 81^o.5$ is 2.7 mm/yr and within latitude $\pm 66^o$ is 2.8 mm/yr, respectively. Figure 5.4 illustrates the formal errors of Figure 5.3 geographically. Averaged formal error with area weights within latitude $\pm 81^o.5$ is 1.6 mm/yr and within latitude $\pm 66^o$ is 1.4 mm/yr. Figure 5.5 presents the geographic trends of sea level as the same as Figure 5.3 except IB corrections are applied to the measurements of altimeters. Area-weighted trend within latitude $\pm 81^0$ equals 2.6 mm/yr and within latitude $\pm 66^0$ is 2.7 mm/yr. Figure 5.6 shows the formal errors of Figure 5.5. Averaged formal error within latitude $\pm 81^o.5$ is 1.3 mm/yr and within latitude $\pm 66^o$ is 1.1 mm/yr. By comparing the trends of global sea level variations averaged within latitude $\pm 81^0.5$ and latitude $\pm 66^0$, the result shows extremely equivalent. The reason should be that the area of oceans within latitude $\pm 81^0.5$ holds 99% of global ocean as the area of oceans within latitude $\pm 66^0$ holds 96% of global ocean. Therefore, the area within latitude $\pm 81^0.5$ is big enough to represent the global ocean and even the ocean area within latitude $\pm 66^0$ is adequate. Compared with global sea level trend without applying IB corrections, the trend with IB corrections is lightly smaller. The magnitude of global sea level trend difference is 0.1 mm/yr and consequently IB corrections can

contribute 0.1 mm/yr to global sea level changes. Nevertheless, the magnitude is smaller than the uncertainty of global sea level trend and the contribution of IB correction on the global sea level trend is not significant. The higher sea level trends occur in the western Pacific Ocean while lower trends appear in the eastern Pacific Ocean. By the same token, this phenomenon occurs in the trends of thermosteric sea level (Figure 5.7), which are determined by integrating from 0 m down to 500 m using WOA01 during 1985–2003. Similarly, the higher trends of sea level and thermosteric sea level also appear in Gulf Stream. Nevertheless, the trends of sea level and thermosteric sea level are diverse in southern ocean, when sea level variations present higher trends but thermosteric sea level changes show more smooth trends, the amplitude of which are smaller than 1 mm/yr and are close to 0 mm/yr. The discrepancy may results from the sampling problem of *in situ* temperature data, which are used to compose the objective model WOA01.

For the comparison of formal errors with and without applying IB corrections, averaged formal error applying IB corrections is 0.3 mm/yr, which is smaller than not applying IB corrections. This means applying IB corrections makes sea level variations smoother and the determination of sea level trend more accurate, the uncertainty is reduced. Geographic formal errors in the area of high latitude are inordinately larger. The possible reason is altimeter data are missing due to sea ice coverage and no TOPEX/POSEIDON measurements. Additionally, some specific areas (up to 5 mm/yr presented by green color) are relatively higher as well. It may be induced by Agulhas current, Gulf Stream, and Kuroshio or inter-decadal signals in measurements.

Figure 5.8 illustrates the time series of global sea level changes, which are observed by 9 altimeter missions without applying IB correction. In the Figure, the relatively residual biases, semi-annual and annual signals are removed. Each curve presents a time series of an altimeter mission, which is determined by averaging sea level anomalies within its coverage with area weights and in a 9-day time interval. The trend of sea level variations and relative residual biases are estimated simultaneously by Equation (5.2) using 9 time series of global sea level changes from 9 missions. In consequence, the trend of global sea level changes is 2.8 mm/yr. The same outcome is shown when the time series is obtain by only averaging sea level anomalies within latitude $\pm 66^0$. Figure 5.9 shows the same as Figure 5.8 except IB corrections are applied to altimeter data. The trend of global ($\pm 81^0$) or $\pm 66^0$ sea level changes are identical at 2.7 mm/yr. The discrepancy between Figure 5.8 and 5.9 is the variations in Figure 5.9 are relative smaller than Figure 5.8 as IB corrections account for the part of sea level signals. The uncertainty of global sea level trend is reasonably given as 0.5 mm/yr according to Church et al. [2004], Nerem et al. [2001], Urban [2000], and Guman [1997].

Geoid change caused by PGR is not the part of sea level variations and consequently it should be corrected to the sea level trend derived from altimeters as is done in tide gauge records generally [Tamisiea et al, 2005]. There are two PGR models used in this study. The first is ICE4G and the other one is BIFROST model with Earth parameters, LT=120km, LMV=1×10^{21} Pas, and UMV=3×10^{21} Pas. The averaged geoid effects in global ocean area are -0.17 mm/yr and -0.28 mm/yr from these two models. As a result, global sea level trends corrected geoid effect without applying IB corrections is equal to 3.0±0.5 mm/yr and with IB corrections equals 2.9±0.5 mm/yr. From now on the rate of sea level trend derived from altimeters is addressed as after correcting for the geoid effect caused by PGR.

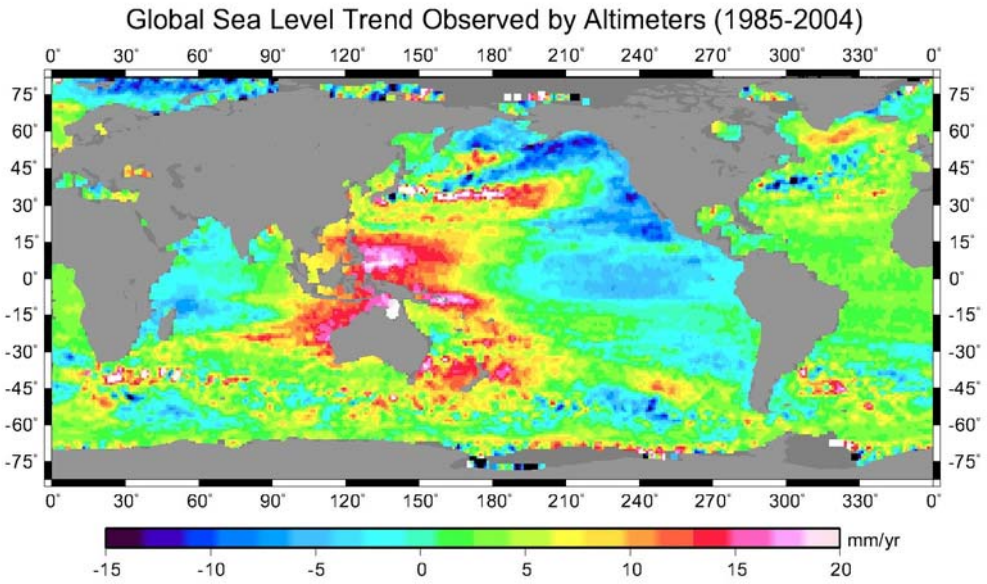

Figure 5.3: Geographical global sea level trends observed by altimeters (1985-2004) (area weighted, 1^0 blocks, latitude $\pm 81^0.5$). No IB corrections are applied.

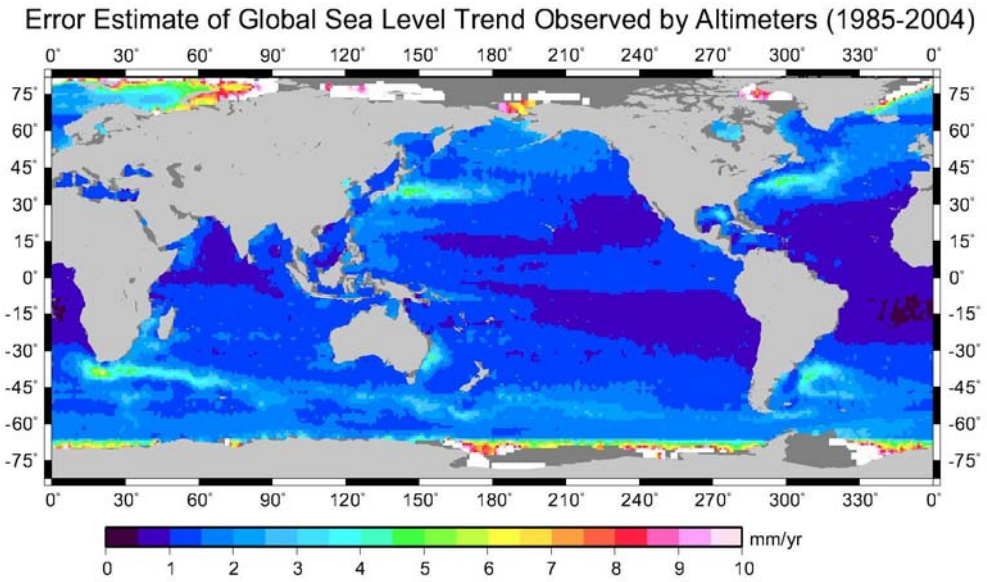

Figure 5.4: Geographical formal errors displayed (latitude weighted, 1^0 blocks, latitude $\pm 81^0.5$). No IB correction is applied.

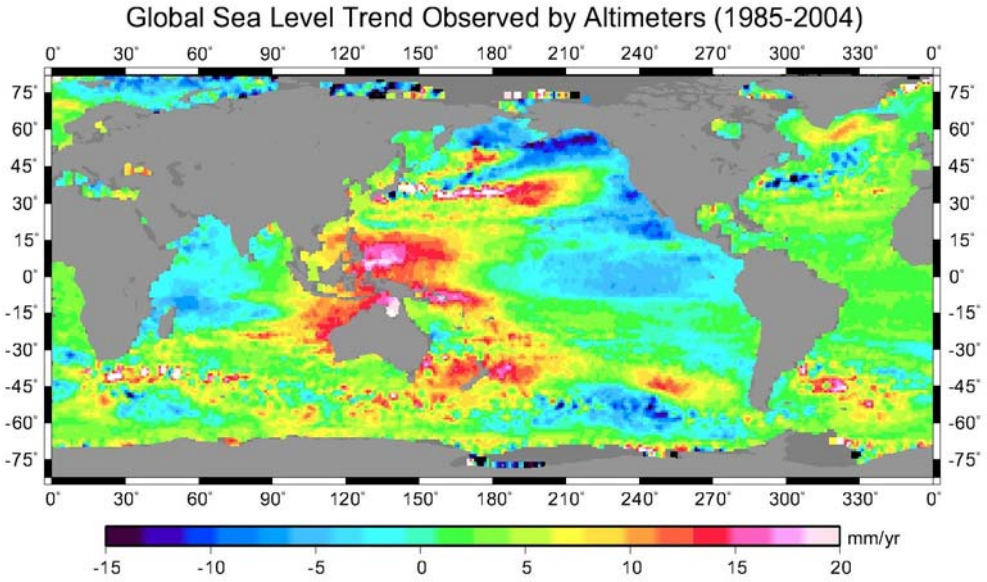

Figure 5.5: Geographical global sea level trends observed by altimeters (1985–2004) (latitude weighted, 1^0 blocks, latitude $\pm 81^0.5$). IB corrections are applied.

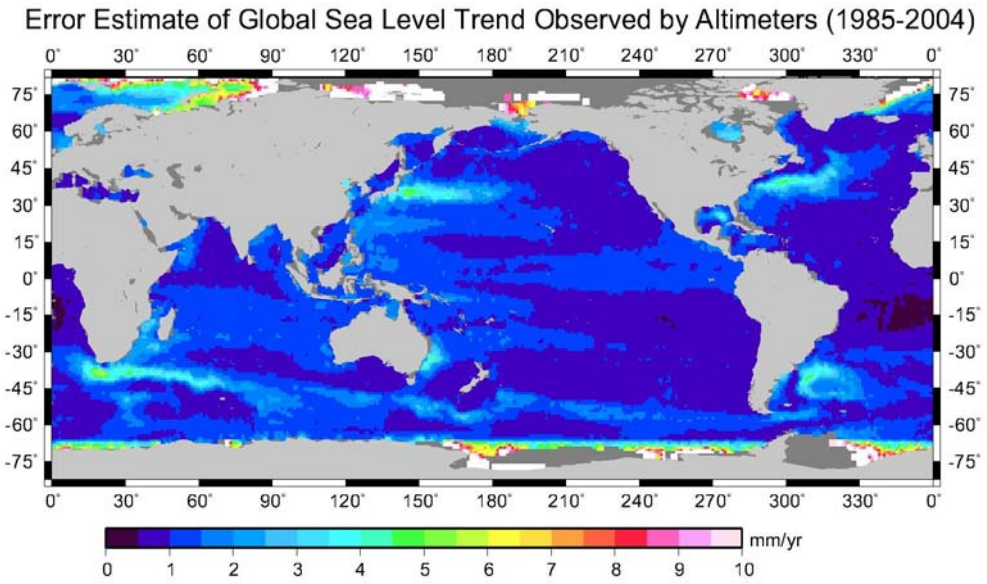

Figure 5.6: Geographical formal errors (latitude weighted, 1^0 blocks, latitude $\pm 81^0.5$). IB correction is applied.

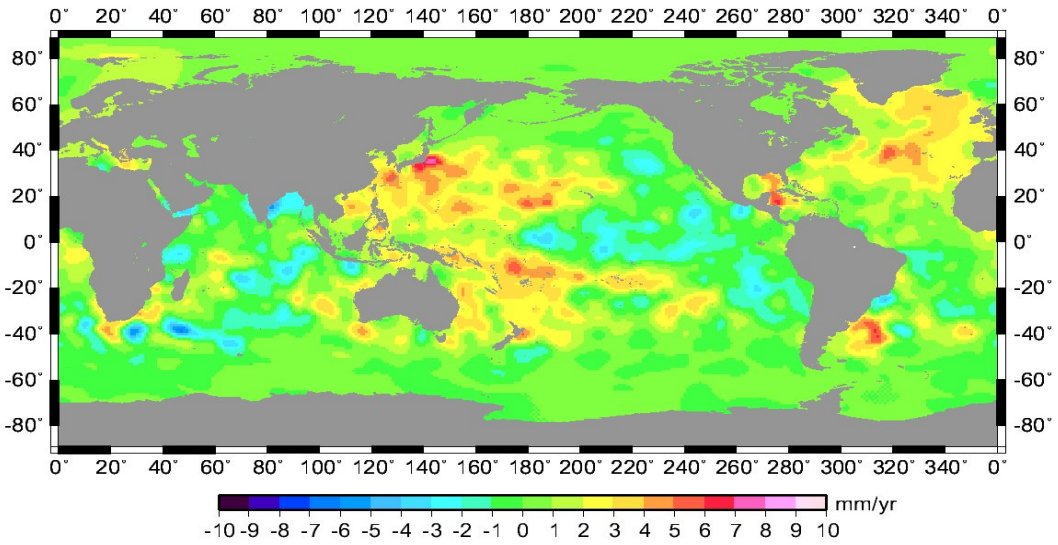

Figure 5.7: Geographical trends of thermosteric sea level, which are determined by integrating from 0 m down to 500 m using WOA01 during 1985-2003.

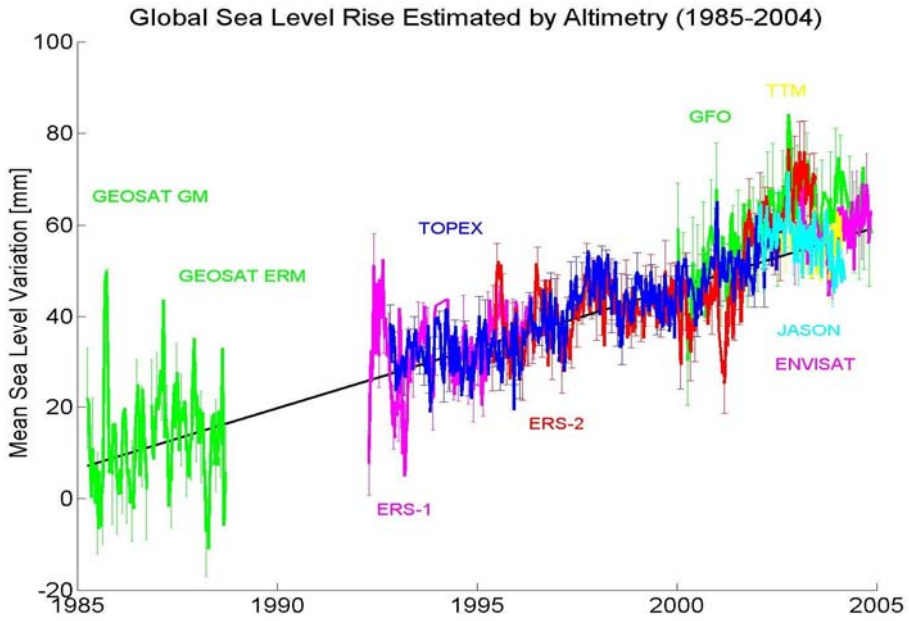

Figure 5.8: Global sea level variations (latitude $\pm 81^0.5$, with error bars) observed by altimeters (1985–2004) with all known corrections applied including instrument drifts except for IB correction. Residual biases relative to TOPEX/POSEIDON have been removed. Trend estimated by simultaneous adjustment of annual, semi-annual, and a slope (shown as a black line).

Residual biases	CASE I	CASE II	CASE III	CASE IV
TOPEX INTERLEAVE MISSION	-0.7 mm	-0.7 mm	-0.7 mm	-0.7 mm
JASON-1	5.0 mm	5.0 mm	5.0 mm	5.0 mm
ERS-1	-2.3 mm	-2.3 mm	17.7 mm	-2.3 mm
ERS-2	5.8 mm	5.8 mm	25.8 mm	5.8 mm
ENVISAT	-10.6 mm	-10.6 mm	-10.6 mm	9.4 mm
GEOSAT/GM	-2.2 mm	17.8 mm	-2.2 mm	-2.2 mm
GEOSAT/ERM	-13.0 mm	7.0 mm	-13.0 mm	-13.0 mm
GFO	-11.2 mm	-11.2 mm	-11.2 mm	8.8 mm
Trend	2.7 mm/yr	2.7 mm/yr	2.7 mm/yr	2.7 mm/yr

Table 5.2: Residual biases relative to TOPEX/POSEIDON and estimated trends.

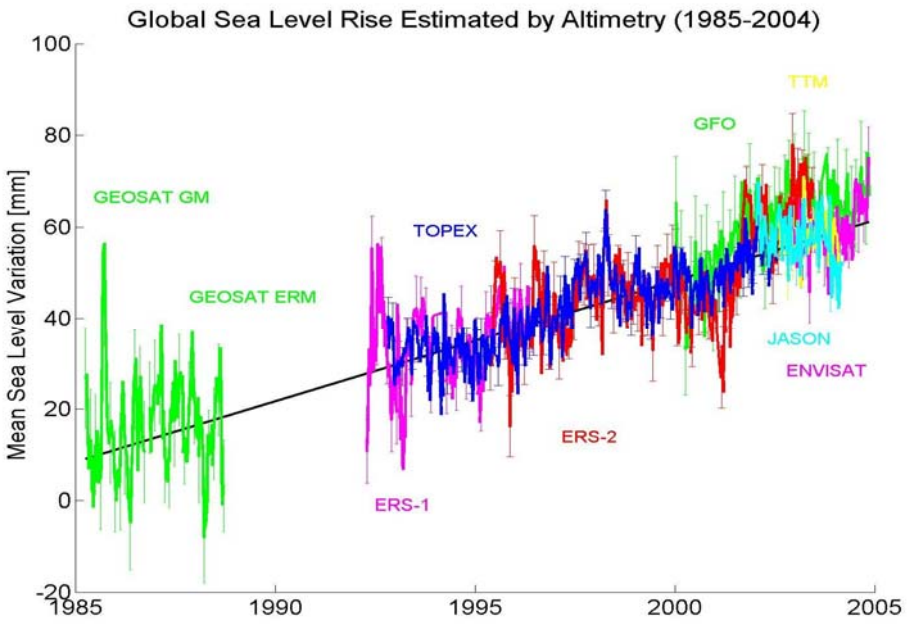

Figure 5.9: Global sea level variations (latitude $\pm 81^0$, with error bars) observed by altimeters (1985-2004) with all known corrections applied including instrument drifts and IB correction. Residual biases relative to TOPEX/POSEIDON have been removed. Trend estimated by simultaneous adjustment of annual, semi-annual, and a slope (shown as a black line).

5.2 Sea Level Trend Observed by Tide Gauge Records

5.2.1 Tide Gauge Records

Two datasets of tide gauge records are used in this study, which are provided by two different global data centers. The first data set are monthly averaged Revised Local Reference (RLR) tide gauge data provided by Proudman Oceanographic Laboratory's (POL's) Permanent Service for Mean Sea Level (PSMSL), which has been responsible for the collection, publication, analysis and interpretation of sea level data from the global network of tide gauges. The latest record in this database ends in 2003. The RLR is defined to be approximately 7000 mm below mean sea level at each station.

The second data set are monthly sea level heights with millimeter unit, which are provided by the Joint Archive for Sea Level (JASL), a collaboration between the University of Hawaii Sea Level Center (UHSLC) and the World Data Center-A for Oceanography, the National Oceanographic Data Center (NODC), and the National Coastal Data Development Center (NCDDC), continues to acquire, quality control, manage, and distribute sea level data as initiated by the Tropical Ocean Global Atmosphere (TOGA) Program, which ended in 1994. The JASL is now an official Global Sea Level Observing System (GLOSS) data center. Tide gauge records can be downloaded from ftp server (http://ilikai.soest.hawaii.edu).

Since tide gauge records are provided by two data centers, the duplicate stations could exist in two databases at the same time by reason of the same raw data sources, so these kinds of data should be edited from either database. In our processing, the trends and correlation coefficients of tide gauge records in both datasets are computed in order to inspect the duplicate stations. If the correlation coefficient is > 0.98, the trend difference is < 0.2 mm/yr, and their position (latitude and longitude) are quite near (<0.2 degree), these two stations are to be considered as the same points and either one should be discarded. It is possible to edit a tide gauge in one dataset and there is no identical station in the other dataset due to extreme proximity of two sites. However, the estimated sea level variations will not vary significantly because a station is adequate to represent sea level change in the specific region. As a consequence, the algorithm resulted in 1,483 tide gauge stations left after combining the two databases according to above described process.

5.2.2 Effect of Atmospheric Pressure on Sea Level Determination

In this study, two atmospheric pressure datasets are used to calculate IB corrections applied to tide gauge records. The first pressure model is provided by the European Centre for Medium-Range Weather Forecasts (ECMWF) 40-year reanalysis (ERA-40), which can provide monthly mean directly in $2.5^o \times 2.5^o$ global grid. ERA-40 is a new European re-analysis data set (http://data.ecmwf.int), which improved considerably upon the earlier reanalysis. It produces and disseminates analyses with higher horizontal resolution, a much more extensive and accurate description of the stratosphere, and finer resolution of the planetary boundary layer.

The other atmospheric pressure model is obtained from the National Centers for Environmental Prediction–National Center for Atmospheric Research (NCEP–NCAR) 50-yr

reanalysis [Kistler et al. 2001] (http://www.cdc.noaa.gov), which is provided by the National Oceanic and Atmospheric Administration Cooperative Institute for Research in Environmental Sciences (NOAA–CIRES) Climate Diagnostics Center, Boulder, Colorado. The resolution of the data set is monthly $2.5^o \times 2.5^o$ global grids with 144x73 points. It should be noted in this study, the IB corrections are applied to tide gauge data records up to 5 decades due to the limitation of the ECWMF (40 years) and the NCEP (50 years) Reanalysis data. For the determination of the 100 year (20^{th} Century) sea level, IB corrections are not applied for tide gauge records prior to 1948. This approximation is justified, as it will be shown later, that the effect of IB corrections on global (i.e., averaged) sea level determined by tide gauges are approximately <0.2 mm/yr. This result also agrees with Ponte [2005].

5.2.3 Determination of Sea Level trend using Tide Gauge Records

Before determining the rate of sea level changes using tide gauge records, the criteria to select tide gauge records in this study should be set up and it is extremely important since tide gauge records of low quality should be edited or down-weighted. The first criterion is the rate of a tide gauge record could not exceed a reasonable value, which is set to 10 mm/yr in this study. If the rate at a tide gauge station is relative high, it means the tide gauge records contains exceeding large local vertical motion, such as the local subsidence due to water usage or oil drilling, or the tide gauge station is located at the estuary (tide gauge records are affected by the water column from river). In addition, the standard deviation of the sea level trend should be <10 mm/yr to avoid noisy tide gauge data. The second criterion is that data gap at a station cannot exceed 30% of the total data span. This procedure can make sure the data quality of tide gauge records and to avoid the error of the estimated trend caused by data gaps. The third criterion is the operating period should be longer than 15 years in order to reduce error resulting from low frequency signals including the decadal signal. The last criterion is the tide gauge should measure the same sea level variations with nearby tide gauges. This criterion can be considered by computing correlation coefficients of tide gauge records. We set that a tide gauge data should have at least 70% of the correlation coefficients with the other gauges located within 3 degree radius (about 300 km) that are bigger than 0.6.

After tide gauge stations are selected in light of the above criteria, the procedure to determine sea level trends using selected tide gauge records has five steps as follows:

Step 1: Fit bias, secular rate, semi-annual and annual signals of each tide gauge station by least squares algorithm:

$$y = a + bt + c\sin(2\pi t) + d\cos(2\pi t) + e\sin(4\pi t) + f\cos(4\pi t), \qquad (5.3)$$

where y are tide gauge measurements and the other parameters are the same as described in Equation (5.2).

Step 2: Parameters estimated by step 1 are used to create pseudo-measurements, which fill in data gaps of tide gauges records. Therefore, tide gauge records keep the original data and take the advantage of no data gap.

Step 3: Average the tide gauge records weighted by standard deviations derived by step 1 at the same epoch to obtain the time series of sea level changes for each of 10^o by 10^o grid cell after removing the relative biases of tide gauge records and applying PGR corrections. Average of all sites in a 10^o by 10^o grid cell can avoid overemphasizing the signals of the area where abundant tide gauges are located.

Step 4: Average all 10^o by 10^o grids with an equal weight to obtain the time series of global sea level variations.

Step 5: Fit the rate of global sea level trend using the time series from step 4 by least squares algorithm using Equation (5.3).

In this study, the trend is determined by traditional Weighted Least Squares (WLS) approach. Other more sophisticated time series analysis mathematical tools are available, including the Monte Carlo Singular Spectrum Analysis (MC-SSA) [Moore et al., 2005], the Empirical Orthogonal Function (EOF) method [Church et al., 2004], and the Multi-Tapers Method (MTM) [Mann and Lees, 1996]. Here we attempt to quantify the difference of using one of these algorithms, the MTM, to apply to sea level determination using tide gauges, and to compare to the conventional WLS approach using in this study (Appendix B). The comparison (Appendix B) shows no significant difference of sea level trends determined using both methods. Therefore, we are satisfied to use the simple WLS approach as the preferred technique for sea level determination.

5.2.4 Results and Discussions

Figure 5.10 illustrates geographic locations of 651 tide gauge stations in the global map, which tally with the described criteria in section 5.2.3. Most tide gauges are located at the north hemisphere, especially the coasts in North America and Europe. The colored circles present the sea level trends of tide gauges using individual time span. Formal errors of sea level trends in Figure 5.10 are displayed in Figure 5.11. The rate of sea level trend is higher when the corresponding former error is relatively larger. Figure 5.12 shows the operating time spans of tide gauge stations. Tide gauge stations located at the coasts of the eastern North American and of the Western Europe have records longer than 50 years, while the stations located at the northern and middle Pacific Ocean have data about 50 years. By comparing Figures 5.11 and 5.12, the tide gauge with longer time span has a smaller formal error of the trend. Figure 5.13 shows the number of monthly observations at 651 tide gauges per year and per month. Obviously, the amount of the measurements between 1950 and 2000, which account for 78% of total measurements, is larger than the other time spans. The maximum amount of observations happens during 1987-1988. The number of measurements decreases dramatically from 1949 back to 1900.

The sea surface tends to respond hydrostatically, either falling or rising, as atmospheric pressure increases or decreases. In general, 1 mbar increase in atmospheric pressure depresses the sea surface by about 10 mm. In contrast, sea surface rises about 10 mm as atmospheric pressure decreases 1 mbar. This effect is referred to as the inverted barometer (IB) effect [Ponte,

2005]. Tide gauge stations are usually located at coastal regions. In a coastal area, sea level responds to atmospheric pressure as well as to large-scale offshore forcing. In many circumstances the direct response induced by local atmospheric pressure forcing is almost isostatic. IB corrections should be applied for the sake of reducing the ‘‘noise’’ related to regional phenomena in the tide gauge records. A more important reason for correcting the tide gauge data with IB corrections relates to the lack of global coverage of the tide gauges. Changes of atmospheric pressure patterns over time could redistribute sea level resulting in no net rise or fall of sea level globally (assuming that water is incompressible). However, with a sparse network of tide gauges this could easily be misinterpreted as a change in global sea level since local barotropic effects could be large at specific regions. Before using surface atmospheric pressure, the global trend should be removed to avoid the artificial trend introduced into sea level trends. The instantaneous IB effect on sea surface height in millimeters is computed from the surface atmospheric pressure, P_{atm} in mbar:

$$IB = -9.948 \times (P_{atm} - P) \tag{5.4}$$

where P is the time varying mean of the global surface atmospheric pressure over the oceans. The scale factor 9.948 is based on the empirical value [Wunsch, 1972] of the IB at mid latitudes. Figure 5.14 shows the averaged sea surface pressure at the locations of 651 tide gauge stations. Surface pressures are interpolated at tide gauge locations and at measured epoch of gauge records from ECMWF and NCEP models. Thereafter, a time series are derived by averaging interpolated surface pressures at the same epoch. Green curve shows sea surface pressures of ECMWF with the trend at -0.008±0.003 mbar/yr, which is approximately equal to 0.08±0.03 mm/yr of sea level changes. Red curve presents sea surface pressures of NCEP with the trend at 0.003±0.003 mbar/yr, which is approximately equal to -0.03±0.03 mm/yr. The correlation coefficient of ECMWF curve and NCEP curve equals 0.98. High correlation addresses the significant errors or the discrepancy in neither ECMWF nor NCEP model. Blue curve presents the difference between ECMWF and NCEP model with mean of 0.22±0.20 mbar (equal to -2.2±2.0 mm) and with a slope of -0.011±0.0005 mbar/yr (0.11±0.005 mm/yr). There is an uneven offset in mid-1970s of blue curve. It may be caused by changing data process in either ECMWF or NCEP but there is no report from two data sets.

Trends of sea level changes determined from 651 tide gauge records are in Table 5.3. Columns 2 and 3 show the trends derived from tide gauge records without and with IB corrections respectively in light of section 5.2.3. In this study, IB corrections are computed using NCEP model because longer time span is available. The trend of sea level changes without applying IB corrections is uniform when the time span of records is shorter than 30 years; however, the sea level trend is around 1.6 mm/yr invariably when using records more than 60 years. The trends of sea level changes with IB corrections are very close to trends without applying IB corrections since the sea level trends responding to surface pressure at gauge stations are lower than ±0.2 mm/yr. To be noticed, column 1 presents the calculated time span and the number of stations used in the determination of sea level trend. The number of stations is not consistent for different time span since some gauge records do not cover the time span we computed.

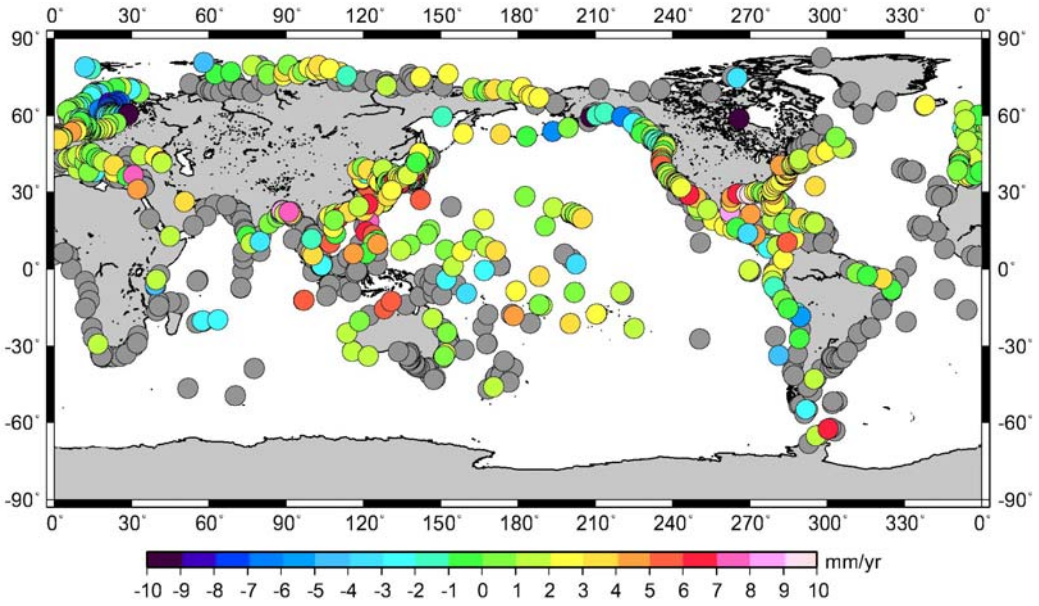

Figure 5.10: Locations of 651 tide gauges and the rates of sea level trends (colored circles). Gray circles present the tide gauge stations rejected by selected criteria.

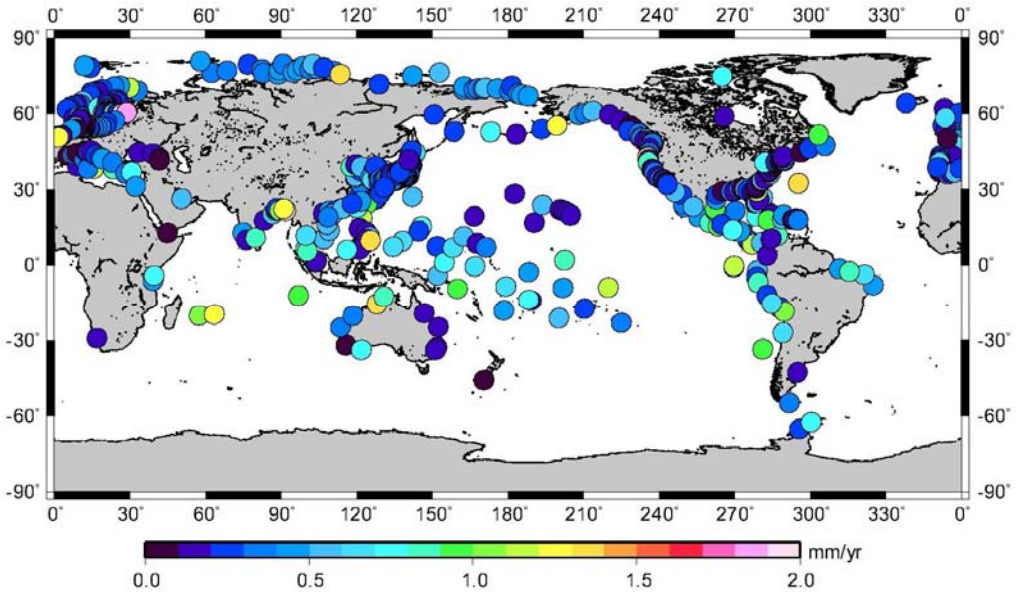

Figure 5.11: Formal errors of secular trends at tide gauge stations in Figure 5.10.

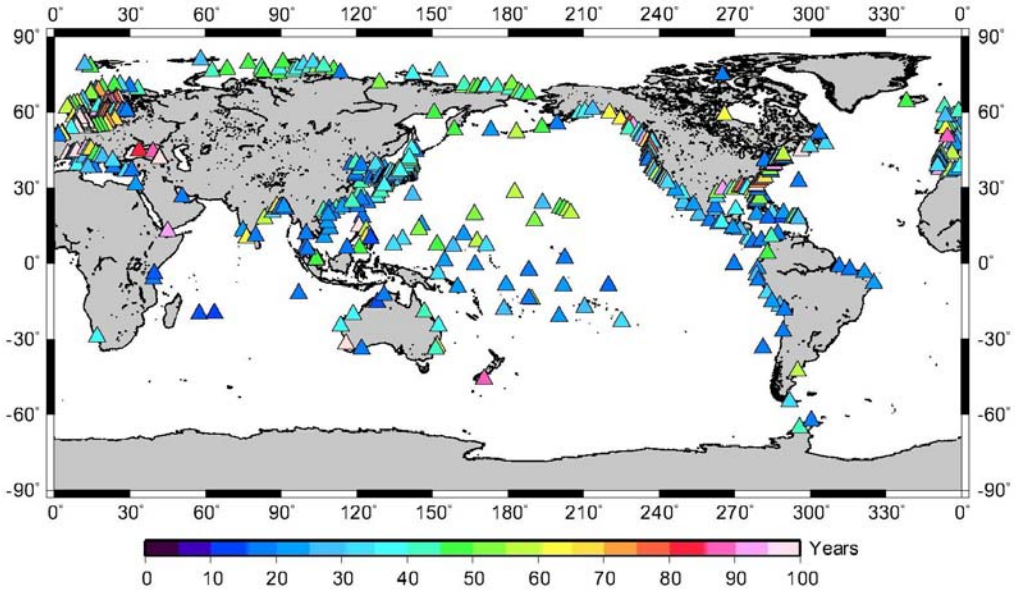

Figure 5.12: Operating time spans of 651 tide gauge records.

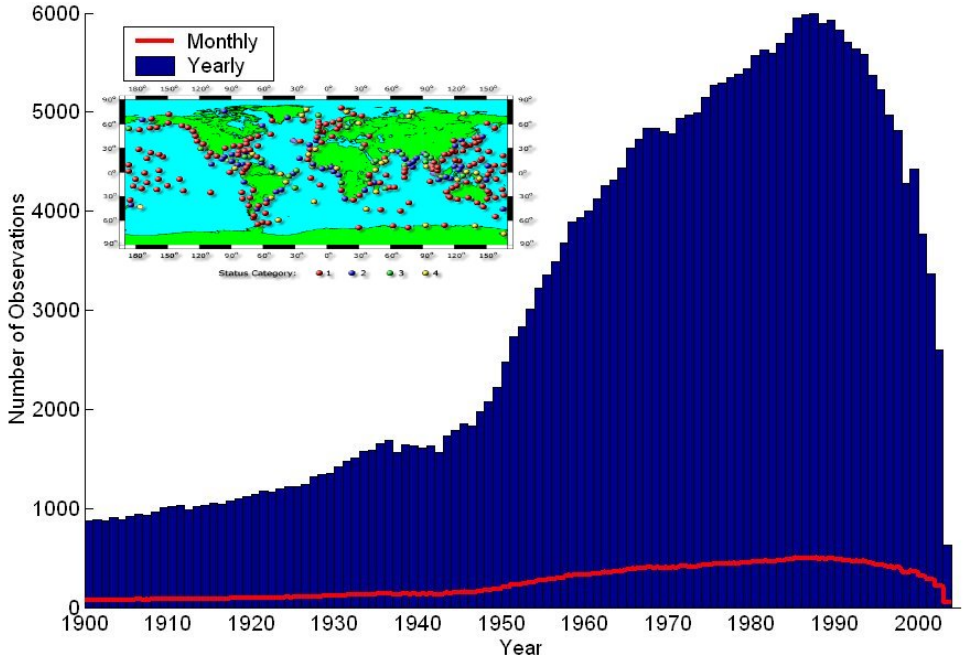

Figure 5.13: Number of monthly observations at 651 tide gauges per year (blue bars) and per month (red curve) and the global distribution of GLOSS gauge stations.

Time span (# of stations)	Sea Level Change (mm/yr) W/O IB Correction	Sea Level Change (mm/yr) W/ IB Correction
1985-2002 (530)	2.88±0.1 (Alt.: 2.9±0.5)	2.68±0.09 (Alt.: 2.8±0.5)
1980-2002 (548)	2.61±0.07	2.53±0.06
1970-2002 (574)	1.81±0.04	1.86±0.03
1960-2002 (616)	1.78±0.02	1.90±0.02
1950-2002 (618)	1.56±0.02	1.63±0.01
1940-2002 (620)	1.6	–
1930-2002 (640)	1.6	–
1920-2002 (644)	1.6	–
1920-2002 (651)	1.6	–
1900-2002 (651)	1.6	–

Table 5.3: Trends of sea level variations determined from 651 tide gauge records in different time spans.

Figure 5.15 shows a comparison of sea level variations determined from altimeters and tide gauges both without applying IB corrections. Annual and semi-annual signals are removed in the figures from now on. The trends (1985-2002) of sea level variations observed by altimeters and gauges are identical and its value is 2.9 mm/yr. Figure 5.16 shows a comparison of sea level variations determined from altimeters and tide gauges both with IB corrections. The trends (1985–2002) of sea level variations observed by altimeters and gauges are 2.8 mm/yr and 2.7 mm/yr, respectively. The trends of sea level changes agree well in both figures even if inter-annual signals are not similar and gauges do not cover globally and evenly. By comparing both cases with and without applying IB corrections, IB effect contributes a small positive trend to sea level trend. Additionally, by analyzing Figure 5.15 and 5.16, the amplitude of sea level variations with IB corrections is smaller than without applying IB corrections.

In Figure 5.17, red curve presents the sea level changes determined from altimeters with IB corrections and the trend equals 2.9 mm/yr (without IB corrections the trend is 3.0 mm/yr) from 1985 to 2004. Blue curve presents the trend derived from tide gauges from 1950 to 2002 with IB correction is equal to 1.6 mm/yr. Trend derived from tide gauge data is also 1.6 mm/yr when no IB corrections applied. The trend derived from 50-year gauge records has about 1 mm/yr lower than 19-year data. Therefore, the trend determined by a short time records could be misinterpreted by a decadal or inter-decadal signals. Figure 5.18 shows the same conclusion as Figure 5.17, which presents the comparison of sea level variations determined from altimeters (1985–2004) and tide gauges (1900–2002). Neither altimeters nor tide gauge data are applied for IB corrections.

In order to examine the stability of determination, the other approach is used to determine the sea level trend. The procedure is almost the same as the description in Section 5.2.5 except for dividing global area into 10^o by 10^o grids. Steps 1 and 2 are the same as in Section 5.2.5. Step 3 is to average all tide gauge records weighted by standard deviations derived by Step 1 at the same time epoch to obtain the sea level changes in form of time series after removing relative biases of tide gauge records and applying PGR corrections. In contrast to Step 3 in section 5.2.3, this approach may overemphasize the signal of areas where large amount of tide gauges are located so the decadal and interdecadal signals show more strongly like El Nino in 1983 and

1997-1998. As a result, the trend shows no difference compared with the method in Section 5.2.3 (see Figure 5.19). The trend derived from tide gauge records during 1900–2002 is 1.5 mm/yr and 3.0 mm/yr during 1985–2002. Therefore, the limited amount of gauge stations seems to be good enough to present global sea level changes although they do not cover globally.

In previous Sections, the comparisons of sea level trends determined from tide gauge records with global averaged sea level from altimeters have been performed, nevertheless, tide gauges do not distribute globally and evenly. Therefore, in order to illustrate whether sea level variations of selected tide gauges and altimeters present the identical sea level trend, a comparison of sea level variations derived from tide gauge records and satellite altimeters, both of which measure the same regions, is being performed during the same time span (1985–2002). Altimetric sea level variations can be derived by averaging geographical sea level changes within 3 degrees of tide gauge locations. As a result, the sea level trend derived from altimeters without applying IB corrections is 3.1 mm/yr while with applying IB corrections the sea level trend drops to 2.8 mm/yr. The result agrees exceptionally well with sea level trend determined using tide gauge records.

If one assumes that the formal error of sea level trend derived from tide gauge records as the true uncertainty, it should be underestimated because other errors caused by IB corrections, PGR corrections, and spatial coverage of tide gauges have not been taken into account. One error model caused by IB corrections could be considered as the trend of the difference between ECMWF and NCEP models at 651 tide gauge stations, which is 0.11 mm/yr. Similarly, the error model due to PGR corrections is assumed to be the mean of differences between the ICE4G and BIFROST model computed with Earth parameters, LT=120 km, LMV= 1×10^{21} Pas, and UMV= 3×10^{21} Pas. The mean of differences at 651 stations is 0.13 ± 0.54 mm/yr. Applying PGR corrections to the sea level trend determined from tide gauge records is a nonlinear problem, so not only the mean value 0.13 mm/yr but also the standard deviation of 0.54 mm/yr could affect the determination of sea level trend. The average of two values, therefore, is being assumed to be the error, 0.33 mm/yr. The last error caused by non-global coverage of tide gauges can be assumed to be the difference of global sea level trends derived from altimeters and gauges during time span of 1985–2004 and the value is less than 0.2 mm/yr. If the data span is longer, like 50 years, this error would decrease to 0.1 mm/yr or smaller. In addition, Douglas [1992, 1997] and Woodworth [1990] concluded that very long tide gauge records (>50 years) do not require global coverage and sparsely and randomly located tide gauge stations show a very consistent trend and there is a lack of acceleration. Therefore, we concluded that the overall uncertainty of sea level trend determined using global tide gauge is reasonable to be given as 0.4 mm/yr.

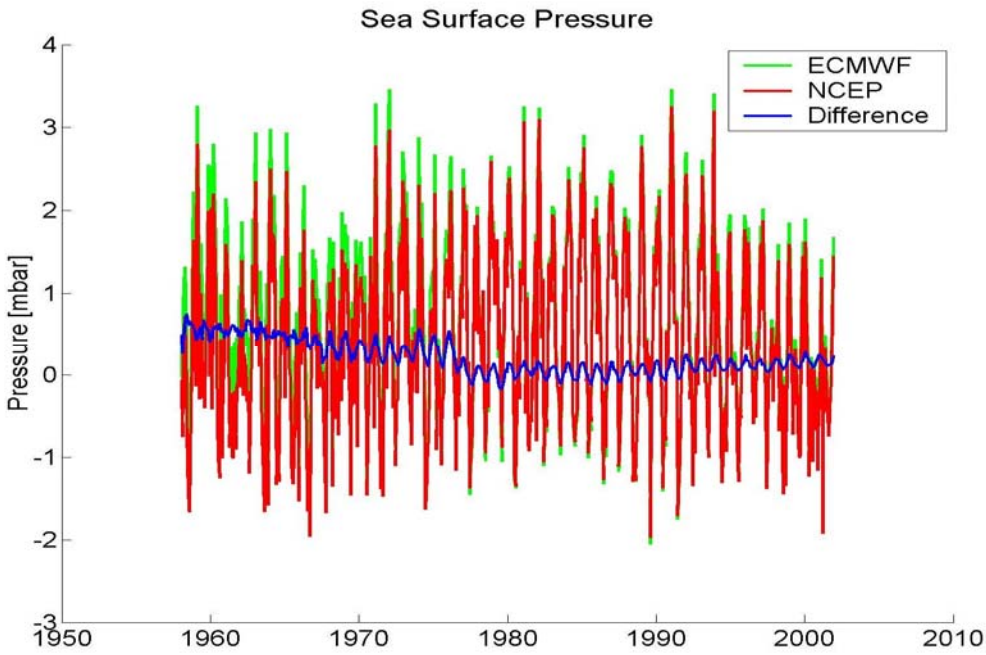

Figure 5.14: Averaged sea surface pressure of monthly tide gauge data (651 stations) in global Ocean. Green curve presents sea surface pressures provided by ECMWF. Red curve presents sea surface pressure provided by NCEP. Blue curve presents the difference of ECMWF and NCEP.

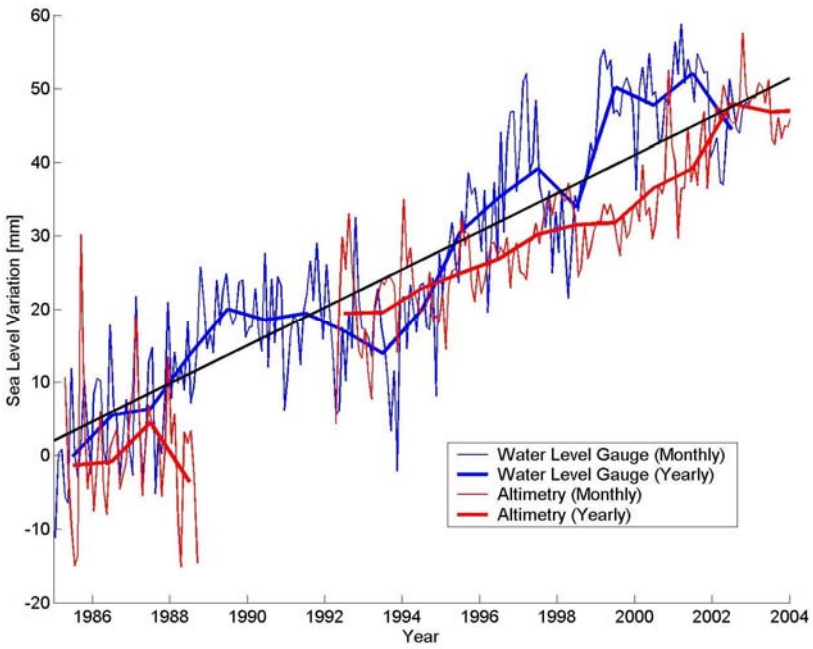

Figure 5.15: Comparison of sea level variations determined from Altimeters and tide gauges. No IB corrections are applied to both altimeters and gauge data.

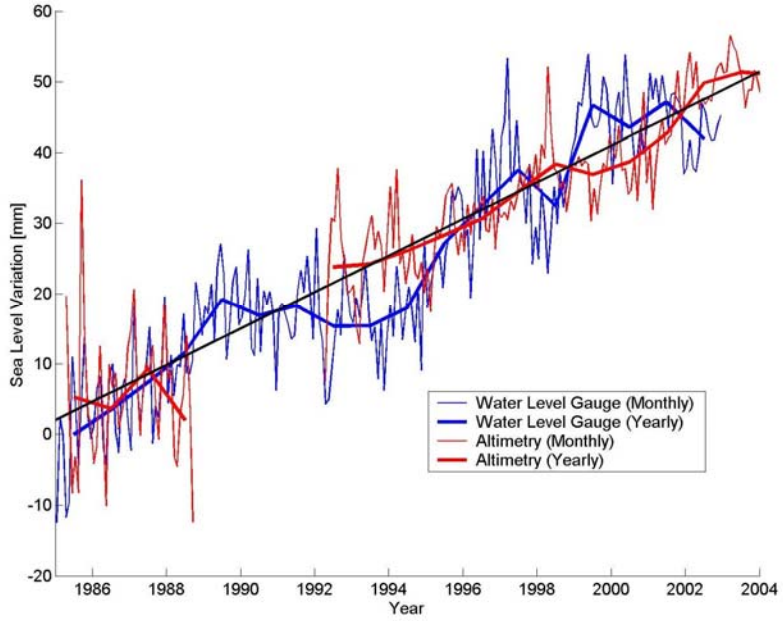

Figure 5.16: Comparison of sea level variations determined from altimeters and tide gauges. IB corrections are applied to both altimeters and gauge data.

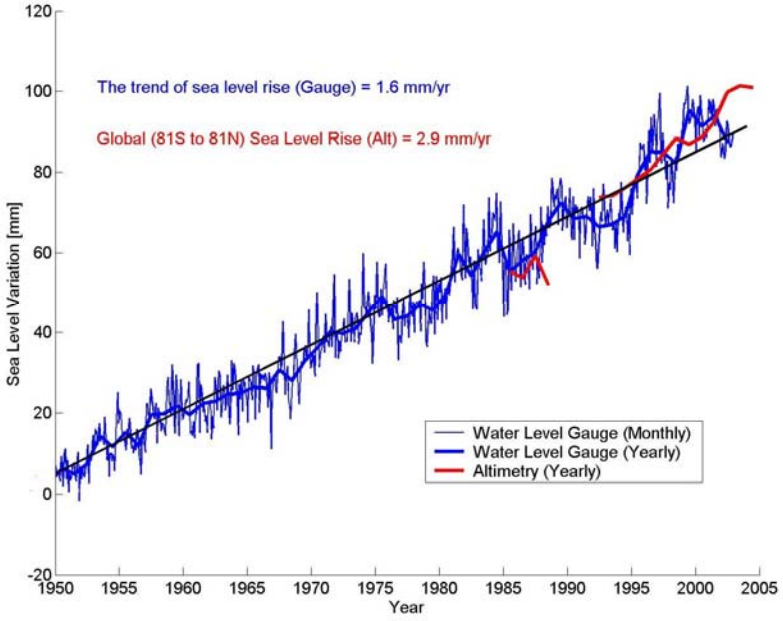

Figure 5.17: Comparison of sea level variations determined from Altimeters and tide gauges. Red curve presents the sea level changes determined from altimeters with IB corrections with a trend at 2.9 mm/yr (without IB corrections the trend is 3.0 mm/yr) from 1985 to 2004. Blue curve presents the trend derived from tide gauges from 1950 to 2002 with IB correction equals 1.6 mm/yr (without IB corrections the trend is 1.6 mm/yr).

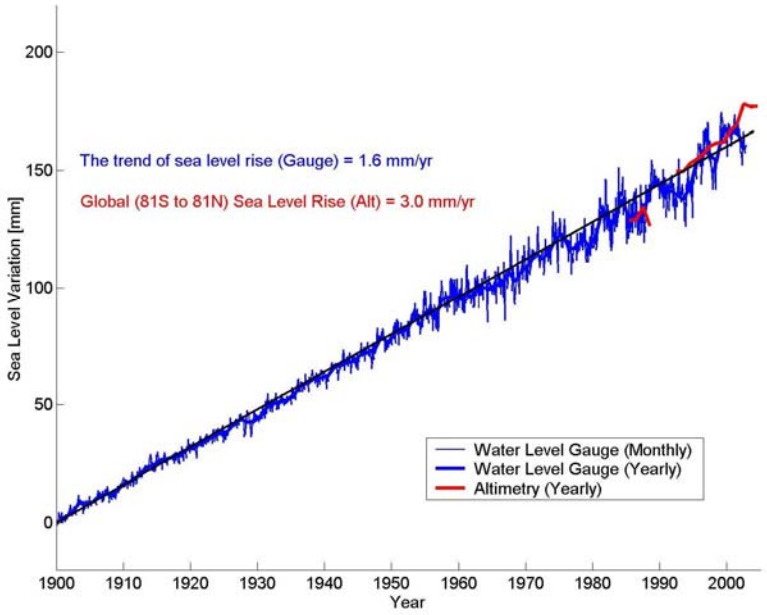

Figure 5.18: Comparison of sea level variations determined from Altimeters and tide gauges. Red curve presents the sea level changes determined from altimeters without IB corrections with a trend at 3.0 mm/yr (with IB corrections the trend is 2.9 mm/yr) from 1985 to 2004. Blue curve presents the trend derived from tide gauges from 1900 to 2002 without IB correction equals 1.6 mm/yr

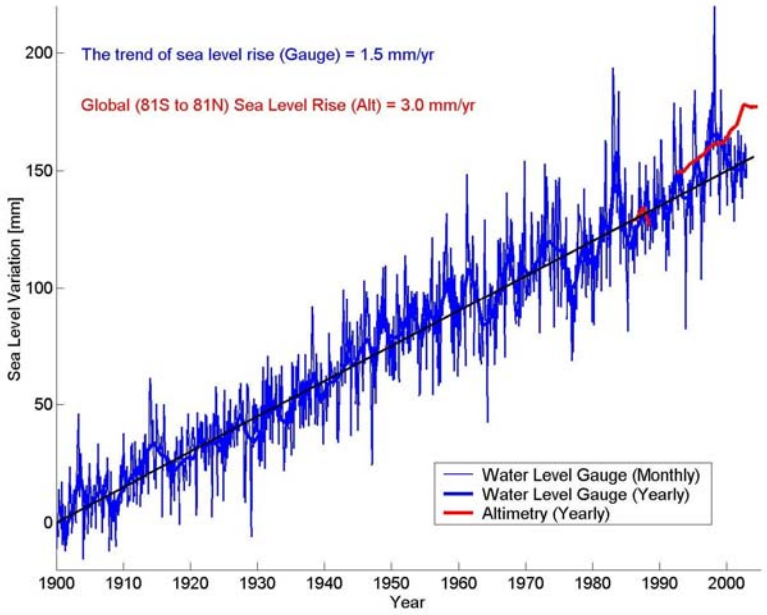

Figure 5.19: Comparison of sea level variations determined from Altimeters and tide gauges. Red curve presents the sea level changes determined from altimeters without IB corrections with a trend at 3.0 mm/yr (with IB corrections the trend is 2.9 mm/yr) from 1985 to 2004. Blue curve presents the trend derived from tide gauges from 1900 to 2002 without IB correction equals 1.5 mm/yr. Not averaging each 10^o by 10^o procedure in the computation when compared with figure 5.18 (see detail description in the text).

5.3 Summary

The rates of global sea level trends during 1985-2002 derived from altimeters (GEOSAT, GFO, ERS-1, ERS-2, ENVISAT, TOPEX/POSEIDON, and JASON-1) and 530 tide gauge stations have been done in this chapter, which are 2.8±0.5 mm/yr and 2.7±0.4 mm/yr, respectively. For 1985-2004, the sea level trend derived from altimeters is equal to 2.9±0.5 mm/yr. Results from the two independent instruments show excellent agreement. Additionally, the rate of sea level variations derived from satellite altimeters, when evaluated near the tide gauge stations, agrees very well at 2.8±0.5 mm/yr. Both cases provide strong confidence for our choice of the 651 tide gauge records for determination of global sea level trend even if they are not distributed evenly or globally. Finally, global sea level trend determined using the 651 tide gauge stations and the developed methodology yields an estimate of 1.6±0.4 mm/yr, which is in good agreement with the previous estimated sea level rise of 1.5 to 2.4 mm/yr and within the error bound [Gornitz, 1982, 1995; Barnett, 1990; Peltier, 1988, 2001; Trupin and Wahr, 1990; Shennan and Woodworth, 1992; Douglas, 1991, 1995, 1997; Mitrovica and Davis, 1995; Ekman, 1998, 2000; Woodworth et al., 1999; Douglas et al., 2001; Mitrovica et al., 2001]. The effect of the atmosphere, i.e., the IB effects on sea level, is assessed using two independent reanalysis atmosphere general circulation models (NCEP and ECMWF). The globally averaged difference of the IB effect is estimated to be around 0.11 mm/yr, agreeing with the conclusion by a similar study [Ponte, 2005].

Recently studies attempt to determine global sea level trend during the last 5 decades using a combination of tide gauge data and altimeter data [Chambers et al., 2002; Church et al., 2004]. The sea level reconstruction; however, is moderately sensitive to variation in the analysis variables, such as tide gauge selection criteria and the number of EOFs used [Jakub et al. 2004]. The largest sensitivity is during the early years of the reconstruction when the least number of tide gauges are available and with relatively larger error in the tide gauge instruments. The errors of reconstructed sea level trends may be caused by short time altimeter data. Time-varying biases (e.g., trends) in the observations will be projected onto the leading EOFs. Because the EOFs used as basis functions are computed over relatively short time intervals, true spatial patterns of global sea level change are not distinct in any one EOF mode. Therefore trends in the tide gauge observations will likely be projected erroneously onto the TOPEX/POSEIDON EOF modes and lead to possible errors. Because of this, any recovered trends from the reconstruction perhaps should be examined with caution. Further study on this topic, i.e., the use of EOF reconstruction to determine global sea level change geographically, is needed.

CHAPTER 6

SEA LEVEL IN ARCTIC AND SUB-ARCTIC OCEANS

In modern climate, ocean circulation is responsible for some half of the poleward heat transport, the remaining half being contributed by the atmosphere [e.g., Piexoto and Oort, 1992]. It has been widely accepted that the Arctic is particularly sensitive to climate variability and is in the midst of a major climate, environmental and societal change *[Study of Environmental Arctic Change (SEARCH) Science Plan,* Morison et al., 2001; Morison et al., 2000]. A comprehensive study on the Arctic system climate, environmental and societal changes undertaken by the Study of Environmental Arctic Change (SEARCH) project [*SEARCH Science Plan,* Morison et al., 2001] describes contemporary changes in the Arctic ocean, in addition to sea ice thinning and its role in a forcing mechanism on climate change, including recent sea level pressure decrease [Polyakov et al., 2003], salinity decrease, temperature increase, diminishing of the cold Halocline layer, and sea level rise in the Russian Seas [Proshutinsky et al., 2001; Proshutinsky et al., 2004]. In particular, Arctic sea ice is sensitive to small changes in vertical oceanic heat flux [Barry et al., 1993], i.e., a flux of 10W/m would melt 1 m of sea ice in a year. Simulations by Manabe et al. [1991] indicate that both sea ice thickness and extent will change markedly in the Arctic in response to gradual increases in *CO2*. Serreze [2003] found a minimum in Arctic sea ice extent and area in the year 2002. Because sea ice governs the interaction between ocean and atmosphere, its thickness or its knowledge is considered to be a critical quantity. Ice thickness not only controls the rate of energy transfer from ocean to atmosphere, but also determines the ice strength, which controls its resistance to motion and deformation [Tucker et al., 1992]. Additionally, major changes in ice thickness will significantly affect the volume of fresh water contributions to the ocean, e.g., Arctic sea ice which advances to the Fram Strait [Kwok and Rothrock, 1999] and melts in the Greenland Sea, where it is associated with deep convection and bottom water formation, and thus plays a major role in global thermohaline overturning [Wunsch, 2002].

In this chapter, we provide a contribution to study the sea level in the Arctic and Sub-Arctic oceans using data from tide gauges and high-latitude observing altimeter satellites. Sea level change in the polar oceans are much less studied primarily because of unavailable of abundant data (i.e., long-term tide gauge sites) due primarily to ice covered oceans/coastal regions causing operation of long-term tide gauges difficult, and to the fact that TOPEX/POSEIDON altimetry only covers the area within $\pm 66^{o}$ in latitude, missing most of the oceans poleward. In this study, ERS-1 and ERS-1 are first calibrated using TOPEX/POSEIDON in the lower latitudes (within $\pm 66^{o}$) and tide gauge records, to remove systematic bias and drift due to problems in the instrument and orbit error. Sea level trend during the period 1985-2004 are then determined using high-latitude observing altimeters ERS-1 and ERS-2 in the Sub-Arctic Ocean. Finally, we provide an updated solution of long-term sea level trend in Arctic Ocean during 1948-2002 using the Arctic Ocean tide gauge records [A. Proshutinsky, personal communication] and address the contributions of barotropic and thermal effects to the observed sea level rise.

6.1 Data Analysis

In this study, GEOSAT/GM, GEOSAT/ERM, ERS-1, ERS-2, and ENVISAT altimeters are used to determine the trend of sea level changes during 1985-2004, which is compared with sea level trend derived from tide gauge records, in the Arctic and Sub-Arctic Oceans. Sea level variations in Arctic and Sub-Arctic Oceans could not be determined from TOPEX/POSEIDON data since TOPEX/POSEDON data only covers latitude $\pm 66^{o}$; however, TOPEX/POSEIDON data which are dual-frequency and thus more accurate can be used to correct or calibrate ERS-1 and ERS-2 data, which have unknown instrument drift problems [R. Francis, personal communication] and errors associated with orbits. For all altimeters, the instrument, media, and geophysical corrections are applied. The atmospheric corrections or inverted barometer (IB) corrections are applied, depending on the need, e.g., for comparison with tide gauge sea level records, which may not have any IB corrections.

In the Arctic and the Sub-Arctic Oceans, Monthly averaged Revised Local Reference (RLR) tide gauge data for 96 stations around the Arctic Ocean from Proudman Oceanographic Laboratory's (POL's) Permanent Service for Mean Sea Level (PSMSL) are used in the study. We adopt the data selecting criteria described in Section 5.2, resulting in the selection of a total of 71 available tide gauges (depicted by triangles in Figure 6.1(a)) for the study.

A barotropic ocean model [A. Prushutinsky, personal communications] is also used to compare with altimeter sea level in this study. The model is forced only by wind stresses and sea level pressure gradients. It is the result of a 2-D model with barotropic ocean and ice dynamics and without ice thermodynamic, and the ice concentration and thickness are from climatology before 1979 and the ice concentration is from observations after 1979 [Proshutinsky et al., 2002]. Wind stresses and sea level pressure gradients are calculated using NCAR/NCEP reanalysis data for 1948–2000.

6.2 Calibration of ERS-1 and ERS-2 Using TOPEX/POSEIDON Altimeter

The NASA/CNESS satellite altimeter mission TOPEX/POSEIDON, which is launched in 1992, is equipped with a dual-frequency altimeter and a nadir-looking microwave radiometer, and designed also with its accurate orbits, to measure sea level changes [Nerem and Mitchum, 2002; Cabanes et al, 2001b]. Since most of the Arctic Ocean is not covered by TOPEX/POSEIDON, other higher latitude observing satellite altimetry satellites including ERS-1, ERS-2, GFO, ENVISAT, and Cryosat are of interest in the problem of polar ocean sea level observations. Since ERS-1 and ERS-2 are less accurate altimeter systems (e.g., single-frequency and lower altitude, causing the orbit accuracy to degrade), and in addition, ERS-1 and ERS-2 have instrument problems associated with the Single Point Target Response (SPTR) errors which create a bias due to thermal anomalies in the altimeter instrument [Richard Francis, personal communication]. The orbit errors on ERS-1 and ERS-2 are due potentially to geographically correlated gravity errors and the unsymmetrical ground-based satellite laser ranging (SLR) stations tracking the satellites. One of the errors manifests in a z-bias or tilt in the radial orbit in the north-south (latitude) direction, resulting in a potential sea level trend error in the polar regions.

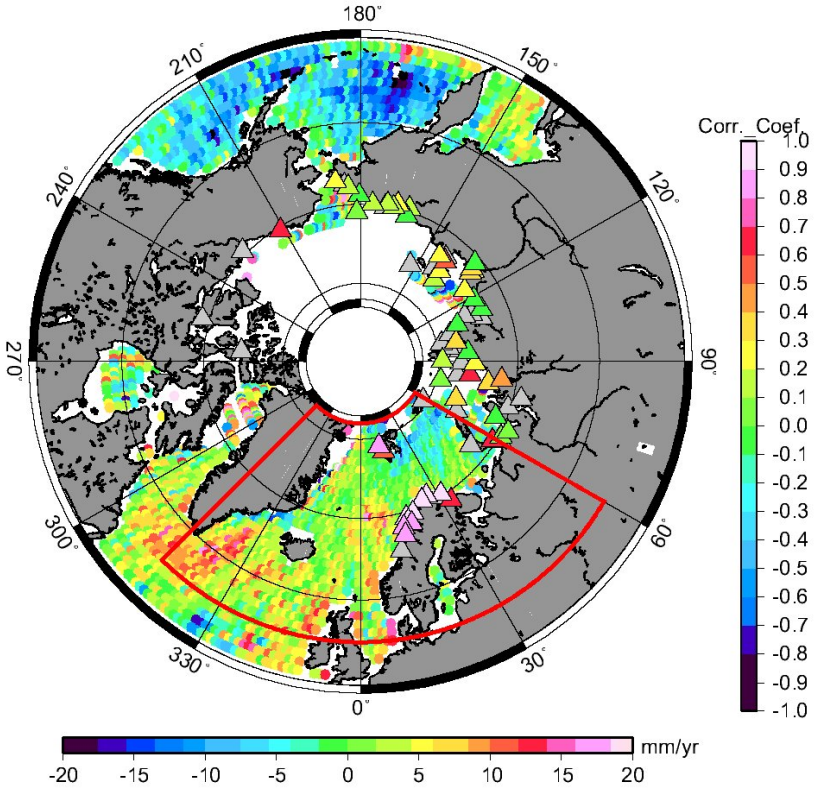
180°
210°
150°
240°
120°
270°
90°
300°
60°
330°
30°
0°
Corr._Coef.
1.0
0.9
0.8
0.7
0.6
0.5
0.4
0.3
0.2
0.1
0.0
-0.1
-0.2
-0.3
-0.4
-0.5
-0.6
-0.7
-0.8
-0.9
-1.0
mm/yr
-20
-15
-10
-5
0
5
10
15
20

(a)

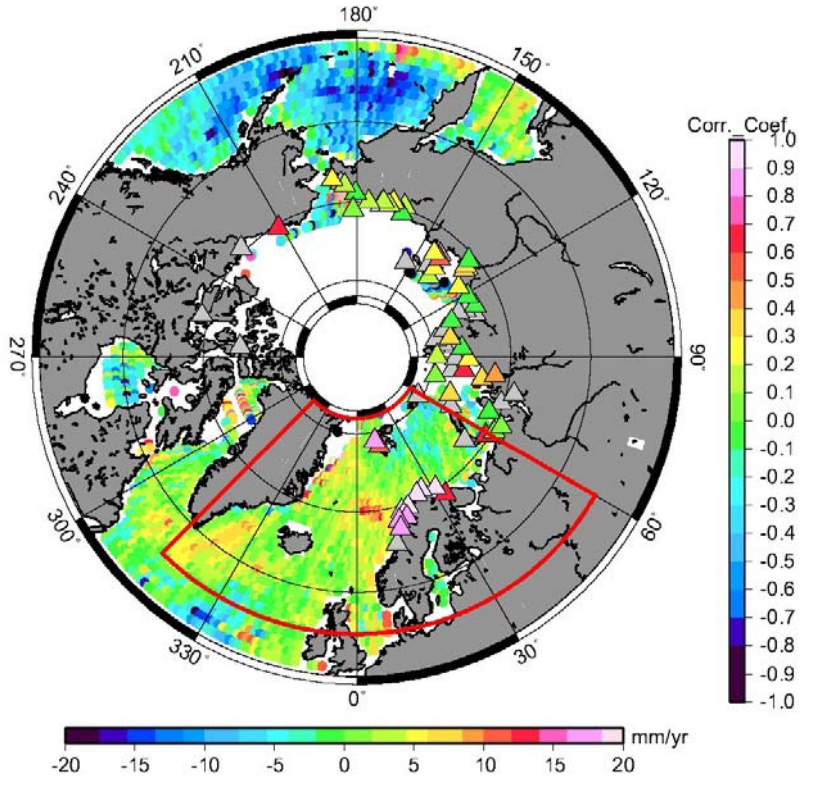
180°
210°
150°
240°
120°
270°
90°
300°
60°
330°
30°
0°
Corr._Coef.
1.0
0.9
0.8
0.7
0.6
0.5
0.4
0.3
0.2
0.1
0.0
-0.1
-0.2
-0.3
-0.4
-0.5
-0.6
-0.7
-0.8
-0.9
-1.0
mm/yr
-20
-15
-10
-5
0
5
10
15
20

(b)

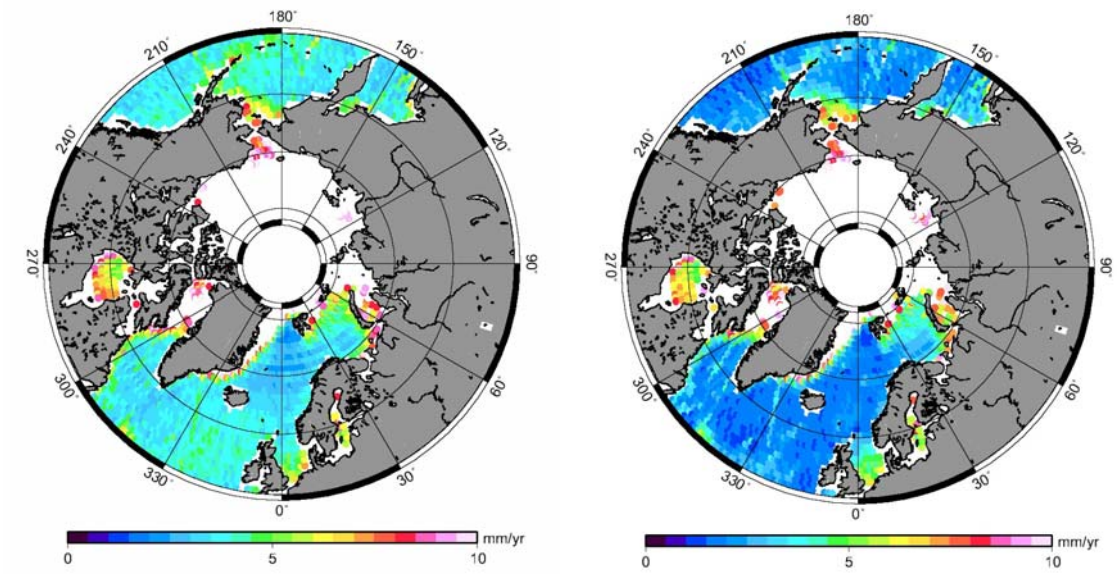

(c) (d)

Figure 6.1: (a) Geographic sea level trends derived from GEOSAT and ERS-1 and ERS-2 without applying IB corrections. (b) Geographic sea level trends derived from GEOSAT and ERS-1 and ERS-2 with IB corrections. (c) Formal errors of (a). (d) Formal errors of (b). Triangles are tide gauge stations from PSMSL.

We validate the ERS-1 and ERS-2 data for sea level by comparing them to the more accurate data from TOPEX/POSEIDON in the lower latitudes, as their observations overlap each other in time. First, we compare ERS-1 and ERS-2 sea level trends with TOPEX/POSEDION sea level trends during the same data span (~10 years) in latitude bands, to provide confidence of the less accurate ERS data used to measure sea level changes in the Arctic Ocean. We first determine the sea level trends using ERS-1 and ERS-2 within latitude 30N~66N, 0N~30N, 30S~0S and 66S~30S, individually as well as using TOPEX/POSEIDON (Figure 6.2). It is evident that the difference of sea level trends is highly correlated with latitude, with ERS-2 drifting more than ERS-1 with respect to TOPEX/POSEIDON. This error is presumably due to the fact that ERS-2 is on zero-gyro for its altimeter Earth-pointing attitude control, which is high-latitude dependent. Instead of formulating an instrumental model to correct for the drifts, which are difficult as there is a lack of spacecraft data to implement the model [Richard Francis, personal communication], we choose to derive an empirical model, fixing TOPEX/POSEIDON in the lower latitude ($\pm 66^0$) as "truth", and model the drifts of ERS-1 and ERS-2 with respect to TOPEX/POSEIDON, which are assumed to be linear depending on latitude as a variable.

$$drift = a + b(dis(\varphi - \varphi_0)) \qquad (6.1)$$

where a is the offset, b is the slope, φ and φ_0 are the latitudes of computed trend difference and the equator, respectively, and $dis(\varphi - \varphi_0)$ is the distance between the locations of computed trend difference and the equator.

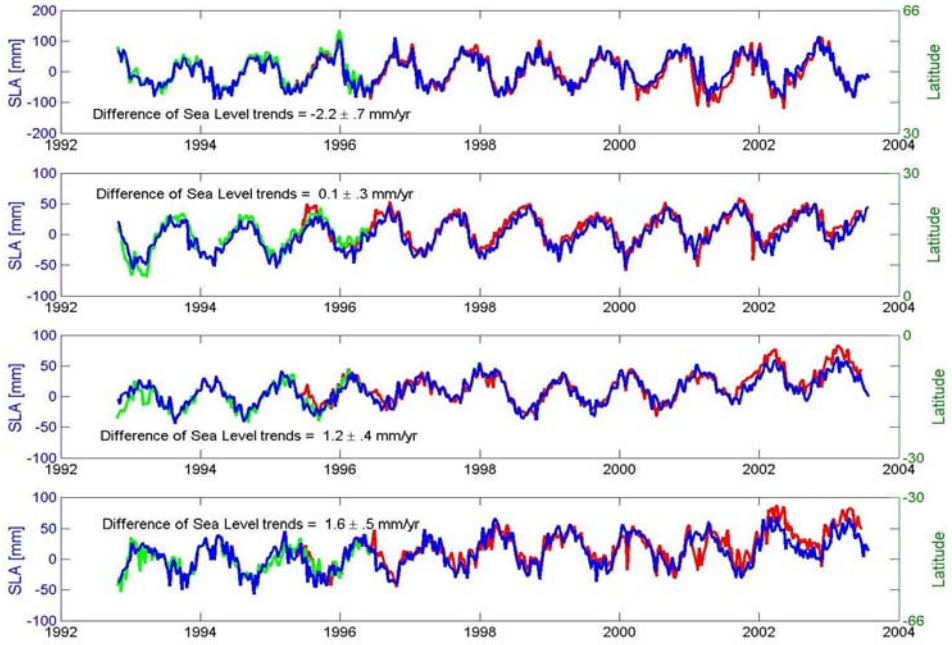

Figure 6.2: Comparison of sea level trends derived from TOPEX/POSEIDON (blue curve), ERS-1(Green curve) and ERS-2 (red curve) within four latitude bands 30N~66N, 0N~30N, 30S~0S and 66S~30S.

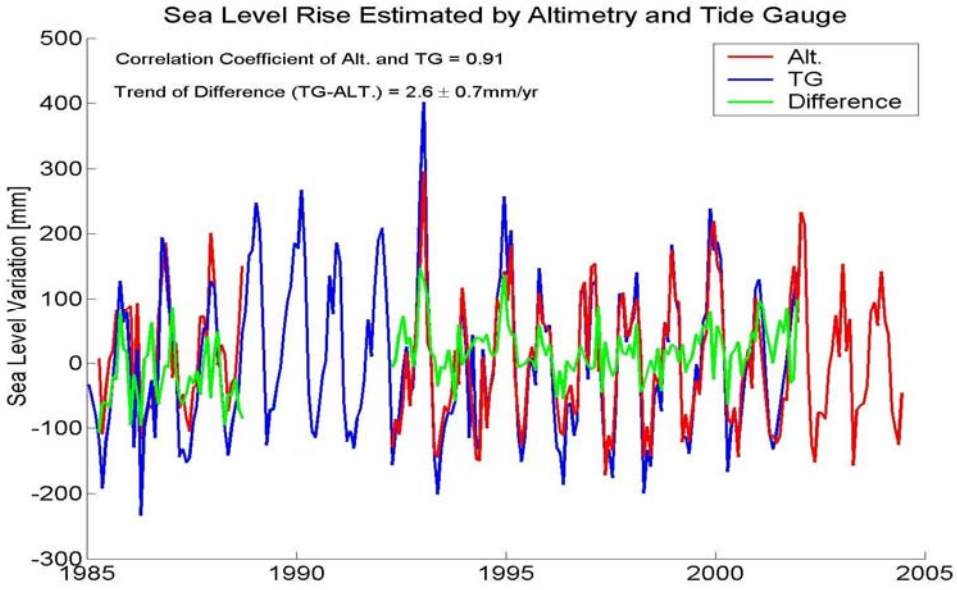

Figure 6.3: Comparison of sea level variations derived from tide gauge data and altimeter data (GEOSAT/GM, GEOSAT/ERM, ERS-1, ERS-2 and ENVISAT) within 3-degree of gauge stations.

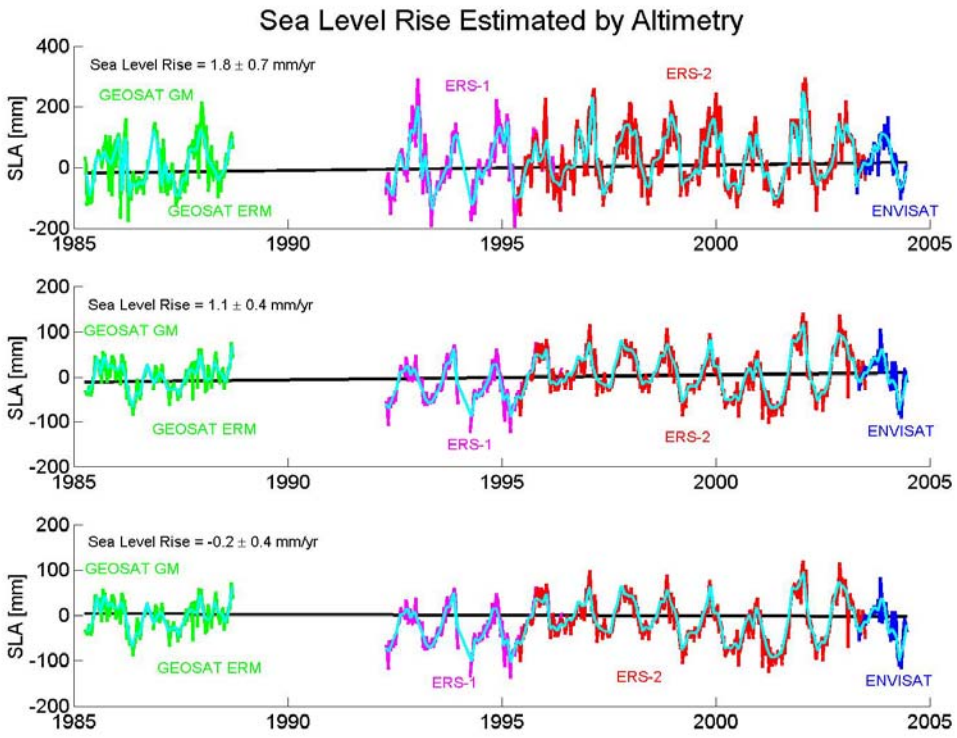

Figure 6.4: Sea level changes are computed within latitude 55N-82N and longitude 315E-60E using GEOSAT/GM, GEOSAT/ERM, ERS-1, ERS-2 and ENVISAT. The drift of Geosat and ERS is applied as 2.4 mm/yr. TOP: Sea level changes without applying IB corrections. MIDDLE: IB corrections are applied. BOTTOM: Remove 0–500 m thermosteric sea level trend derived from Levitus et al. [2005].

φ is assumed to be the middle of latitude band. As a result, unknown parameters a and b can be solved using trend differences as observations in Equation (6.1) by the least squares approach. The resulting adjustment yields a combined drift of ERS-1 and ERS-2 sea level (with respect to TOPEX/POSEIDON) in Arctic (and the Sub-Arctic) Ocean can be predicted as $2.4 \pm 0.6 mm/yr$ using the estimated a and b. However, when averaging ERS-1 and ERS-2 altimeter data globally with equal area weights, the drift (with respect to TOPEX/POSEIDON) averages to zero if global sea level is computed using ERS-1 and ERS-2. This is why there is no drift correction for ERS altimeters when determining global sea level trend.

Additionally, altimeters are also being validated or calibrated using tide gauge records in order to further verify the calibration constants using lower latitude data from TOPEX/POSEIDON. First of all, a correlation coefficient of sea level changes derived from a tide gauge station and altimeter data, which are within 3 degree of the tide gauge station, is computed. Triangles in Figure 6.1 (a) show the correlation coefficients of 71 tide gauge records and altimeter data. Gray color means that there is no data from the specific tide gauges during 1985–2004. After analyzing the coefficients, it is found that the tide gauge stations with correlation coefficients>0.8 are located entirely in the Barents Sea, which may result from local sea level differences or the lack of altimeter data in other (ice-covered) areas. It is found that the quality of the altimeter measurements is better in the Barents Sea. The explanation could be that

the sea ice covers most area of Arctic Ocean or the Sub-Arctic Ocean in the winter season or permanently near the North polar region and as a result, degrading the altimeter sea level data in the other regions. For this reason we selected the region (Fig. 6.1a), which covers latitude 55N-82N and longitude 315E-60E, for calibrating ERS altimeter sea level data and to compute sea level changes. Ten tide gauge stations are shown in Table 6.1, all of which have the correlation coefficients>0.8 when compared with altimeter data, are used to compute sea level variations. Altimeter data within 3 degree of 10 tide gauge stations are used to determine sea level changes. Figure 6.3 presents a comparison of sea level changes derived from gauge data and altimeter data including GEOSAT/GM, GEOSAT/ERM, ERS-1, ERS-2, and ENVISAT. It indicates that sea level changes derived from altimeters and from tide gauge records are highly correlated. The trend of sea level difference between two different data is 2.6±0.7 mm/yr. This estimated drift agrees well with the previous estimate when comparing with TOPEX/POSEIDON data but both cases have large uncertainties. Therefore, applying a drift of 2.4 mm/yr for ERS-1 and ERS-2 in the selected region is reasonable but should be carefully.

6.3 Sea Level Changes Derived from Altimeter Data and Tide Gauge Records

In accordance with Section 6.2, a drift correction of 2.4 mm/yr is applied for ERS-1 and ERS-2 data to compute sea level changes in Sub-Arctic Ocean, latitude 55N-82N and longitude 315E-60E. Upper panel of Figure 6.4 shows the sea level change derived from altimeters without applying IB corrections (using ECMWF operational run pressure field) with the trend at 1.8 mm/yr. Middle panel of Figure 6.4 shows that the sea level change with IB corrections with trend at 1.1 mm/yr. Accordingly, the trend of sea level change responding to atmospheric pressures in this region is 0.7 mm/yr, which is significantly larger than the contribution of global averaged atmospheric pressures [e.g., Ponte, 2005]. Lower panel of Figure 6.4 presents the sea level change after subtracting the trend (1985–2003) of thermosteric sea level derived from Levitus et al. [2005], which equals 1.3 ± 0.4 mm/yr. The residual trend of sea level changes is –0.2 mm/yr, indicating that the most of the signals have been explained to be due to the barotropic response and the thermal expansion of the ocean. However, the uncertainty of residual trend is quite high primarily because of the short data span. The remaining signals contributing to the sea level trend include wind, precipitation, evaporation, halosteric sea level, river flow and melting of sea ice. However, these contributions are much smaller than IB and thermosteric sea level, which have also been concluded by Proshutinsky et al. [2001 and 2004]. Fig. 6.1 shows the geographical sea level trends and the corresponding formal errors for the studing region determined using satellite altimetry. Figure 6.1(a) shows the geographic sea level trends derived from GEOSAT and ERS-1 and ERS-2 without applying IB corrections while (b) shows geographic sea level trends with IB corrections. Figures 6.1(c) and (d) indicate the formal errors of Figures 6.1(a) and (b), respectively. The fluctuation in Figure 6.1(b) is significantly smaller than Figure 6.1(a), while the formal errors in Figure 6.1(d) are relative lower than Figure 6.1(c), hence the contribution of atmospheric pressures to sea level changes is essentially larger in the Arctic and the Sub-Arctic Oceans than global average.

Figure 6.5 shows that the sea level trends during the time span of 1985-2000 from the barotropic ocean model [Proshutinsky et al., 2002, courtesy, A. Proshutinsky]. White color indicates invalid data. The averaged trend in the entire area is 0.3±1.0 mm/yr while the averaged

sea level trend in the selected area described above is 0.8 ±1.0 mm/yr (red curve in Figure 6.6). Blue line is the sea level changes derived from altimeters after removing steric sea level from WOA01, which are monthly climatology data and only present the semi-annual and annual variations and then do not contain the secular trend signal. The sea level variations derived from the barotropic model and steric-corrected altimeter data are compatible and the correlation coefficient is 0.63. In order to compute the sea level trend, yearly objective analyzed data are used to compute thermosteric sea level trend. The trend of sea level changes derived from altimeters after the removing thermosteric sea level trend equals 0.5 mm/yr. Therefore, the steric-corrected and the barotropic model sea level agree well in terms of the secular trend and they are highly correlated.

The sea level trend during the time span of 1948–2002 has been also determined using 71 tide gauge data from PSMSL and the Arctic Ocean gauge data courtesy of A. Prushutinsky. The sea level trend is equal to 1.92±0.14 mm/yr when ICE4G is applied. If BIFROST model computed with LT of 120 km, UMV of 1×10^{21} Pas and LMV of 3×10^{21} Pas, is used, the rate changes to 2.03±0.14 mm/yr; however, if UMV is set to 0.5×10^{21} Pas, the rate is equal to 1.93±0.14 mm/yr, which agrees with the previous estimated sea level rate when applying ICE4G. Next, IB corrections are applied to tide gauge data by means of atmospheric pressures from NCEP model. In order to assess the quality of atmospheric pressures in Arctic Ocean, a comparison of two atmospheric models is done. Figure 6.7 shows the averaged atmospheric pressures, which are interpolated from NCEP and ECMWF models at 71 tide gauge locations. Green curve shows sea surface pressures of ECMWF and the trend equals –0.057±0.014 mbar/yr, which is approximately equal to 0.57±0.14 mm/yr of sea level changes. Red curve presents sea surface pressures of NCEP and the trend is –0.051±0.013 mbar/yr, which is approximately equal to 0.51±0.13 mm/yr. The correlation coefficient of ECMWF pressure and NCEP pressure is high at 0.998. Blue curve presents the difference of ECMWF and NCEP model, which has the mean at 0.45±0.33 mbar (–4.5±3.3 mm) and has the estimated trend at 0.006±0.001 mbar/yr (–0.06±0.01 mm/yr). The estimated long-term (1948–2002) sea level trends in the Arctic Ocean based on tide gauge data vary from 1.55 mm/yr, 1.59 mm/yr, and 1.53 mm/yr with identical former errors of 0.9 mm/yr when applying IB corrections using NCEP model. This result with estimates using a longer data span and using other PGR models (ICE4G and the BIFROST models) is in excellent agreement with Proshutinsky et al. [2004].

PSMSL ID	Longitude (degree)	Latitude (degree)	Correlation Coefficients
025021	11.9333	78.9333	0.84
040001	31.1000	70.3333	0.91
040015	25.9833	70.9833	0.91
040021	23.6667	70.6667	0.90
040031	18.9667	69.6500	0.91
040041	16.1500	69.3167	0.92
040061	16.5500	68.8000	0.92
040081	17.4167	68.4333	0.88
040091	14.4833	68.2167	0.88
040101	14.3833	67.2833	0.90

Table 6.1: Tide gauge stations with correlation coefficients >0.8.

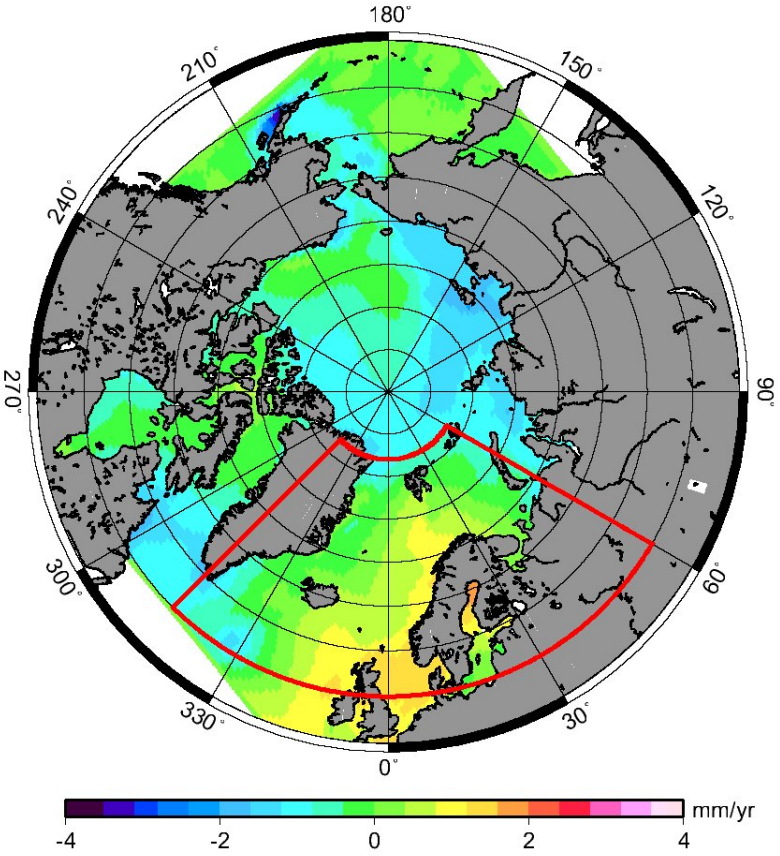

Figure 6.5: Sea level trends from a barotropic ocean model (1985-2000). A 2-D model forced by wind stresses and sea level pressure gradients [Prushutinsky et al., 2002].

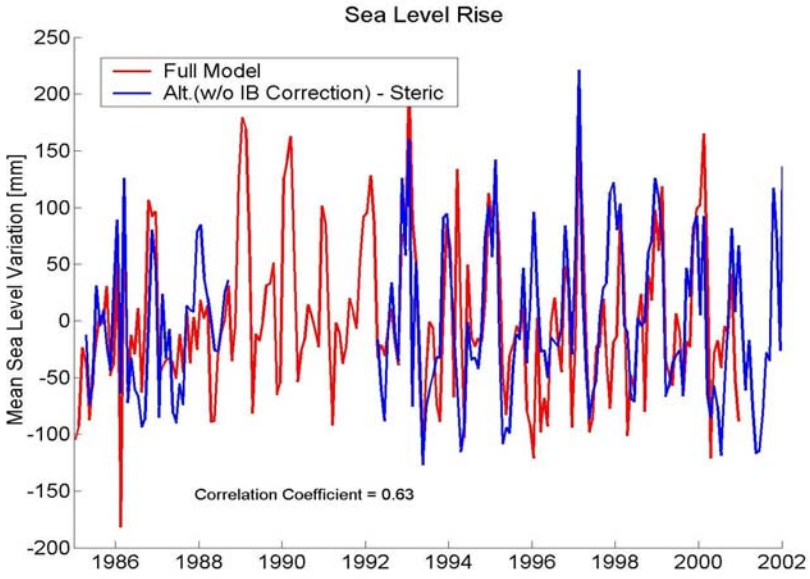

Figure 6.6: Comparison of steric-corrected sea level changes and simulated sea level changes in the selected region, latitude 55N-82N and longitude 315E-60E.

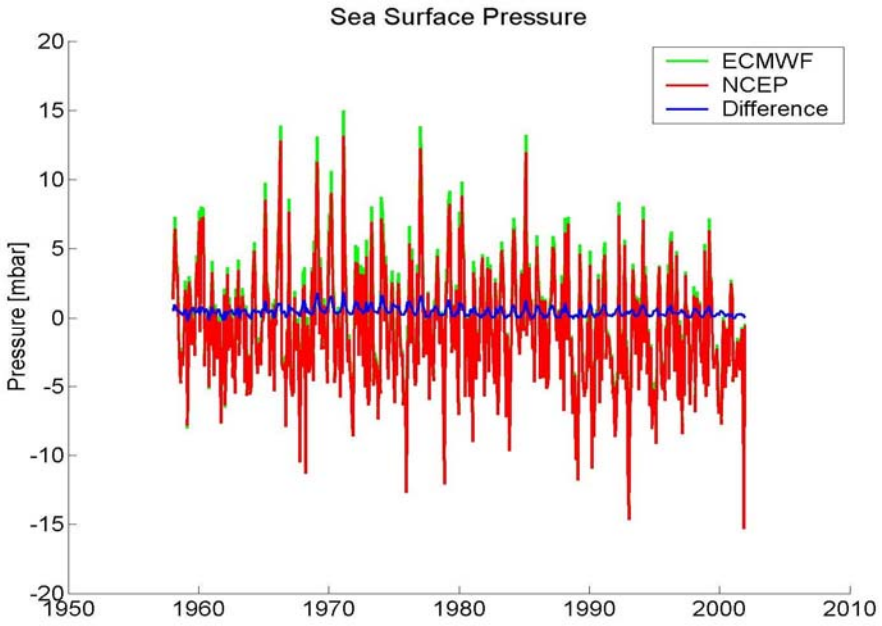

Figure 6.7: Sea surface pressure of PSMSL at tide gauges (71 stations) in Arctic Ocean.

6.4 Summary

In this study, the combined drift of ERS altimeters has been identified after comparing with TOPEX/POSEIDON, and removed. The drift rate is estimated as 2.4 mm/yr. After applying the drift correction, the sea level trend in latitude 55N-82N and longitude 315E-60E (Sub-Arctic Ocean) is estimated at 1.8 mm/yr, which can be characterized to be caused primarily by sea surface atmospheric pressures and thermosteric sea level trend. It is noticed that the uncertainty is too large (or the altimeter data span is to short) to have complete confidence in stating the conclusion. However, the estimated trend agrees well with the simulated sea level based on ocean general circulation model in the Arctic region provided by Prushutinsky et al. [2002]. In addition, sea level trend in Arctic Ocean during the period 1948–2002 is estimated to be 1.9–2.0 mm/yr when using different PGR models and tide gauge data. After applying the IB corrections using NCEP model, the sea level rise reduces to 1.5–1.6 mm/yr. In conclusion, the effect of surface atmospheric pressures is a much more important contribution to sea level trend in Arctic Ocean (0.4 mm/yr) than globally (0.11 mm/yr) [e.g., Ponte, 2005].

GEOSAT and ENVISAT have not been calibrated in this study to determine sea level changes but the influence is expected to be small primarily because of the relative short time spans of data. In the future work, a comprehensive calibration of all altimeters should be done in order to determine the sea level trend more precisely. In addition, more contemporary altimeter missions can be added to extend the time span, which can potentially avoid the errors caused by decadal or inter-decadal signals when computing a secular trend.

CHAPTER 7

ACCELERATION OF SEA LEVEL RISE IN THE 1990s?

The coastlines are the most populated regions in the world, and developed cities largely locate in the area taking advantage of water-base transportation and living quality. At the LGM (Last Glacial Maximum) about 21,000 years ago, sea level was much lower than present at approximately 125 m. Coastal resorts, like New Orleans and Miami Beach, had a few hundred km more shoreline during LGM; however, they are not located on the coasts right next to the ocean. Recent studies indicate that the global sea level is rising in the range of 1.5 to 2.4 mm/yr [e.g., Douglas, 2001; Mitrovica et al., 2001; Church et al., 2004] so the populated area of human is continuing to diminish. The other notable open question is whether global sea level rise accelerates in the 1990s [Carton et al., 2005], which could result from accelerated global warming presumably because of anthropogenic cause [Hansen et al., 2004]. Gregory et al. [2001] and Church et al. [2001] indicate an acceleration of sea level rise during the 20th Century and beyond in response to increasing concentration of greenhouse gases through climate model projections. However, Douglas [1992] and Woodworth [1990] consider sea level records contain a considerable amount of interannual and decadal variability so no definite long term acceleration of sea level has been identified using the 20th Century data alone. The other possible reason for one not to be able to detect sea level acceleration may be the sparse tide-gauge network [Gregory et al., 2001].

The global sea level rise in the 20th Century is estimated at 1.8 mm/yr [Church et al, 2004; Douglas, 2001] while sea level rise derived from TOPEX/POSEIDON satellite altimetry since 1993 is 3.1±0.4 mm/yr [Cazenave and Nerem, 2004], which is more than 50% more than the long-term rate of 1.8 mm/yr. In addition, Willis et al. [2005] and Carton et al. [2005] indicate a commensurate more rapid rise of thermosteric sea level during 1993–2001 as compared with the centennial estimate. Although the rate of sea level rise during the TOPEX/POSEIDON period is larger than the averaged rate of rise over the 51-year period, Church et al. [2004] confirms there is no significant increase in the rate of rise by visual inspection and fitting a quadratic to the time series.

Recent studies attempt to answer the question if the thermosteric and the total sea level are accelerating in the 1990s. Willis et al. [2004], Antonov et al. [2005], and Ishii et al. [2005] determined the trends of thermosteric sea level (0–700 m) during 1993–2003 are 1.6±0.3 mm/yr, 1.23±0.2 mm/yr, and 1.8±0.2 mm/yr respectively while the long-term trend is estimated to be close to 0.4 mm/yr [Antonov et al., 2005] during the time span of 1955–2003. The thermosteric sea level trends are significantly different in these two time spans and the acceleration of thermosteric sea level looks obviously in 1993-2003 time windows if only comparing the values of the trends. Willis et al. [2004] reported it is not possible to identify whether the recent increase in ocean warming is due to an acceleration of heat uptake by the ocean or is simply decadal variability with the present time series since the warming rate in the early 1970s is comparable to the present rate. Carton et al. [2005] claimed dynamic height during 1993-2001 increases at a global rate of 2.3±0.8 mm/yr, a substantial acceleration beyond the multi-decadal

steric sea level trend of 0.5 mm/yr (Figure 1 of his paper). However, the same dramatic increase of dynamic heights also occurred during 1970–1980 in the same figure. Therefore, the increase of rate during 1993–2001 could be caused by interdecadal signals. Hansen et al. [2005] reported recent evidence of the Earth's energy imbalance (0.85 ± 0.15 W/m^2 more absorption than emission of the Sun's energy) and cited studies as confirmations of his study based on last decade's accelerated thermosteric sea level rise [Willis et al., 2004] and TOPEX/POSEIDON altimeter observed sea level rise [Cazenave and Nerem, 2004].

Studies mentioned above which examines whether sea level or thermosteric sea level accelerates only depends on the rates estimated during different time spans; therefore, a more robust method should be introduced to answer the question: is global sea level rise accelerating during the last decade? One reliable approach is hypotheses testing, which can be used to check the information maybe stemming from preceding or additional measurements or even based on supposition available to the unknown parameters. In this Chapter, an attempt to answer the question whether sea level derived by tide gauge data and thermosteric sea level accelerate will be done by hypothesis testing. Additionally, the minimum time span required for obtaining a stable sea level trend is also analyzed.

7.1 Data Analysis

7.1.1 Tide Gauge Records

In order to examine whether sea level rise accelerates, sea level trends will be determined by overlapping 10-year data, so tide gauge stations with longer time span and without big data gaps are the prime candidate to avoid the errors caused by lacking of data. Monthly averaged Revised Local Reference (RLR) tide gauge data of 27 stations from Proudman Oceanographic Laboratory's Permanent Service for Mean Sea Level (PSMSL) are the suitable selection, which are suggested by Douglas et al. [2001]. These gauges should conform to the requirements that the gauge records must be long, free of vertical motions due to plate tectonics, adequately correctable for GIA using existing models, and have trends insensitive to small changes in their record length or be capable of being edited in a justifiable manner based on oceanographic consideration. The latest record in 27 gauges ends in 2001. The records with the longest time span extend from mid-1800 to 2001; however, all records that were used exceed 70 years.

7.1.2 World Ocean Atlas and Database 2001 [Levitus et al., 2005]

The data set of $1°\times1°$ grid temperature anomalies is provided as yearly means for the upper 700 m from 1955 to 2003 and 5-year means down to 3000 m from 1955 to 1998 by Levitus et al. [2005]. They computed yearly global $1°\times1°$ grids at non-uniformly spaced depth levels using the raw temperature profiles, based on an objective analysis scheme. By analyzing the data set, Levitus et al. [2005] reported that globally-averaged ocean heat content (0-3000 m) increased by 14.5×10^{22} joules between 1955 and 1998, corresponding to a net ocean mean temperature warming of 0.037°C during the past 50 years at a rate of 0.20 Wm^{-2} (per unit area of Earth's total surface area). For the world ocean the linear trend of heat content (0–3000 m layer for 1955–1998) is 0.33×10^{22} J/year.

In addition, annual temperature and salinity data from WOA01 are in the format of one-degree objectively analyzed mean. Maximum depth for annual objective analyses reaches 5500 m (33 layers).

7.2 Hypothesis Testing

As it is well known, least squares algorithm can deal with the estimation of unknown parameters. Using variances and covariances of the estimates, the dispersion matrix of the estimates about their expected values could be determined. According to the dispersion matrix of the estimates, the interval of estimates can be given. For instance, one, two and three times of a standard deviation are considered for about 68%, 95% and 99% confidence of t-distribution respectively, to provide the range of errors. However, no statistical result addresses whether the estimate is significantly reliable, so the hypothesis testing should be used in the study. Hypothesis testing intends to check the information may be stemming from preceding or additional measurements or even based on supposition, which may be information available for the unknown parameters; for example, the acceleration of sea level rise is supposed as 0 for the additional information in this study. The acceptance or rejection of the hypothesis results from the hypothesis testing under a given error probability. First of all, Gauss-Markov (GM) model should be introduced and written as [e.g., Koch, 1999]:

$$y = \underset{n\times m}{A}\,\xi + e \quad with \quad e \sim (0, \sigma_0^2 P^{-1}) \text{ and } rank(A) = m, \tag{7.1}$$

where n is the dimension of observation vector, y; A is the design matrix, m is the size of the state vector (unknown parameters), ξ ; e is random error vectors, σ_0^2 is a priori variance associated with the weight matrices, P . The hypotheses for the parameters ξ are introduced into the linear Gauss-Markoff model as linear function.

$$w = \underset{l\times m}{K}\,\xi, \;\; rank(K) = l, \;\; rank(A^T, K^T) = m, \tag{7.2}$$

where l is the number of constrain equations or the so-called pseudo-observations, w. K is the design matrix for the constrain equations. Combination of Equation (7.1) and (7.2) is used to be called Gauss-Markoff model with fixed constraints as well. Hence, for the univariate model the general hypothesis can be formulated as

$$H_0 : w = K\xi \text{ vs. } H_a : w \neq K\xi. \tag{7.3}$$

Then the test statistic T can be written as:

$$\begin{aligned} &T : \frac{R/l}{\Omega/n - rank(A)} \sim F_\alpha(l, n - rank(A)), \text{ with} \\ &\Omega = (y - AN^{-1}c)^T P(y - AN^{-1}c), \\ &R = (w - KN^{-1}c)^T (KN^{-1}K^T)^{-1}(w - KN^{-1}c), \end{aligned} \tag{7.4}$$

where F is F-distribution (Fisher distribution). α is the lower $\alpha - percentage$ point. $N = A^T PA$ and $c = A^T Py$. With a significant level of α the null hypothesis H_0 is therefore rejected if

$$T > F_\alpha(l, n - rank(A)). \tag{7.5}$$

Or accepted if

$$T \le F_\alpha(l, n - rank(A)). \tag{7.6}$$

Acceptance indicates the hypothesis of estimates is confident under the given lower $\alpha - percentage$ point, while rejection indicated the hypothesis of estimates is unmeaning.

7.3 Sea Level Trend Determined from Tide Gage Data

Trend of sea level variations can be calculated using two steps in this study. First of all, sea level trend with the formal error is determined by fitting bias, slope, annual and semi-annual signals at each tide gauge station. Secondly, sea level changes are derived by averaging all selected tide gauge records at the same epoch, which are weighted by the computed formal errors derived from the first step. The top panel of Figure 7.1 shows the sea level variations derived from 27 tide gauges. As the result, the trend of sea level variations is equal to 1.8 mm/yr, which shows an excellent agreement with Douglas [2001].

In order to examine whether tide gauge records contain the lower frequency signals, including decadal or inter-decadal signals, the trends of sea level variations are determined using different time periods of time. Therefore, the variations of trends in different time spans could result from the low frequency signals of sea level changes. Table 7.1 and upper panel of Figure 7.2 show the sea level trends determined using different time spans. The rate of sea level trend derived from tide gauge records with time span shorter than 20 years can not be presented stably and is relative larger than the time span longer than 20 years. In conclusion, the sea level trend derived from TOPEX data alone [e.g., Nerem and Mitchum, 2001; Cabanes et al., 2001b; Cazenave and Nerem, 2004] with less than 10 years of data can not interpret the true sea level trend and its larger rate of 3.0 mm/yr could not address an acceleration of sea level rise even if the sea level trend determined from about 100 years of tide gauge records equals 1.8 mm/yr [Douglas, 2001].

Hypothesis testing is presented here in order to answer the question if the sea level rise is accelerating in the 1990s. The lower panel of Figure 7.1 illustrates the trends of sea level variations, which are determined by overlapping 10-year tide gauge records. Trends are plotted at the centers of 10-year periods. Obviously there is an interdecadal signal after 1950. For the sake of understanding whether the sea level rise is accelerating, the slope of 10-year trends is fit by a linear regression and therefore hypothesis testing in Section 7.2 can be introduced. In light of Equation (7.1) and (7.2), the formula is re-written as follows:

$$y_i = \begin{bmatrix} 1 & t \end{bmatrix} \begin{bmatrix} a \\ b \end{bmatrix} + e_i \text{ and } w = \begin{bmatrix} 0 & 1 \end{bmatrix} \begin{bmatrix} a \\ b \end{bmatrix} = 0 , \quad (7.7)$$

where y_i is the overlapping 10-year trend of sea level variations, t is time at the center of 10-years period, a is offset, and b is slope. The latter of Equation (7.7) is additional information of the unknown parameter, b, based on supposition. It supposes the acceleration of sea level rise is equal to zero. Afterward, test statistics T can be computed according to Equation (7.4):

$$T = 1.2426 < F_{0.05}(1,90) = 3.95$$

On account of data lack before 1905 in most of 27 tide gauges, the case only using time span 1905 to 2000 is examined as well. The test statistics T is:

$$T = 0.0068 < F_{0.05}(1,85) = 3.96$$

Both cases are accepted hypothesis H_0 and consequently slope $b = 0$ is true with a significant level of 95%, which means sea level trend does not accelerate from 27 tide gauge records in 1900–2000 and 1905–2000.

Time span (years)	Sea level Trend (mm/yr)
1902-2000: 99	1.77±0.02
1912-2000: 89	1.80±0.03
1922-2000: 79	1.86±0.03
1932-2000: 69	1.68±0.04
1942-2000: 59	1.52±0.05
1952-2000: 49	1.52±0.06
1962-2000: 39	1.70±0.09
1972-2000: 29	1.63±0.15
1981-2000: 20	1.84±0.26
1982-2000: 19	1.76±0.28
1985-2000: 16	2.68±0.35
1987-2000: 14	3.45±0.44
1992-2000: 9	2.72±0.85

Table 7.1 Sea level trends derived from 27 tide gauges [Douglas, 2001] using different time spans.

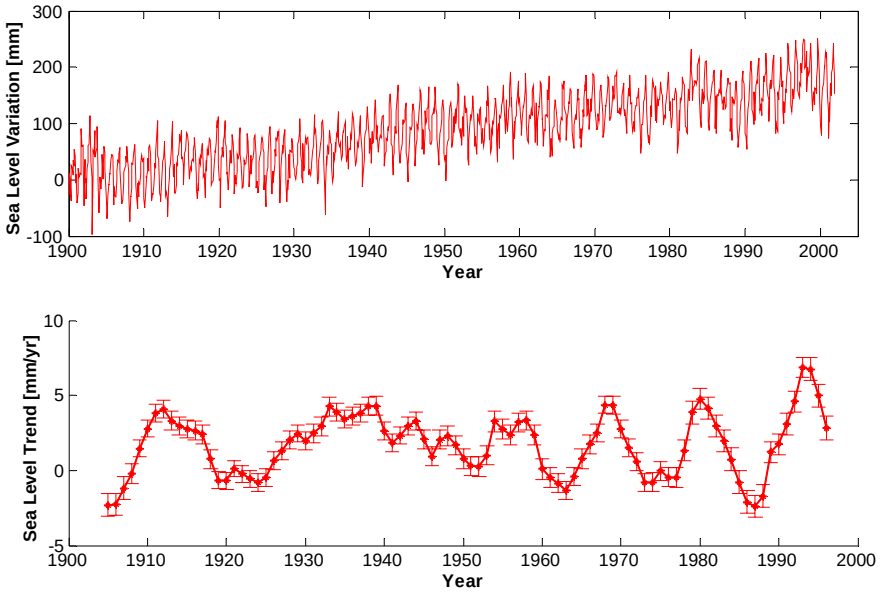

Figure 7.1: Top: Sea level variations derived from 27 tide gauges [Douglas, 2001]. Bottom: Trend of sea level variation is determined by overlapping 10-year data. Trends are plotted at the centers of 10-year periods.

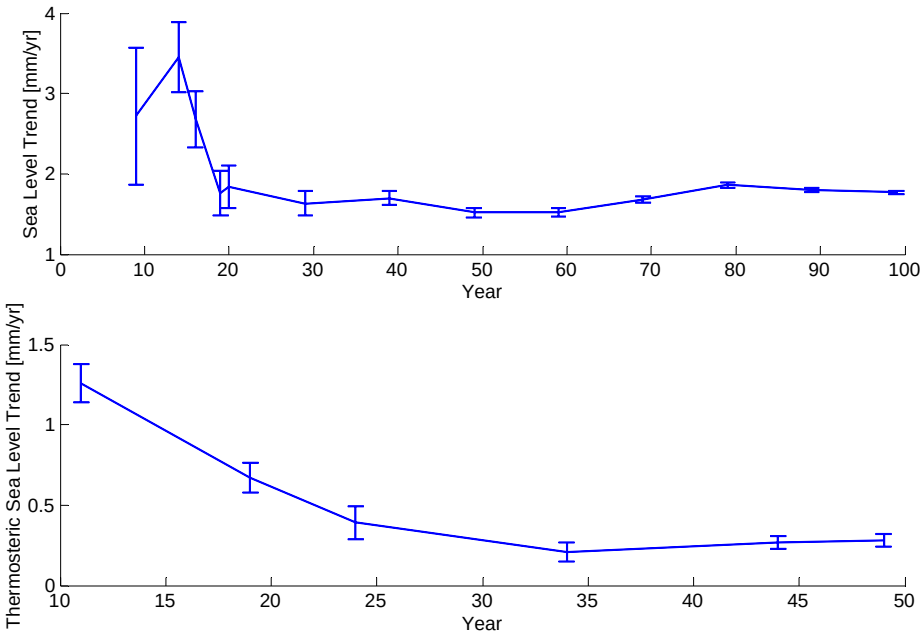

Figure 7.2: Top: Trends of sea level variations derived from 27 tide gauges [Douglas, 2001] using different time spans (Table 7.1). Bottom: Trends of thermosteric sea level variations, which are calculated from temperatures of WOA01 [Levitus, 2005], using different time spans (Table 7.2).

7.4 Thermosteric Sea Level Trends

Since the coverage of tide gauge stations is non-global or uneven, the analysis is attempted to do in terms of thermosteric sea level changes, which can be computed by means of globally grid temperature data. After choosing a long-time-averaged temperature and salinity as reference datum, the steric sea level can be expressed as follows in accordance with Equation (3.7):

$$h_{steric} = \int_{z_1}^{z_2} \left(\frac{1}{\rho(S,T,p)} - \frac{1}{\rho_0(S_0,T_0,p_0)} \right) dz , \tag{7.8}$$

where $S_0, T_0,$ and p_0 are the mean salinity, temperature and pressure data, respectively. S is the salinity of sea water, T is the temperature of sea water, p is the sea pressure, z is vertical distance. $\rho(S,T,p)$ is the density of sea water, and $\rho_0(S,T,p)$ is the mean density of water. In this study, since only the analyzed annual mean fields of temperature data as a reference and yearly temperature data during 1955-2003 of WOA01 are provided, thermosteric sea level can be computed alone. In addition, even if the salinity data are available, salinity change may results from sea ice melting, which can not change the sea water volume. Therefore, it is difficult to distinguish water volume and water mass change due to salinity change so halosteric sea level variations could not be counted.

The upper panel of Figure 7.3 shows thermosteric sea level variations averaged globally from 1955 to 2003 by area weights, which are computed by integrating from 0 m down to 500 m using Equation (7.8). Trend of thermosteric sea level variations determined by linear regression is 0.28±0.04 mm/yr, which is relative small compared with sea level trend derived from 27 tide gauge data, 1.8 mm/yr. As the same as the sea level variations derived from tide gauges data, trends of thermosteric sea level variations using different time spans are computed in order to test whether there is existence of low frequency signal. Table 7.2 and the bottom of Figure 7.2 show that the thermosteric sea level trends are varying when time spans are changing. The thermosteric sea level trend decreases while time span increases. However, when time span used to determine the trend of thermosteric sea level is longer than 30 years, the rate changes slightly and is close to 0.3 mm/yr.

The upper panel of Figure 7.4 presents the trends of thermosteric sea level variations, which are determined by overlapping 10-year data using linear regression. The rates of the trends are plotted at the centers of 10-year periods. In addition to fitting by linear regression, the low frequency of signal can be fit simultaneously if available, so the frequency analysis should be done. The bottom panel of Figure 7.3 shows the amplitude with respect to the frequency computed by the Fourier Transformation (FT) using annual time series of thermosteric sea level variations. The largest amplitude is at frequency of 0.0625 cycles per year, which is equal to the period of 16 years. Because the FT analysis presents a 16-year signal exists in thermosteric sea level variations, the same computation is repeated as for the top panel of Figure 7.4 except for adding a 16-year period to linear regression (bottom panel of Figure 7.4). Nevertheless, whether thermosteric sea level is accelerating could not be identified distinctly; consequently, the rates of

10-year trends fit either by linear regression (case I) or by linear regression plus 16-year period (case II) are used to do hypotheses testing as described in Section 7.2 and Equation (7.7).

For case I, the test statistics T

$$T = 0.5031 < F_{0.05}(1,38) = 4.10$$

For case II, the test statistic T

$$T = 0.6895 < F_{0.05}(1,38) = 4.10$$

If first two data points are eliminated, the test statistics T

$$T = 0.0076 < F_{0.05}(1,36) = 4.12$$

All cases show null hypotheses are accepted. Consequently, the slope $b = 0$ is true with a significant level of 95%. This analysis proves thermosteric sea level rise does not accelerate during 1955–2003 according to the available temperature data.

7.5 Summary

In this Chapter, the minimum data span of sea level or thermosteric sea level data in form of time series for the determination of a stable sea level trend is discussed. Time span of sea level variations derived from 27 tide gauges needs more than 20 years to obtain a stable rate while the time span of thermosteric sea level changes needs more than 30 years of data. The reason for determining a stable rate using thermosteric sea level variations needs more years than using sea level changes is probably that the thermosteric sea level signal contains the strong amplitude of interdecadal signal (~16-year period). In addition, the statistic approach was provided to check whether sea level or thermosteric sea level trend is accelerating in the 1990s. Both cases indicate that there is no evidence that sea level acceleration occurred in the 1990s. However, future work is warranted to use longer historical records with reliable quality.

Time span (years)	Thermosteric sea level trend (mm/yr)
1955-2003: 49	028±0.04
1960-2003: 44	027±0.04
1970-2003: 34	0.21±0.06
1980-2003: 24	0.39±0.10
1985-2003: 19	0.67±0.09
1993-2003: 11	1.26±0.12

Table 7.2: Thermosteric sea level trends determined from different time spans.

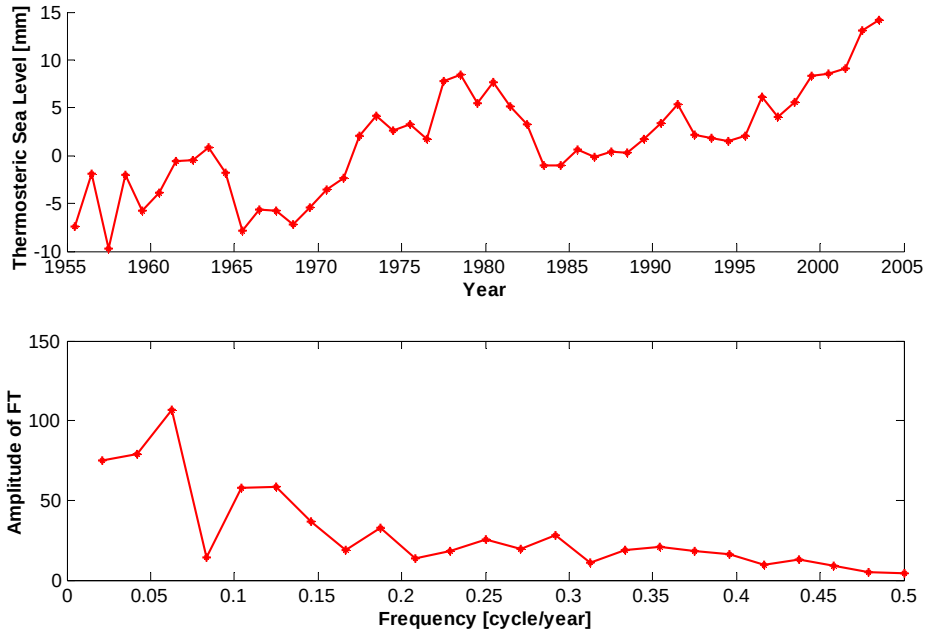

Figure 7.3: Top: The time series of annual thermosteric sea level (mm) averaged globally from 1955 to 2003. Bottom: The Fourier Transformation (FT) of the annual time series of thermosteric sea level changes.

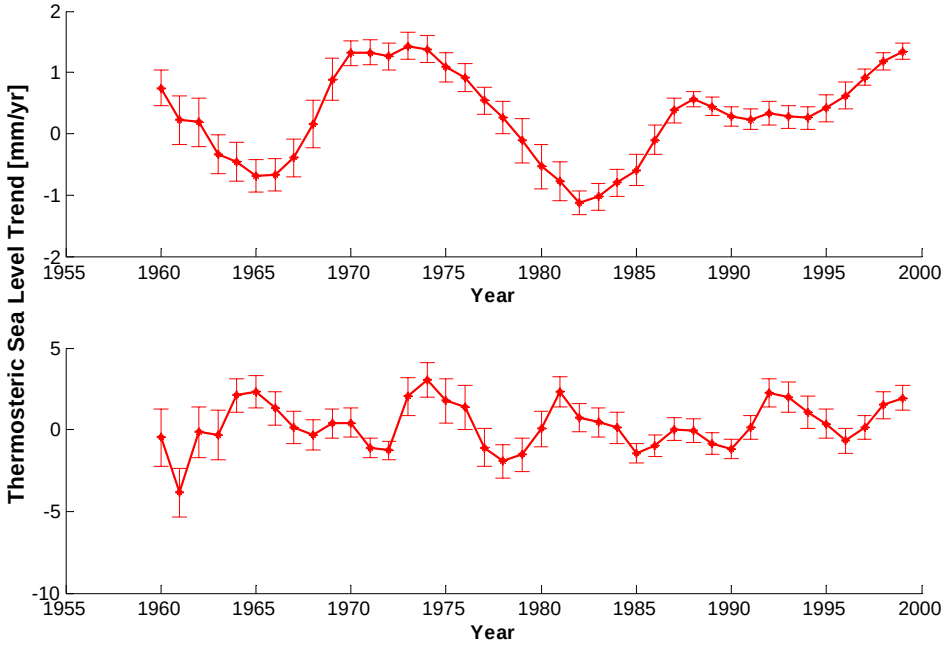

Figure 7.4: Trends of thermosteric sea level changes are determined using overlapping 10-year data. Trends are plotted at the centers of 10-year periods. Top: The trends are fitted by the linear equation. Bottom: The trends are fitted by the linear equation plus 16-year period.

CHAPTER 8

DETERMINATION AND CHARACTERIZATION OF SEA LEVEL RISE

Global sea level rise can only be partially explained by a number of competing geophysical processes, each of which is a complex process within the Earth-atmosphere-ocean-cryosphere-hydrosphere system. The sea level changes are result of a number of forcing factors, which include but not limited to steric sea level, mass variations of ice sheets and mountain glaciers, ocean currents, atmospheric circulation, terrestrial water storage and human-impoundment of water in reservoirs. For the problem of determination of sea level changes using tide gauge data, the direct and indirect effect of vertical motions (crustal uplift and the associated geoid change) should be considered. The contemporary estimate of the 20th century sea level rise primarily used data from coastal tide gauges and correcting the postglacial rebound effect. The estimated sea level rise is 1.5 to 2.4 mm/yr [Gornitz, 1982, 1995; Barnett, 1990; Peltier, 2001; Ekman, 2000; Woodworth et al., 1999; Douglas et al., 2001; Mitrovica et al., 2001]. One of the most recent determination of the 20th Century sea level rise using tide gauges [Douglas et al., 2001; Peltier, 2001], 1.84±0.35 mm/yr, is slightly higher than the central value of the IPCC study [Church et al., 2001] of 1.5 mm/yr, but within their estimated range of 1.0 to 2.0 mm/yr. However, several studies have recognized that sea level redistributions associated with present-day mass variations are non-uniform due to self-gravitational effects (Section 1.4) [Mitrovica et al., 2001; Plag, 2005; Conrad and Hanger, 1997; Meier, 1984]. In addition, Levitus [2005] shows significantly geometric variations of thermosteric sea level trends as shown in Chapter 3. Therefore, the one primary limitation to determine global sea level variations using tide gauge data is the poor global distribution of tide gauge stations.

In order to mitigate this problem, Plag and Jüttner [2001], Plag [2005], Mitrovica et al. [2001], and Tamisiea et al. [2001] demonstrated utilizing tide gauge data as observations to approximate the predicted geometries (geographical patterns) of sea level changes due to forcing factors by Weighted Least Squares (WLS) adjustment. The approach estimates the amplitudes of geometries and interpolates sea level trends between gauges. As a result, the geometries of global sea level trends due to all forcing factors including in the analysis are achieved. The analyses of Mitrovica et al. [2001] and Tamisiea et al. [2001] only adopted the amplitudes of the contributions due to Antarctic and Greenland ice sheets, and uniform variations of steric sea level as unknown parameters while assumed the contributions of PGR and mountain glaciers are known to be applied to observations of tide gauge data selected by Douglas [1997]. The estimated global sea level rise ranges 1.6–2.0 mm/yr associated to different models. The contributions of Greenland ice sheet and Antarctic ice sheet with uniform variations to global sea level trend range 0.4–0.6 mm/yr and 0.4–1.0 mm/yr respectively. The reason to determine the sum of the contributions of Antarctic ice sheet and uniform variations is sea level variation due to Antarctic mass flux at these selected tide gauges are relatively flat, which is presumably caused by the fact that there is no tide gauge station located at or near Antarctica. Plag and Jüttner [2001] did the same analysis using more tide gauges but mountain glaciers are not accounted for. Their updated solution has been addressed in Plag [2005]. The estimated trend of

sea level ranges from 0.70 to 0.95 mm/yr associated to different models. The contributions of Greenland ice sheet and Antarctic ice sheet to global sea level trend range 0.05-0.15 mm/yr and 0.26-0.50 mm/yr, respectively.

In this Chapter, the geometries or spatial patterns of global sea level changes due to three ice sources, global PGR models, and thermosteric sea level variations are assumed to be known, and we combine nearly 600 tide gauge data and multiple mission altimeter data to estimate the respective contributions and the resulting global sea level trend using two numerical techniques: Weighted Least Squares (WLS) and the elementwise-weighted total least squares (EW-TLS). First, we conduct a simulation study to validate the numerical procedure, and then we use the real data (~100 years of tide gauge data from ~600 sites and two decades of satellite altimetry data) for the determination of the 20th Century sea level rise.

8.1 Data Analysis

Three predicted geometries of normalized global sea level variations, which are computed for the case of present-day ice mass variations in Antarctica and Greenland as well as the set of the mountain glaciers and ice sheets tabulated by Meier [1984] (Hereafter, the Meier model) and provided by Mitrovica et al. [2001] (J. Mitrovica, personal communications). In Antarctica and Greenland ice sheets, the mass variations are assumed to be uniform over the two regions. The results are normalized by the equivalent sea level changes for each mass flux event, which is uniform and set as a contribution of global sea level rise as 1 mm/yr [Mitrovica et al., 2001]. The predicted geometry due to Antarctic ice source has a distinct zonal component, while the geometry due to Greenland ice sheet illustrates more variations along longitude in the northern hemisphere. The correlation coefficients of three predicted geometries are calculated in global ocean using1×1degree grids. The correlation coefficient between the predicted geometries of Antarctica and of Greenland is –0.20 and between the geometries of Antarctica and Meier model is –0.18. Both cases above show anti-correlations. Nevertheless, if weighted by area when computing the correlation coefficients, the values turn to 0.19 and 0.10, respectively. The reason is that significantly anti-correlated values occur in the Polar regions, which occupy tiny areas relative to global ocean. The correlations coefficients between the geometries of Meier model and Greenland without and with area weights are 0.47 and 0.42, respectively. They are highly correlated.

Thermosteric sea level trends are used to account for the volume of sea level changes, which are not induced in mass variations. WOA01 and Ishii05 are used in this study and both are calculated by integrating from 0 m down to 500 m (see Chapter 3). For WOA01, the secular trends of 1×1grids are calculated by the least squares fit of a degree one polynomial. For Ishii05, the secular trends of 1×1grids are calculated by the least squares fit of a degree one polynomial with extra semi-annual and annual signals. More detail has been described in Chapter 3.

Tide gauge data are used as observations in this study. According to the selected criteria as described in Chapter 5, there are 651 stations available. However, there is no thermosteric sea level data available around some of the tide gauge stations, which were edited. There are 585 stations left after editing. Next, the secular trends of 585 stations are calculated individually using least squares fit of a degree one polynomial with extra parameters representing the semi-

annual and annual signals. IB corrections are applied to tide gauge records using the NCEP model.

In addition to three predicted geographical patterns of ice melt sources and thermosteric sea level, PGR signal is also included in tide gauge data, so PGR should be considered in the estimation. In order to estimate the effect of the errors in PGR models, a number of PGR models are used to examine in the adjustment. Selected PGR models include ICE4G VM2 and numerical predictions of GIA with BIFROST GPS estimates of vertical crustal motions (hereafter the BIFROST model) with six sets of Earth parameters, lithospheric thickness (LT), upper mantle viscosity (UMV) and lower mantle viscosity (LMV). The symbol of a PGR model is presented as LT_UMV_LMV. LT is set as 120 kilometer. UMV is set as 0.5×10^{21} Pas or 1×10^{21} Pas. LMV is set as 1×10^{21} Pas, 3×10^{21} Pas, or 10×10^{21} Pas.

The vertical motion at each gauge station derived from the combination of altimeters and tide gauge data could be used as observations in an adjustment. Altimeter data are averaged monthly after removing the biases relative to TOPEX/POSEIDON in light of the description in Chapter 5. Both altimeter and tide gauge data are not applied IB corrections in order to remain consistent.

Any adjustment is restrained by the correlation of observations and forcing factors, which consist of the design matrix. For the sake of studying the correlation of observations and forcing factors, the correlation coefficients are calculated between the contributions of three ice sources, PGR models, and thermosteric sea level, which are interpolated at 585 gauge stations. Furthermore, the correlation coefficients between different forcing sources are computed as well. Table 8.1(a) illustrates the correlation coefficients of different PGR models and sea level trends at 585 tide gauge records. ICE4G and BIFROST models with different Earth parameters are highly correlated and correlation coefficients are higher than 0.74. The correlation coefficients between PGR models and sea level trends are larger than 0.37, which means PGR contributes to sea level changes essentially. If BIFROST models with LMV 1×10^{21} Pas are eliminated, the correlation coefficients of PGR models and sea level trends become larger. Afterward, the mentioned correlation coefficients previously have been changed from 0.74 to 0.87 and from 0.37 to 0.44, respectively. ICE4G shows the largest correlation coefficient of 0.46. Table 8.1(b) shows the correlation coefficients of three ice sources, WOA01, Ishii05, ICE4G, and sea level trends of 585 tide gauges. The correlation coefficients indicate these forcing factors and observations are inter-correlated at 585 tide gauge stations. Among these forcing factors, ICE4G has the highest correlation with sea level trends. The predicted geometries of Antarctica and Greenland do not show the expected anti-correlated at the 585 stations because there are quite few stations in the polar regions, where extreme anti-correlation occurs. Table 8.1(c) shows the correlation coefficients of different PGR models with three ice sources, WOA01, Ishii05, and sea level trends of 585 tide gauges to test the effect of errors from PGR models. The correlation coefficients of ICE4G with three ice sources, thermosteric sea level trends and sea level trends are relative larger than other PGR models. BIFROST models with LMV 1×10^{21} Pas present the lower correlations than other PGR models. In addition, the means of differences between PGR models with standard deviations are computed and shown in Table 8.2. Similarly, BIFROST models with LMV 1×10^{21} Pas display relative larger differences compared with other PGR

models. Similarly, the mean of difference between WOA01 and Ishii05 is also computed and the value is 0.055 mm/yr with a standard deviation of 0.270 mm/yr.

	ICE4G	120_1_1	120_1_3	120_1_10	120_p5_1	120_p5_3	120_p5_10	SLT
ICE4G	1.000							
120_1_1	0.737	1.000						
120_1_3	0.871	0.927	1.000					
120_1_10	0.865	0.892	0.983	1.000				
120_p5_1	0.752	0.987	0.927	0.897	1.000			
120_p5_3	0.897	0.859	0.980	0.970	0.977	1.000		
120_p5_10	0.896	0.799	0.957	0.974	0.820	0.983	1.000	
SLT	0.462	0.365	0.439	0.442	0.383	0.455	0.453	1.000

Table 8.1(a): Correlation coefficients between different PGR models and sea level trends of 588 tide gauge stations. SLT: relative sea level trend derived from tide gauge data.

	Ant	Green	Meier	WOA01	Ishii05	Ice4g	SLT
Ant	1.00						
Green	0.187	1.00					
Meier	0.065	0.327	1.00				
WOA01	-0.138	-0.055	0.093	1.00			
Ishii05	-0.175	-0.051	0.064	0.921	1.00		
Ice4g	0.166	0.315	0.268	0.324	0.329	1.00	
SLT	0.013	0.259	0.253	0.167	0.193	0.462	1.00

Table 8.1(b): The correlation coefficients of three ice sources, WOA01, Ishii05, ICE4G, and sea level trends of 585 tide gauges. SLT: relative sea level trend derived from tide gauge data.

	Ant	Green	Meier	WOA01	Ishii05	SLT
ICE4G	0.166	0.315	0.268	0.324	0.329	0.462
120_1_1	0.025	0.097	0.141	0.339	0.280	0.365
120_1_3	0.045	0.202	0.151	0.357	0.337	0.439
120_1_10	0.053	0.170	0.193	0.322	0.325	0.442
120_p5_1	0.002	0.125	0.155	0.300	0.254	0.383
120_p5_3	0.039	0.238	0.148	0.339	0.333	0.455
120_p5_10	0.050	0.203	0.180	0.311	0.326	0.453

Table 8.1(c): Correlation coefficients of different PGR models with three ice sources, WOA01, Ishii05, and sea level trends of 585 tide gauges. SLT: relative sea level trend derived from tide gauge data.

	ICE4G	120_1_1	120_1_3	120_1_10	120_p5_1	120_p5_3	120_p5_10
ICE4G	0.000						
120_1_1	-0.037±0.765	0.000					
120_1_3	0.106±0.757	0.143±0.600	0.000				
120_1_10	0.128±0.816	0.165±0.732	0.023±0.282	0.000			
120_p5_1	-0.087±0.674	-0.050±0.503	-0.193±0.917	-0.215±1.006	0.000		
120_p5_3	0.058±0.472	0.095±0.573	-0.048±0.446	-0.071±0.548	0.145±0.606	0.000	
120_p5_10	0.105±0.597	0.142±0.784	0.000±0.428	-0.023±0.384	0.192±0.874	0.048±0.321	0.000

Table 8.2: Means of differences between PGR models with standard deviations.

8.2 Methodology

Ideally all forcing factors introduced in the previous sections to cause sea level changes should be estimated. However, sufficient models are not completely available to predict all forcing factors, so only some available main factors can be taken into consideration for estimations. Based on the available models and observations, the total predicted sea level changes can be formed from these three ice sources, steric sea level, PGR and other sources. They can be expressed as follows:

$$\begin{aligned} S_T(\theta_j,\varphi_j) &= V_O \times S_O^n(\theta_j,\varphi_j) + V_A \times S_A^n(\theta_j,\varphi_j) \\ &+ V_G \times S_G^n(\theta_j,\varphi_j) + V_M \times S_M^n(\theta_j,\varphi_j) + V_P \times P(\theta_j,\varphi_j) \end{aligned}, \tag{8.1}$$

where j is the index of tide gauge station; θ_j and φ_j are the longitude and latitude of index j station; $S^n(\theta_j,\varphi_j)$ are the patterns of normalized sea level changes contributed by Antarctic ice sheet, Greenland ice sheet, Meier model, steric sea level, and others; V_A, V_G and V_M are the amplitude of sea level variations associated with each of three ice systems; V_O is the amplitude of steric sea level variations; $P(\theta_j,\varphi_j)$ is Glacier Isostatic Adjustment (GIA) model or called PGR; $P(\theta_j,\varphi_j)$ can be separated as crustal radial motion, $\dot{u}(\theta_j,\varphi_j)$, and the geoid effect, $G(\theta_j,\varphi_j)$; V_P is the scale factor of PGR, and $S_T(\theta_j,\varphi_j)$ are sea level trend observations by tide gauges.

Additionally, if observations are introduced by combining tide gauge data and altimeter data, Equation (8.1) can be simply re-written as follows:

$$S_V(\theta_j,\varphi_j) = V_P \times \dot{u}(\theta_j,\varphi_j), \tag{8.2}$$

where $S_V(\theta_j,\varphi_j)$ is the total crustal radial motion due to PGR and the combination of altimeter data and tide gauge data can provides observations of this quantity. Assuming $j = 1,...,n$, Equation (8.1) and Equation (8.2) can be combined and re-written as follows:

$$\begin{bmatrix} S_T(\theta_1,\varphi_1) \\ \vdots \\ \vdots \\ S_T(\theta_n,\varphi_n) \\ S_V(\theta_1,\varphi_1) \\ \vdots \\ \vdots \\ S_V(\theta_n,\varphi_n) \end{bmatrix} = \begin{bmatrix} S_A^n(\theta_1,\varphi_1) & S_G^n(\theta_1,\varphi_1) & S_M^n(\theta_1,\varphi_1) & S_O^n(\theta_1,\varphi_1) & P(\theta_1,\varphi_1) \\ \vdots & \vdots & \vdots & \vdots & \vdots \\ \vdots & \vdots & \vdots & \vdots & \vdots \\ S_A^n(\theta_n,\varphi_n) & S_G^n(\theta_n,\varphi_n) & S_M^n(\theta_n,\varphi_n) & S_O^n(\theta_n,\varphi_n) & P(\theta_n,\varphi_n) \\ 0 & 0 & 0 & 0 & \dot{u}(\theta_1,\varphi_1) \\ \vdots & \vdots & \vdots & \vdots & \vdots \\ \vdots & \vdots & \vdots & \vdots & \vdots \\ 0 & 0 & 0 & 0 & \dot{u}(\theta_n,\varphi_n) \end{bmatrix} \times$$

$$\begin{bmatrix} V_A \\ V_G \\ V_M \\ V_O \\ V_P \end{bmatrix}, \tag{8.3}$$

The vector on the left side of Equation (8.3) is the observations provided by altimeters and tide gauge data. The first term on the right side is formed from three ice sources, PGR, and thermosteric sea level in this study. The second term on right side is the unknown parameters, which present the amplitudes of forcing factors.

8.3 Weighted Least Squares (WLS)

Equation (8.3) can be seen as Gauss-Markov (GM) model:

$$y = A\xi + e \qquad with \quad e \sim (0, \sigma_0^2 P^{-1} = \Sigma), \tag{8.4}$$

where $A = \begin{bmatrix} S_A^n(\theta_1,\varphi_1) & S_G^n(\theta_1,\varphi_1) & S_M^n(\theta_1,\varphi_1) & S_O^n(\theta_1,\varphi_1) & P(\theta_1,\varphi_1) \\ \vdots & \vdots & \vdots & \vdots & \vdots \\ \vdots & \vdots & \vdots & \vdots & \vdots \\ S_A^n(\theta_n,\varphi_n) & S_G^n(\theta_n,\varphi_n) & S_M^n(\theta_n,\varphi_n) & S_O^n(\theta_n,\varphi_n) & P(\theta_n,\varphi_n) \\ 0 & 0 & 0 & 0 & \dot{u}(\theta_1,\varphi_1) \\ \vdots & \vdots & \vdots & \vdots & \vdots \\ \vdots & \vdots & \vdots & \vdots & \vdots \\ 0 & 0 & 0 & 0 & \dot{u}(\theta_n,\varphi_n) \end{bmatrix}$, $y = \begin{bmatrix} S_T(\theta_1,\varphi_1) \\ \vdots \\ \vdots \\ S_T(\theta_n,\varphi_n) \\ S_V(\theta_1,\varphi_1) \\ \vdots \\ \vdots \\ S_V(\theta_n,\varphi_n) \end{bmatrix}$,

$\xi = \begin{bmatrix} V_A \\ V_G \\ V_M \\ V_O \\ V_P \end{bmatrix}$, e are random error vectors, σ_0^2 is the unknown priori variance associated with the weight matrix, P, and Σ is a variance-covariance matrix. In addition, the dimension of y is $2n \times 1$, the dimension of A is $2n \times m$, e is $2n \times 1$, and the dimension of ξ is $m \times 1$.

The solution of Equation (8.3) derived by Least Squares (LESS) or Best Linear Unbiased Estimation (BLUE) could be expressed as:

$$\hat{\xi} = (A^T PA)^{-1}(A^T Py). \tag{8.5}$$

$$\hat{D}\{\hat{\xi}\} = \hat{\sigma}_0^2 (A^T PA)^{-1}, \quad with \quad \hat{\sigma}_0^2 = (y^T Py - (A^T Py\hat{\xi}))/(n-m), \tag{8.6}$$

where $\hat{\xi}$ is the estimation of ξ, $\hat{D}\{\hat{\xi}\}$ is the post-dispersion matrix of $\hat{\xi}$, and $\hat{\sigma}_0^2$ is the estimation of σ_0^2.

The detailed description to introduce models and data into above equations will be acquainted as follows. First of all, the relative sea level trends with formal errors (ε_{S_T}) derived from tide gauge data with IB corrections (Equation 5.4) using the NCEP reanalysis model, and vertical motions with formal errors (ε_{Sv}) determined by combining altimeter and tide gauge data [Nerem and Mitchum, 2002; Kuo et al., 2004b] which produce the observation vector, y, and the variance-covariance matrix, Σ. In the initial exercise, Σ is set as a diagonal matrix, which means there is no correlation between observations. The diagonal elements of Σ are set as $\varepsilon_{S_T}^2$ or $\varepsilon_{S_v}^2$. Column 1 (or 3) of Table 8.3 shows the estimates of forcing factors using three ice sources, ICE4G, and thermosteric sea level from WOA01 (or Ishii05). Similarly, we do the same test expect for the variance-covariance matrix of Σ. We set Σ as a non-diagonal matrix. The element of Σ presenting the correlation of two measurements can be set to be equal to $0.1\times\sqrt{(\varepsilon_{S_T}^2\varepsilon_{S_v}^2)}$ and the diagonal elements are identical as the previous case. Columns 2 and 4 of Table 8.3 show the estimates of forcing factors using the non-diagonal matrix of Σ. A comparison of columns 1 and 2 or columns 3 and 4 shows the good consistency of the estimated rates when Σ matrix is diagonal or non-diagonal and then the estimated variance component of the later case is slightly bigger than former case. In addition, the element of Σ matrix is also set as $0.3\times\sqrt{(\varepsilon_{S_T}^2\varepsilon_{S_v}^2)}$, which makes higher correlation between two observations. As a result, the changes of the estimated rates contributing to global sea level variations are only around 0.01 mm/yr level, which is small enough to be ignored. The reason could be that ε_{Sv} is relative larger than ε_{S_T}. Therefore, in the convenience of computations, Σ matrix is considered as a diagonal matrix in the following content.

A comparison of using different thermosteric sea level models (columns 1 and 3 or columns 2 and 4) indicates the rate for Antarctic ice sheet is really depending on a selected thermosteric sea level. Consequently any errors in the models of thermosteric sea level will bias the estimated rate of Antarctic ice sheet since the most tide gauge stations are located in the north hemisphere as the fluctuation of the geometry due to Antarctic ice sheet appears in the southern hemisphere (close to Antarctica), thus there is no redundancy of observations to get optimal estimates.

The dependency of the estimated trends of the forcing factors resulting from the selection of PGR models is presented in Table 8.4 and 8.5. Table 8.4 shows the estimated trends for all forcing factors using three ice sources, WOA01, and BIFROST PGR models with different Earth parameters. Table 8.5 shows the same as Table 8.4 except using thermosteric sea level from Ishii05 instead of WOA01. By examining Table 8.3, 8.4, and 8.5, the contributions of three ice sources are entirely positive, which means three ice sheets are melting. The contribution of Meier model is approximately not affected by the selection of PGR models, while the contributions of Antarctic ice sheet and Greenland ice sheet vary using different PGR models especially the

BIFROST models with lower mantle viscosity (LMV) for 1×10^{21} Pas. The selection of PGR models also affects the contribution of the scale factor of PGR and the scale changes considerably, but the variations are quite small in terms of sea level changes because averaged PGR model with area weights in global ocean is almost close to zero.

Excluding the BIFROST model with 1×10^{21} Pas LMV, the contribution of Antarctic ice sheet ranges 0.29 – 0.50 mm/yr to global sea level change. Additionally, the sea level change contributed by Greenland ice sheet ranges 0.57 - 0.71 mm/yr while the contribution of Meier model ranges 0.65 - 0.72 mm/yr. The trend of thermosteric sea level changes ranges 0.05 - 0.15 mm/yr. As a result, the total sea level change ranges 1.78 - 1.87 mm/yr with a formal error of 0.23 mm/yr.

	1948-2003 I	1948-2003 II	1948-2003 III	1948-2003 IV
V_A (mm/yr)	0.48±0.13	0.48±0.13	0.41±0.14	0.41±0.14
V_G (mm/yr)	0.57±0.15	0.59±0.15	0.58±0.15	0.59±0.15
V_M (mm/yr)	0.65±0.10	0.65±0.09	0.66±0.09	0.66±0.09
V_O (mm/yr)	0.08±0.03	0.08±0.03	0.13±0.04	0.13±0.04
V_P	0.72±0.10	0.72±0.10	0.69±0.09	0.69±0.10
$\hat{\sigma}_0^2$ (mm/yr)^2	13.79	13.98	13.70	13.89
TSLT	1.78	1.80	1.78	1.79

Table 8.3: Estimated trends resulting from three ice sources, ICE4G, and thermosteric sea level (WOA01 and Ishii05) using 1948 – 2003 tide gauge records and nearly 15 years multi-altimeters. IB correction is applied to tide gauge data using NCEP model. TSLT: Total sea level trend is sum of all forcing factors.

I: WOA01 are used.
II: The correlation between observations, y , are considered. WOA01 are used.
III: Ishii05 are used.
IV: The correlation between observations, y , are considered. Ishii05 are used.

PGR	V_A	V_G	V_M	V_O	V_P	$\hat{\sigma}^2$	TSLT
120_1_1	0.22±0.13	0.75±0.15	0.75±0.10	0.11±0.03	0.34±0.09	14.50	1.83
120_1_3	0.42±0.13	0.66±0.15	0.71±0.09	0.06±0.03	0.45±0.07	14.05	1.85
120_1_10	0.36±0.13	0.71±0.15	0.66±0.10	0.09±0.03	0.39±0.07	14.17	1.82
120_p5_1	0.26±0.13	0.75±0.15	0.74±0.10	0.10±0.03	0.72±0.16	14.40	1.85
120_p5_3	0.50±0.14	0.60±0.15	0.72±0.10	0.05±0.03	0.68±0.09	13.85	1.87
120_p5_10	0.43±0.13	0.65±0.15	0.67±0.10	0.08±0.03	0.51±0.07	13.95	18.3

Table 8.4: Estimated trends resulting from three ice sources, different PGR models, and WOA01 using 1948 – 2003 tide gauge records and nearly 15 years multi altimeters. IB correction is applied to tide gauge data using NCEP. TSLT: Total sea level trend is sum of all forcing factors.
*Symbols in Column 1 show the Earth parameters used in PGR models. They are presented as a_b_c. where a is lithospheric thickness (LT). The unit is kilometer. b is upper mantle viscosity (UMV). The unit is Pas. b means $b\times10^{21}$ Pas. p5 is equal to 0.5. c is lower mantle viscosity (LMV). The unit is Pas. c means $c\times10^{21}$Pas.

PGR	V_A	V_G	V_M	V_O	V_P	$\hat{\sigma}^2$	TSLT
120_1_1	0.13±0.13	0.76±0.15	0.75±0.10	0.17±0.04	0.34±0.08	14.32	1.81
120_1_3	0.33±0.14	0.67±0.15	0.71±0.10	0.12±0.04	0.42±0.07	13.95	1.83
120_1_10	0.29±0.13	0.71±0.15	0.67±0.10	0.15±0.04	0.37±0.07	14.06	1.82
120_p5_1	0.18±0.13	0.76±0.15	0.74±0.10	0.17±0.04	0.70±0.15	14.23	1.85
120_p5_3	0.41±0.14	0.61±0.15	0.72±0.10	0.11±0.04	0.64±0.09	13.77	1.85
120_p5_10	0.35±0.14	0.66±0.15	0.68±0.10	0.13±0.04	0.48±0.07	13.87	1.82

Table 8.5: Estimated trends resulting from three ice sources, different PGR models, and Ishii05 using 1948 – 2003 tide gauge records and nearly 15 years multi altimeters. IB correction is applied to tide gauge data using NCEP model. TSLT: Total sea level trend is sum of all forcing factors.

8.4 Elementwise-Weighted Total Least Squares (EW-TLS)

In essence, OLS only takes care of the independently distributed errors affecting only the observation vector, y. However, in this study the designed matrix, A, is composed of forcing models (sea level changes from three ice systems, thermosteric sea level, and PGR models), which contain errors practically. Hence the WLS can not handle this data set properly. Here, EW-TLS is introduced to include the observation equation, in which the independently distributed errors not only affect the observation vector but also affect the design matrix A. In addition, the model covers the whole class of problem $A\xi \approx y$, in which the errors in each element are proportional to its size and is therefore an important extension of the class TLS problems studied so far. The Gauss-Markoff model can be re-written as follows:

$$y - e = (A + E_A)\xi, \tag{8.7}$$

$$E\{[E_A, e]\} = 0; C\{[E_A, e]\} = 0, \tag{8.8}$$

$$D\{e\} = \sigma_{iy}^2 \text{ and } D\{E_A\} = \sigma_{ij}^2, \tag{8.9}$$

where $I \equiv \{1,2,...,n\}$; $J \equiv \{1,2,...,m\}$; $\sigma_{ij}^2 \forall ij \in I \times J$ and $\sigma_{iy}^2 \forall i \in I$; There are two approaches to solve equations of a EW-TLS problem here :

(1) Premoli and Rastello [2002] – approach I

This paper proposes an original algorithm solving general EW-TLS problems. It is based on the minimization of the weighted Frobenius norm (WFN) of the errors, expressed in terms of the sum of ratios of quadratic forms. WFN of data and observation errors:

$$F(\xi, E_A, e) = \sum_{i \in I} (\Delta a_i^T S_i^{-1} \Delta a_i + e_i^2 \sigma_{iy}^{-2}), \tag{8.10}$$

where $E_A = \Delta a_i = [\Delta a_{i1}, \Delta a_{i2}, ..., \Delta a_{in}]^T$ and $S_i \equiv diag(\sigma_{i1}^2, \sigma_{i2}^2, ..., \sigma_{im}^2)$

According to Premoli and Rastello [2002], Equation (8.10) can be re-written as:

$$F(\xi) = \sum_{i \in I} \left(\frac{\xi^T a_i - y_i}{\xi^T S_i \xi + \sigma_{iy}^2}\right)^2 (\xi^T S_i \xi + \sigma_{iy}^2) = \sum_{i \in I} \left(\frac{(\xi^T a_i - y_i)^2}{\xi^T S_i \xi + \sigma_{iy}^2} \right). \tag{8.11}$$

The gradient of the WFN is approximated by the gradient of a parametric quadratic form (PQF), here expressed as $Q(\xi, \hat{\xi})$. A generic value $\hat{\xi}$ is a sufficiently small neighborhood D^*. By zeroing of the gradient of $Q(\xi, \hat{\xi})$, the values $\hat{\hat{\xi}}$ approximating the minimization can be obtained.

$$\hat{\hat{\xi}} = [A^T Z^* A - G^*]^{-1} A^T Z^* y, \tag{8.12}$$

where $Z^* \equiv diag(\varsigma_1^*, \varsigma_2^*, ..., \varsigma_n^*)$ with $\varsigma_i^* = \dfrac{1}{\hat{\xi}^T S_i \hat{\xi} + \sigma_{iy}^2} \quad i \in I$,

$G^* \equiv diag(\gamma_1^*, \gamma_2^*, ..., \gamma_n^*)$ with $\varsigma_i^* = \sum_{i \in I} \left(\dfrac{\sigma_{ij}(a_i^T \hat{\xi} - y_i)}{\hat{\xi}^T S_i \hat{\xi} + \sigma_{iy}^2} \right)^2 \quad j \in J$.

The minima of a sequence of these PQFs converge to the global minimum of the WFN of errors within a few iterations. The algorithm steps are as follows:

(i) Compute $\hat{\xi}$ by considering data as WLS problem

(ii) Calculate

$Z^* \equiv diag(\varsigma_1^*, \varsigma_2^*, ..., \varsigma_n^*)$ with $\varsigma_i^* = \dfrac{1}{\hat{\xi}^T S_i \hat{\xi} + \sigma_{iy}^2} \quad i \in I$.

$G^* \equiv diag(\gamma_1^*, \gamma_2^*, ..., \gamma_n^*)$ with $\varsigma_i^* = \sum_{i \in I} \left(\dfrac{\sigma_{ij}(a_i^T \hat{\xi} - y_i)}{\hat{\xi}^T S_i \hat{\xi} + \sigma_{iy}^2} \right)^2 \quad j \in J$.

(iii) Calculate $\hat{\hat{\xi}} = [A^T Z^* A - G^*]^{-1} A^T Z^* y$.

(iv) Calculate $\|\Delta\xi\| = [\hat{\hat{\xi}} - \hat{\xi}]^T [\hat{\hat{\xi}} - \hat{\xi}] / m$.

(v) If $\|\Delta\xi\| \geq \varepsilon^2 \left\|\hat{\hat{\xi}}\right\|$, $\hat{\xi} = \hat{\hat{\xi}}$ and go to step (ii).

(vi) If $\|\Delta\xi\| < \varepsilon^2 \left\|\hat{\hat{\xi}}\right\|$, the algorithm converges to an equilibrium point of WFN. $\hat{\hat{\xi}}$ are the final estimates.

An unbiased estimate of the variance component σ_0^2 is obtained by

$$\hat{\sigma}_0^2 = \sum_{i \in I} \left(\frac{(\hat{\hat{\xi}}^T a_i - y_i)^2}{\hat{\hat{\xi}}^T S_i \hat{\hat{\xi}} + \sigma_{iy}^2} \right) \Big/ (n - m). \tag{8.13}$$

In addition, an (approximate) variance-covariance matrix for the EW-TLS is given by

$$\hat{D}\{\hat{\hat{\xi}}\} \approx \hat{\sigma}_0^2[A^T Z^* A - G^*]^{-1} A^T Z^* P^{-1} Z^{*T} A[A^T Z^* A - G^*]^{-1}. \quad (8.14)$$

(2) Kukish and Huffel [2004] - approach II

Kukish and Huffel [2004] solve the multivariate measurement error model $A\xi \approx y$. The errors in [A,y] are rowwise independent but within each row the errors may be correlated. Premoli and Rastello [2002] approach, therefore, is to solve a special case of the EW-TLS problem, where A and ξ are vectors and all errors are non-correlated with elementwise differently sized variance. Therefore, approach II is an extension of approach I. In this study, approach I is suitable for the data of this study to solve the problem, so approach II is used to verify the result and equations are simplified for only one set of data and non-correlated with elementwise differently sized variance. The algorithm of Kukish and Huffel [2004] is described as follows:

$$\frac{1}{2}\frac{dQ(\xi)}{d\xi} = \Phi(\xi, Z) = \sum_{i=1}^{n} a_i (a_i^T \xi - y_i^T) G_i^{-1}(Z),$$
$$- \sum_{i=1}^{n} P \cdot S_i Z G_i^{-1}(Z)(\xi^T a_i - y_i)(a_i^T \xi - y_i^T) G_i^{-1}(Z), \quad (8.15)$$

where $Q(\xi)$ is the objective function, which is the quadratic form and is used to determine ξ when it is minimized. $P = [I_m; 0_{m\times 1}]$, $S_i = \mathrm{cov}(\sigma_{ij}, j = 1,....,m+1)$, and $Z = Z(\xi) = [\xi^T, -I_1]^T$. The minimum point of $\hat{\xi}$ exists with probability tending to 1 when $\Phi(\xi, Z) = 0$. The proposed iterative algorithm is as follows:

(i) compute an approximation $\hat{\xi}$ by considering data as WLS problem.

(ii) compute $Z = Z(\xi) = [\hat{\xi}^T, -I_1]^T$, and find $\hat{\hat{\xi}}$ from the optimization problem using Newton algorithm.

$$\min_{\xi \in \Re^{m\times 1}} \left\| \Phi(\xi, Z) \right\|_F^2$$

(iii) calculate $\left\| \Delta\xi \right\| = [\hat{\hat{\xi}} - \hat{\xi}]^T [\hat{\hat{\xi}} - \hat{\xi}]/m$.

(iv) if $\left\| \Delta\xi \right\| \geq \varepsilon^2 \left\| \hat{\hat{\xi}} \right\|$, $\hat{\xi} = \hat{\hat{\xi}}$ and go to step (ii).

(v) if $\left\| \Delta\xi \right\| < \varepsilon^2 \left\| \hat{\hat{\xi}} \right\|$, $\hat{\hat{\xi}}$ are the final estimates.

8.5 Simulation

Before real data processing, the simulated data are used to prove the algorithm. In this simulation, only Equation (8.1) is used to produce simulated data and, however, Equation (8.2) is

neglected. $V_O \times S_O^n(\theta_j, \varphi_j)$ only accounts for thermosteric sea level variations. V_A, V_G, V_M, V_O, and V_P are all set to 1. $S^n(\theta_j, \varphi_j)$ is interpolated from the patterns of sea level variations caused by Antarctic ice sheet, Greenland ice sheet, Meier model, and thermosteric sea level changes at 27 tide gauges [Douglas, 2001]. $P(\theta_j, \varphi_j)$ is interpolated from ICE4G VM2 model. According to Equation (8.1), $S_T(\theta_j, \varphi_j)$ is computed by means of $S^n(\theta_j, \varphi_j)$, $P(\theta_j, \varphi_j)$, $V_A, V_G V_M, V_O$, and V_P. Figure 8.1 illustrates the simulated values of three ice sources, PGR, thermosteric sea level, and sea level changes. Subsequently, random noises are added to $S_T(\theta_j, \varphi_j)$, $S^n(\theta_j, \varphi_j)$ and $P(\theta_j, \varphi_j)$ by producing in the light of the normal distribution with a zero mean and a square root of variance. Square roots of variances in $S^n(\theta_j, \varphi_j)$ (Antarctica, Greenland and Meier) are all set close to zero, which means the errors are relative small. And square roots of variances in $S_O^n(\theta_j, \varphi_j)$, $P(\theta_j, \varphi_j)$, and $S_T(\theta_j, \varphi_j)$ are set to 0.3 mm/yr, 0.2 mm/yr, and 0.1 mm/yr, respectively.

Thereupon, $V_A, V_G V_M, V_O$, and V_P, which present unknown parameters, could be estimated by regarding as WLS and EW-TLS problems using $S_T(\theta_j, \varphi_j)$, $S^n(\theta_j, \varphi_j)$ and $P(\theta_j, \varphi_j)$. After 1200 times of repeated runs, the averaged estimates and the estimated variance components are shown in Table 8.6. Both approaches to solve EW-TLS problem obtain identical and nearly perfect results, which are closer to set value 1, while the approach to solve WLS problem results in a maximum difference of 0.307 mm/yr. From the view of estimated variance component, which presents the "quality-of-fit", the solution of EW-TLS problem illustrates the advantage of fit in contrast to the solution of WLS problem.

In the second simulation, more simulated tide gauge stations are introduced. V_A, V_G, V_M, V_O, and V_P are set as 0.6 mm/yr, 0.3 mm/yr, 0.5 mm/yr, 0.3 mm/yr, and 1, respectively. $S^n(\theta_j, \varphi_j)$ can be interpolated from the geometries of sea level variations caused by Antarctic ice sheet, Greenland ice sheet, Meier model, and thermosteric sea level trends for 1×1 degree grids as well as $P(\theta_j, \varphi_j)$ could be interpolated from ICE4G VM2 model for 1×1 degree grids. Afterwards, $S_T(\theta_j, \varphi_j)$ is computed according to Equation (8.1) using $S^n(\theta_j, \varphi_j)$, $P(\theta_j, \varphi_j)$, $V_A, V_G V_M, V_O$, and V_P, which are set as the description above. There are only 1,413 grids in the computation, which are around 2-degree area of selected 585 tide gauge stations, used to do adjustment. Figure 8.2 illustrates the simulated values of three ice sources, PGR, thermosteric sea level and sea level changes in 1,413 grids. As the same as Figure 8.1, simulated data from three ice sources show relative smaller amplitudes of variations than from thermosteric sea level and PGR model. Similarly, random noises have to be added to data as the first simulation. Table 8.7 shows the estimated force factors. The solution of EW-TLS problem achieves a perfect result, which obtain nearly values as we originally set. In contrast, the solution of WLS problem makes the error up to 0.14 mm/yr for ice sheets and 0.28 for PGR. The estimated variance component derived from EW-TLS is smaller than from WLS. The bottom line, therefore, shows EW-TLS provides an excellent method of adjustment when the design matrix contains errors. In addition,

the global total sea level trend is calculated and its value equals 1.70 mm/yr, which is identical with the simulated global sea level trend we set. The area-weighted sea level trend of 1413 grids is equal to 1.77 mm/yr. In this case, the method cannot present the benefit obviously of this point, so only the part of 1,413 grids are chosen to do adjustment, in which 300 grids and 100 grids are randomly selected. For the case of 300 grids, the area-weighted sea level trend is 1.52 mm/yr. The global total sea level trend derived by EW-TLS equals 1.70 mm/yr. For the 100-grid case, the area-weighted sea level trend is equal to 1.12 mm/yr while the global total sea level trend derived by EW-TLS is equal to 1.70 mm/yr. As a result, the total sea level trend can be entirely recovered regardless of how many grids are selected when the number of grids is relative larger than unknown parameters.

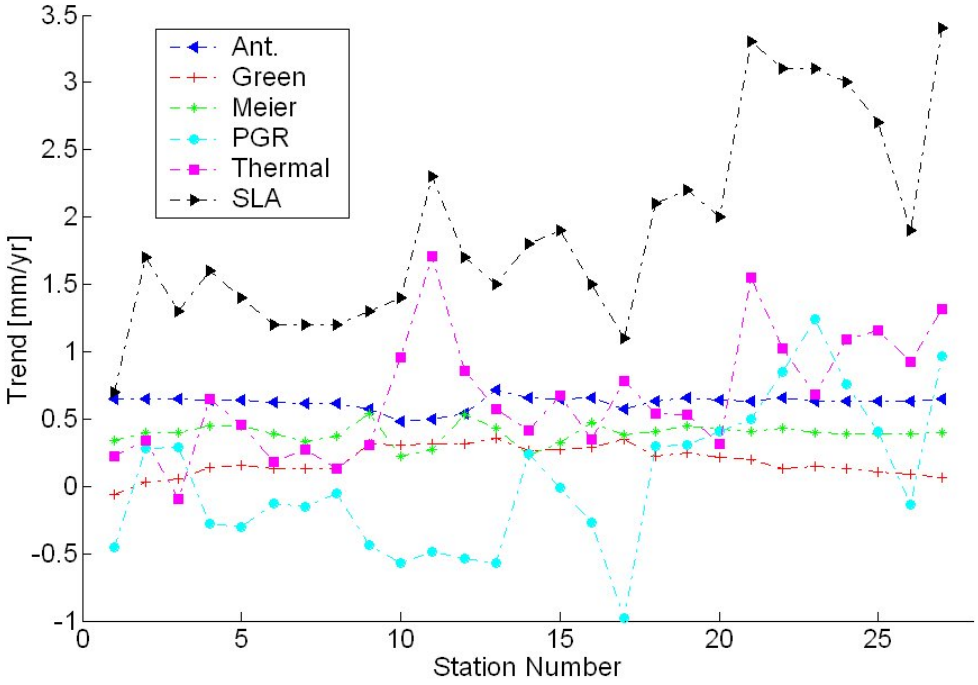

Figure 8.1: Simulated values of three ice sources, PGR, thermosteric sea level, and sea level variations at 27 tide gauge stations.

Forcing factors / True values	WLS	EW-TLS Approach I	EW-TLS Approach II
V_A / 1 (mm/yr)	1.307	1.020	1.020
V_G / 1 (mm/yr)	1.196	1.055	1.055
V_M / 1 (mm/yr)	0.841	0.988	0.988
V_O / 1 (mm/yr)	0.744	0.971	0.971
V_P / 1	0.951	1.019	1.019
$\hat{\sigma}_0^2$ (mm/yr)^2	10.438	0.908	0.908

Table 8.6: Estimated trends resulting from simulated data interpolated from three ice sources, thermosteric sea level and ICE4G in 27 tide gauge stations.

Forcing factors / True values	WLS	EW-TLS Approach I	EW-TLS Approach II
V_A / 0.6 (mm/yr)	0.708	0.600	0.600
V_G / 0.3 (mm/yr)	0.161	0.299	0.299
V_M / 0.5 (mm/yr)	0.520	0.500	0.500
V_O / 0.3 (mm/yr)	0.303	0.300	0.300
V_P / 1.0	0.718	1.000	1.000
$\hat{\sigma}_0^2$ (mm/yr)^2	4.690	1.000	1.000

Table 8.7: Estimated trends resulting from simulated data interpolated from three ice sources, thermosteric sea level, and ICE4G in 1413 grids.

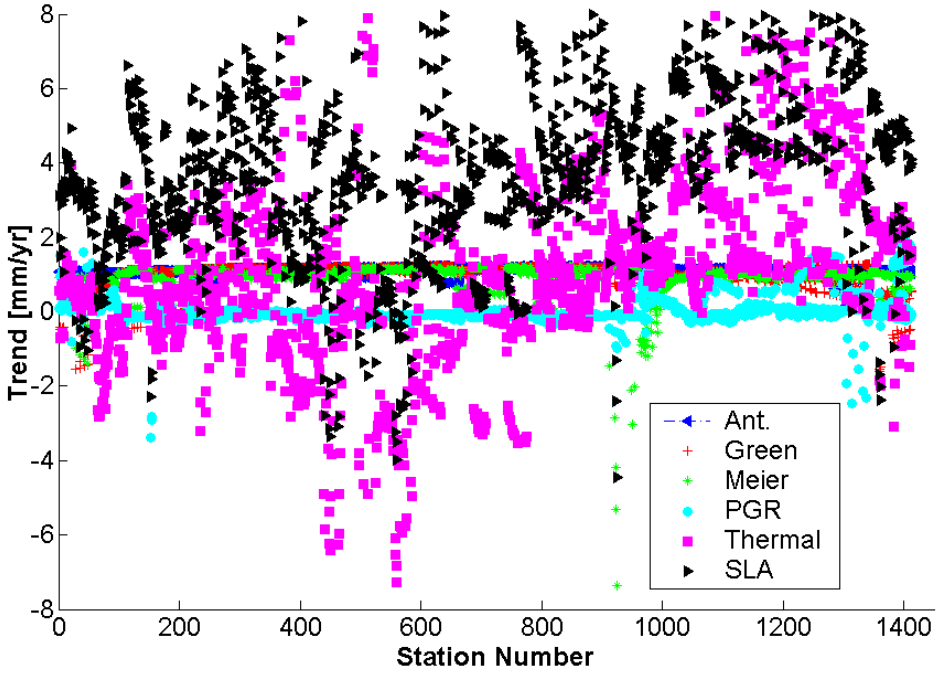

Figure 8.2: Simulated values of three ice sources, PGR, thermosteric sea level, and sea level changes in1413 grids, which are around 2-degree area of 585 gauge stations.

8.6 Solutions from EW-TLS and Discussions

After demonstrating the advantage of the solution for EW-TLS problem in section 8.5, approach I for solving EW-TLS problem is employed to determine forcing factors and total sea level trend using the same data in section 8.3. The same procedure as described in section 8.3, relative sea level trends with formal errors (ε_{S_T}), which are derived from tide gauge data with IB corrections in light of Equation (5.4), and vertical motions with formal errors(ε_{S_V}), which are determined by combining altimeter and gauge data [Nerem and Mitchum, 2002; Kuo et al., 2004b], can consist of observations, y. Let $\sigma_{iy}^2 = \varepsilon_{S_T}^2$ and $\sigma_{iy}^2 = \varepsilon_{S_v}^2$. σ_{ij}^2 are set according to the

errors of three ice sources, thermosteric sea level, and different PGR models. However, in this study the errors of these models are not exactly available, so σ_{ij}^2 cannot be assigned accurately. In the computation, the errors of three ice sources were assumed to be nearly zero and test few pairs of the errors for different thermosteric sea level trends and PGR models. In the first case, thermosteric sea level from WOA01 is used and the errors of WOA01 and PGR are set as 0.10 and 0.05 mm/yr, respectively. The estimates are shown in Table 8.8. In the second case, thermosteric sea level trends from Ishii05 are used and the errors of Ishii05 and PGR are set as 0.10 and 0.05 mm/yr, respectively. The estimates are shown in Table 8.9. By analyzing Table 8.8 and 8.9, the contribution of Meier model presents approximately not to be affected by the selection of PGR models. The contributions of two ice sources from Antarctica and Greenland vary as different PGR models are used, especially PGR models with lower mantle viscosity (LMV) of 1×10^{21} Pas. The selection of PGR models also affects the contribution of the scale factors of PGR models and the scale factors change considerably, but the variation is very small in terms of sea level change because averaged PGR in global ocean is pretty close to zero. Excluding the PGR models with 1×10^{21} Pas LMV, the contributions to global sea level changes of Antarctic ice sheet, Greenland ice sheet, and Meier model range from 0.28 mm/yr to 0.56 mm/yr, from 0.56 mm/ye to 0.72 mm/yr, and from 0.62 mm/yr to 0.71 mm/yr, respectively. Besides, the contribution of thermosteric sea level change ranges from 0.04 mm/yr to 0.16 mm/yr. And the total sea level trend ranges from 1.77 mm/yr to 1.88 mm/yr with a formal error of 0.23 mm/yr.

In accordance with correlation coefficients of sea level changes derived by tide gauges with WOA01 and Ishii05, the errors of WOA01 and Ishii05 are set as 0.3 and 0.2 mm/yr because Ishii05 is higher correlated with sea level change. Additionally, the error of PGR is set as 0.05 mm/yr. Tables 8.10 and 8.11 show the estimates of two cases. The dependency of the estimated trends from the forcing factors results on the selection of PGR models present the similar phenomena as shown in Table 8.8 and 8.9. Excluding the PGR models with 1×10^{21} Pas LMV, the contributions to global sea level trend of Antarctic ice sheet, Greenland ice sheet, Meier model, and thermosteric sea level are 0.16 – 0.42 mm/yr, 0.59 – 0.74 mm/yr, 0.61 – 0.70 mm/yr, and 0.07 – 0.22 mm/yr, respectively. The total sea level change ranges from 1.73 to 1.85 mm/yr with a formal error of 0.28 mm/yr.

Compared with WLS solution, there is no significant difference for adopting EW-TLS. The estimated variance component from EW-TLS is slightly smaller than from WLS, which means EW-TLS provides quality-of-fit improvement. The formal errors of the estimated forcing factors from EW-TLS are somewhat bigger than from WLS, which means the solution from EW-TLS problem has an expected loss-in-efficiency. The global total sea level trends by summing the contributions of three ice sources and thermosteric sea level, which are determined from WLS and EW-TLS problems, are accordant. Furthermore, the rate of sea level trend determined using 585 tide gauge stations in light of chapter 2 is 1.62 mm/yr. It is relative smaller than the rate determined from WLS and EW-TLS but the difference is not notable because the difference is smaller than the uncertainty. In the computation by EW-TLS using real data, the estimates do not demonstrate the excellence as well as in simulation. The possible reason is the errors of models to form the design matrix are not controlled well. The real errors of three ice sources, thermosteric sea level, and PGR models are not available and only a constant value to present the

error of each model was given. Besides, whether the errors distribute randomly is not known well either.

Considering the estimated variance component to find a best quality-of-fit case, the case using Ishii05 and ICE4G, the errors of which are set as 0.20 and 0.05 mm/yr respectively, is selected. The contributions of Antarctic ice sheet, Greenland ice sheet, and Meier model are 0.36±0.16mm/yr, 0.59±0.15 mm/yr, and 0.62±0.10 mm/yr, respectively. The estimated thermosteric sea level is equal to 0.17±0.05 mm/yr. Figure 8.3 shows the estimated forcing factors described above, containing contributions of three ice sources and thermosteric sea level. As a result, the global total sea level trend determined by summing the contributions of three ice sources and thermosteric sea level is 1.74±0.24 mm/yr, which is slightly larger than the determination described in Chapter 2. The error of 0.24 mm/yr is presented by one standard deviation and only considers 68 % confidence; however, it can be twice of a standard deviation, 0.48 mm/yr, to be more reliable (95 % confidence). Figure 8.4 illustrates the geographic global sea level trends during 1948-2003 by summing the contributions of three ice sources and thermosteric sea level. The higher trends appear in the middle latitude while lower trends occur in the high latitude. The reason is melting ice sheets are located at high latitude and are the dominant to sea level changes. When ice sheets melt, the sea level decreases near the ice sheets.

In addition to tide gauge records with period of 1948–2003, the estimates of global sea level changes using tide gauges of 1900-2003 are also determined, but no IB corrections are applied to gauge data. However, the IB effect should be very small referring to Figure 5.14. Considering the same models and errors as using in Figure 8.3 and Figure 8.4, the solutions of WLS and EW-TLS are shown in Table 8.12 and both estimates are the same. The contributions of Antarctic ice sheet, Greenland ice sheet, and Meier model are 0.80±0.14mm/yr, 0.56±0.12 mm/yr, and 0.31±0.08 mm/yr, respectively. The estimated thermosteric sea level is equal to 0.06±0.04 mm/yr. Figure 8.5 presents the geographic sea level trends of each forcing factors during 1900–2003, which is not consistent with Figure 8.3 in consequence of deficiency of tide gauge data before 1948. As a result, the global total sea level trend determined by summing the contributions of three ice sources and thermosteric sea level equals 1.73±0.42 mm/yr (95 % confidence), which is consistent with previous estimates using the time span of 1948–2003. Figure 8.6 illustrates the geographic total sea level trends during 1900–2003. As the same as in Figure 8.4, the higher trends appear in the middle latitude while lower trends occur in the high latitude and sea level trends drop near the Greenland; however, the amplitude of sea level variations in Figure 8.6 is smaller than in Figure 8.4. In addition, sea level trends near Antarctica in Figure 8.6 are lower than in Figure 8.4 as a result of more contributions from Antarctic ice sheet to sea level.

Compared with previous studies (Table 8.13), the estimated thermosteric sea level trend is smaller than the observed thermosteric sea level trend [Levitus et al., 2005]; however, the value at the lower bound cited in the second IPCC report (0.2–0.7 mm/yr). The estimated contribution of ice sheets is higher than previous studies of 0.45 mm/yr yet within the twice of an uncertainty. The estimated contribution of mountain glaciers has a good agreement with Ahrendt et al. [2002] with the difference within one uncertainty. To be noticed, hydrological and anthropogenic effects are not accounted in this study, which may bias the estimates, especially the similar geometries of models. The reason for inconsistency of estimates and recent

measurements may be the measurements could be inaccurate (lack of adequately long data span) and also that the model does not include present day data (therefore the spatial pattern is inaccurate).

In Equation (8.4), the block of zeros in the design matrix A should be treated as non-random. However, it is not practically applicable to this problem at this time primarily because there is no model suitable in this time. The newest researches only treat the weight matrix of observations as an identity matrix for TLS, which can consider non-random elements in design matrix [Schaffrin et al., 2005]. For the sea level case, the solutions are significantly more sensitive to data weights. If one uses an identity matrix as a weight matrix, the result will not an optimal solution and could be incorrect. In computation, the relatively small errors (large weights) are assigned to $D\{E_A\} = \sigma_{ij}^2$ corresponding to these zero elements in order to force non-random elements not change. Additionally, errors of observations corresponding to non-random elements are relatively large, $\varepsilon_{S_T}^2 << \varepsilon_{S_v}^2$, which makes the effect of treating non-random elements as random more slight. Therefore, numerically the result is no different in this case when treating the block of zeros in the design matrix A as random.

	V_A (mm/yr)	V_G (mm/yr)	V_M (mm/yr)	V_O (mm/yr)	V_P	$\hat{\sigma}_0^2$ $(\text{mm/yr})^2$	TSLT (mm/yr)
ICE4G	0.54±0.14	0.56±0.15	0.62±0.10	0.07±0.03	0.84±0.11	13.52	1.79
120_1_1	0.22±0.13	0.77±0.15	0.74±0.10	0.10±0.03	0.38±0.10	14.26	1.83
120_1_3	0.44±0.14	0.66±0.15	0.70±0.09	0.06±0.03	0.48±0.08	13.86	1.86
120_1_10	0.37±0.14	0.72±0.15	0.65±0.10	0.09±0.03	0.41±0.07	13.97	1.83
120_p5_1	0.37±0.14	0.83±0.15	0.67±0.10	0.06±0.04	1.24±0.27	14.04	1.93
120_p5_3	0.56±0.14	0.59±0.15	0.71±0.09	0.04±0.03	0.79±0.11	13.61	1.90
120_p5_10	0.45±0.14	0.65±0.15	0.65±0.10	0.08±0.03	0.55±0.08	13.76	1.83

Table 8.8: Estimated trends resulting from three ice sources, PGR, and thermosteric sea level using different PGR models and WOA01. The errors of WOA01 and PGR are set as 0.10 and 0.05 mm/yr respectively. Time span of tide gauges is 1948-2003. TSLT: Total sea level trend is sum of all forcing factors.

	V_A	V_G	V_M	V_O	V_P	$\hat{\sigma}_0^2$	TSLT
Ice4g	0.46±0.14	0.57±0.15	0.62±0.10	0.12±0.04	0.80±0.11	13.42	1.77
120_1_1	0.12±0.13	0.77±0.15	0.74±0.10	0.18±0.04	0.36±0.09	14.04	1.81
120_1_3	0.33±0.14	0.67±0.15	0.70±0.09	0.13±0.04	0.44±0.07	13.74	1.83
120_1_10	0.28±0.14	0.72±0.15	0.65±0.10	0.16±0.04	0.38±0.07	13.84	1.81
120_p5_1	0.25±0.14	0.83±0.15	0.67±0.10	0.15±0.04	1.12±0.25	13.86	1.90
120_p5_3	0.46±0.14	0.61±0.15	0.71±0.09	0.10±0.04	0.73±0.11	13.52	1.88
120_p5_10	0.36±0.14	0.66±0.15	0.66±0.10	0.13±0.04	0.52±0.08	13.66	1.81

Table 8.9: Estimated trends resulting from three ice sources, PGR, and thermosteric sea level using different PGR models and Ishii05. The errors of Ishii05 and PGR are set as 0.10 and 0.05 mm/yr respectively. Time span of tide gauges is 1948-2003. TSLT: Total sea level trend is sum of all forcing factors.

	V_A	V_G	V_M	V_O	V_P	$\hat{\sigma}_0^2$	TSLT
Ice4g	0.42±0.17	0.59±0.15	0.61±0.10	0.11±0.05	0.77±0.13	13.44	1.73
120_1_1	0.02±0.17	0.77±0.15	0.73±0.10	0.20±0.06	0.24±0.13	14.03	1.72
120_1_3	0.30±0.19	0.69±0.15	0.70±0.09	0.12±0.06	0.41±0.11	13.79	1.81
120_1_10	0.20±0.17	0.74±0.15	0.64±0.10	0.16±0.05	0.34±0.09	13.81	1.74
120_p5_1	0.21±0.20	0.82±0.15	0.67±0.10	0.14±0.07	0.97±0.38	13.92	1.84
120_p5_3	0.47±0.20	0.61±0.15	0.70±0.09	0.07±0.06	0.73±0.15	13.61	1.85
120_p5_10	0.30±0.17	0.68±0.15	0.65±0.10	0.14±0.05	0.48±0.10	13.64	1.77

Table 8.10: Estimated trends resulting from three ice sources, PGR, and thermosteric sea level using different PGR models and WOA01. The errors of WOA01 and PGR are set as 0.30 and 0.05 mm/yr respectively. Time span of tide gauges is 1948-2003. TSLT: Total sea level trend is sum of all forcing factors.

	V_A	V_G	V_M	V_O	V_P	$\hat{\sigma}_0^2$	TSLT
Ice4g	0.36±0.16	0.59±0.15	0.62±0.10	0.17±0.05	0.74±0.12	13.35	1.74
120_1_1	0.01±0.15	0.78±0.15	0.73±0.10	0.26±0.04	0.29±0.10	13.87	1.78
120_1_3	0.22±0.16	0.69±0.15	0.70±0.09	0.18±0.06	0.39±0.08	13.64	1.79
120_1_10	0.16±0.16	0.73±0.15	0.66±0.10	0.22±0.06	0.34±0.08	13.71	1.77
120_p5_1	0.13±0.16	0.83±0.15	0.67±0.10	0.21±0.06	0.97±0.27	13.74	1.72
120_p5_3	0.37±0.17	0.62±0.15	0.70±0.09	0.14±0.06	0.67±0.12	13.47	1.83
120_p5_10	0.25±0.16	0.68±0.15	0.66±0.09	0.19±0.06	0.47±0.09	13.56	1.78

Table 8.11: Estimated trends resulting from three ice sources, PGR, and thermosteric sea level using different PGR models and Ishii05. The errors of Ishii05 and PGR are set as 0.20 and 0.05 mm/yr respectively. Time span of tide gauges is 1948–2003. TSLT: Total sea level trend is sum of all forcing factors.

	V_A	V_G	V_M	V_O	V_P	$\hat{\sigma}_0^2$	TSLT
WLS	0.76±0.12	0.59±0.12	0.33±0.08	0.06±0.03	1.16±0.07	13.07	1.74
EW-TLS	0.80±0.14	0.56±0.12	0.31±0.08	0.06±0.04	1.27±0.08	12.36	1.73

Table 8.12: Estimated trends resulting from three ice sources, PGR, and thermosteric sea level using different PGR models and Ishii05. The errors of Ishii05 and PGR are set as 0.20 and 0.05 mm/yr respectively. Time span of tide gauges is 1900-2003. TSLT: Total sea level trend is sum of all forcing factors.

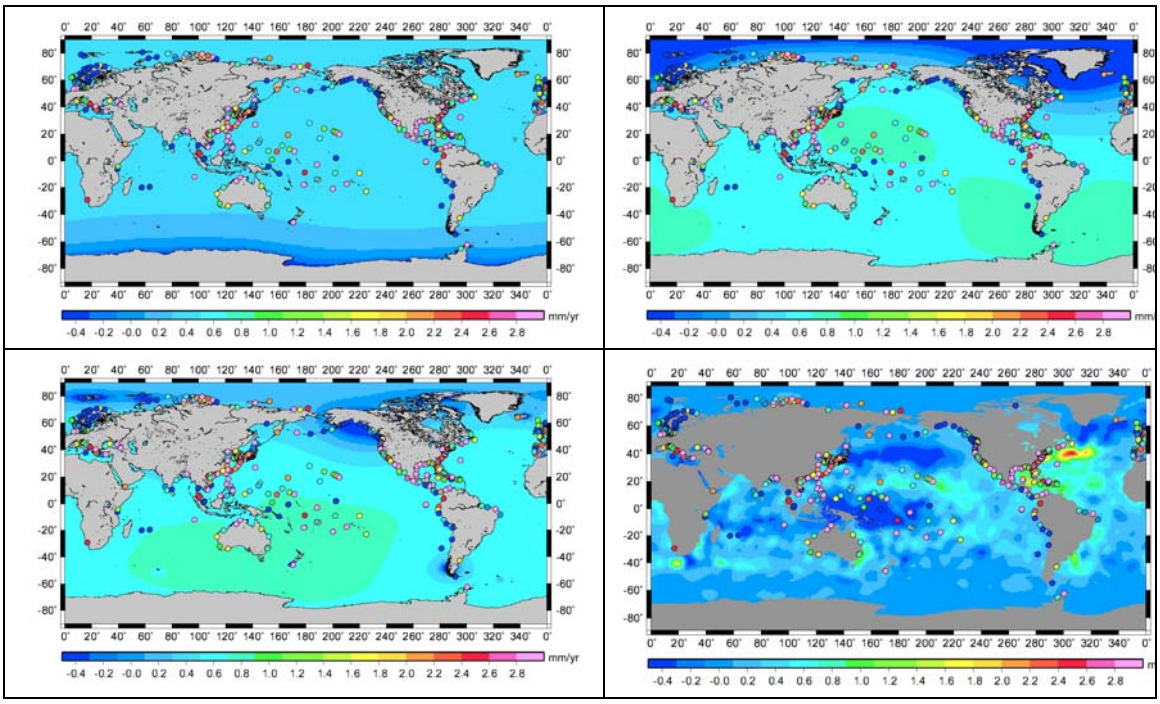

Figure 8.3: Left-Top: sea level trends contributed by Antarctic ice sheet; Right-Top: sea level trends contributed by Greenland ice sheet; Left-Bottom: sea level trends contributed by mountain glaciers and ice sheets tabulated by Meier [1984]; Right-Bottom: sea level trends contributed by thermosteric sea level. Time span of tide gauges is 1948–2003. Circles are tide gauge stations.

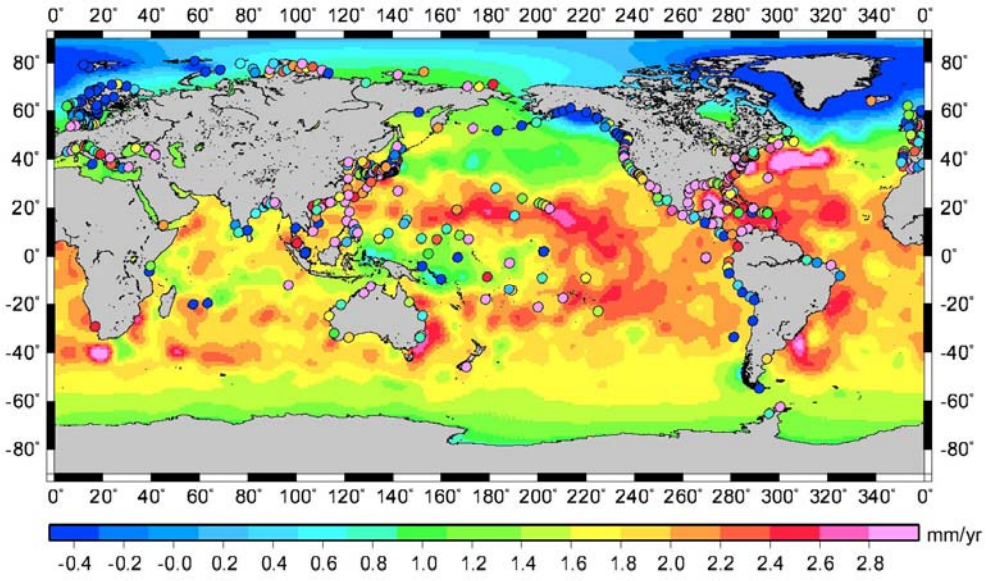

Figure 8.4: Geographical sea level trends during 1948–2003. Circles are tide gauge stations.

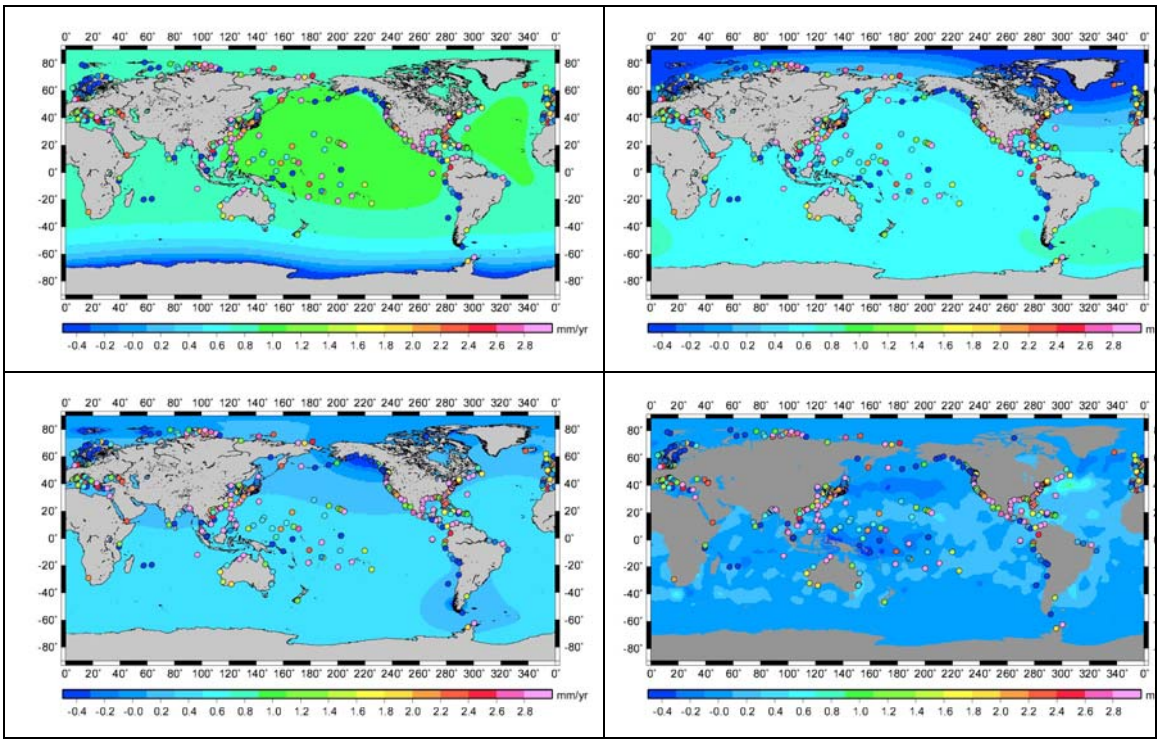

Figure 8.5: Left-Top: sea level trends contributed by Antarctic ice sheet; Right-Top: sea level trends contributed by Greenland ice sheet; Left-Bottom: sea level trends contributed by mountain glaciers and ice sheets tabulated by Meier [1984]; Right-Bottom: sea level trends contributed by thermosteric sea level. Time span of tide gauges is 1900–2003. Circles are tide gauge stations.

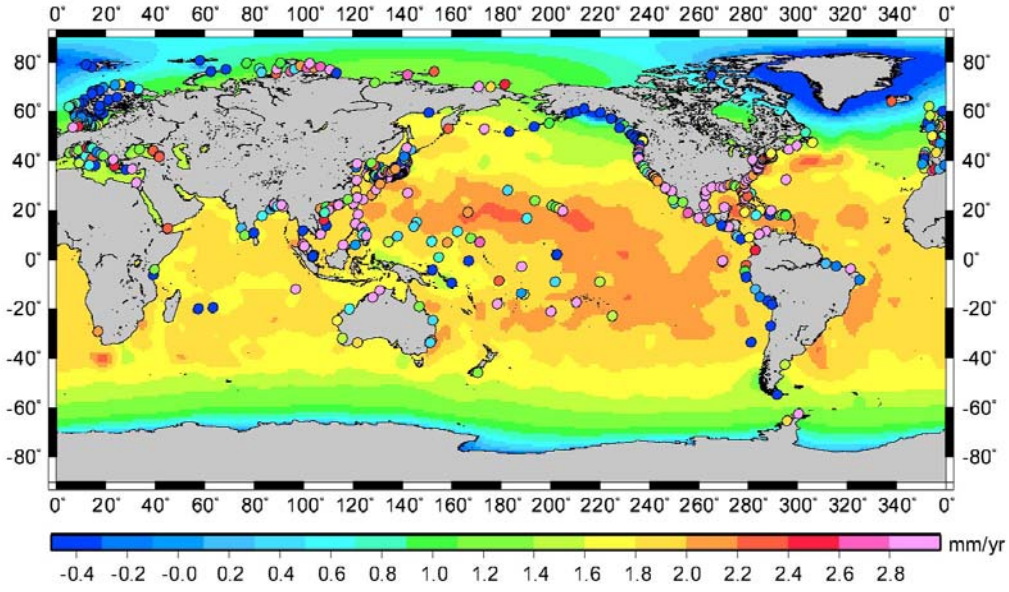

Figure 8.6: Geographical sea level trends during 1900–2003. Circles are tide gauge stations.

	Previous Study	Previous Study	This study (1948-2002)
Steric (mm/yr)	0.4 (1957-1996) [Levitus et al., 2005]		0.17±0.05
Glaciers (mm/yr)	0.51 [Ahrendt et al., 2002]		0.62±0.10
Ice sheets (mm/yr)	0.45 (0.20, ~0.07, 0.11, 0.07 mm/yr for Greenland, Antarctica, Patagonia, Canadian) [Krabill et al. 2004; Rignot et al., 2005 ; Thomas et al., 2005]		0.94±0.22
Hydrological (mm/yr)	0.0-0.12 [Ngo-duc et al., 2005 ; Milly et al 2003]		
Anthropogenic (mm/yr)	0.05		
Total Sea Level Trend (mm/yr)	1.41 to 1.53	1.8 [Douglas, 2001; Church et al., 2004]	1.74±0.48

Table 8.13: Comparisons of the contributions to global sea level trend from different sources.

8.7 Summary

In this Chapter, global sea level trend is determined combining altimeter data and 585 tide gauge records based on geographic patterns predicted by PGR models, the geometries due to melting of three ice sources, and thermosteric sea level trend. The amplitudes of each of the geophysical contributions and the scale factor to the PGR model are simultaneously estimated to determine the global sea level trend for the 20th Century and for last 5 decades (or hundred years) using of WLS and EW-TLS approaches. The solution of EW-TLS problem presents an excellent determination of sea level trend and amplitudes of forcing factors using simulated data while the solution of EW-TLS problem gives similar determinations with a slightly smaller estimated variance component compared with the solution of WLS problem using *in situ* data. The possible reason is the errors of models used to form the design matrix are not known well and only give each model a constant value. Therefore, one of the future works is to develop more realistic error models, for example, the use of ICE5G and the model specific to Antarctica. More accurate error models produce a more robust design matrix which would improve the estimates.

Considering the estimated variance component to find the best quality-of-fit case, the contributions of Antarctic ice sheet, Greenland ice sheet and Meier model during 1948-2002 are 0.36±0.16mm/yr, 0.59±0.15 mm/yr, and 0.62±0.10 mm/yr, respectively. The estimated thermosteric sea level is equal to 0.17±0.05 mm/yr. These estimates agree with previous researches within twice of the uncertainty. As a result, the global total sea level trend for the 50 year case is 1.74±0.48 mm/yr (95% confidence, or 2σ), which is slightly larger than the determination of 1.6 mm/yr in Chapter 5 and is close to the estimates of 1.8 mm/yr reported by Church et al. [2004] and Douglas [2001]. The 20th Century sea level determination is estimated to be 1.73±0.42 mm/yr (95% confidence or 2σ) with the contributions of facing factors at 0.80±0.14mm/yr, 0.56±0.12 mm/yr, and 0.31±0.08 mm/yr in order. The comparison of estimates and measurements is inconsistent since the measurements could be inaccurate (lack of adequately long data span) and also that the model does not include present day data (therefore

the spatial pattern is inaccurate). In this study, hydrological and anthropogenic effects are not accounted for, which may bias the estimates, especially if the models have similar geometries. Therefore, these models should be included in future research.

CHAPTER 9

CONCLUSIONS AND FUTURE WORK

Global sea level variation is determined mainly using tide gauge data, which are measuring the heights of sea surface relative to a fixed point on the adjacent land. For that reason, the vertical crustal motions could complicate the measurements of tide gauge stations. The contemporary method is to adopt a specific postglacial rebound (PGR) model to correct for vertical motions at tide gauge sites for the determination of global sea level trend. In this dissertation a new method, which takes advantage of using the accurately absolute sea level from altimeters and the long time spans of tide gauge records, to estimate the absolute vertical motions in Fennoscandia, Alaska, and Great Lakes has been presented. The uncertainty of the estimated vertical motions reduces significantly to less than 0.5 mm/yr in semi-enclosed ocean or lakes and about 1 mm/yr in the open ocean compared with the traditional approach at more than 1-2 mm/yr [e.g., Nerem and Mitchum, 2002]. The estimated vertical motions agree well with GPS solutions in Baltic Sea and Alaska region; however, the estimated vertical motions are not consistent with GPS solution in Great Lakes, but agree well with the ICE4G PGR model. At present, various GPS vertical solutions are largely inconsistent with each other even though different analysis centers or researchers primarily used similar data sets [Snay et al., 2002]. The large discrepancy between GPS solutions and altimetry-tide gauge vertical motion determination may be caused by different GPS solution methodologies, processing philosophy, or using different reference frames or fixing different stations.

In the Baltic Sea region and Alaska, excellent agreement between the different independent solutions verifies the accuracy and robustness of our (and the GPS) techniques. The future work to improve the approach is to lengthen the time span of altimeter data. In this way, the accuracy of the absolute vertical motion estimates should be improved. Extension of TOPEX/POSEIDON data span using JASON and linking with GEOSAT (1984–1989) would provide an avenue for this improvement. In the adjustment, the adjacent tide gauge stations are assumed to measure the identical sea level variations; however, this assumption could be not exactly correct when the local phenomenon dominates the sea level like currents. Hence, the assumption can be improved by introducing sea level trends from circulation models, such as ECCO model. In addition, analyzing in detail the correlation between gauge data and altimeter data to compose an accurate weight matrix can improve the algorithm as well.

Steric sea level is a major component of sea level rise in addition to ocean mass variations, so the comprehensive analysis of steric sea level should be done by *in situ* data and the objective analyzed models. Grid temperature data of WOA01 and Ishii05 have been employed to compute thermosteric sea level. Additionally, thermosteric sea level and steric sea level have been also computed using *in situ* data of OSD. From the analysis, global thermosteric sea level trend of upper (0-500m) layers is about 70% of the deep ocean (0-3000m) when using the objective analyzed models, whereas thermosteric sea level trends integrated from 0 down to 500 m and down to 1000 m using OSD have a consistent trend in Eastern Pacific, where large numbers of hydrographic observations exist. The discrepancy of this conclusion may be caused

by inadequate sampling by *in situ* profiles, particularly in the Southern Hemisphere or Gulf Stream [Miller at al., 2004]. Therefore, a more careful analysis on the deep ocean such as 500 m–3000 m or 500 m–5500 m is needed in the future. Halosteric sea level changes contributing relative small to steric sea level variations have been verified using OSD and its sign is positive. The rise of halosteric sea level means salinity decrease, which may be interpreted in terms of both sea ice melting and fresh water added to the oceans. Melting water of sea ice does not change sea level while fresh water flowing to the oceans from the continents does.

Although *in situ* data or objective analyzed models are available to compute steric sea level variations, the serious problem of sampling stands in the southern ocean and near the region of North Pole like Arctic Ocean. However, if mass variations or fresh water flowing into oceans can be understood more accurately over the past 50 years, it may help us to understand the steric sea level. An assessment of the first release of the GRACE observations of the Southern Ocean mass variations (April/May 2002–April 2004) are provided using ENVISAT radar altimetry corrected for steric sea level using NOAA's WOA01 climatology, and the ocean bottom pressure data of ECCO model. The annual signal of ocean mass variations in general agrees well between the GRACE and the steric-corrected TOPEX altimetry globally, while the steric-corrected ENVISAT altimeter and GRACE are not compatible in the Southern Ocean and East Antarctica when the isotropic filter smoother, the non-isotropic filter smoother, and a preliminary solution of regional inversion using GRACE *in situ* potential measurements. The causes of the discrepancy can be attributed to the errors in the steric sea level primarily due to lack of data in the Southern Ocean, or possible ENVISAT data sampling problem due to sea ice. Therefore, if the sampling problem of ENVISAT can be overcome or the place there is sea ice less, the role of GRACE observing long-wavelength mass variations has a potential to improve the estimates of the steric sea level over the Southern Ocean.

Finally, the AGOS arrays are beginning to lengthen the spatial and temporal coverage of the steric measurements in the ocean, and combining with satellite altimetry and GRACE, it is expected that the quantification and understanding of steric sea level in the decades to come will improve.

The global sea level trends during the period of 1985–2002 derived by altimeters and tide gauge records are 2.9±0.5 mm/yr and 2.7±0.4 mm/yr, respectively. Additionally, the rate of sea level variations derived by satellite altimeters, which measure the same regions as the tide gauge stations do, is equal to 2.8±0.5 mm/yr. Three cases present an excellent agreement. Both tests confide us that selected tide gauge records complying with the setting criteria are good enough to account for global sea level trend even if gauges have not been distributed evenly and globally. Therefore, global sea level trend is being determined from 651 tide gauge stations finally and the outcome shows a consistent value, 1.6±0.4 mm/yr, during the time span of 1948–2002. Additionally, the sea level trend keeps constantly with the rate at 1.6 mm/yr when the time span is longer than 54 years (1948–2002).

The other approach to overcome the problem of gauge distribution is to determine and characterize global sea level using gauge records and altimeter data combining with geophysical models. The rate and characterization of global sea level trend have been determined and explained by the solutions of WLS and EW-TLS problems using the combination of altimeter

data, 585 tide gauge records, PGR models, the geometries of sea level trends caused by three ice sources, and thermosteric sea level trends derived from temperature data. The solution of EW-TLS problem has an excellent result, which recovers the values set for the simulated data while the solution of WLS problem makes errors of approximately 0.3 mm/yr using the simulated data. Nevertheless, the solutions of EW-TLS and WLS problems make a similar result using the real data because the errors of models to form the design matrix are not available exactly. The EW-TLS solution yields the estimated sea level trends contributed by melting ice from the Antarctic, Greenland and mountain glaciers to be 0.80±0.14 mm/yr, 0.56±0.12 mm/yr. and 0.31±0.08 mm/yr, respectively; the estimated contribution from the thermosteric effect to be 0.06±0.04 mm/yr, and the estimated scale of the GIA (ICE-4G) model to correct tide gauge sea level data is 1.27±0.08. The resulting 20th Century (1900–2002) global sea level trend is estimated to be 1.73±0.42 mm/yr (95% confidence or 2σ) after summing the above forcing factors. The estimate of the resulting last 50 year (1948–2002) global sea level trend is 1.74±0.48 mm/yr (95% confidence or 2σ) with the contributions at 0.36±0.16mm/yr, 0.59±0.15 mm/yr, 0.62±0.10 mm/yr, and 0.17±0.05 mm/yr. The estimated sea level trend is the comparable with 1.6±0.4 mm/yr, which is determined only using tide gauge records. By comparing the estimates with measurements, it shows an inconsistency because the measurements could be inaccurate (lack of adequately long data span) and also that the model does not include present day data (therefore the spatial pattern is inaccurate).

To computing the solution of EW-TLS problem, the errors of geophysical models used to form the design matrix should be known accurately in contrast to only giving a constant value for a model. Therefore, to analyze the real errors of models in the future is a necessary work to improve the determination. Recently, more contemporary models are going to be released like ICE5G. More accurate models can consist of more perfect design matrix. Additionally, hydrological and anthropogenic effects are not accounted in this computation, which may bias the estimates, especially the similar geometries of models. Therefore, these models should be included in the future work.

Arctic region is particularly sensitive to climate variability and is in the midst of a major climate, environmental and societal change, so it is important and worth paying attention to study the sea level changes here. Because of the lack of altimeter data due to sea ice coverage, sea level variations are determined only in a selected area of latitude 55N-82N and longitude 315E-60E. The sea level trend in the region is estimated at 1.8 mm/yr using altimeters, in which ERS-1 and ERS-2 are calibrated by TOPEX/POSEIDON, and this trend can be characterized by the sea surface atmospheric pressures and the thermosteric sea level trend with a quite large uncertainty. In Arctic Ocean, sea level trend during the period of 1948-2002 has also been estimated at 1.9-2.0 mm/yr when applying different PGR models. After applying IB corrections to tide gauge data, the rate reduces to 1.5-1.6 mm/yr. Thus it can be seen the effect of surface atmospheric pressures is an important contribution to sea level trend in Arctic Ocean with respect to global ocean. GEOSAT and ENVISAT have not been calibrated in this study to determine sea level changes but the influence is slight on account of the relative short period of data. For the future work, a comprehensive calibration of all altimeters should be done in order to determine the sea level trend more precisely. Additionally, more contemporary altimeter missions can be added to extend the time span, which can potentially avoid the errors caused by decadal or inter-decadal signals when computing secular trend.

Time span of sea level derived from 27 tide gauge stations should be more than 20 years to obtain a stable rate while time span of thermosteric sea level should be more than 30 years of data. The reason for why thermosteric sea level variations needs more years to derive a stable rate could be that thermosteric sea level contains the strong amplitude of the interdecadal signal (about 16-year period). Whether sea level rise is accelerating in the 1990s is an important question for researchers because acceleration of sea level rise could make the populated area to disappear more quickly. As a conclusion of this study, sea level variations derived from 27 tide gauge data and thermosteric sea level changes indicate that there is no evidence to address sea level acceleration in the 1990s by means of the available time span of data by the statistic approach. The future work, however, should be studied using longer historical records. But the major problem could be the quality of the historical data, which have not yet been under adequate quality control.

REFERENCES

Arendt, A. A., K. A. Echelmeyer, W. D. Harrison, C. S. Lingle, and V. B. Valentine, Rapid wastage of Alaska glaciers and their contribution to rising sea level, *Science*, 297, 383-386, 2002.

Andersen, O. B., and J. Hinderer, Global inter-annual gravity changes from GRACE: Early results, *Geophys. Res. Lett.*, 32, L01402, doi:10.1029/2004GL020948, 2005.

Antonov, J. I., S. Levitus, and T. P. Boyer, Steric sea level variations during 1957-1994: Importance of salinity, *J. Geophys. Res.*, 107(C12), 8013-8021, 2002.

Antonov, J. I., S. Levitus, and T. P. Boyer, Thermosteric sea level rise, 1955-2003, *Geophys. Res. Lett.*, 32, L12602, doi:10.1029/2005GL023112, 2005.

Aoki, S., Large-scale variations of sea level in the Southern Ocean, Joint Asia-Pacific Space Geodynamics (APSG/AOGS) Session, Proc. Asia Oceanic Geosciences Society (AOGS) Meeting, Singapore, 2004.

Barnes, D. F., No measurable gravity change at Glacier Bay regional uplift area, *U.S. Geol. Surv. Circ.*, 939, 88-90, 1984.

Barnett, T. P., Recent changes in sea level: a summary in sea level change (National Research Council), 37-51, National Academy Press, Washington D.C., 1990.

Barnett, T. P., D. W. Pierce, and R. Schnur, Detection of anthropogenic climate change in the world's ocean, *Science*, 292, 270-274, 2001.

Barry, R. G., M. C. Serreze, J. A. Maslanik, and R. H. Preller, The Arctic sea ice-climate system: observations and modeling, *Rev. Geophys.*, 31, 397-422, 1993.

Beyer, W. H., Standard mathematical tables and formulae, CRC press, Boca Raton, Fla., 1991.

Blewitt, G., H.-P. Plag, R. Gross, P. Clarke, D. Lavallée, and T. Van Dam, Monitoring sea level change: reference frames, Earth's changing shape & gravity field, NASA Sea Level Workshop, Landover, MD, 2005.

Bonnefond P., P. Exertier, O. laurain, Y. Merard, A. Orsoni, G. Jan, and E. Jeansou, Absolute calibration of Jason-1 and Topex/Poseidon altimeters in Corsica, *Marine Geodesy*, 261-284, doi: 10.1080/01490410390253487, 2003.

Boyer, T. P., M. E. Conkright, S. Levitus, D. Johnson, J. I. Antonov, T. O' Brien, C. Stephens, and R. Gelfeld, NOAA Atlas NESDIS 22, World Ocean Database 1998 Volume 5: Temporal distribution of station data temperature and salinity profiles, U.S. Gov. Printing Office, Washington, D.C., 108, 1998.

Boyer, T. P., J. I. Antonov, S. Levitus, and R. Locarnini, Linear trends of salinity for the World Ocean, 1955-1998, *Geophys. Res. Lett.* , 32, L01604, doi:1029:2004GL021791, 2005.

Cabanes, C., A. Cazenave, and C. Le Provost, Sea level rise during the 1990s and past 40 years: new insight from satellite and in situ observations, *Science*, 194, 840-842, 2001a.

Cabanes, C., A. Cazenave, and C. Le Provost, Sea level changes from TOPEX/POSEIDON altimetry for 1993-1999 and warming of the southern oceans, *Geophys. Res. Lett.*, 28, 9-12, 2001b.

Caccamise, D. J., II, M. A. Merrifield, M. Bevis, J. Foster, Y. L. Firing, M. S. Schenewerk, F. W. Taylor, and D. A. Thomas, Sea level rise at Honolulu and Hilo, Hawaii: GPS estimates of differential land motion, *Geophys. Res. Lett.*, 32, L03607, doi:10.1029/2004GL021380, 2005.

Calmant, S., K. Cheng, G. Jan, C. Kuo, C. Shum, Y. Yi, V. Ballu and M. Bouin, Comparison of sea surface height derived from satellite altimetry and from ocean bottom pressure gauges: The SW Pacific MOTEVAS Project, *Marine Geodesy*, 27 (3–4), Special Issue on Jason-1 Calibration/Validation Part III, 597-613, 2004.

Carton, J. A., B. S. Giese, and S. A. Grodsky, Sea level rise and the warming of the oceans in the Simple Ocean Data Assimilation (SODA) ocean reanalysis, *J. Geophys. Res.,* 110, C09006, doi:10.1029/2004JC002817, 2005.

Cazenave, A., K. Dominh, F. Ponchaut, L. Soudarin, J. F. Cretaux and C. Le Provost, Sea level changes from Topex/Poseidon altimetry and tide gauges, and vertical crustal motions from DORIS, *Geophys. Res. Lett.,* 26(14), 2077–2080, 1999.

Cazenave, A., F. Remy, K. Dominh, and H. Douville, Global ocean mass variation, continental hydrology and the mass balance of Antarctica ice sheet at seasonal time scale, Geophys. Res. Lett., 27, 3755–3758, 2000.

Cazenave, A., and R. S. Nerem, Present-day sea level change: observations and causes, *Reviews of Geophysics,* 42(3), RG3001, doi:10.1029/2003RG000139, 2004.

Chambers, D. P., C. A. Melhaff, T. J. Urban, D. Fuji, and R. S. Nerem, Low-frequency variations in global mean sea level: 1950–2000. *J. Geophys. Res.,* 107(C4), 3026, doi:10.129/2001JC001089, 2002.

Chambers, D. P., S. A. Hayes, J. C. Ries, and T. J. Urban, New TOPEX sea state bias models and their effect on global mean sea level, *J. Geophys. Res.,* 108(C10), 3305, doi:10.1029/2003JC001839, 2003.

Chambers, D. P., J. Wahr and R. S. Nerem, Preliminary observations of global ocean mass variations with GRACE, *Geophys. Res. Lett.,* 31, L13310, doi:10.1029/2004GL020461, 2004.

Chao, B., Man-made lakes and global sea level, *Nature,* 370, 258, 1994

Chao, B., T. Farr, J. LaBrecque, R. Bindschadler, B. Douglas, E. Rignot. C. Shum, J. Wahr and NASA Solid Earth Science Working Group (SESWG), Understanding sea level changes, IGARSS Meeting, Toronto, Canada, June 24-28, 2002.

Chen, J. L., C. R. Wilson, R. J. Eanes, and R. S. Nerem, Geophysical interpretation of observed geocenter variations, *J. Geophys. Res.,* 104(B2), 2683– 2690, 1999.

Chen, J. L., C. K. Shum, C. R. Wilson, D. P. Chambers, and B. D. Tapley, Seasonal sea level change from TOPEX/POSEIDON observation and thermal observation, *J. of Geodesy,* 73, 638-647, 2000.

Cheng, K. C., Radar altimeter absolute calibration using GPS water level measurements, *Master thesis*, Ohio State University, 2001.

Cheng, K., S. Calmant and C. Shum, Absolute calibration of satellite radar altimeters in Lake Erie, and Vanuatu, South Pacific, 27th General Assembly of the EGS in Nice, France, April 21–26, 2002.

Church, J. A., J. Gregory (Lead Authors), P. Huybrechts, M. Kuhn, K. Lambeck, M. Nhun, D. Qin, and P. L. Woodworth (Lead Authors), Change in sea level, In 26 contributing authors, Intergovernmental Panel Climate Committee (IPCC) Working Group 1 (WG1) Third Assessment Report, Chapter 11, 2001.

Church, J. A., N. J. White, R. Coleman, K. Lambeck, and J. X. Mitrovica, Estimates of regional distribution of sea level rise over the 1950-2000 period, *J. of Clim.,* 17, 2609-2625, 2004.

Conkright, M. E., H. E. Garcia, T. D. O'Brien, R. A. Locarnini, T. P. Boyer, C. Stephens, and J. I. Antonov, World Ocean Database 2001, vol. 1, Introduction [CD-ROM], NOAA Atlas

NESDIS, vol. 42, edited by S. Levitus, 159 pp., Govt. Print. Off., Washington, D.C., 2002.

Conrad, C. P., and B. H. Hager, Spatial variations in the rate of sea level rise caused by the present-day melting of glaciers and ice sheets, *Geophys. Res. Lett.*, 24, 12, 1503-1506, 1997.

Christensen, E., B. Haines, S. Keihm, C. Morris, R. Norman, G. Purcell, B. Williams, B. Wilson, G. Born, M. Parke, S. Gill, C. Shum, B. Tapley, R. Kolenkiewicz, R. Nerem, Calibration of TOPEX/POSEIDON at platform harvest. *J. Geophys. Res.*, 99, (C12), 24,465–24,485, 1994.

Cullition, T. J., M. A. Warren, T. R. Goodspeed, D. G. Remer, C. M. Blackwell, and J. J. McDonough III, 50 years of population change along the nation's coast, 1960-2010, Rockwille, Maryland, Strategic Assessment Branch, National Ocean Service, National Oceanic and Atmospheric Administration, 41, 1990.

Davis, J. L., P. Elosequi, J. X. Mitrovica, and M. E. Tamisiea, Climate-driven deformation of the solid Earth from GRACE and GPS, *Geophys. Res. Lett.*, 31, L24605, doi:10.1029/2004GL021435, 2004.

Dettinger, M.D., Ghil, M., Strong, C.M., Weibel, W., and Yiou, P., 1995: Software expedites singular-spectrum analysis of noisy time series, Eos, Trans. American Geophysical Union, v. 76(2), p. 12, 14, 21.

Douglas, B. C., Global sea level rise, *J. Geophys. Res.*, 96(C4), 6981-6992, 1991.

Douglas, B. C., Global sea level acceleration, *J. Geophys. Res.*, 97(C8), 12,699-12,706, 1992.

Douglas, B. C., Global sea rise: a redetermination, *Surveys in Geophysics*, 18, 279-292, 1997.

Douglas, B. C., Sea level change in the era of the recording tide gauge, In B. C. Douglas, M. S. Kearney, and S. P. Leatherman (Eds.), Sea Level Rise; History and Consequences, Chapter 3, Academic Press, 2001.

Dyurgerov, M. B., and Meier, M.F., Glaciers and Changing Earth System: a 2004 snapshot, INSTAAR, 37, Boulder, 2005.

Dyurgerov, M. B., and L. Carissa, Observational evidence of increases in freshwater inflow to the Arctic Ocean, *Carter.Arctic, Antarctic, and Alpine Research*, 36, 1, 117-122, 2004.

Farrell, W. E., and J. T. Clark, On postglacial sea level, *Geophys. J. R. Astron. Soc. 46*, 647-667, 1976.

Fan, Y., H. Van del Dool, K. Mitchell, and D. Lohmann, A 51-Year reanalysis of the U.S. land-surface hydrology, *GEWEX News*, 13, 2, 6, 2003.

Fukumori, I., R. Raghunath, L. L. Fu, and Y. Chao, Assimilation of TOPEX/POSIEDON altimeter data into a global ocean circulation model: How good are the results?, *J. Geophys. Res.*, 104(C11), 25,647-25,665, 1999.

Fukumori, I., A partitioned Kalman filter and smoother, *Monthly Weather Review*, 130, 1370-1383, 2002.

Ekman, M., The world's longest continued series of sea level observations, *Pure and Applied Geophysics*, 127, 73-77, 1988.

Ekman, M., Determination of global sea level rise and its change with time, *Small Pub. In Hist. Geophys.*, 7, 19, 2000.

Ghil M., R. M. Allen, M. D. Dettinger, K. Ide, D. Kondrashov, M. E. Mann, A. Robertson, A. Saunders, Y. Tian, F. Varadi, and P. Yiou, Advanced spectral methods for climatic time series, *Rev. Geophys.*, 40(1), 3.1-3.41, 10.1029/2000GR000092, 2002.

Gill, A. E., Atmosphere-Ocean Dynamics, Academic Press, New York, 1982.

Gille, S. T., Warming of the Southern Ocean since the 1950s, *Science*, 295, 1275-1277, 2002.
Gille, S. T., Decadal-scale temperature variability in the southern ocean, IUGG2003, Sapporo, Japan, 2003.
Gille, S. T., How nonlinarities in the equation of state of seawater can confound estimates of steric sea level change, *J. Geophys. Res.*, 109, C03005, doi:10.1029/2003JC002012, 2004.
Gornitz, V., S. Lebedeff, and J. Hansen, Global sea level trends in the past century, *Science*, 215, 1611-1614, 1982.
Gornitz, V., Monitoring sea level changes, *Climatic Change*, 31, 515-544, 1995.
Greatbatch, R. J., A note on the representation of steric sea level in models that conserve volume rather than mass, *J. Geophys. Res.*, 99(C6), 12,767-12,771, 1994.
Gregory, J., J. A. Church, G. J. Boer, K. W. Dixon, G. M. Flato, D. R. Jackett, J. A. Lowe, S. P. O'Farrell, E. Roeckner, G. L. Russell, R. J. Stouffer, and M. Winton, Comparison of results from several AOGCMs for global and regional sea-level changes 1900-2100, *Climate Dynamics*, 18, 225-240, 2001.
Guman, M. D., Determination of global mean sea level variations using multi-satellite altimetry, *Ph.D. dissertation*, The University of Texas at Austin, 1997.
Haines, B., D. Dong, G. Born, and S. Gill, The harvest experiment: monitoring Jason-1 and Topex/Poseidon from California Offshore Platform, *Marine Geodesy*, 239–259, doi: 10.1080/01490410390253487, 2003.
Han, S. C., C. Jekeli, and C. K. Shum, Time-variable aliasing effects of ocean tides, atmosphere, and continental water mass on monthly mean GRACE gravity field, *J. Geophys. Res.*, 109(B4), B04403, doi:10.1029/2003JB002501, 2004a.
Han, S. C., C. K. Shum, D. Alsdorf, K. W. Seo and C. Wilson, High-resolution recovery and validation of GRACE hydrological signals, Eos Trans. AGU, 85(47), Fall Meet. Suppl., Abstract C22C-01, San Francisco, 2004b.
Han, S. C., The efficient determination of global gravity field from satellite-to-satellite tracking mission, Celestial Mechanics and Dynamical Astronomy, 88, 69-102, 2004c.
Han, S. C., C. K. Shum, C. Jekeli, and D. Alsdorf, Improved estimation of continental water storage changes from GRACE satellite-to-satellite tracking data, in press, *Geophys. Res. Lett.*, 2005a.
Han, S. C., C. K. Shum, C. Jekeli, C. Y. Kuo, C. Wilson, and K. W. Seo, Non-isotropic filtering of grace temporal gravity for geophysical signal enhancements, *Geophys. J. Int.*, 163(1), 18-25, doi:10.1111/j.1365-246X.2005.02756.x, 2005b.
Hansen, J., et al., Earth's Energy Imbalance: Confirmation and Implications. *Science* 308, 1431-1435, 2005.
Hayne, G. S., and D. W. Hancock, Topex side B Sigma0 calibration table adjustment, NASA, Goddard Space Flight Center, Wallops Flight Facility, 2000.
Heiskanen, W. A., and H. Moritz, Physical geodesy, Institute of Physical Geodesy, Technical University, Graz, Austria, 1987.
Hendricks, J. R., R. R. Leben, G. H. Born, and C. J. Koblinsky, Empirical orthogonal function analysis of global TOPEX/Poseidon altimeter data and implications for detection of global sea level rise, *J. Geophys. Res.*, 101(C6), 14,131– 14,146, 1996.
Ishii, M., M. Kimoto, and M. Kachi, Historical ocean subsurface temperature analysis with error estimates. *Mon. Wea. Rev.*, 131, 51-73, 2003.
Ishii, M., M. Kimoto, K. Sakamoto, and S. I. Iwasaki, Historical ocean subsurface temperature analysis with error estimates-revised, *Monthly Weather Review*, submitted, 2005.

Jakub, T., R. S. Nerem, E. W. Leuliette, D. P. Chambers, and L. Miller, Reconstruction of global mean sea level variations using altimeter and tide gauge data: A sensitivity analysis, OSTST Meeting, St. Petersbury, Florida, 2004.

Johansson, J. M., J. L. Davis, H. G. Scherneck, G. A. Milne, M. Vermeer, J. X. Mitrovica, R. A. Bennett, B. Jonsson, G. Elgered, P. Elósegui, H. Koivula, M. Poutanen, B. O. Rönnäng, and I. I. Shapiro, Continuous GPS measurements of postglacial adjustment in Fennoscandia 1. Geodetic results, *J. Geophys. Res.*, 107(B8), doi:10.1029/2001JB000400, 2002.

Kaula, W.M., The terrestrial environment: Solid earth and ocean physics, NASA Rep. Study at Williamstown, MA, NASA CR-1579, 1969.

Kistler, R., E. Kalnay, W. Collins, S. Saha, G. White, J. Woollen, M. Chelliah, W. Ebisuzaki, M. Kanamitsu, V. Kousky, H. van den Dool, R. Jenne, and M. Fiorino, The NCEP–NCAR 50-year reanalysis: Monthly means CD-ROM and documentation, *Bull. Amer. Meteor. Soc.*, 82, 247–267, 2001.

Koch, K., Parameter estimation and hypothesis testing in linear models, 2nd edition, Springer, 1999.

Krabill, W., W. Abdalati, E. Frederick, S. Manizade, C. Martin, J. Sonntag, R. Swift, R. Thomas, W. Wright, and J. Yungel, Greenland ice sheet: High-elevation balance and peripheral thinning, *Science*, 289, 428-430, 2000.

Krabill, W., E. Hanna, P. Huybrechts, W. Abdalati, J. Cappelen, B. Csatho, E. Frederick, S. Manizade, C. Martin, J. Sonntag, R. Swift, R. Thomas, and J. Yungel, Greenland Ice Sheet: Increased coastal thinning, *Geophys. Res. Lett.*, 31, L24402, doi:10.1029/2004GL021533, 2004.

Kukush, A., and S. Van Huffel, Consistency of elementwise-weighted total least squares estimator in a multivariate errors-invariables model AX=B, *Metrika*, 59, 75–97, DOI 10.1007/s001840300272, 2004.

Kuo, C. Y., C. K. Shum, A. Braun, I. Fukumori, Z. Xing, and Y. Yi, Southern Ocean sea level variation studies using steric data, GRACE ocean mass variations and ocean modeling, Proc. Gravity, Geoid and Space Mission, Porto, Portugal, 2004a.

Kuo, C. Y., C. K. Shum, A. Braun, and J. X. Mitrovica, Vertical crustal motion determined by satellite altimetry and tide gauge data in Fennoscandia, *Geophys. Res. Lett.*, 31, L01608, doi:10.1029/2003GL019106, 2004b.

Kuo, C. Y., C. K. Shum, S. C. Han, Y. Yi, A. Braun, K. Shibuya, K. Doi, and K. Matsumoto, Oceanic mass constraint studies in East Antarctica Ocean, submitted, *J. of Geodynamics*, 2005.

Kwok, R., D. A. Rothrock, G. F. Stern, and H. L. Cunningham, Determination of ice age using Lagrangian observations of ice motion, *IEEE Trans. Geosci. Remote Sens.*, 33 (2), 392-400, 1995.

Lambert, A., T. S. James, and L. H. Thorleifson, Combining geomorphological and geodetic data to determine postglacial tilting in Manitoba, *J. of Paleolimnology*, 19, 365–376, 1998.

Larsen, C. F., K. A. Echelmeyer, J. T. Freymueller, and R. J. Motyka, Tide gauge records of uplift along the northern Pacific-North America plate boundary, 1937 to 2001, *J. Geophys. Res.*, 108(B4), 2216, doi:10.1029/2001JB001685, 2003.

Larson, K. M., and T. van Dam, Measuring postglacial rebound with GPS and absolute gravity, *Geophys. Res. Lett.*, 27, 23, 3925-3928, 2000.

Lee, T., and I. Fukumori, Interannual to decadal variation of tropical-subtropical exchange in the Pacific Ocean: boundary versus interior pycnocline transports, *J. of Clim.*, 16, 4022-4042, 2003.

Levitus, S., T. P. Boyer, World Ocean Atlas 1994, Vol. 4: Temperature. NOAA Atlas NESDIS 4, U.S. Gov. Printing Office, Wash., D.C., 117, 1994.

Levitus, S., J. I. Antonov, T. P. Boyer, and C. Stephens, Warming of the world ocean, *Science*, 287, 2225-2229, 2000.

Levitus, S., J. I. Antonov, J. Wang, T. L. Delworth, K. W. Dixon, and A. J. Broccoli, Anthropogenic warming of Earth's climate system, *Science*, 292, 267-270, 2001.

Levitus, S., J. I. Antonov, and T. P. Boyer, Warming of the world ocean, 1955–2003, *Geophys. Res. Lett.*, 32, L02604, doi:10.1029/2004GL021592, 2005.

Liebsch, G., K. Novotny, R. Dietrich, and C. Shum, Comparison of multi-mission altimetric sea-surface heights with tide gauge observations in the Southern Baltic Sea, *Marine Geodesy*, 25, 213–234, 2002.

Lin, J., Correction of tide gauge measurements to absolute sea level by vertical land motion solution, *Master Thesis*, The Ohio State University, August, 2000.

Lombard, A., A. Cazenave, P. Y. Le Traon, and M. Ishii, Contribution of thermal expansion to present-day sea level change revisited, *Global and Planetary Change*, 47, 1 –16, 2005.

Mäkinen, J., and V. Saaranen, Determination of post-glacial land uplift from the three precise levellings in Finland, *J. of Geodesy*, 72, 516–529, 1998.

Mainville, A., and M. Craymer, Present-day tilting of the Great Lakes region based on water level gauges, *Geological Society of America Bulletin*, in review, 2003.

Manabe, S., M. J. Stouffer, R. J. Spelman, and K. Bryan, Transient responses of a coupled ocean atmosphere model to gradual changes of atmospheric CO2. Part 1: Annual mean response, *J. of Clim.*, 4, 785-818, 1991.

Mann, M.E. and Lees, J.M., Robust estimation of background noise and signal detection in climatic time series, *Clim. Change*, 33, 409-445, 1996.

Marshall, J. C., A. Adcroft, C. Hill, L. Perelman, and C. Heisey, A finite-volume incompressible Navier Stokes model for studies of the ocean on parallel computers, *J. Geophys. Res.*, 102(C3), 5753-5766, 1997.

McCarthy, D., IERS Conventions, IERS Technical Note 21, 1996.

McPhaden, M., and D. Zhang, Slowdown of the meridional overturning circulation in the upper Pacific Ocean, *Nature*, Vol. 415, 603–608, 2002.

Meier, M. F., Contribution of small glaciers to global sea level, *Science*, 226, 1418-1421, 1984.

Meier, M. F., Wahr, J. M., Sea level is rising: Do we know why?, *Proc. Natl. Acad. Sci. U. S. A.*, 99, 6524-6526, 2002.

Meier, M. F., D. B. Bahr, M. B. Dyurgerov, and W. T. Pfeffer, Comment on "The potential for sea level rise: New estimates from glacier and ice cap area and volume distribution" by S. C. B. Raper and R. J. Braithwaite, *Geophys. Res. Lett.*, 32, L17501, doi:10.1029/2005GL023319, 2005.

Miller, L., and Douglas, B. C., Mass and volume contributions to 20th century global sea level rise, *Nature*, 248, 407-409, 2004.

Miller, L., and Douglas, B. C., On the rate and causes of 20th century sea level rise, *Phil. Trans.*, in press, 2005.

Millero, F. J., and A. Poisson, International one-atmosphere equation of state for sea water, *Deep-Sea Res.*, 28A, 625-629, 1981.

Milly, P. C. D., A. Cazenave, and M. C. Gennero, Contribution of climate-driven change in continental water storage to recent sea-level rise, *Proc. Natl. Acad. Sci. U. S. A.*, 100, 13,158–13,161, 2003.

Milne, G. A., J. X. Mitrovica, and J. L. Davis, Near-field hydro-isostasy: The implementation of a revised sea-level equation, *Geophys. J. Int.*, 139, 464-482, 1999.

Milne, G. A., J. L. Davis, J. X. Mitrovica, H. Scherneck, J. M. Johansson, M. Poutanen, and H. Koivula, Space-geodetic constraints on glacial isostatic adjustment in Fennoscandia, *Science*, 291(5512), 2381–2385, 2001.

Mitrovica, J. X., and J. L. Davis, Present-day post-glacial sea level change far from the late Pleistocene ice sheets: Implications for recent analyses of tide gauge records, *Geophys. Res. Lett.*, 22(18), 2529-2532, 1995.

Mitrovica, J. X., M. E. Tsimplis, J. L. Davis, and G. A. Milne, Recent mass balance of polar ice sheets inferred from patterns of global sea-level change, *Nature*, 409, 1026-1029, 2001.

Moore, J. C., A. Crinsted, and S. Jevrejeva, New tools for analyzing time series relationships and trends, Eos, 86, 24, 226& 232, 2005.

Morison, J., K. Aagaard, and M. Steele, Recent environmental changes in the Arctic, *A review Arctic*, 53, 4, 2000.

Morison, J., V. Alexander, L. Codispoti, T. Delworth, B. Dickson, H. Eicken, J. Grebmeier, J. Kruse, J. Overland, J. Overpeck, P. Schlosser, M. Serreze, and J. Walsh (Eds.), Study of Environmental Arctic Change (SEARCH) Science Plan, http://psc.apl.washington.edu/search/, 2001.

Morris, C.S., and S.K. Gill, Evaluation of the TOPEX/POSEIDON altimeter system over the Great Lakes, *J. Geophys. Res.*, 99(C12) 24,52724,540, 1994.

Munk, W., Twentieth century sea level: an enigma, *Proc. Natl. Acad. Sci. USA*, 99, 10, 6550-6555, 2002.

Murphy, C.M., P. Moore, and P. L. Woodworth, Short-arc calibration of the ERS-1 and TOPEX/POSEIDON altimeters utilising in-situ data, *J. Geophys. Res*, 101(C6), 14,191-14,200, 1996.

Nakada, M., and K. Lambeck, The melting history of the late Pleistocene Antarctic ice sheet, *Nature*, 333, 36-40, 1988.

Nerem, R. S., and G. T. Mitchum, Observations of sea level change from satellite altimetry, In B. C. Douglas, M. S. Kearney, and S. P. Leatherman (Eds.), Sea Level Rise: History and Consequences, Chapter 6, Academic Press, 2001.

Nerem, R. S., and G. T. Mitchum, Estimates of vertical crustal motion derived from differences of TOPEX/Poseidon and tide gauge sea level measurements, *Geophys. Res. Lett.*, 29, 19, doi:10.1029/2002GL015037, 2002.

Nerem, R. S., D. P. Chambers, E. W. Leuliette, G. T. Mitchum, and W. White, A multidisciplinary investigation of present-day sea level change, NASA Sea Level Workshop, Landover, MD, 2005.

Ngo-Duc, T., K. Laval, J. Polcher, A. Lombard, and A. Cazenave, Effects of land water storage on global mean sea level over the past half century, *Geophys. Res. Lett.*, 32, L09704, doi:10.1029/2005GL022719, 2005.

Nicholls, R. J., and S. P. Leatherman, Global sea-level rise, In K. Strzepek and J. B. Smith (Eds.), As Climate Changes: Potential Impacts and Implications, Cambridge University Press, Cambridge, 1994.

Pagiatakis, S. D., and P. Salib, Historical relative gravity observations and the time rate of change of gravity due to postglacial rebound and other tectonic movements in Canada, *J. Geophys. Res.*, 108(B9), 2406, doi:10.1029/2001JB001676, 2003.

Pattullo, J., W. Munk, R. Revelle, and E. Strong, The seasonal oscillation in sea level, *J. Mar. Res.*, 88-156, 1955.

Peltier, W. R., Global sea level and Earth rotation, *Science*, 240, 895-901, 1988.

Peltier, W. R., Postglacial variations in the level of the sea: implications for climate dynamics and solid Earth Geophysics, *Rev. of Geophys.*, 36(4), 603-689, 1998.

Peltier, W. R., Global glacial isostatic adjustment and modern instrumental records of relative sea level history, In B. C. Douglas, M. S. Kearney, and S. P. Leatherman (Eds.), Sea Level Rise: History and Consequences, Chapter 4, Academic Press, 2001.

Peltier, W. R., Global glacial isostatic adjustment: Palaeogeodetic and space-geodetic tests of the ICE-4G (VM2) model, *J. Quaternary Science*, 17, 5-6, 491-510, 2002.

Piexoto, J. P., and A. H. Oort, The physics of climate, American Institute of Physics, New York, 1992.

Plag, H. P., and H. U. Juttner, Inversion of global tide gauge data for present-day ice load changes, *Memoirs of Nat. Inst. of Polar Res.*, 54, 2001.

Plag, H. P., Recent relative sea level trends: An attempt to quantify the forcing factors, *Phil Trans.*, in press, 2005.

Polyakov, I. V., R. V. Bekryaev, G. V. Alekseev, U. Bhatt, R. L. Colongy, M. A. Johnson, A. P. Maskshtas, and D. Walsh, Variability and trends of air temperature and pressure in the maritime Arctic, 1875-2000, *J. of Clim.*, 6, 12, 2067-2077, 2003.

Pond, S., and G. L. Pickard, Introductory dynamical oceanography, second edition, 1983.

Ponte, R. M., Low frequency sea level variability and the inverted barometer effect, *J. of Atmospheric and Oceanic Technology*, in review, 2005.

Premoli, A., and M. L. Rastello, The parametric quadratic form method for solving total least squares problems with elementwise weighting. In Van Huffel S, Lemmerling P (Eds), Total Least Squares and Errors-in-Variables Modeling: Analysis, Algorithms and Applications, Kluwer Academic Publishers, 67–76, 2002.

Proshutinsky, A., V. Pavlov, and R. H. Bourke, Sea level rise in the Arctic Ocean, *Geophys. Res. Lett.*, 28(11), 2237-2240, 2001.

Proshutinsky, A., J. Zhang, G. Holloway, N. Steiner, S. Hakkinen, D. Holland, R. Gerdes, C. Koeberle, M. Johnson, W. Maslowski, W. Walczowski, W. Hibler, and J. Wang, Variability of the Arctic Ocean sea surface heights: Model intercomparison results, EOS. Trans. AGU, 83(19), Spring Meeting, Suppl., Abstract #GC51A-03, 2002.

Proshutinsky, A., I. M. Ashik, E. N. Dvorkin, S. Hakkienen, R. A. Krishfield, and W. R. Peltier, Secular sea level change in the Russian sector of the Acrtic Ocean, *J. Geophys. Res.*, 109, C03042, doi:10.1029/2003JC002007, 2004.

Raper, S. C. B., and R. J. Braithwaite, The potential for sea level rise: New estimates from glacier and ice cap area and volume distributions, *Geophys. Res. Lett.*, 32, L05502, doi:10.1029/2004GL021981, 2005a.

Raper, S. C. B., and R. J. Braithwaite, Reply to comment by M. F. Meier et al. on "The potential for sea level rise: New estimates from glacier and ice cap area and volume distributions," *Geophys. Res. Lett.*, 32, L17502, doi:10.1029/2005GL023460, 2005b.

Reynolds, R. W., and T. M. Smith, Improved global sea surface temperature analysis using optimum interpolation, *J of Clim.*, 7, 929-948, 1994.

Ries, J. C., Low degree harmonics in GRACE monthly solutions, Joint CHAMP/GRACE Science Meeting, Potsdam, Germany, 2004.

Rignot, E., G. Casassa, S. Gogineni, P. Kanagaratnam, W. Krabill, H. Pritchard, A. Rivera, R. Thomas, J. Turner, and D. Vaughan, Recent ice loss from the Fleming and other glaciers, Wordie Bay, West Antarctic Peninsula, *Geophys. Res. Lett.*, *32*, L07502, doi:10.1029/2004GL021947, 2005.

Sahagian, D. L., F. W. Schwartz, and D. K. Jacobs, Direct anthropogenic contributions to sea level rise in the twentieth century, *Nature*, 367, 54-56, 1994.

Schaffrin, B., I. Lee, Y. Felus, and Y. Choi, Total Least-Squares (TLS) for Photogrammetric Straight-line and Plane Adjustment, *Photogrammetric Record*, Submitted, 2005.

Schöne, T., M. Forberg, R. Galas, and C. Reigber, GPS-buoys for lifetime RA drift monitoring, AGU Fall Meeting, EOS Trans. AGU, 83(47), Fall Meet. Suppl., Abstract 0S52A-0189, 2002.

Schüler, T., B. Zimmermann, B. Riedl, and G.W. Hein, Radar altimeter calibration of the Envisat satellite: An autonomous system of high-precision for instantaneous sea surface height determination. Proc. NTM 2003 - National Technical Meeting, Anaheim, CA, 2003.

Serreze, M. C., A record minimum in arctic sea ice extent and area in 2002, *Geophys. Res. Lett.*, 30, 3, 1110-1113, 2003.

Shennan, I., and P. L. Woodworth, A comparison of late Holocene and twentieth-century sea-level trends from the UK and North Sea region, *Geophys. J. Int.*, 109, 1, 96-105, 1992.

Shum, C. K., C. Zhao, Y. Yi, C. Reigber, A. Braun, T. Schoene, D. Wolf, and P. L. Woodworth, Determination and characterization of global mean sea level change, Proc. ERS-ENVISAT Symposium, Gothenburg, Sweden, 2000.

Shum, C. K., P. Luk, Y. Yi, C. Zhao, A. Braun, and P. L. Woodworth, Determination of 20th century global sea level rise, APSG Workshop, Shanghai, China, 2001a.

Shum, C. K., C. Zhao, Y. Yi, P. Luk and J. Lillibridge, Quality assessment of GFO sensor and data products, GFO Calibration/Validation Meeting, NOAA Lab. for Satellite Altimetry, Silver Spring, MD, 2001b.

Shum, C. K., C. Y. Kuo, and J. X. Mitrovica, Glacial isostatic adjustment in the Great Lakes region inferred by tide gauges and satellite altimetry, Spring AGU Meeting, Washington D.C., 2002a.

Shum, C. K., C. Y. Kuo, A. Braun, and Y. Yi, 20th century sea level rise: a geophysical perspective, Proc. 90th Journees Luxembourgeoises de Geodynamique, Council of Europe, European Network on Geodynamics, Luxembourg, 2002b.

Shum, C. K., Y. Yi, K. C. Cheng, C. Y. Kuo, A. Braun, S. Calmant, and D. P. Chamber, Calibration of Jason-1 altimeter over Lake Erie, *Marine Geodesy*, 26:335-354, doi: 10.1080/01490410390253487, 2003a.

Shum, C. K., C. Y. Kuo, A. Braun, and Y. Yi, 20th century sea level rise, IUGG2003, Sapporo, Japan, 2003b.

Shum, C. K., S. C. Han, C. Y. Kuo, K. W. Seo, and C. Wilson, Assessment of GRACE time-variable gravity observables: A new filtering technique to enhance signal spatial resolutions, Eos Trans. AGU, 85(47), Fall Meet. Suppl., Abstract G31C-0814, San Francisco, 2004.

Sigman, D. M., S. L. Jaccard, and G. H. Haug, Polar ocean stratification in a cold climate, *Nature*, 428, 59-63, 2004.

Snay, R., M. Chin, D. Coner, T. Soler, C. Zervas, J. Oyler, M. Craymer, S. I. Gutman, C. K.

Shum, K. C. Cheng, and C. Y. Kuo, Great Lakes continuous GPS (CGPS) network for geodynamics, meteorology and safe navigation, Weikko A. Heiskanen Symposium In Geodesy: Celebrating 50 years in Geodetic Science at the Ohio State University, Ohio State University, Columbus, Ohio, 2002.

Song, T., and V. Zlotnicki, Subarctic ocean-bottom-presure oscillatin and its link to the tropical Pacific ENSO oscillation, *J. of Clim.*, in press, 2005.

Stephens, C., J. I. Antonov, T. P. Boyer, M. E. Conkright, R. Locarnini, and T. D. O'Brien, World Ocean Atlas 2001 Volume 1: Temperature [CD-ROM], edited by S. Levitus, NOAA Atlas NESDIS 49, U.S. Govt. Printing Office, Washington, D. C, 2002.

Sturges, W., and B. G. Hong, Decadal variability of sea level, In B. C. Douglas, M. S. Kearney, and S. P. Leatherman (Eds.), Sea Level Rise: History and Consequences, Chapter 7, Academic Press, 2001.

Swenson, S., and J. Wahr, Methods for inferring regional surface-mass anomalies from Gravity Recovery and Climate Experiment (GRACE) measurements of time-variable gravity, *J. Geophys. Res.*, 107(B19), 2193, doi:10.1029/2001JB000576, 2002.

Tamisiea, M. E., J. X. Mitrovica, R. S. Nerem, E. W. Leuliette, and G. A. Milne, Correcting atellite-derived estimates of global mean sea level change for glacial isostatic adjustment, *Geophys. J. Int.*, in press, 2005.

Tamisiea, M. E., J. X. Mitrovica, G. A. Milne, and J. L. Davis, Global geoid and sea level changes due to present-day ice mass fluctuation, *J. Geophys. Res.*, 106 (B12), 30,849-30,863, 2001.

Tapley, B. D., S. Bettadpur, M. Watkins, and C. Reigber, The Gravity Recovery and Climate Experiment: Mission overview and early results, *Geophys. Res. Lett.*, 31, 9, 10.1029/2004GL019920, 2004a.

Tapley, B. D., S. Bettadpur, J. C. Ries, P. F. Thompson, and M. M. Watkins, GRACE measurements of mass variability in the Earth system, *Science*, 305, 503-505, 2004b.

Thomas, R., Accelerated Sea-Level Rise from West Antarctica, *Science*, 306, 255-258, 2005.

TOPEX Team, Side B testing status, Special report, http://topex.wff.nasa.gov/sideb_status.html, NASA GSFC Wallop Flight Facility, Observational Science Branch, Wallops Flight Facility, Wallops Island, VA, 2000.

Trupin, A., and J. Wahr, Spectroscopic analysis of global tide gauge sea level data, *Geophys. J. Int.*, 100, 441-453, 1990.

Trupin, A., C. K. Shum and C. Zhao, A comparison of methods of altimetry and gravity inversion to measure components of the global water budget, In J. X. Mitrovica and R. Vermeersen (Eds.), Gravity and Glacial Isostacy in the Earth System, AGU Monograph Series, 2001a.

Trupin, A., and C. K. Shum, Determinations of polar ice mass balance from gravity, IAG Symposium Series, 123, M. Sideris (Eds), 171-178, Springer-Verlage Berlin Heidelberg, 2001b.

Tucker, W., R. Anderson, J. Newton, C. Wales, G. Newton, and T. Luallin, Accuracy of submarine ice draft measurements, In A. Thorndike, C. Parkinson, and D. Rothrock (Eds.), Report of the Sea Ice Thickness Workshop, B22-B24, University of Washington, Seattle, WA: Polar Science Center, 1992.

Tushingham, A. M., and W. R. Peltier, Ice-3G: A new global model of late Pleistocene deglaciation based upon geophysical predictions of postglacial relative sea level, *J. Geophys. Res.*, 96, 4497–4523, 1991.

Tushingham, A. M., Postglacial uplift predictions and historical water levels of the Great Lakes, *Journal Great Lakes Research,* 18, 440-455, 2002.

UNESCO, Tenth report of the joint panel in ocean graphic tables and standards, UNESCO Technical Papers in Marin Sci., 36, UNESCO, Paris, 1981.

Urban, T. J., J. C. Ries, B. D. Tapley, and C. K. Shum, The integration of twenty-five years of sea-level measurements from satellite altimetry, IUGG Symposia, JSG11, Birmingham, UK, 1999.

Urban, T. J., The integration and applications of multi-satellite radar altimetry, *Ph.D. dissertation*, The University of Texas at Austin, 2000.

Urban, T. J., T. Pekker, B. D. Tapley, G. Kruizinga, and C. K. Shum, A multiyear comparison of wet troposphere corrections from TOPEX/Poseidon, ERS-1 and ERS-2 microwave radiometers and the European Centre for Medium-range Weather Forecasts model, *J. Geophys. Res.*, 106(C9), 19657-19669, 2001a.

Urban, T. J., and D. P. Chambers, Observed sea level rise from multi-satellite altimetry, *J. of Phys. Chem. Earth*, in review, 2001b.

Varekamp, J. C., E. Thomas, and O. Van de Plassche, Relative sea level rise and climate change over the past 1500 years, *Terra Nova*, 4, 293-304, 1992.

Wadhams, P., and W. Munk, Ocean freshening, sea level rising, sea ice melting, *Geophys. Res. Lett.*, 31, L11311, doi:10.1029/2004GL020039, 2004.

Warrick, R. A., C. Le Provost, M. F. Meier, J. Oerelemans, and P. L. Woodworth, Change in sea model: An adjective mechanism, *Atmosphere-Ocean*, 29, 197-231, 1996.

Wahr, J., Deformation induced by polar motion, *J. Geophys. Res.*, 90, 9363–9368, 1985.

Wahr, J., M. Molenaar, and F. Bryan, Time variability of the Earth's gravity field: Hydrological and oceanic effects and their possible detection using GRACE, *J. Geophys. Res.*, 103(B12), 30, 205-30,229, 1998.

Wahr, J., S. Swenson, V. Zlotnicki, and I. Velicogna, Time-variable gravity from GRACE: First results, *Geophys. Res. Lett.*, 31, L11501, doi:10.1029/2004GL019779, 2004.

Watson, C., R. Coleman, N. White, J. Church, and R. Govind, Absolute calibration of Topex/Poseidon and Jason-1 using GPS buoys in bass strait, Australia, *Marine Geodesy*, 285-304, doi: 10.1080/01490410390253487, 2003.

White, N., R. Coleman, J. Church, P. Morgan and S. Walker, A southern hemisphere verification for the TOPEX/POSEIDON satellite altimeter mission, *J. Geophys. Res.*,99 (C12), 24,505–24,516, 1994.

Willis, J. K., D. Roemmich, and B. Cornuelle, Interannual variability in upper-ocean heat content, temperature and thermosteric expansion on global scales, *J. Geophys. Res.*, 109, C12036, doi:10.1029/2003JC002260, 2004.

Wingham, D. J., A. J. Ridout, R. Scharoo, R. J. Arthern, and C. K. Shum, Antarctic elevation change from 1992 to 1996, *Science*, 16, 282, 1998.

Woodworth, P. L., A search for accelerations in records of European mean sea level, *Int. J. Climate*, 10, 129-143, 1990.

Woodworth, P. L., M. N. Tsimplis, R. A. Flather, and I. A. Shennan, A review of the trends observed in British Isles mean sea level data measured by tide gauges, *Geophys. J. Int.*, 136, 651-670, 1999.

Woodward, R. S., On the form and position of mean sea level, *US Geol. Surv. Bull. 48*, 87-170, 1888.

Wunsch, C., Bermuda sea level in relation to tides, weather and baroclinic fluctuations, *Rev. Geophys. Space Phys.*, 10, 1-49, 1972.

Wunsch, C., What is the thermohaline circulation? *Science*, 298, 1179-1120. 2002.

Wunsch, C. and R. Ferrari, Vertical mixing, energy, and the general circulation of the oceans, *Annu. Rev. Fluid Mech. 2004*, 36:281–314, doi:10.1146/annurev.fluid.36.050802.122121, 2004.

Yi, Y., Determination of gridded mean sea surface from TOPEX, ERS-1 and GEOSAT altimeter data, *Report. 434*, Dept. of Geodetic Science and Surveying, The Ohio State University, Columbus, 9363-9368, 1995.

Yi, Y., OSU Stackfile, Department of Civil and Environmental Engineering and Geodetic Science, The Ohio State University, Columbus, Ohio, USA, 2000.

Zhao, D., D. Christensen, and H. Pulpan, Tomographic imaging of the Alaska subduction zone, *J. Geophys. Res.*, 100(B4), 6487–6504, 1995.

Zhang, T., O. W. Frauenfeld, M. C. Serreze, et al., Spatial and temporal variability in active layer thickness over the Russian Arctic drainage basin, *J. Geophys. Res*., 110, doi:10.1029/2004JD005642, 2005.

Zlotnicki, V., Y. T. Song, J. Wahr, I. Fukumori, D. Menemenlis, and A. Haider, Bottom pressure signals in the Pacific Ocean observed by GRACE, *Advances in Geosciences*, summitted, 2005.

Zwally, H. J., A. C. Brenner, J. A. Major, R. A. Bindschadler, and J. G. Marsh, Growth of Greenland ice sheet: Measurement, *Science*, 246, 1587-1589, 1989.

APPENDIX A

THE EQUATION OF STATE

The equation of state defined by the Joint Panel on Oceanographic Tables and Standards (UNESCO,1981) fits available measurements with a standard error of 3.5 ppm for pressure up to 1000 bars, for temperatures between freezing and 40° C, and for salinities between 0 to 42 (Millero and Poisson, 1981). The density $\rho\,(kg \times m^{-3})$ of sea water as a function of pressure p (in bars), temperature t (in $^{\circ}C$), and practical salinity S is given by

$$\rho(S,t,p) = \rho(S,t,0)/[1 - p/K(S,t,p)] \quad \text{.....(A.1)}$$

where $K(S,t,p)$ is the secant bulk modulus.

$$\begin{aligned}
&\rho(S,t,0) = \\
&+ 999.842594 + 6.793952\times10^{-2}\times T - 9.095290\times10^{-3}\times T^2 \\
&+ 1.001685\times10^{-4}\times T^3 - 1.120083\times10^{-6}\times T^4 + 6.536332\times10^{-9}\times T^5 \\
&+ 8.24493\times10^{-1}\times S - 4.0899\times10^{-3}\times T\times S + 7.6438\times10^{-5}\times T^2\times S \\
&- 8.2467\times10^{-7}\times T^3\times S + 5.3875\times10^{-9}\times T^4\times S - 5.72466\times10^{-3}\times S^{3/2} \\
&+ 1.0227\times10^{-4}\times T\times S^{3/2} - 1.6546\times10^{-6}\times T^2\times S^{3/2} + 4.8314\times10^{-4}\times S^2
\end{aligned} \quad \text{.....(A.2)}$$

The secant bulk modulus is given by:

$$\begin{aligned}
&K(S,t,p) = \\
&19652.21 + 148.4206\times T - 2.327105\times T^2 + 1.360477\times10^{-2}\times T^3 \\
&- 5.155288\times10^{-5}\times T^4 + 3.239908\times p + 1.43713\times10^{-3}\times T\times p \\
&+ 1.16092\times10^{-4}\times T^2\times p - 5.77905\times10^{-7}\times T^3\times p + 8.50935\times10^{-5}\times p^2 \\
&- 6.12293\times10^{-6}\times T\times p^2 + 5.2787\times10^{-8}\times T^2\times p^2 + 54.6746\times S \\
&- 0.603459\times T\times S + 1.009987\times10^{-2}\times T^2\times S - 6.1670\times10^{-5}\times T^3\times S \\
&+ 7.944\times10^{-2}\times T\times S^{3/2} + 1.6483\times10^{-2}\times T\times S^{3/2} - 5.3009\times10^{-4}\times T^2\times S^{3/2} \\
&+ 2.2838\times10^{-3}\times p\times S - 1.0981\times10^{-5}\times T\times p\times S - 1.6078\times10^{-6}\times T^2\times p\times S \\
&+ 1.91075\times10^{-4}\times p\times S^{3/2} - 9.9348\times10^{-7}\times p^2\times S + 2.0816\times10^{-8}\times T\times p^2\times S \\
&+ 9.1697\times10^{-10}\times T^2\times p^2\times S
\end{aligned}$$

.....(A.3)

APPENDIX B

MULTI-TAPER METHOD (MTM)

The Multi-Taper method (MTM) of spectral analysis provides a novel approach for spectral estimation of a time series which is believed to exhibit a spectrum containing both continuous and singular components and signal reconstruction from selected spectral components. This method has been widely applied to problems in geophysical signal analysis, including analyses of atmospheric and oceanic data, paleoclimate data geochemical tracer data, and seismological data [Ghil et al., 2002]. In this study, the Singular Spectrum Analysis - Multitaper Method (SSA-MTM) Toolkit was used as a means to estimate spectra of a time series, to decompose a time series into trends, oscillatory components, and noise, and to reconstruct the contributions of selected components of a time series [Ghil et al., 2002; Dettinger et al., 1995]. The detail of theory has been introduced in Ghil et al. [2002] and Mann and Lees [1996].

The procedure to determine a trend of sea level variations derived from tide gauge data is as follows. First at all, a time series of sea level changes is calculated in light of chapter 7 (blue curve in the upper panel of Figure B.1). Then the time series of sea level changes can be decomposed into trends, oscillatory components, and noise by MTM. Figure B.2 present the spectra derived by MTM. Four additional smooth curves are shown for the 50%, 90%, 95%, and 99% significance levels relative to the estimated noise background in increasing vertical progression. Secondly, a time series is reconstructed from selected components, which have the periods longer than half of the time span of the original sea level time series. For instance, if a time series lasts 50 years, the components with longer than 25-year period could be used in reconstruction. The red curve in the upper panel of Figure B.1 shows the reconstructed time series of sea level using four selected frequencies, 0.0005 cycle/month, 0.0044 cycle/month, 0.0117 cycle/month, and 0.0171 cycle/month, which show 99% significance levels relative to the estimated noise background. Finally, the trend can be determined by the linear regression using the reconstructed time series. For spectral analysis, the time series of sea level variations is considered as a combination of harmonic signals, which are periodic or quasi-periodic signals, and narrowband (anharmonic), quasi-oscillatory signals which may exhibit phase and amplitude modulation, and intermittent oscillatory behavior. If only harmonic signals are considered, a continuous spectrum (in the case of a colored noise or a chaotic system) will be broken down into spurious lines with arbitrary frequencies and possibly high *F*-values [Ghil et al., 2002].

Table B.1 and the lower panel of Figure B.1 show the trends determined from different time spans of 27 tide gauge data. Sea level changes of two time spans, 1992-200 and 1982-2000, are assumed to only contain harmonic signals because trends do not exist when assuming sea level variations contain both harmonic and narrowband signals. The trends are more stable when time spans of gauge data are more than 20 years. Compared with Table 7.3, which results are determined by Least Squares approach, both methods address the difficulty to derive a trend when using a time series with a short time span.

Time span (years)	Sea level Trend (mm/yr)
1902-2000: 99	1.77±0.005
1912-2000: 89	1.79±0.007
1922-2000: 79	1.70±0.009
1932-2000: 69	1.51±0.004
1942-2000: 59	1.43±0.000
1952-2000: 49	1.40±0.001
1962-2000: 39	1.40±0.006
1972-2000: 29	1.48±0.015
1981-2000: 20	1.76±0.085
1982-2000: 19	1.86±0.096*
1985-2000: 16	3.00±0.080
1987-2000: 14	3.88±0.073
1992-2000: 9	3.43±0.318*

Table B.1: Sea level trends derived from 27 tide gauges [Douglas, 2001] using different time spans. * means sea level variations are assumed to only contain harmonic signals.

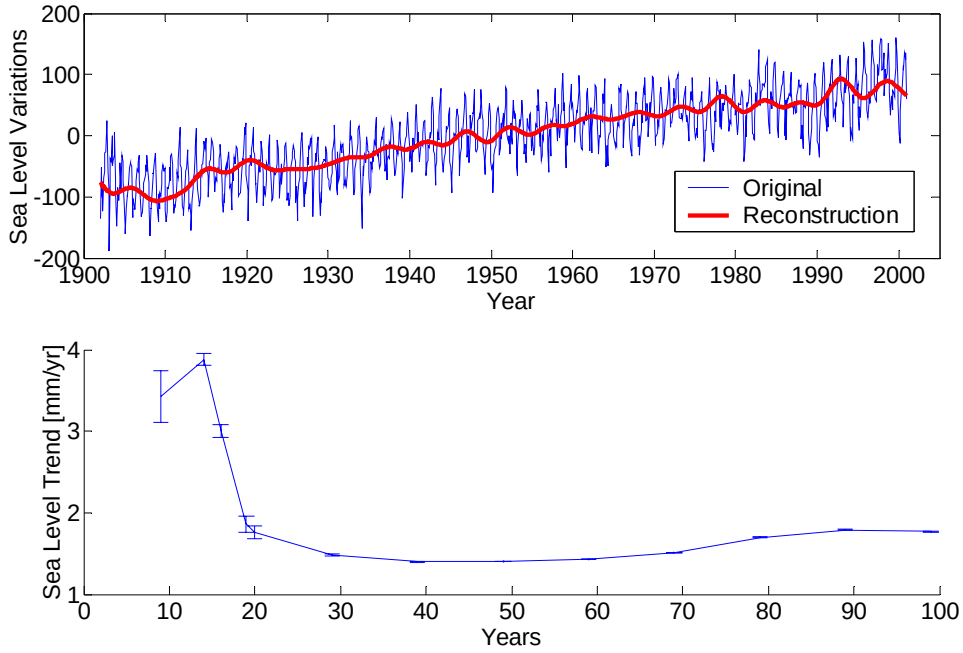

Figure B.1: Top: Sea level variations derived from 27 stations [Douglas, 2001] during 1902-2000 (blue curve). Red curve is the reconstructed time series. Bottom: Sea level trends determined from different time spans of gauge data.

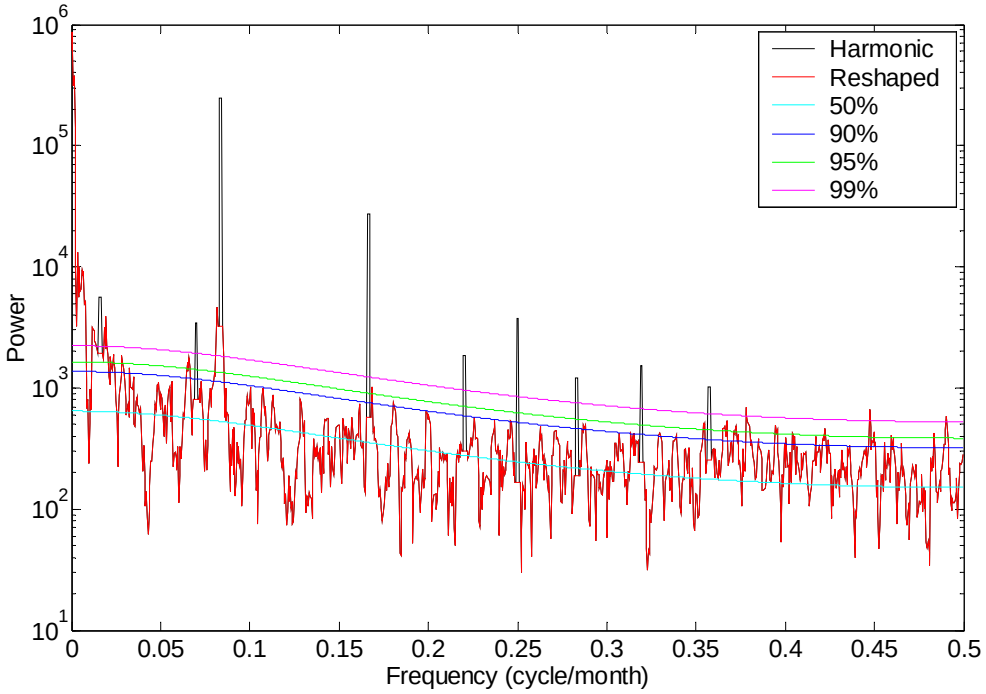

Figure B.2: Spectrum derived by MTM. Four additional smooth curves are shown, in increasing vertical progression, for the 50%, 90%, 95%, and 99% significance levels relative to the estimated noise background.